INTERFERENCE CHARACTERISTICS OF PULSE-TIME MODULATION

E. R. KRETZMER

TECHNICAL REPORT NO. 92

MAY 27, 1949

RESEARCH LABORATORY OF ELECTRONICS
MASSACHUSETTS INSTITUTE OF TECHNOLOGY

The research reported in this document was made possible through support extended the Massachusetts Institute of Technology, Research Laboratory of Electronics, jointly by the Army Signal Corps, the Navy Department (Office of Naval Research) and the Air Force (Air Materiel Command), under Signal Corps Contract No. W36-039-sc-32037, Project No. 102B; Department of the Army Project No. 3-99-10-022.

MASSACHUSETTS INSTITUTE OF TECHNOLOGY
Research Laboratory of Electronics

Technical Report No. 92 May 27, 1949

INTERFERENCE CHARACTERISTICS OF PULSE-TIME MODULATION*

E. R. Kretzmer

ABSTRACT

The interference characteristics of pulse-time modulation are analyzed mathematically and experimentally; particular forms examined are pulse-duration and pulse-position modulation. Both two-station and two-path interference are considered. The theoretical analysis consists, first, of a quantitative formulation of the defects imparted on the pulses by the interference; second, of a detailed evaluation of the resulting disturbance in the receiver output, based on auto-correlation analysis. The experimental investigation is aimed at close duplication of the various conditions encountered in practice: two-station interference is produced by use of separate transmitters, while two-path interference is simulated by means of a mercury delay line. Detailed results are presented in numerous graphical plots. Two-station interference is characterized by a virtually complete predominance of the stronger of the two signals, and by noise of more or less random character. Under some conditions, the noise is sufficiently weak to permit fair reception when the two signal levels differ by less than 1 db, while other situations permit acceptable reception only with level difference larger than 6 db. These general statements apply to both pulse-duration and pulse-position modulation, simplex and multiplex. Two-path interference in the case of simplex pulse-duration modulation, is characterized by the linear superposition of the two identical but time-staggered modulating signals. All interference effects, both in theory and practice, are found to be directly dependent on the all-important slicing process. For best results, the "slice" must be very thin and the slicing level should be adjustable.

* This report is identical with a thesis of the same title submitted by the author in partial fulfillment of the requirements for the degree of Doctor of Science in Electrical Engineering at the Massachusetts Institute of Technology.

TABLE OF CONTENTS

CHAPTER 1

PULSE-TIME MODULATION

Pulse-time modulation, usually abbreviated PTM, may be defined as modulation in which the time of occurrence of the pulse edges of a pulse train is varied from exact periodicity by samples of the modulating signal. Pulse-duration modulation and pulse-position modulation, abbreviated PDM and PPM, respectively, are particular forms of pulse-time modulation which differ fundamentally only in the relative timing variations of the two edges of each pulse; these two sets of timing variations are different in the case of pulse-duration modulation, but are generally identical in the case of pulse-position modulation. In both cases, however, information is conveyed only by the time position of the pulse edges relative to their periodic positions in the unmodulated pulse train.

Amplitude keying, frequency-shift keying and other methods may be used to transpose the pulses into a frequency range suitable for radio transmission. The method considered in this paper is the amplitude-keying method, whereby the modulated train of d-c pulses is converted into a corresponding train of r-f pulses with the transmitter idle during the periods between pulses. The shape and time of build-up and decay of the transmitted pulses determine the transmission bandwidth, which, for a given shape, is inversely proportional to the time interval. The pulse repetition frequency, in accordance with the sampling principle, must exceed twice the width of the modulating-signal band in order to make the faithful reproduction of the signal possible.

The time between pulses can be utilized for the transmission of other similar pulse trains modulated by different signals, to form a so-called time-division multiplex or multi-channel system. Results for both single-channel and multi-channel systems are obtained in this paper.

The history of pulse-time modulation, as applied to the transmission of speech and music, dates back to the nineteen-twenties and nineteen-thirties. In 1924, R. A. Heising applied for a patent which was granted in 1924 under the title "Transmission System", and which described a method similar to modern pulse-duration modulation.[1] Other American patents, as well as a series of British patents, describing pulse-time modulation and various methods for producing it, appeared during the period 1934-41.[2,3] During this

period, PDM found application in a few experimental decimeter-wave links in Europe, but the actual development and use of PTM in its various forms did not begin until after the beginning of World War II, when its use was prompted by the development of radar and by the advantages which PTM appeared to have for military communication. This work was kept secret during the war; since 1945, however, it has been appearing in the technical literature, along with the more recent results of research and development work on pulse-time modulation and other types of pulse modulation. Although somewhat overshadowed by pulse-code modulation at the present time, pulse-time modulation has taken its place alongside the older types of modulation; it is in commercial use to a considerable extent, mostly in the form of pulse-position modulation used in time-division multiplex radio links.

The early patents, although obscured by the more recent publications, form an important part of the history of PTM, since they disclose some interesting and useful viewpoints. The duration-modulated pulses used to key the transmitter in a PDM system, and re-obtained at the receiver after detection, are shown in Fig. 1. While the transmitted-pulse envelopes must be rounded rather than rectangular because of the transmission-bandwidth limitation, the pulses eventually obtained in the receiver after detection and limiting can be considered as perfectly rectangular, as will be shown later.

These pulses are more than a particular kind of sub-carrier modulated by a signal in a special way: they constitute another method of representing the signal function by a two-valued (on-off) function. The pulse train is seen to have an average value which is proportional to the instantaneous value of the signal, and while it does contain additional undesired components, these can be largely removed by the simple process of filtering which may be performed by the ear. The remaining inherent distortion is a function of several variables, and has been treated in the literature.[4] On the other hand, the pulse-train representation of the signal has certain advantages which stem mostly from the fact that amplitude is not a variable and linearity is not required in handling the signal. The purpose of the very early patent of Heising was the design of a transmitter, more efficient than the usual AM transmitter because it did not have to be linear throughout. Its essential difference from the ordinary AM system is that a large supersonic voltage is mixed with the modulating signal voltage, overloading the amplifier stages, and producing duration-modulated pulses as shown in Fig. 2. These contain the signal without the distortion that would result if the signal alone were

passed through a nonlinear amplifier. Before actual transmission, a filter removes the high-frequency components, leaving the usual AM wave. The same principle of effectively converting a signal into an equivalent duration-modulated pulse train finds application in other instances where it is desirable or necessary to convey the signal through a nonlinear device, as is the case in magnetic recording.

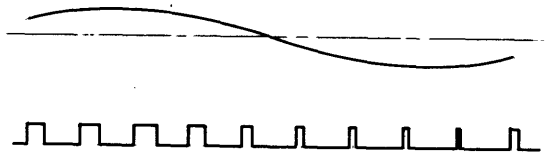

Fig. 1 Duration-modulated pulses.

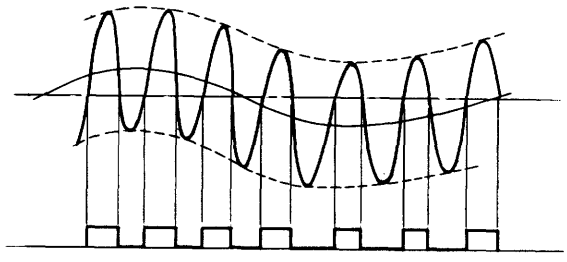

Fig. 2 Heising's method of forming PDM.

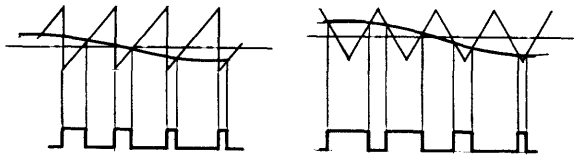

Fig. 3 Asymmetrical and "symmetrical" PDM.

The modern method for generating PTM is based on the same principle, (Fig. 2), refined somewhat by a patent granted to R. D. Kell[2] in 1936, and still further refined in more recent development work. The modulation process, which consists of slicing a high-frequency saw-tooth voltage at a variable level determined by the instantaneous signal value, is shown in Fig. 3 for so-called asymmetrical and "symmetrical" PDM. The latter is enclosed in quotation marks because, although both edges shift, they do not, in general, shift by exactly equal and opposite amounts.

Pulse-position modulation evolved directly from pulse-duration modulation[2] from the realization that it is wasteful to transmit relatively long pulses when only the timing of their edges conveys information, and that greater power economy can be obtained by merely marking these edges by pulses of constant duration. These new pulses may have minimum duration possible for the available bandwidth, which means that they consist merely of a rise and decay without any flat portion intervening. At the receiver, the space between the two

pulses marking the two edges of the original duration-modulated pulse can be "filled in" to reproduce the original pulse, so that the overall system differs essentially only in its transmission characteristics. While some systems used in England during World War II had PPM which was derived from "symmetrical" PDM, more recent PPM systems use only one position-modulated pulse per sampling period for each channel and one unmodulated pulse which may serve as a time reference or marker pulse to a large number of time-interlaced modulated pulses called channel pulses. The marker pulse and the channel pulse of any one channel can be regarded as marking the fixed leading edge and the time-modulated trailing edge, respectively, of an asymmetrically duration-modulated pulse; but such a duration-modulated pulse need not exist anywhere in the system. Even the reconversion of the pulses into the original audio signal can be performed without first converting to PDM, although this has been the most common practice in the past. It should be pointed out that, in fact, even PDM does not necessarily have to be considered in the light of the basic characteristic discussed above - that is, the approximate equivalence of the duration-modulated pulse train to the modulating signal. The so-called sampling principle (see page 7) states that a signal having frequency components up to f_c can be faithfully reproduced from samples taken periodically at a minimum rate $2f_c$;[5,6] it is entirely possible to convert such samples into pulses of corresponding durations, reconvert these durations into the original samples except for a constant delay, and reproduce the original signal without any inherent distortion being introduced in the process. However such methods are not generally used, and are mentioned only for the sake of completeness.

The first advantage claimed for pulse-time modulation in the earliest patents was greater transmitter efficiency, but added claims of improved signal-to-noise ratio and the general benefits of nonlinearity became the dominating factor as early as the middle nineteen-thirties. Principal reasons for the wartime use of pulse-time modulation systems were, besides those already mentioned, the superiority of time-division multiplex over frequency-division multiplex, which makes possible lighter equipment with lower cross-talk between channels, as well as the fact that the use of the microwave spectrum was desirable and microwave tubes could be more easily pulse-modulated than amplitude- or frequency-modulated.

The literature on pulse-time modulation has dealt with descriptions of

systems and circuit techniques, spectrum analyses, and derivations of signal-to-noise-ratio-formulas. Although so-called pulse techniques are a well-established art, their application to PTM, particularly PPM, has not yet resulted in standard circuits for performing various functions. While many of the same principles have been used in various equipments, the exact methods and circuits are still being improved. A presentation of those used in the experimental part of the research reported here will be found in the appendix.

Spectrum analyses for various modulation types have become a standard textbook ornament, and their significance, especially with sinusoidal modulation, is sometimes overrated. Generally, they give information about the transmission bandwidth, the distribution of energy over the band, and other items. In the case of pulse modulation, including PTM, the bandwidth is largely determined by the shortest rise or decay time occurring in the pulse train, and modulation may have little effect. A spectrum analysis of the modulated pulse train is of interest for another reason: it shows exactly what will be heard if the pulses are fed to the loudspeaker without any nonlinear or demodulation process intervening. In some cases where a nonlinear demodulator is normally used, the spectrum will therefore show how private the system is when conventional receivers are used. For example, it shows that position-modulated pulses of the type normally used do contain enough signal component to be heard directly, and that by a slight modification this component can be eliminated. More important, in the case of pulse-duration modulation, where no nonlinear process is ordinarily used, the spectrum analysis gives the type and amount of distortion to be expected at the output as a function of the variables involved. Since position-modulated pulses are usually converted to duration-modulated pulses for demodulation, such results are applicable to PPM as well as PDM. This subject has received a considerable amount of attention in the literature; this was stimulated by the fact that some authors obtained partially wrong results, because they failed to take into account the exact law of modulation. For the details, the reader is referred to another paper by the writer.[4] Some of the salient points can be mentioned here: The spectrum of the d-c pulses, in the absence of modulation, consists of lines at the pulse repetition frequency p and its harmonics np. Modulation by a sinusoid of frequency q produces additional spectral lines, one at frequency q which represents the useful signal component, and an infinite set at frequencies $np \pm mq$ with m any integer and n any integer except zero. So-

called intermodulation distortion results because some of these components fall into the audio band and cannot be separated from the useful or desired components, as shown in Fig. 4. The only components apt to be significant

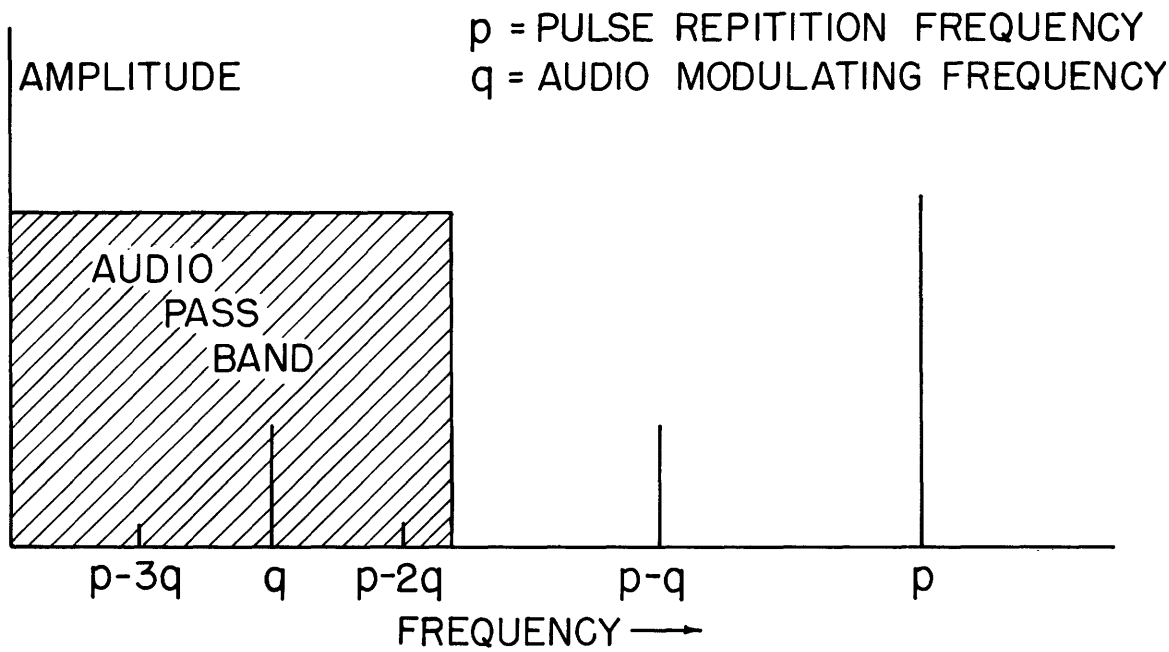

Fig.4 Audio spectrum of duration-modulated pulses.

are those of frequencies p-q and p-2q. The former is of the same magnitude as the useful signal component of frequency q and is in fact an exact inversion of this; it occurs in any periodic sampling process and the necessity for its exclusion from the audio band is responsible for the basic rule that the sampling frequency must exceed twice the highest signal frequency in order to make faithful reproduction possible. The latter component, at frequency p-2q, ranges from a fraction of one per cent of the desired component in the case of low-index symmetrical PDM, through several per cent for low-index asymmetrical PDM such as is obtained in most present-day PPM systems, to about 30 per cent in the case of high-index PDM which is possible only on single-channel applications. In the latter case, it may be necessary to exclude the p-2q component, which would call for a pulse-repetition frequency more than three times the highest modulating frequency. However, the intermodulation distortion is generally much less severe than indicated by the above figures,

because the spectral components in question fall into the audio band only when caused by relatively high values of the signal frequency q, where the signal magnitude is relatively small; this makes the index of modulation effectively smaller as far as the undesired components are concerned, and their magnitude decreases rapidly with decreasing index.

The sampling principle, mentioned earlier, can also be clarified by similar spectrum considerations. True samples of a signal may be regarded as pulses which are so short in duration that the signal is substantially constant during the duration of one pulse. The height of each pulse is proportional to the instantaneous value of the signal. The spectrum of the amplitude-modulated train of short pulses is readily obtained by multiplying the Fourier series for the unmodulated pulses by the modulating signal, that is, the signal which is being sampled. It resembles the PDM spectrum, shown in Fig. 4, but differs from it essentially in that each harmonic of the pulse-repetition frequency, np, has only a single set of side bands, $np \pm q$, instead of the infinite set $np + mq$. As a consequence, the lowest-frequency component other than the signal frequency, q, is the first prf side band, p-q, so that the signal of frequency q or any lower frequency can be completely separated and reproduced perfectly if p-q exceeds q. This requirement is met, of course, if p, the sampling frequency, exceeds 2q, twice the highest signal frequency. Although obtained on the basis of sinusoidal steady-state analysis, the result applies also if q is the top-frequency component of a complex signal wave; this follows from the linear relationship between the modulating signal and the corresponding AM side bands. Consequently, the first-side-band spectrum, p-q, is an exact mirror image of the signal spectrum q, even if q now represents a continuous spectrum ranging from $\omega = 0$ to $\omega = q$.

Derivations and discussions of signal-noise relations have formed a large fraction of the published work on PTM, the object being to compare PTM to other transmission systems with regard to their susceptibility to random noise. Such derivations have ranged all the way from simple, somewhat superficial, but usually adequate analyses[7,8,9,10,11] to more detailed and sophisticated analyses.[12] Most of the articles have treated only the simpler and more important signal-to-noise ratio behavior above the so-called threshold, where the pulse amplitude exceeds twice the peak noise amplitude at the receiver input. Below threshold, the noise-reducing properties of the

system are no longer utilized, and the relations are more complicated. In order to clarify the presentation of the principles involved, and to pave the way for the interference analysis in the next chapter, the all-important technique of double-limiting or slicing will be described. Since the desired information is contained solely in the relative timing of the pulse edges, all amplitude variations of less than one-half pulse amplitude during or between pulses, can be eliminated at the receiver by accepting only a thin horizontal slice of each pulse, at about half the pulse height and only a few per cent of this height in thickness. The importance of performing this slicing process effectively and correctly is greater than one might infer from some published accounts of theory and practice; this is especially true in the various cases of nonrandom interference treated in this paper. The slicing process does more than merely eliminate amplitude variations. It also establishes the time of occurrence of a pulse edge - namely as that time at which the edge crosses the slicing level, the thickness of the slice being assumed negligible. After the slicer, which usually follows the i-f stages and detector and precedes, or in part comprises, the video stages, there is no such strict bandwidth limitation as in the transmission medium. The slices are therefore amplified to form pulses which may be assumed perfectly rectangular for all analysis purposes. The slicing and video amplification processes can actually be carried out concurrently, and it is a simple matter to make the slicing level adjustable over a wide range.* Adjustability of the slicing level is desirable not only in equipment designed for interference experiments, in which the slicing level is an important variable, but also in practical receivers operating under conditions where there is any chance of interference of any type.

The mechanism which controls signal-noise relations in PTM systems operating above threshold is based on time shifts of the pulse edges. Noise can reach the output only by shifting a pulse edge from its correct position. The noise voltage admitted, for random thermal or tube noise, is directly proportional to the square root of the bandwidth, but the amount by which a given disturbance shifts the pulse edge is also directly proportional to the rise or decay time of the pulse edge and hence inversely proportional to the

---

* Equipment designs are shown and discussed in Appendix V

bandwidth. Consequently the noise voltage reaching the output is inversely proportional to the square root of the bandwidth, so that PTM, like FM, exhibits a wideband gain.* In the case of PDM, no additional first-order factors enter, so that the signal-to-noise ratio improvement or wideband gain expressed as a voltage ratio is proportional to the square root of the bandwidth. On the other hand, in the case of PPM, widening the system bandwidth brings in another factor, in that it permits a proportionate reduction in the pulse duration and hence in the duty factor, since the pulses are of constant duration and therefore need consist essentially only of a rise and decay. As a result of the lower duty factor, the peak transmitted power can be raised in direct proportion for the same average power, which effectively increases the signal voltage in proportion to the square root of the bandwidth, thereby making the signal-to-noise ratio improvement directly proportional to the system bandwidth. Furthermore, since this signal increase with increasing bandwidth just matches the noise increase at the receiver input, PPM maintains its threshold independent of the bandwidth, unlike systems such as FM or PDM, in which the input carrier remains constant and is eventually swamped by the noise if the bandwidth is raised sufficiently. (The latter occurs despite the fact that the output signal-to-noise ratio improves, if the input carrier is above threshold.)

Variables other than system bandwidth will of course, also enter the signal-noise relations and, in addition to the dependence on the different variables, the constant factors of proportionality can readily be found to give complete signal-to-noise ratio formulas such as have been derived in various papers. Of principal interest and importance, however, is the dependence of signal-noise relations on system bandwidth.

The literature has not contained any material, either theoretical or experimental, dealing with the susceptibility to interference of pulse-time modulation systems, where the interference is not random noise but originates from another transmitter, or even from the same transmitter by so-called multipath transmission. On the other hand, the interference characteristics

---

* Wideband gain is a term generally used to designate the signal-to-noise ratio improvement possible in certain modulation systems with increasing bandwidth. It may be interpreted as the ratio of the actual output signal-to-noise ratio to that which would be obtained in a conventional AM system operating under identical conditions, except for system bandwidth.

of AM and FM have received a great deal of attention in the past. They are well known in the case of AM, where multipath interference causes fading and distortion often observed in overseas shortwave reception, and interference between separate transmitters results in the superposition of their modulating signals as well as annoying beat notes. In the case of FM, interference characteristics, notably those associated with multipath transmission* are still being studied, but the so-called capture effect observed when two transmissions interfere is a widely-publicized phenomenon.

While the interference characteristics of pulse-time modulation have not been treated in the literature, suggestions that the subject needs consideration have appeared as well as conjectures as to the severity of the disturbances resulting from certain interference conditions.[13,14,15,16,17] A mathematical paper[18], entitled "Pulse Distortion: The Probability Distribution of Distortion Magnitudes due to Interchannel Interference in Multi-Channel Pulse Transmission Systems", treats a related problem but has little bearing on the interference characteristics of pulse-time modulation.

* Quarterly Progress Reports, 1946-1949, Research Laboratory of Electronics, Massachusetts Institute of Technology.

CHAPTER 2

EFFECTS OF INTERFERENCE IN PULSE-TIME MODULATION SYSTEMS

The term "interference" is intended to apply to signals other than the desired signal which enter the receiver and reach the detector because they have the same or nearly the same carrier frequency as the desired signal. Two general types of interference are considered in this paper: two-station interference and two-path interference. (The desired signal always consists of time-modulated pulses, either PDM or PPM.) The interfering signal may be a similar transmission, or possibly one using a different type of modulation, if any, in the case of two-station interference; on the other hand, it must be identical to the desired signal in the case of multipath interference, where only a single source is involved. Multipath interference is a phenomenon commonly encountered as a result of reflections from the ionosphere in the 2 to 30 Mc range and at higher frequencies from buildings.

Interference can reach the output of a pulse-time modulation receiver in the three ways illustrated in Fig. 5, if the previously described slicing process is used. The top picture represents one of the desired pulses as it would appear after detection and before slicing. with three shorter interfering pulses in different positions. The resulting slicer output is shown at the bottom; the effect of the interference on this slicer output must be considered in order to determine how the interference will manifest itself in the final output. A long desired pulse and shorter interfering pulses are shown merely for convenience in illustrating the various possibilities. The height of the desired pulse is taken to be unity, the height of the interfering pulses is designated by the letter "a", and the slicing level by the letter "s". Since the desired-pulse height is unity, "a" is also the ratio of the amplitude of the two signals, or, in short, the interference ratio. This ratio can vary only between zero and one, inasmuch as the smaller signal will always be considered as interference.* The slicing level "s" is actually that level expressed as a fraction of the desired-pulse height and is usually between zero and one.

---

* It is not, in general, possible to receive the weaker of two interfering signals, unless some particular difference in their characteristics makes their partial or total separation possible.

The first and simplest possibility illustrated in Fig. 5 is that of an interfering pulse occurring during the interval between two desired pulses. If $a < s$, it will not pierce the slicing level and will therefore have no effect; if $a > s$, a spurious pulse is produced in the slicer output, which may be gated out, under certain conditions, by virtue of its relative time of occurrence. More important, however, it is always possible to prevent the interfering pulse from piercing the slicing level and having any effect so long as the interference ratio is below one, by raising $\underline{s}$ just above $\underline{a}$, that is, by satisfying the condition $s > a$.*

The second possibility shown in Fig. 5 is that of an interfering pulse occurring during a desired pulse. The magnitude of the resultant depends on the radio-frequency phase difference between the two pulse carriers. If this is near 180°, partial cancellation will occur, and the resultant may, therefore, go below the slicing level, causing a portion of the desired pulse to be missing in the slicer output. In fact, if the interfering pulse is long enough to overlap the entire desired pulse, it may never reach the slicing level, and the entire pulse will be missing from the output, just as though it had never been transmitted. The possibility of thus having all or part of a desired pulse fail to reach the output can be eliminated by lowering the slicing level far enough to satisfy the relation $s < 1-a$.

It is to be noted that the two conditions $s > a$ and $s < 1-a$ are conflicting requirements when $\underline{a}$ is between one-half and one, but either one or the other can always be satisfied, and both can be satisfied simultaneously if the interference ratio is less than one-half ($a < \frac{1}{2}$) by setting the slicing level at one-half ($s = \frac{1}{2}$). This means that the two interference effects discussed so far can be avoided entirely with interference ratios less than one-half, and either one or the other can always be avoided. The second possibility, which may be descriptively called the missing-pulses effect, turns out to be the more important of the two and will be discussed in greater detail later in this chapter.

The third possibility illustrated in Fig. 5 is one which must be reckoned with for any interference ratio. If interference is present during the build-up or decay of the desired pulse, it will, in general, alter the time at which the slicing level is pierced. Consequently, the rectangular

---

* Underlining of symbols such as $\underline{a}$ and $\underline{s}$ is merely intended to make them stand out.

pulse at the slicer output may have one or both of its edges shifted from their correct positions. Such undesired time shifts naturally constitute errors, since the desired information is also conveyed by pulse-edge time shifts.

It is entirely possible for all three of the interference effects discussed to appear simultaneously, and two will invariably occur when the interference ratio exceeds one-half. These phenomena form the basis for a large part of the work presented in this paper, and they will therefore be discussed in detail in the remainder of this chapter. The time-shift effect is perhaps of somewhat greater fundamental importance than the missing-pulses effect and will therefore be treated first.

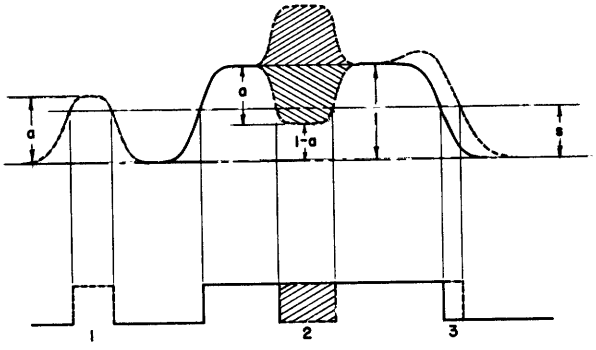

Fig.5 Three ways in which interference may enter PTM systems.

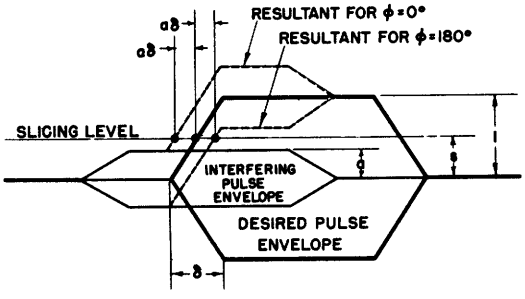

Fig.6 Pulse-edge time shift caused by interference.

2.1 The Time-Shift Effect

Because relative timing variations are the basis of pulse-time modulation, the analysis of the time-shift effect in PTM is analogous to an analysis of the rate of phase shift in FM or the change in the envelope in AM caused by interference. The ultimate aim of such an analysis is, of course, a theoretical prediction of the effect of the interference on the audio output. The purpose of the analysis which follows is to relate the time-shift to the various parameters involved, in order to set the stage for the subsequent evaluation of its effect in the next chapter. The following variables have to

be considered:

The shape of the pulse edges;
The rise and decay times of the pulse edges;
The interference ratio, a;
The slicing level, s;
The radio-frequency phase difference, ϕ.

In order to solve the problem, a definite pulse-edge shape should be assumed, which then makes it possible to write a relation between the time shift Δt and the above-listed parameters. The simplest shape mathematically, and one which gives sufficiently accurate results under many conditions, is a purely linear rise and decay. Under certain other conditions, it is necessary to assume pulses with edges formed by simple exponentials and pulses of Gaussian shape, rather than the trapezoidal pulses with linear edges.

A pictorial explanation of the time-shift phenomenon is shown in Fig. 6 for the case of linear pulse edges, which will be considered first. The heavy lines outline the envelope of the desired pulse, and the envelope of an interfering pulse is shown overlapping the leading edge of the desired pulse. Normally, in the absence of interference, this leading edge would pierce the slicing level at the point indicated by the middle one of the three small circles. The two broken lines indicate the resultant of the two pulses for two extreme values of the radio-frequency phase difference, ϕ, namely 0° and 180°. If $\phi = 0°$, the leading edge is effectively advanced by an amount $\Delta t_{max} = a\delta$, that is, the product of interference ratio and rise time, for any value of slicing level between a and 1-a. For $\phi = 180°$, the edge is delayed by the same amount. For intermediate values of the phase difference, ϕ, there are time shifts which fall between these two extremes; an expression relating them to ϕ and the other variables will now be derived.

If the time origin is chosen at the starting point of the desired pulse, the leading edge of the actual r-f pulse may be described by (1).

$$f_1(t) = \frac{t}{\delta} \cos(\omega t + \alpha). \qquad 0 < t < \delta \tag{1}$$

The interference, which is constant in amplitude during the time interval of interest is given by (2).

$$f_2(t) = a \cos(\omega t + \beta). \qquad 0 < t < \delta \tag{2}$$

In these two expressions, α and β are the phase angles of the two r-f pulses, and the r-f phase difference is given by $\phi = \beta - \alpha$. Since detection occurs before slicing in the receiver, only the envelope of the resultant is of interest. The magnitude of this envelope is given by the resultant of the two vectors representing $f_1(t)$ and $f_2(t)$ in the vector diagram of Fig. 7.

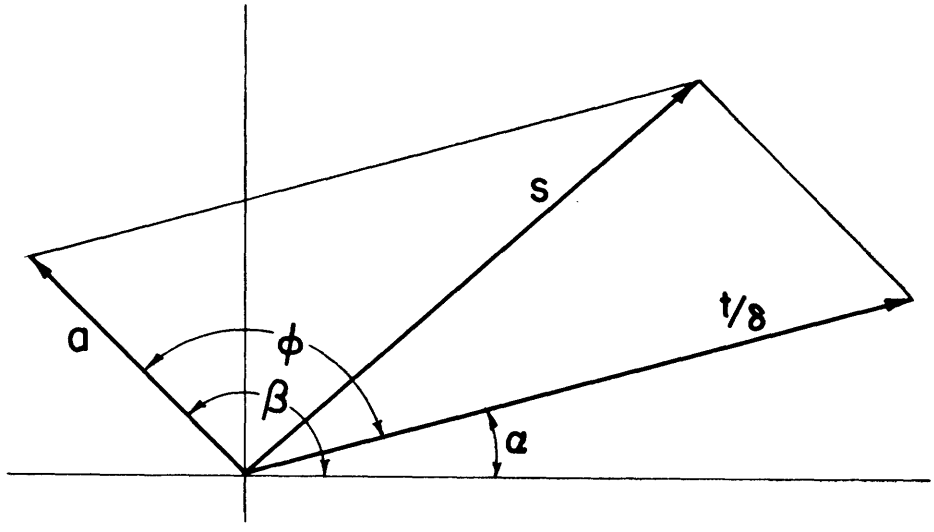

Fig.7 Vector diagram for determining the time shift of linear pulse edges

The present problem is to find the instant of time at which the resultant passes the value s of the slicing level. It is therefore only necessary to equate the resultant to s and solve the equation thus obtained for t. The magnitude of the resultant of two vectors of magnitudes b and c, respectively, with included angle ϕ is given by $\sqrt{b^2 + c^2 + 2bc \cos \phi}$. Applying this to the parallelogram of Fig. 7, and equating the resultant to s, one obtains (3).

$$\sqrt{\left(\frac{t}{\delta}\right)^2 + (a)^2 + 2(a)\left(\frac{t}{\delta}\right)\cos \phi} = s . \qquad 0 < t < \delta \tag{3}$$

This can be written in the standard quadratic equation form as follows:

$$\left(\frac{t}{\delta}\right)^2 + 2a\cos\phi\left(\frac{t}{\delta}\right) + (a^2 - s^2) = 0 \,. \qquad (4)$$

Solving for (t/δ) by means of the quadratic formula and retaining only the solution which gives a positive value for t, denoted by t_1, one obtains

$$t_1 = \delta(-a\cos\phi + \sqrt{s^2 - a^2\sin^2\phi}\,). \qquad a < s < 1-a \qquad (5)$$

The value of t_1 represents the time at which the pulse edge pierces the slicing level and at which the new edge is therefore formed at the slicer output. In the absence of any interference, this time, denoted by $t_\bullet$ is given by

$$t_\bullet = \delta s \,. \qquad (6)$$

The quantity of interest is the time shift of the pulse edge from its normal position, and this is found by subtracting (5) from (6), which gives

$$\Delta t = t_\bullet - t_1 = \delta(s + a\cos\phi - \sqrt{s^2 - a^2\sin^2\phi}\,). \qquad a < s < 1-a \qquad (7)$$

This can be written in normalized form as follows:

$$\frac{\Delta t}{s\delta} = 1 + \frac{a}{s}\cos\phi - \sqrt{1 - \left(\frac{a}{s}\right)^2\sin^2\phi}\,. \qquad a < s < 1-a \qquad (8)$$

A plot of this normalized time shift as a function of the phase difference ϕ for various values of a/s will be found in Fig. 8. The function approaches a cosine wave as the value of a/s approaches zero and, as a/s approaches 1, the function becomes a half-wave rectified sinusoid. Except in the limit $(a/s) \to 0$, Δt is seen to have positive values over a larger range of values of ϕ, and the magnitude of the average of the positive values exceeds that of the average of the negative values. In short, advances of the leading edge are favored over delays. In the case of trailing pulse edges, the time shift relations are exactly the same, except that the algebraic sign of Δt is reversed, so that advances and delays of the leading edges correspond to delays

and advances, respectively, of the trailing edges. Therefore the trailing edge of a pulse is delayed over a larger range of values of ϕ than the range over which it is advanced.

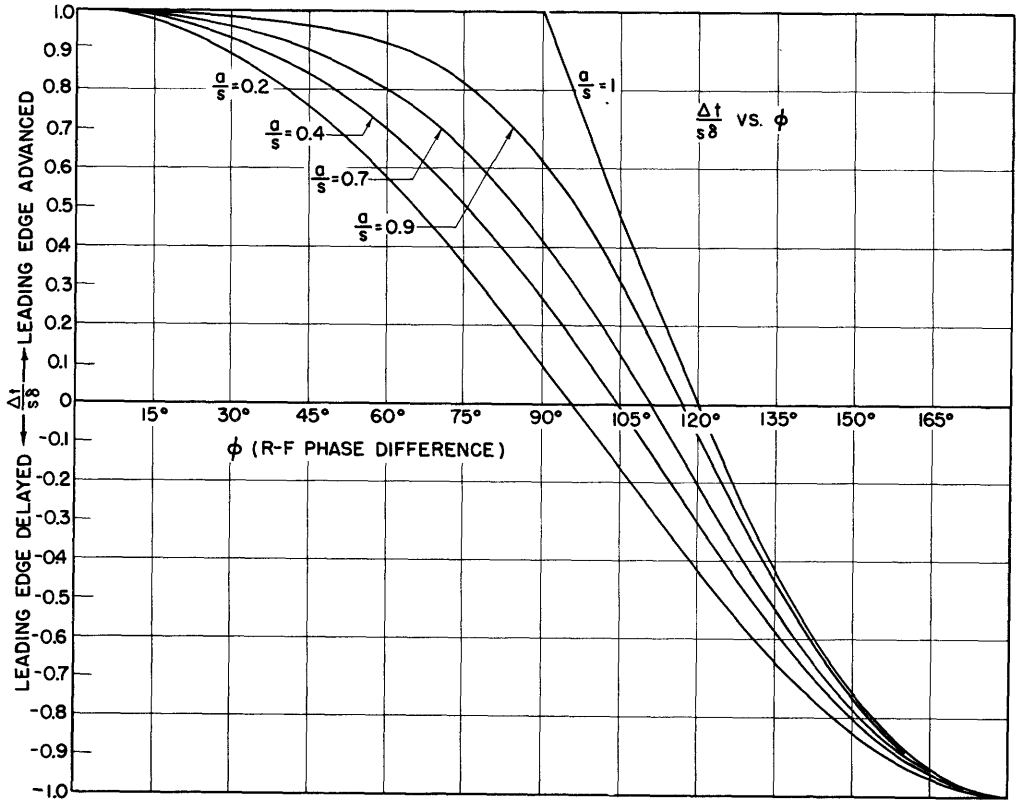

Fig.8 Normalized time shift $\Delta t/s\delta$ vs. r-f phase difference ϕ for several values of a/s (linear pulse edges); s = slicing level, a = interference ratio.

The value of s is generally fixed in a given system; s is constant or possibly controlled by a, while a is either constant or varying at a rate which is low compared to the pulse-repetition frequency. On the other hand, the value of ϕ is generally variable from pulse to pulse, and the variations are random in the great majority of cases. Consider, for a moment, what governs the successive values of ϕ under various conditions of interference: a number of factors must enter such considerations, but the crux of the matter is whether or not either or both of the two r-f signals are coherent within themselves. A continuous sinusoid which has no frequency variations is called coherent, inasmuch as its phase at any instant of time can be predicted relative to the phase at a different time. When the same sinusoid is frequency-modulated by speech or music, this is no longer true, since the modulation is random or statistical in nature. The function is then incoherent with itself, or, stated in another way, its auto-correlation - a

concept which will be introduced in the next chapter - approaches zero for large values of the time difference between the two sets of values being correlated. A pulsed carrier such as is generally transmitted by a PTM transmitter is not coherent from pulse to pulse when even the least amount of time modulation is imposed on the pulses, and not even truly coherent in the total absence of modulation unless very special relations exist between the radio frequency and the pulse-repetition frequency. This is true because the pulses generally used are generated by keying an oscillator, so that the r-f builds up in the same manner on successive pulses. Consequently, a small departure from periodicity of the leading pulse edges, such as is generally effected in most types of PTM, eliminates the coherence that might exist as a result of the integral relationship between radio frequency and pulse-repetition frequency. It is possible, however, to generate and transmit r-f pulses which are perfectly coherent with each other regardless of their time modulation. This can be done, for example, by gating the oscillator output, allowing the oscillator to operate continuously rather than keying it. The resulting r-f pulses are portions of a perfect sinusoid, and they are therefore coherent among themselves, no matter what their distribution in time may be. Needless to say, each individual r-f pulse is generally coherent within itself.

What is the effect of all this on the values of the r-f phase difference ϕ? Briefly, the answer is that incoherence on the part of either or both signals will cause random variations in ϕ, while coherence on the part of both signals will cause systematic changes, if any, in the value of ϕ from pulse to pulse, as will be explained below.

First consider the more important case in which at least the desired signal consists of r-f pulses which are incoherent with each other. Each time that interference overlaps a desired pulse, or part of it, ϕ has a different random value, quite independent of previous values. The overlap may extend over the entire pulse (as it always must if the interference is a continuous wave), so that the values of ϕ governing the respective shifts of the leading and trailing edges of that pulse are identical or at least simply related. For example, they will be the same if the radio frequencies are identical, or 180° different if the radio frequencies differ by half the reciprocal of the pulse duration. The result is that pulse-edge time shifts occurring on different pulses are uncorrelated, while shifts experienced by

the two edges of the same pulse may or may not be correlated depending on the exact circumstances. The latter is of less importance than the randomness of the time shifts from pulse to pulse.

Next consider the case in which both r-f signals are coherent within themselves. The resulting behavior of successive values of ϕ and hence of the successive time shifts depends chiefly on the radio-frequency difference. In the case of two-path interference, with the time-delay difference between the two paths constant, the two r-f waves are synchronous if the radio frequency is sufficiently stable. The same will be true, even if the r-f pulses are incoherent with each other, if the delay difference is smaller than the pulse duration, so that the interfering pulse is really the same pulse as the desired pulse with which it is overlapping. The condition of synchronism which exists in these cases causes the phase difference ϕ to be the same on successive pulse overlaps, the value of ϕ being determined by the delay difference and the radio frequency. The result is that all the pulse-edge time shifts will be alike, provided, of course, that $\underline{\delta}$, $\underline{a}$, and $\underline{s}$ remain constant. If the two interfering coherent signals originate from separate sources, their radio frequencies are not generally identical, so that successive values of ϕ are different but follow a systematic pattern of variation. These values are merely samples of the phase difference which is continuously changing linearly (corresponding to a constant frequency difference). As a result, the pulse-edge time shifts vary from edge to edge in a predictable fashion. When the desired pulse edges are time-modulated, particularly if the radio-frequency difference is several times as large as the pulse repetition frequency of the desired signal, the presence of modulation tends to impart a somewhat random character on the sequence of ϕ and Δt values. Similarly, the duty factor of the interference affects the sequence of ϕ and Δt values, a small duty factor making it appear more random, since pulse overlaps occur less frequently.

As previously indicated, a pulsed carrier generally does not have any coherence between its successive pulses, so that the case of the totally random sequence of ϕ values is of greater practical significance than the possibilities discussed in the preceding paragraph. Therefore, unless otherwise stated, the phase-difference values will be assumed to be random, with each value having an equal probability of being anywhere between zero and 360°. This means that the pulse-edge time shifts are also random, as previously discussed, but their extreme values and their probability distribution between

these extremes are subject to the relation expressed in (7) on page 16, and plotted in normalized form in Fig. 8. Physically, this means that the values of the time shifts Δt have the same statistical characteristics as the ordinates corresponding to a series of arbitrarily chosen abscissas on one of the curves of Δt vs. ϕ. The distribution of the resulting ordinates is the same as the amplitude distribution of the curve which was randomly sampled. The amplitude distribution of a continuous periodic function is simply a quantity which expresses the relative amounts of time it spends at various values; it is therefore proportional to the average of the reciprocal slope magnitudes at any ordinate value. In the case of simple periodic functions such as $\frac{\Delta t}{s\delta}(\phi)$, where there is only one slope magnitude at any ordinate value, the amplitude distribution at any ordinate equals the reciprocal of the slope magnitude at that ordinate. In mathematical language, if the simple periodic function is $x(\phi)$, and its amplitude distribution is denoted by $A(x)$, then

$$A(x) = \frac{k}{\left|dx/d\phi\right|} \quad . \tag{9}$$

The probability distribution of the random samples of $x(\phi)$, that is, the probability distribution of the time shifts if $x(\phi) = \Delta t(\phi)$, is equal to $A(x)$ with k so chosen as to make the area under the curve of $A(x)$ vs. x equal to unity. The quantity $P(x)dx$ equals the probability of any one of the values of x being between x and $x + dx$, and if the extreme possible values are $-x_o$ and $+x_o$, the integral $\int_{-x_o}^{x_o} P(x)dx$ includes all possible values of x and is therefore equal to unity.

For small values of a/s, $\frac{\Delta t}{s\delta}(\phi)$ as given by (8) can be approximated by $\frac{\Delta t}{s\delta}(\phi) = \frac{a}{s}\cos\phi$, or $\frac{\Delta t}{a\delta} = \cos\phi$, provided that $a < s < 1-a$. The maximum magnitude of the time shift Δt will be denoted by x_o, so that the following approximate relation gives the time shift for small values of a/s.

$$\Delta t(\phi) = x_o \cos\phi \quad . \tag{10}$$

In order to find the probability distribution of the pulse-edge time shifts for small values of a/s, ($\frac{a}{s} < 0.2$), such as will be encountered with interference ratios in the order of one-tenth or less, (or with reduced accuracy for higher ratios as well), it is merely necessary to evaluate the amplitude

distribution A(x) of (10). Application of (9) yields

$$A(x) = \frac{k}{x_o \sin \phi} = \frac{k}{\sqrt{x_o^2 - x^2}} \cdot (-x_o < x < x_o) \cdot \qquad (11)$$

The probability function P(x) is obtained by evaluating k as follows:

$$\int_{-\infty}^{\infty} P(x)\,dx = \int_{-x_o}^{x_o} P(x)\,dx = \int_{-x_o}^{x_o} \frac{k\,dx}{\sqrt{x_o^2 - x^2}} = 1 \; ;$$

$$\int_{-x_o}^{x_o} \frac{k\,dx}{\sqrt{x_o^2 - x^2}} = k \sin^{-1}\left(\frac{x}{x_o}\right)\Big]_{-x_o}^{x_o} = \pi k = 1 \; ;$$

$$\therefore \quad k = \frac{1}{\pi} \cdot$$

Substitution of this value for k in (11) gives

$$P(x) = \frac{1/\pi}{\sqrt{x_o^2 - x^2}} \cdot (-x_o < x < x_o) \cdot \qquad (12)$$

The plot in Fig. 9 is more descriptive than the algebraic expression, showing how the values of x crowd at the two extremes, where the cosine wave "spends most of its time". The probability distribution of the pulse-edge time shifts will be utilized in the next chapter in the determination of the output noise resulting from the time shifts.

The calculation of P(x) for the exact expression given by (8) is more involved and leads to a more complicated result. It is of interest to find P(x) for the limiting case, $(\frac{a}{s}) = 1$, for which $\Delta t(\phi)$ assumes the shape of a half-wave rectified sinusoid. Substitution of $(\frac{a}{s}) = 1$ in (8) yields

$$\frac{\Delta t}{s\delta}(\phi) = \frac{\Delta t}{a\delta}(\phi) = 1 + \cos \phi - \left[\cos \phi\right]. \qquad (0 < a = s < \tfrac{1}{2}) \qquad (13)$$

Maintaining the notation $a\delta = x_o$ and using x to denote the variable Δt, one obtains the function $x(\phi) = x_o(1 + \cos \phi - [\cos \phi])$, the amplitude distribution of which is to be determined. Physical reasoning provides the simplest way of obtaining this amplitude distribution of this function, since it has much in common with (10). Its value during exactly half of the period is $+x_o$, while during the remaining half it traces out the negative half of the cosine wave exactly as (10), except multiplied by a factor of two and moved upwards by an amount x_o. For this half of the function, therefore, the amplitude distribution curve has the appearance of the left half of the curve in Fig. 9, but stretched out over the entire range from $-x_o$ to $+x_o$. In order to obtain the corresponding probability distribution, k must be evaluated so as to make the area under the curve equal to one-half. The other half probability is all concentrated at $x = x_o$ and is representable by a "slot" of infinite height, infinitesimal width, and area equal to one-half. Because of this singularity, the resulting probability distribution is most easily expressed in integral form as follows:

$$\int_{-\infty}^{\infty} P(x)\,dx = \int_{-x_o}^{x_o} P(x)\,dx = \int_{-x_o}^{x_o} \frac{(1/\pi)\,dx}{\sqrt{(2x_o)^2 - (x - x_o)^2}} + \tfrac{1}{2}[]_{\text{at } x = x_o} \qquad (14)$$

The same is shown graphically in Fig. 10.

The probability distribution curves of Fig. 7 and Fig. 8 can be superimposed on the picture of a typical pulse at the slicer output and thus show physically how likely the edges are to be found in any position. This is shown in Fig. 11, in which it must be remembered that positive values of time shift Δt or x correspond to advances (shifts to the left) for the leading edge and to delays (shifts to the right) for the trailing edge.

Although the quantitative apects of the preceding analysis were based on the idealized linear pulse edges, they are nevertheless applicable in many PDM cases (particularly for small interference ratios), since the actual pulse edges are nearly linear over portions of their total extent. However, for interference ratios close to one-half, it is desirable, in the case of pulse-duration modulation, to base all computations on transmitted pulses with simple exponential edges. The relation between pulse-edge time shifts and the other parameters will therefore next be derived for exponential pulse edges

which are shown in the pictorial explanation of time shifts in Fig. 12 (similar to that shown in Fig. 6 for linear edges). It can be seen that, unlike the linear case, the exponential case exhibits asymmetry between the leading and trailing edges, so that separate expressions have to be obtained for each of the two edges. Their envelopes for unity amplitude are given by $1 - \epsilon^{-t/\lambda}$ and $\epsilon^{-t/\lambda}$, with the time origins chosen independently to coincide with the beginning of the edge, and with λ the time constant of the exponential. The normalized time parameter t/λ will be denoted by h_ℓ for the leading edge and h_t for the trailing edge. The development of Eqs. (1) through (8) will now be repeated for these exponential pulse edges, with the various steps being carried out concurrently for the leading edge and the trailing edges.

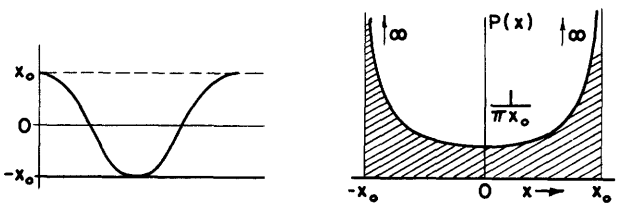

Fig.9 Amplitude-probability distribution of sinusoid.

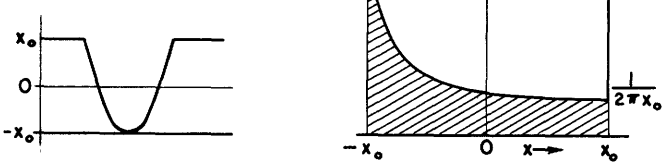

Fig.10 Amplitude-probability distribution of a half-wave-rectified sinusoid.

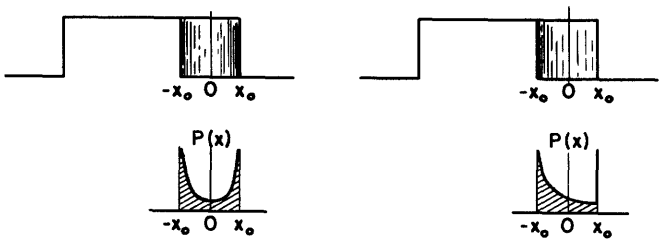

Fig.11 Pulse-edge time-shift probability distributions.

The edges of the desired r-f pulse may be described by (15).

$$f_{1\ell}(t) = (1 - \epsilon^{-h_\ell})\cos(\omega t + \alpha), \qquad f_{1t}(t) = (\epsilon^{-h_t})\cos(\omega t + \alpha). \qquad (15)$$

$$h_\ell,\ h_t > 0$$

The interference, as before, is given, over the time interval of interest, by

$$f_2(t) = a\cos(\omega t + \beta). \tag{2}$$

In order to find the time at which the resultants of $f_{1\ell}$ and f_2 as well as of f_{1t} and f_2 pass through the slicing level $\underline{s}$, exactly the same vector diagram as in Fig. 7 is applied, except with the vector magnitude t/δ replaced by $(1 - \epsilon^{-h_\ell})$ and (ϵ^{-h_t}) respectively. Forming the expression for the resultant and equating it to $\underline{s}$ for each edge, and squaring both sides, one obtains

$$(1 - \epsilon^{-h_\ell})^2 + a^2 + 2a(1 - \epsilon^{-h_\ell})\cos\phi = s^2 . \qquad a < s < 1-a$$

$$(\epsilon^{-h_t})^2 + a^2 + 2a(\epsilon^{-h_t})\cos\phi = s^2 . \tag{16}$$

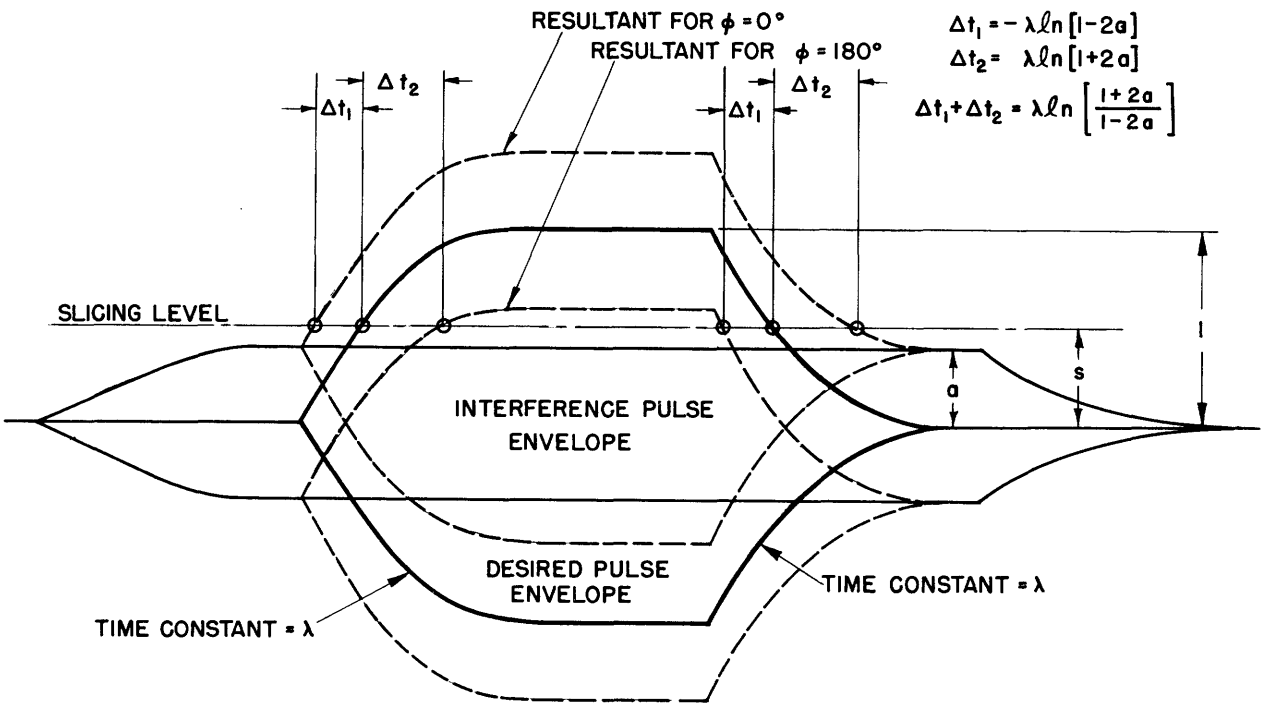

Fig.12 Pulse-edge time shifts caused by interference.

These are quadratic equations in $(1 - \epsilon^{-h_\ell})$ and (ϵ^{-h_t}), respectively, and

the solutions are given by (17).

$$(1 - \epsilon^{-h_\ell}) = -a\cos\phi \pm \sqrt{s^2 - a^2\sin^2\phi} \quad .$$

$$(\epsilon^{-h_t}) = -a\cos\phi \pm \sqrt{s^2 - a^2\sin^2\phi} \quad . \tag{17}$$

Only the positive sign in front of the radical corresponds to a physical solution. Solving for the values of normalized time, relative to the starting time of the pulse edge, and, as in (5), adding the subscript 1 to show that these values represent specific solutions, one obtains

$$h_{\ell 1} = -\ell n(1 + a\cos\phi - \sqrt{s^2 - s^2\sin^2\phi}) \; ;$$

$$a < s < 1-a$$

$$h_{t1} = -\ell n(-a\cos\phi + \sqrt{s^2 - a^2\sin^2\phi}) \; . \tag{18}$$

The corresponding solutions in the absence of interference are

$$h_{\ell_o} = -\ell n(1-s), \qquad h_{t_o} = -\ell n(s), \qquad a < s < 1-a \tag{19}$$

and the time shifts of the pulse edges are found by taking the difference of (18) and (19) as follows.

$$\Delta h_\ell = h_{\ell_o} - h_{\ell 1} = \frac{\Delta t_\ell}{\lambda} = \ell n(1 + a\cos\phi - \sqrt{s^2 - s^2\sin^2\phi}) - \ell n(1-s); \tag{20A}$$

$$\Delta h_t = h_{t_o} - h_{t1} = \frac{\Delta t_t}{\lambda} = \ell n(s) - \ell n(-a\cos\phi + \sqrt{s^2 - a^2\sin^2\phi}). \tag{20B}$$

$$a < s < 1-a$$

This result corresponds to (8) for the case of linear pulse edges, and the entire discussion about random and nonrandom time shifts applies equally here. The relationship between the normalized time shifts Δh and the phase difference ϕ is plotted in Fig. 13 and Fig. 14 for two different values of interference ratio a for a slicing level $s = \frac{1}{2}$. which will be shown to be

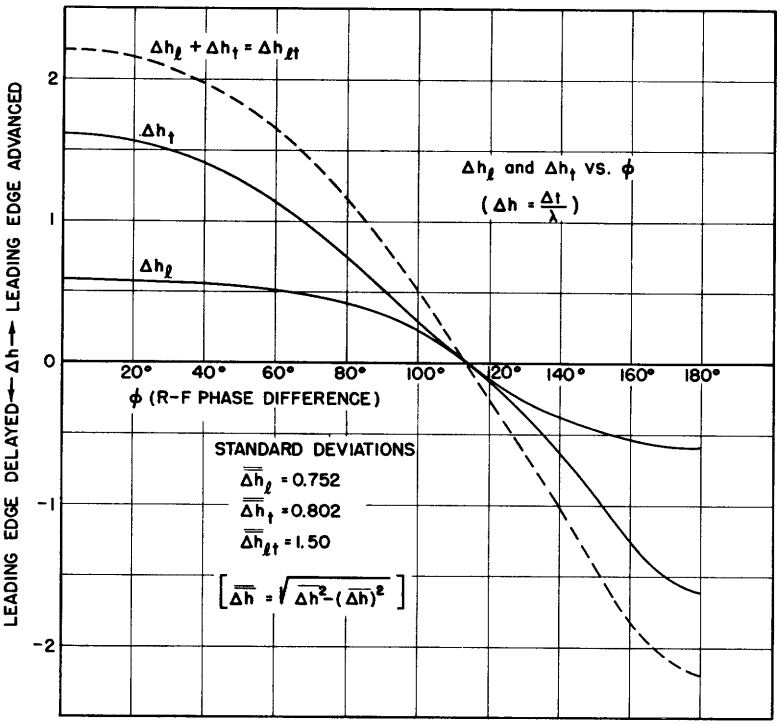

Fig.13 Normalized time shifts Δh_ℓ and Δh_t ($\Delta h = \Delta t/\lambda$) versus r-f phase difference ϕ for a = 0.4, s = 0.5 (exponential pulse edges); λ = time constant, s = slicing level, and a = interference ratio.

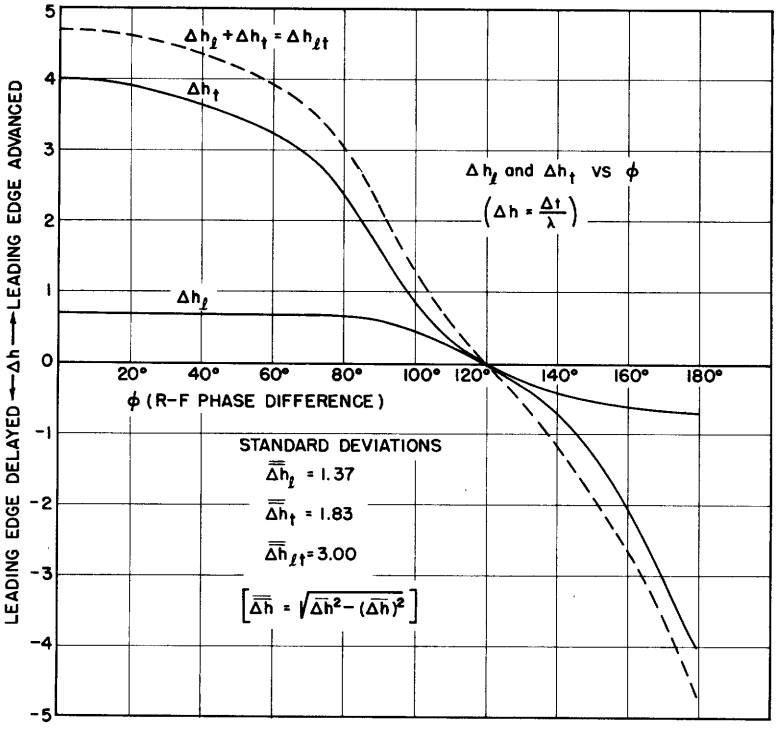

Fig.14 Normalized time shifts Δh_ℓ and Δh_t ($\Delta h = \Delta t/\lambda$) versus r-f phase difference ϕ for a = 0.49, s = 0.50 (exponential pulse edges); λ = time constant, s = slicing level, a = interference ratio.

optimum in general for $\underline{a} < \frac{1}{2}$. Since Δh_ℓ is different from Δh_t, a measure of their combined effect on the duration of the pulse is desirable. Inasmuch as Δh_ℓ is a measure of the advance of the leading edge and Δh_t of the delay of the trailing edge, a suitable index is given by $\Delta h_{\ell t} = \Delta h_\ell + \Delta h_t$, and this has also been included on the plots. It is readily seen that the curves $\Delta h_{\ell t}$ have the same principal characteristics of asymmetry as do the corresponding curves for large values of a/s with linear pulse edges, so that the corresponding time-shift probability distributions are not radically different. Of greater importance is the fact that the increase in peak time shift with increasing interference ratio is exponential rather than linear. For a linear pulse edge, the peak-to-peak time shift - that is, the difference between the time-shift extremes - is given by $2a\phi$, as can be verified by substituting $\phi = 0$ and 180° in (7). This is unchanged for any slicing level above $\underline{a}$ and below $\underline{1-a}$. For exponential pulse edges, with the slicing level at $\underline{s} = \frac{1}{2}$, the corresponding quantity is given by $\lambda \ell n(\frac{1+2a}{1-2a})$, $(a < \frac{1}{2})$, as can be verified from (20). This peak-to-peak time shift is the same for both edges as long as $\underline{s} = \frac{1}{2}$, because of the antisymmetry of the two edges (see Fig. 12): when $\phi = 0$, with $\underline{a}$ not much below one-half, the leading edge is advanced by a small amount, and the trailing edge delayed by a large amount: when $\phi = 180^\circ$, the leading edge is delayed by the same large amount, and the trailing edge advanced by the same small amount. When the two time shifts are added, as in Figs. 13 and 14, the asymmetry in the excursions of each pulse edge cancels out, and the peak deviations in either direction are the same. This is also shown in Fig. 12.

It has been mentioned that the optimum slicing level for $\underline{a} < \frac{1}{2}$ is generally $\underline{s} = \frac{1}{2}$, and that this is therefore usually used unless the interfering signal is "taller" than one-half the height of the desired pulses. There are three different reasons for this, which will be discussed in turn. The first and most important reason is the fact that the effective pulse-edge slope is usually greatest at $\underline{a} = \frac{1}{2}$. Regardless of the shape of the pulse edges, the time shift is given by $\Delta t = \frac{a}{\mu} \cos \phi$ (in which μ denotes the slope of the pulse edge at the slicing level, this slope being based on the unity pulse amplitude) in the limit as $\underline{a}$ approaches zero. More specifically, the above is approximately true so long as the desired pulse edge is approximately linear over the amplitude range s-a to s+a. This means that, for all values of ϕ and for a given value of $\underline{a}$, the pulse-edge time shifts are

inversely proportional to the pulse-edge slopes at the slicing level. Consequently, to minimize the time shifts caused by interference, the slicing level should be set where the magnitude of the slope of the edge concerned is a maximum. When the two edges of each pulse do not have mirror-image symmetry, and the timing of both is of equal importance in the final demodulation process (as is generally the case in PDM with the exponential pulse edges analyzed above), then the sum of the reciprocal slope magnitude of the two edges should be minimized. This can be done mathematically as follows: the two edges are given by $y = 1 - \epsilon^{-h_\ell}$ and $y = \epsilon^{-h_t}$. Their slopes are equal to their respective derivatives, which can be expressed in terms of the ordinate y as follows:

$$\text{leading-edge slope} = dy/dh_\ell = \epsilon^{-h_\ell} = 1 - y$$

$$\text{trailing-edge slope} = dy/dh_t = -\epsilon^{-h_t} = -y \; . \qquad (21)$$

The expression to be minimized is the sum of the reciprocal magnitudes $(1 - y)^{-1} + (y)^{-1}$, and the ordinate value y for which it is a minimum will be the optimum value for the slicing level s. Differentiation with respect to y leads to the equation

$$(1 - y)^{-2} - (y)^{-2} = 0 \; . \qquad (22)$$

The solution of (22) is $y = s_{opt.} = \frac{1}{2}$. The same conclusion can also be reached by minimizing the expression for the actual pulse-edge time shift, but the above method is simpler. In the case of the Gaussian pulse shape, which will be discussed shortly, the same result can be obtained even more directly, since each edge individually has its maximum slope at one-half the peak value. Linear pulse edges are not subject to this particular optimization, but the other, second and third,reasons previously mentioned still maintain the best slicing level at one-half for this case as well. The second reason is the simple fact that all the relations discussed hold only for $a < s < 1-a$, and this condition can be satisfied for interference ratios a up to one-half only if $s = \frac{1}{2}$, otherwise only up to lower values of a, namely s or 1-s, whichever is the smaller. The third reason is apparent from the plots of $\frac{\Delta t}{s\delta}(\phi)$ in Fig. 8. Although the peak-to-peak amplitude of $\Delta t(\phi)$

does not depend on $\underline{s}$, the shape of the curve, e.g., for a = 0.1, varies from the half-wave-rectified sinusoid for $\underline{s = a}$, and tends towards a cosine wave as $\underline{s}$ is raised to one-half; the mean deviation of the corresponding probability distribution consequently becomes smaller, which makes the resulting output disturbance smaller.

Referring to Fig. 12, which shows the envelope of a desired pulse with exponential edges, the constant envelope of the interfering signal, as well as the envelopes of the extreme possible resultants, one finds many of the mathematically derived time-shift characteristics almost obvious for the extreme cases of $\phi = 0°$ and 180°. The region between the broken lines representing these extreme resultants will be filled in completely if a large number of pictures with different values of ϕ are superimposed. With the actual scattered values of ϕ, every possible resultant will sooner or later be covered. An oscillogram taken at the detector output will show just this, of course, for the positive half of the envelopes only, because of the detector rectification. If the interference is intermittent, as it will be when originating from another pulse transmitter with pulse-repetition frequency different from that of the desired signal, then the oscillogram should show not only all the possible resultants but also the unimpaired desired pulse and the level of the interference. (The interfering pulse will not generally appear as such, since the CRO sweep would be in synchronism with the desired pulses only.) Such an oscillogram, taken with an interference ratio of approximately one-third is shown in Fig. 15. Note that the time-shift distribution shows up in the density of the shaded areas.

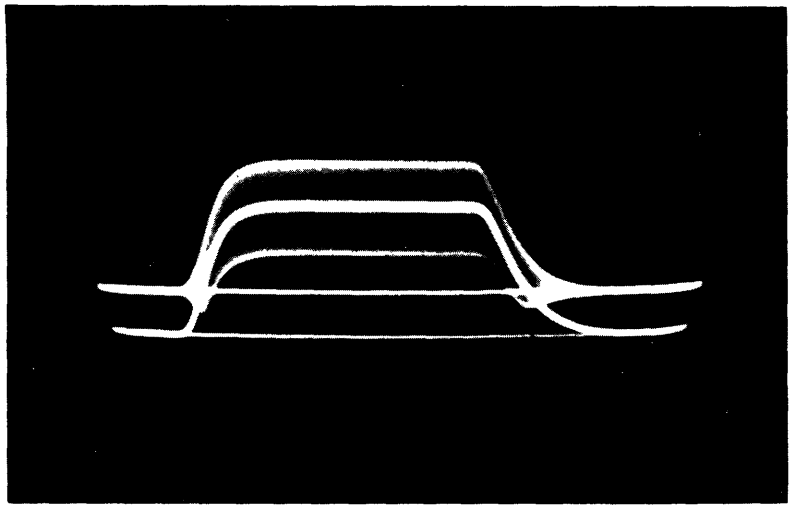

Fig.15 Oscillogram of detector output showing desired pulse and effect of interference.

Two different pulse-edge shapes have been treated with regard to their time shifts caused by interference which is substantially constant during the time of the edge. A third type will be found particularly useful for PPM, where short pulses without flat tops are used. The mathematical function used is the Gaussian error function, which describes an entire pulse from start to finish rather than only a pulse edge. The pulse is bell-shaped, which approximates very closely the optimum pulse shape when the available bandwidth is used to the best advantage achievable in practice. The Gaussian function is useful not only for describing the desired pulses if these come from a PPM transmitter, but also the interfering pulses if they are short pulses without flat tops.

The pulse envelope is given by the general expression $y = A\epsilon^{-k(\frac{t}{d})^2}$. If one evaluates k such that $\underline{d}$ denotes the pulse duration at half the pulse height, then the result is k = 2.77, and the pulse envelope of unity height is given by

$$y = \epsilon^{-2.77(\frac{t}{d})^2} . \qquad (23)$$

The time origin is at the center of the pulse, and while neither side ever actually reaches zero, negligible values are approached very rapidly.

In order to find the pulse-edge time shifts caused by interference which is substantially constant over the pulse duration, the method of the vector diagram in Fig. 7 is again used, except that the magnitude of the variable vector is equal to $\underline{y}$ of (23) instead of t/δ. The expression equating the resultant of the desired pulse and the interference to the slicing level $\underline{s}$ then becomes, after squaring both sides and letting $(\frac{t}{d}) = h$,

$$\epsilon^{-5.54h^2} + a^2 + 2a\epsilon^{-2.77h^2}\cos\phi = s^2. \qquad a < s < 1-a \qquad (24)$$

This equation is quadratic in $\epsilon^{-2.77h^2}$ and the solution is

$$h_1 = \pm\sqrt{-\frac{1}{2.77}\ln(-a\cos\phi + \sqrt{s^2 - a^2\sin^2\phi})} . \qquad (25)$$

The negative and positive solutions for h correspond, respectively, to the time instants at which the leading and trailing edges pass the slicing level $\underline{s}$. The solutions are equal and opposite because of the perfect symmetry about

the time origin. However, this symmetry exists only so long as the radio frequencies of the two interfering signals are not too far different to make ϕ change appreciably from the leading edge to the trailing edge. The solutions for h in the absence of interference are $h_o = -0.5$ and $h_o = +0.5$, for $s = \frac{1}{2}$, the pulse duration being unity in terms of the normalized time parameter h. More generally, in terms of s, these solutions are

$$h_o = \pm\sqrt{\frac{1}{2.77}\,\ell n\left(\frac{1}{s}\right)} \quad . \tag{26}$$

The normalized time shift Δh is given by $h_1 - h_o$, as follows.

$$\Delta h = h_1 - h_o = \frac{\Delta t}{d} = \sqrt{-\frac{1}{2.77}\,\ell n\left(-a\cos\phi + \sqrt{s^2 - a^2\sin^2\phi}\right)} - \sqrt{-\frac{1}{2.77}\,\ell n\, s} \quad . \tag{27}$$

$$(a < s < 1-a)$$

A plot of this function for one particular set of values of a and s is shown in Fig. 16. It is seen to have characteristics similar to those of the

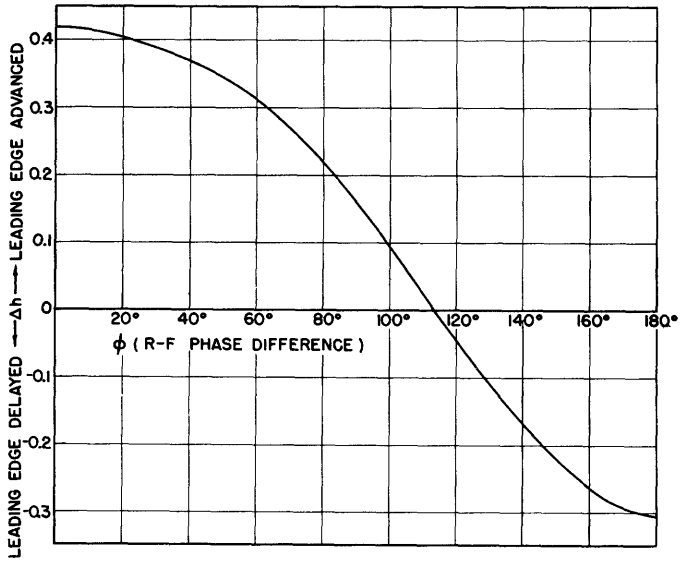

Fig. 16 Normalized time shift Δh ($=\Delta t/d$) *vs.* r-f phase difference ϕ for a = 0.40, s = 0.50 (gaussian pulse shape);
d = pulse duration measured between half-voltage points,
s = slicing level,
a = interference ratio.

previously presented plots of time shifts *versus* r-f phase difference. Positive time shifts (corresponding to increased pulse duration) are favored over negative shifts for three reasons: (1) the time shifts are positive for more than half of the 360-degree range; (2) the peak positive time shift, at $\phi = 0$, is larger than the peak negative shift, at $\phi = 180°$, and (3) the shape

is such as to help make the magnitude of the average of the positive values exceed that of the average of the negative values.

Although it is intended to present in this chapter only the more fundamental aspects of interference phenomena such as the time-shift effect, it will be of interest to widen the scope of the analysis somewhat by removing the restriction that the interference must be substantially constant in amplitude during the time interval of interest. If the interference is a continuous unmodulated or frequency-modulated carrier, then the results found are directly applicable; if it is amplitude-modulated by an audio signal, the interference ratio $\underline{a}$ varies somewhat from pulse to pulse, which can be easily taken into account. Interfering pulses such as those used in PDM have, on the average, flat tops which are no longer in duration than the combined rise and decay times. Therefore, when it comes to practical computations, as will be seen in Chapter 4, the interfering pulses can be assumed rectangular, so that a given desired pulse edge is either shifted as analyzed in the preceding treatments, or it is not shifted at all.

On the other hand, if the interference consists of minimum-duration pulses, and particularly if the desired pulses are similar, then it is preferable to treat the situation somewhat differently. The effective interference level changes as fast as the edges of the desired pulse rise and fall, and should therefore be treated on an instantaneous basis rather than on an averaging basis. This applies particularly to multipath interference in PPM and to two-station interference between PPM systems. The Gaussian pulse shape introduced on page 30 will again be used, this time not only to describe the desired pulse, but also to describe the interfering pulse. The method of determining the relation between the pulse-edge time shift and the variables involved is the same as that used before, except that all vectors in the diagram of Fig. 7 now have time-variable magnitudes, and there is an additional variable, namely the relative phasing or time difference between the two pulses.

The desired pulse will be a Gaussian pulse of half-height duration $\underline{d}$, or normalized duration unity, where the normalized time variable is $h = t/d$. It has unity amplitude and is identical with the pulse used in the previous analysis on pages 30 and 31. The interfering pulse has the same duration, but different amplitude, denoted by $\underline{a}$ and, instead of being positioned symmetrically about the origin like the other pulse, it is advanced from this position by an amount ℓ in terms of the normalized time parameter; of course,

ℓ may be negative as well as positive. The algebraic expressions for the desired and interfering pulses, respectively, are given by $f_1(h)$ and $f_2(h)$ in (28).

$$f_1(h) = \epsilon^{-2.77(h)^2} \cos(\omega t + \alpha) \ ,$$

$$f_2(h) = a\epsilon^{-2.77(h + \ell)^2} \cos(\omega t + \beta) \ , \qquad (28)$$

in which $\beta - \alpha = \phi$. The envelopes of the pulses are shown in Fig. 17.

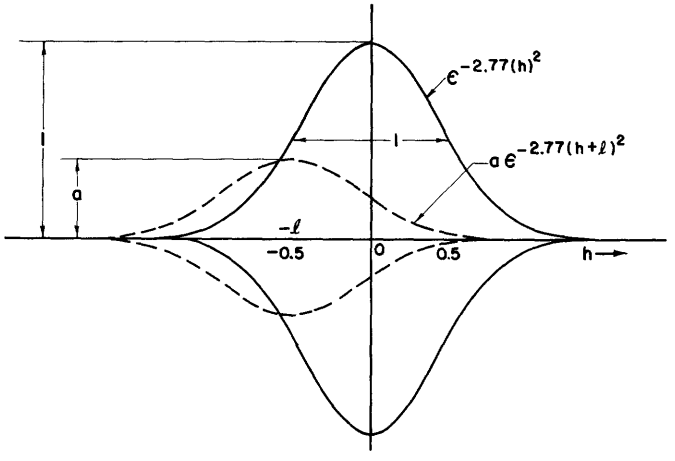

Fig.17 Envelopes of desired and interfering pulses of gaussian shape.

Recalling the vector-diagram addition of the two components (Fig. 7), applying it to $f_1(h)$ and $f_2(h)$ of (28), and equating the resultant to the slicing level, one obtains, after squaring both sides

$$\epsilon^{-5.54h^2} + a^2\epsilon^{-5.54(h + \ell)^2} + 2a\epsilon^{-2.77[h^2 + (h + \ell)^2]}\cos\phi = s^2 \ . \qquad (29)$$

$$(a < s < 1\text{-}a)$$

Except for special values of some of the parameters, this equation can not be solved analytically. Only point-by-point trial-and-error or graphical solutions are possible, and values obtained by such methods will be found tabulated and plotted in the section on PPM interference. They are not included at this point, since they would add little to the present discussion.

In connection with the mathematical results obtained in this chapter, the

following point should be made clear. The time-shift equations have been labelled so as to be subject to the restriction $a < s < 1-a$. Actually, this indicates that the expression for Δt exists for all values of ϕ only so long as s is within the specified limits. The lower limit for s is necessary regardless of ϕ, to prevent the interference from piercing the slicing level and giving completely erroneous results. If the upper limit is exceeded, there will be a range of values of ϕ, extending symmetrically about 180°, in which there will be no real solution for Δt. This means simply that the pulse edge never reaches or crosses the slicing level, since the resultant is always smaller than s, so that the pulse or part of the pulse will be missing from the slicer output. Therefore, if this is correctly interpreted, the restriction on s can be relaxed to read $s > a$.

2.2 The Missing-Pulses Effect

The missing-pulses effect is strictly a "below-threshold phenomenon"; since the interference is too large to be"eliminated" by the slicer, it reaches the output through a different mechanism than the modulating signal. The effect does not have an exact counterpart in other types of modulation. The variables on which it is dependent are the same as those listed on page 14, except that the pulse-edge shape need not be taken into account, for all but the very short pulses used in PPM.

As a starting point it will be assumed that the interference is of constant amplitude a, that it completely overlaps every desired pulse, that the radio-frequency difference between desired and interfering signals is much less than the reciprocal of the longest desired pulse, and that there is no coherence between different pulses. Such a situation may arise if a continuous constant-amplitude wave, such as an FM signal, interferes with PDM or PPM reception; the interference can also be another pulse signal with identical pulse-repetition frequency and phase; or, in the absence of modulation, it can be a replica of the desired pulse train delayed through multipath transmission by an exact integral multiple of the pulse-repetition period. The results of these assumptions are that either every desired pulse is entirely present, in which case it is generally subject to the time-shift effect, or that the whole pulse is completely missing; further, the r-f phase difference ϕ is random from pulse to pulse with all values equally likely.

Clearly, if the slicing level s is higher than $1-a$, then the resultant

of the desired and interfering signals will fall below $\underline{s}$ (namely, at $\underline{1-a}$)when $\phi = 180°$, and still, though to a lesser degree for a certain range of values on both sides of 180°. This range of values depends on $\underline{s}$ and $\underline{a}$, as will be shown. It will be denoted by 2θ. The probability that ϕ, for any one pulse, will fall within the range $180° \pm \theta$ is $\theta°/\ 180°$, or θ/π if θ is expressed in radians. This will then also be the probability that any pulse is missing. Before deriving a mathematical expression for this probability in terms of known quantities, it is desirable to state what the most important combinations of $\underline{a}$ and $\underline{s}$ are likely to be in practice, so that the emphasis can be placed correctly in the mathematical work.

When the interference ratio $\underline{a}$ is below one-half, the slicing level $\underline{s}$ is generally set at one-half, just half-way between $\underline{a}$ and $\underline{1-a}$ for reasons stated previously. In that case no pulses will be missing. A possible exception to the $s = \frac{1}{2}$ rule occurs in certain two-path interference cases, where the slicing level may be set much lower (as will be seen in Chapter 5). The possibility of missing pulses is even more remote here, since $s \ll 1-a$. As $\underline{a}$ is increased in these cases, the missing-pulses effect occurs only when $\underline{a}$ is near one, when it exceeds $1-s$, so that interest is centered on values of $\underline{s}$ near zero and $\underline{a}$ near unity. In the majority of interference situations, however, as $\underline{a}$ is increased beyond one-half, $\underline{s}$ must be increased to stay above $\underline{a}$ in order to prevent the interference from piercing the slicing level. On the other hand, raising the slicing level increases the probability of a resultant pulse not reaching it, and consequently the best compromise is $\underline{s} = \underline{a}+$, that is , the slicing level is just above the interference level. Mathematically, this most important condition will be specified as $\underline{s} = \underline{a}$, so that interest is focussed on $\frac{1}{2} < a = s < 1$.

The borderline condition under which the resultant of the two signals just equals the slicing level, with the amplitudes $\underline{1}$ and $\underline{a}$ and the r-f phase difference ϕ, is given by

$$a^2 + 1 + 2(a)\cos\phi = s^2 \ . \qquad (30)$$

The solution is as follows:

$$\cos\phi = \frac{s^2 - a^2 - 1}{2a} \ , \qquad \theta = \phi - \pi \ ,$$

$$\cos\theta = \frac{1 + a^2 - s^2}{2a} \ , \qquad \theta = \cos^{-1}\left(\frac{1 + a^2 - s^2}{2a}\right) \ . \qquad (31)$$

The result given by (31) is perfectly general, as far as the values of a and s are concerned. This is confirmed, (when s and a are such that no pulses can be missing), by the fact that there is no real solution in (31) or (32). The probability that a given pulse is missing is also equal to the fraction of pulses missing out of a very large number of pulses; it will be denoted by F and equals θ/π, as explained previously.

$$F = \frac{\theta}{\pi} = \frac{1}{\pi} \cos^{-1}\left(\frac{1 + a^2 - s^2}{2a}\right) . \qquad (32)$$

This general result can now be applied to the two different sets of combinations of a and s which are of practical importance. First, the less important case, in which a is close enough to unity (≥ 0.98) to justify the approximation $a \approx 1$, will be considered. The result is

$$F_{a=1} = \frac{1}{\pi}\cos^{-1}\left(1 - \frac{s^2}{2}\right) \approx \frac{s}{\pi} . \qquad (33)$$

The practical application of (33) will be found in the treatment of incoherent two-path PDM interference.

The more significant case is that for which s = a. Substitution of this conditions into (32) gives the simple relation (34).

$$F_{s=a} = \frac{1}{\pi} \cos^{-1}\left(\frac{1}{2a}\right) . \qquad (34)$$

This important relation is plotted in Fig. 18 for interference ratios from

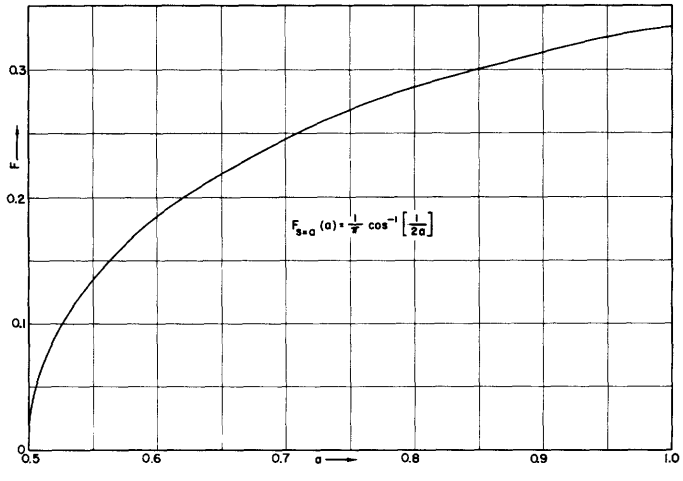

Fig.18 Fraction of missing pulses, F, versus interference ratio, a, for slicing level s = a; $F_{s=a}(a) = (1/\pi) \cos^{-1}[1/2a]$.

0.5 up to 1.0. The fraction of missing pulses reaches a maximum of one-third for $\underline{a} = 1$, which is approached rapidly as $\underline{a}$ increases above 0.5. Therefore, under the conditions stated at the beginning of this analysis, with $\underline{a}$ close to unity, one out of every three pulses will be missing at the slicer output. Since ϕ is random, each pulse, regardless of what happened to its predecessors, has the same probability, namely one-third, of not reaching the output. The effect of this on the final output will be taken up in the next chapter. The condition described here is severe in that all desired pulses are completely overlapped by interference. More generally, if the interference consists of pulses, this total overlap will be replaced by a fractional overlap, which means that, on the average, only a certain fraction, P, of the desired pulse is overlapped by interference. This part of the pulse, rather than the entire pulse, is then subject to the same probability of being missing at the slicer output. Some of the desired pulses may still be overlapped completely, some partially, and some not at all, but the overlapped portions of different pulses are still governed by the same probability. The total fraction of the pulse train missing at the output will then be $\underline{F}P$, or P/3, if $\underline{a}$ is not far below one. Those pulses or portions of pulses that do reach the output are subject to the pulse-edge time-shift effect in accordance with the formulas derived in this chapter, with $(a/s) = 1$, and with the restriction $a < s < 1-a$ removed and replaced by $a < s < 1$.

In continuing the analysis of the missing-pulses effect, it will be convenient to revert to the original assumption that each desired pulse is completely overlapped by constant-amplitude interference. In accordance with the discussion of coherence and incoherence on pages 18 and 19, it is possible for ϕ to vary systematically, if both the desired and interfering signals are coherent within themselves. In that case the same fraction of pulses would still be missing, but not in the same random fashion. Also, as mentioned previously, it is possible, in the case of totally coherent two-path interference with fixed delay difference, that the r-f phase difference ϕ will be constant at a value determined only by the delay difference and the precise value of the radio frequency.* In this case the probability is 1-F that all pulses will reach the output and F that none of the pulses will reach

* This can occur only if the radio frequency is sufficiently stable (see 5.31).

the output, if there is no control whatever over the radio-frequency or the delay difference. However, as will be shown in 5.32, this is one of the situations in which the slicing level may be lowered below a and even below 1-a to avoid all possibility of missing pulses, if the system is a single-channel system, and the signal-to-random-noise ratio is sufficiently high.

Unlike the time-shift effect, the missing pulses effect loses its true form when the radio frequencies are different enough to cause a decisive variation in ϕ during a single pulse. It therefore applies only to actual common-channel interference. The phenomenon which takes place if the radio-frequency difference is several times the reciprocal of the pulse-overlap duration is best illustrated by an oscillogram taken at the detector output, before slicing (Fig. 19). In this illustration, a desired pulse is almost

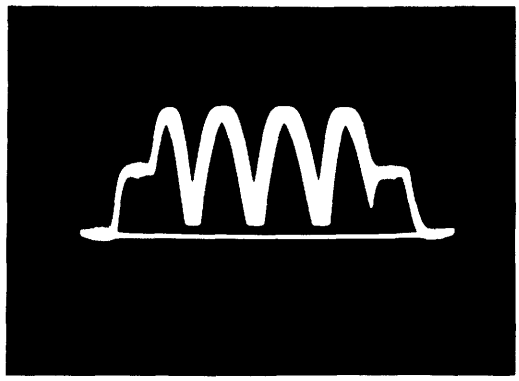

Fig.19 Oscillogram of detector output showing interference beats.

totally overlapped by an interfering pulse; the result is the familiar beat phenomenon (alternate reinforcement and cancellation as the phase difference ϕ changes continuously). Though present also when the interference ratio a is less than one-half, these beats have no effect for the same reason that there are no missing pulses: the slicing level s can be set between a and 1-a. In the present case of $\frac{1}{2} < a < 1$, each beat means a portion of the resultant will fall below the slicing level, so that the pulse at the slicer output will have small pieces missing at regular intervals. The fractional portion of the pulse missing at the output is still equal to F, given by (32). However, the effect can no longer be called random, regardless of the incoherence of the interfering signals, since it is primarily a systematic effect within each pulse, rather than an effect taking place from pulse to pulse. If the r-f pulses are coherent with each other, then the beat is coherent throughout, as is the case in the oscillogram of Fig. 19, which is a

superposition of a very large number of successive pulses.

This situation, as presented, is likely to be encountered only with pulses of rather long duration, such as may be used in PDM, and not with minimum-duration pulses as commonly used in PPM. In the latter case, the radio-frequency difference must generally have a larger absolute value to produce one or more complete phase reversals of ϕ within a single pulse, so that only a very strong adjacent-channel interfering signal could produce a sufficiently high interference ratio at the detector. In addition, the limited high-frequency response of the video stages including the slicer may cause the gaps in the pulses to be filled in when the r-f difference becomes several megacycles.

The quasi-missing-pulses effect encountered when the interfering signals differ considerably in radio frequency, as would be true in adjacent-channel interference, is not nearly so important as the true missing pulses effect encountered only in common-channel interference or multipath interference. The principal reason for this is the fact that its manifestation at the output is much less severe. The question of how the various interference effects manifest themselves in the receiver output will be treated in detail in the next chapter.

CHAPTER 3

AUTO-CORRELATION ANALYSIS OF OUTPUT NOISE RESULTING FROM INTERFERENCE IN PULSE-TIME MODULATION SYSTEMS

In the preceding chapter, the mechanism of the two interference effects, the time-shift effect and the missing-pulses effect, was examined in detail. In this chapter, these effects will be pursued further in order to learn how they affect the output of the receiver.

3.1 Auto-Correlation Analysis

Both the time-shift and the missing pulses effects are generally random phenomena; in the special cases in which they are not random, the prediction of the receiver output presents no problem, and need not be considered at this point. The theory of random or statistical phenomena or processes has not, until relatively recently, begun to take its rightful place in communication engineering. Transient analysis and steady-state sine-wave analysis are being supplemented by methods utilizing the statistics of the signal which is actually to be transmitted; the realization of the fact that the basic problem of communication is a statistical one is creating new horizons in the philosophy of system design. Credit for this is due N. Wiener[19] and C. E. Shannon.[20] Wiener's work has been of extremely wide scope with a large variety of possible applications, while Shannon's work has been directed specifically at the problem of transmission of information. That aspect of it which has direct application to communication and related systems is being ably expanded and presented by Y. W. Lee.* Most of the work in this chapter is based on material obtained from this presentation.

One of the important tools in the statistical treatment of communication problems is the concept of auto-correlation, first used by G. I. Taylor,[21] and then brought to the foreground on a rigorous basis by N. Wiener.[19] It is a device for transforming a random function, which is infinite in extent along the time axis and therefore can not be handled by the usual mathematical methods, into an analytic function or a statistical parameter which characterizes the original time function with respect to its spectrum and time

* Electr. Eng. Course 6.563, M.I.T., taught by Prof. Y. W. Lee.

distribution. The evaluation and use of the auto-correlation function figure prominently in this chapter.

Before proceeding with the mathematical analyses, it should be stated that the exact aim of this chapter is to evaluate the ultimate consequences of time shift and missing pulses. Both of these are random in character and therefore give rise to a random type of noise in the output which is, in fact, difficult to distinguish from random thermal or tube noise. Since this noise is generally either the only or the only significant manifestation of the interference, it is of primary importance to find its total power in the output, as well as its spectral distribution, with the final goal of predicting the output signal-to-noise ratio under various interference conditions. The desired information is furnished by the so-called power-density spectrum or power spectrum, which is obtained by operating on the auto-correlation function. For the sake of clarity and completeness, the work will be undertaken on a somewhat more general basis than might be considered necessary to solve only the immediate problem at hand. The two effects will first be analyzed in their most basic or simple form, and the additions or modifications necessary to adapt the results to the more complex interference situations will be made in the following chapters where these situations will be discussed individually.

The relations involving the power spectrum and the auto-correlation function can be derived as follows. Beginning with two functions of frequency $g_1(\omega)$ and $g_2(\omega)$ which are the Fourier transforms of the analytic functions $f_1(\tau)$ and $f_2(\tau)$, one can easily show, by ordinary Fourier transform methods, that the following relation holds:

$$\int_{-\infty}^{\infty} g_1(\omega)\overline{g_2}(\omega)\epsilon^{j\omega\tau}d\omega = \frac{1}{2\pi}\int_{-\infty}^{\infty} f_1(t)f_2(t+\tau)dt \ . \qquad (35)$$

Letting

$$f_2(\tau) = f_1(\tau) \ ,$$

$$g_2(\omega) = g_1(\omega) \ ,$$

one obtains

$$\int_{-\infty}^{\infty} |g_1(\omega)|^2 \epsilon^{j\omega\tau} d\omega = \frac{1}{2\pi} \int_{-\infty}^{\infty} f_1(t) f_1(t+\tau)\, dt \ . \qquad (36)$$

If $f_1(\tau)$ is a random function, infinite in extent, then both integrals of (36) will be infinite, but they can be made finite again, so that the equation is still valid, by dividing both sides by a very large period as indicated in (37); ($f_1(\tau)$ is now a random function.)

$$\lim_{T\to\infty} \frac{1}{2T} \int_{-\infty}^{\infty} |g_1(\omega)|^2 \epsilon^{j\omega\tau} d\omega = \lim_{T\to\infty} \frac{1}{2\pi} \frac{1}{2T} \int_{-T}^{T} f_1(t) f_1(t+\tau)\, dt \ . \qquad (37)$$

In (36), where $f_1(\tau)$ represents an analytic function, such as a single voltage pulse, $g_1(\omega)$ gives the spectral distribution in volts per radian/sec. In (37), where $f_1(\tau)$ is a random voltage function, $g_1(\omega)$ does not exist, but the quantity

$$\lim_{T\to\infty} \frac{\pi |g_1(\omega)|^2}{T}$$

does exist; it has the dimensions volt^2 per radian/sec, or watts per radian/sec if a one-ohm resistance level is assumed. This quantity therefore gives the amount of power in a one-radian-per-second bandwidth as a function of radian frequency and is referred to as the power-density spectrum, or simply power spectrum, denoted by $\Phi_{11}(\omega)$. Substitution of this in (37) results in the following important equation:

$$\int_{-\infty}^{\infty} \Phi_{11}(\omega) \epsilon^{j\omega\tau} d\omega = \lim_{T\to\infty} \frac{1}{2T} \int_{-T}^{T} f_1(t) f_1(t+\tau)\, dt \ . \qquad (38)$$

The left-hand side of (38) is the inverse Fourier transform of the power spectrum $\Phi_{11}(\omega)$; it equals the quantity on the right-hand side, which is known as the auto-correlation of $f_1(t)$, denoted by $\varphi_{11}(\tau)$. The auto-correlation being the inverse Fourier transform of the power spectrum, it then follows that the power spectrum is the Fourier transform of the auto-correlation function,

as given by (39).

$$\Phi_{11}(\omega) = \frac{1}{2\pi} \int_{-\infty}^{\infty} \varphi_{11}(\tau) \epsilon^{j\omega\tau} d\tau \ . \tag{39}$$

Regarding the method of derivation, it will be noted that in Eqs. (35), (36) and (37) the parameter τ signifies the independent variable, time, and t represents a time-shift variable.* In (38) and (39) their rôles have been tacitly interchanged. The auto-correlation function

$$\varphi_{11}(\tau) = \lim_{T \to \infty} \frac{1}{2T} \int_{-T}^{T} f_1(t) f_1(t + \tau) dt \ , \tag{40}$$

is a function of τ and has the physical significance which will be described only if τ is taken as the time-shift variable and t as the independent variable, time.

Defined in words, the auto-correlation of a function of time (or any other variable along the abscissa, e.g., distance) for any given value of time shift τ, is the product of the function over a large enough stretch of the independent variable to be completely representative of the entire function and the same function shifted by an amount τ over the same large interval of the abscissa variable, divided by this large interval. More briefly, it is the average over that long interval, or over all time, of the product of the function and the function shifted by the amount τ. Each averaging process furnishes only a single point in the curve of $\varphi_{11}(\tau)$ *vs.* τ. The process of obtaining one such value is illustrated in Fig. 20. In reality, the time shift τ is a continuous variable rather than a discrete one.

Inasmuch as the power spectrum is the function to be determined and is simply related to the auto-correlation, the auto-correlation holds the key to the analysis. The first and major part of the problem is, therefore, to find the auto-correlation function of the time functions of interest (the rectangular pulse train with random-edge-time shifts and the rectangular

*This bears no relation to the time-shift effect.

pulse train with randomly missing pulses). Since a low-pass filter is usually associated with the audio system, and the spectrum of the original pulse train is known, attention should be focussed on the random component, the component which causes the audible noise (as well as inaudible supersonic noise) at the output. Thus, while the entire auto-correlation function is first determined, its component corresponding to the nonrandom part of the pulse train is soon discarded since it has no direct bearing on the problem. This procedure of separating the two components after the auto-correlation is obtained is much simpler than a similar separation would be on the original time function.

3.2 Auto-Correlation of One-Edge Time-Shift Noise

The first step in finding the auto-correlation of the pulse train with randomly shifted edges is naturally to find the auto-correlation without time shifts, when the time function is perfectly periodic, and then to find the effect of small time shifts. The most frequently used symbols are defined below.

- E = pulse height (volts at 1 ohm).
- d_o = average pulse duration.
- d = duration of a given pulse.
- x_o = maximum shift (Δt_{max}) of pulse edge from its unshifted position.
- x = actual shift (Δt) of a given pulse edge from its normal position (positive if it makes pulse longer, negative if it makes it shorter).
- $P(x)$ = probability distribution of x.
- τ = time-shift parameter associated with auto-correlation, the independent variable of the auto-correlation.
- t = the independent variable, time.
- T = the pulse-repetition period.
- p = the pulse-repetition frequency in radian measure.

Certain simplifying assumptions will be made at the outset in order to make the development easier to follow. (None of these, as will be shown later, affect the result in any way.) One edge of each pulse, namely the trailing edge, will be subject to a random shift, limited for the time being to one-

third of the normal pulse duration ($x_o < \frac{1}{3} d_o$) for reasons which will soon become apparent. For similar reasons, the maximum pulse duration d_o+x_o will be limited to one-half of the period T. Also, $p(x)$ will be assumed symmetrical, so that d_o is both the "unshifted" pulse duration and the average "shifted" pulse duration.

The task of determining the auto-correlation function for rectangular pulses is actually easier than for most other time functions. The multiplication of the function by its shifted replica merely amounts to noting the amount of overlap between the shifted and unshifted pulses. Clearly, this overlap varies linearly with τ, and the auto-correlation of the perfectly periodic pulse train is the periodic sequence of triangles shown at the top of Fig. 21. Because of the perfect periodicity, the overlap situation for any one pulse is the same as for all others, so that a single pulse-repetition period is representative of the behavior over a very long period. The average value of the product of the two overlapping pulses in one period is $\frac{E^2}{T} d_o$ when the overlap extends over the entire pulse duration, i.e., when τ is zero. This is the value of $\varphi_{11}(0)$ and also equals the average power of the time function. When τ is not zero, but smaller than d_o so that there is partial overlap, then the average value of the product is given by

$$\varphi_{11}(\tau) = \frac{E^2}{T}(d_o - |\tau|) \quad . \qquad (|\tau| < d_o) \tag{41}$$

If τ is increased enough to make any and every pulse coincide not with its own shifted replica but with the replica of the next pulse or any other pulse, the same pattern repeats exactly, since all the pulses are identical. Therefore, $\varphi_{11}(\tau) = \frac{E^2}{T}(d_o - |\tau + nT|)$, where n is an integer such that $|\tau + nT| < d_o$.

If all the trailing edges are subject to random time shifts, then the various pulses and hence the various overlaps are no longer identical, and this has the following effects:

1. The value of $\varphi_{11}(0)$ is the same as before, if the average pulse duration is d_o, and the same linear decrease given by (41) occurs, but only for values of τ small enough so that <u>all</u> pulses still partially overlap their shifted replicas, that is, only so long as the shift τ is smaller than the minimum pulse duration ($\tau < d_o - x_o$).

2. As τ begins to exceed the minimum pulse duration, $[(d_o-x_o) < \tau < (d_o+x_o)]$,

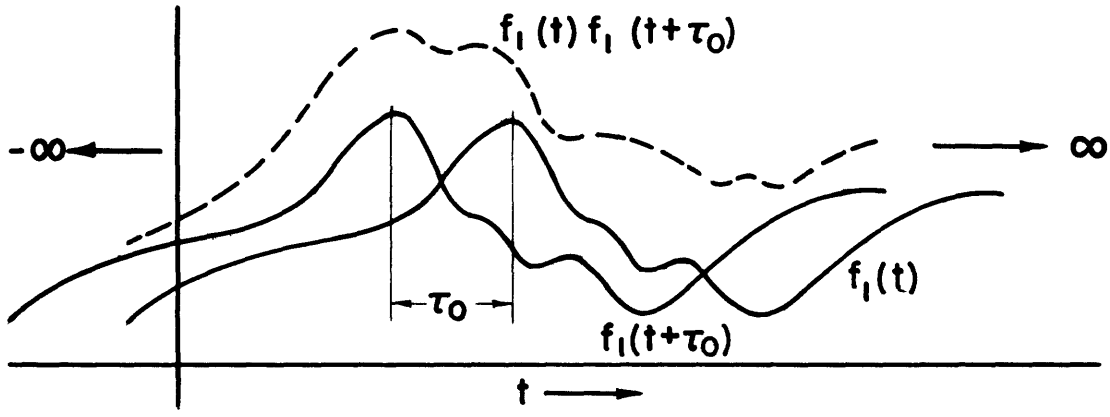

Fig.20 Obtaining the auto-correlation for $\tau = \tau_0$;
$\varphi_{11}(\tau_0) = f_1(t)\ f_1(t+\tau_0)$.

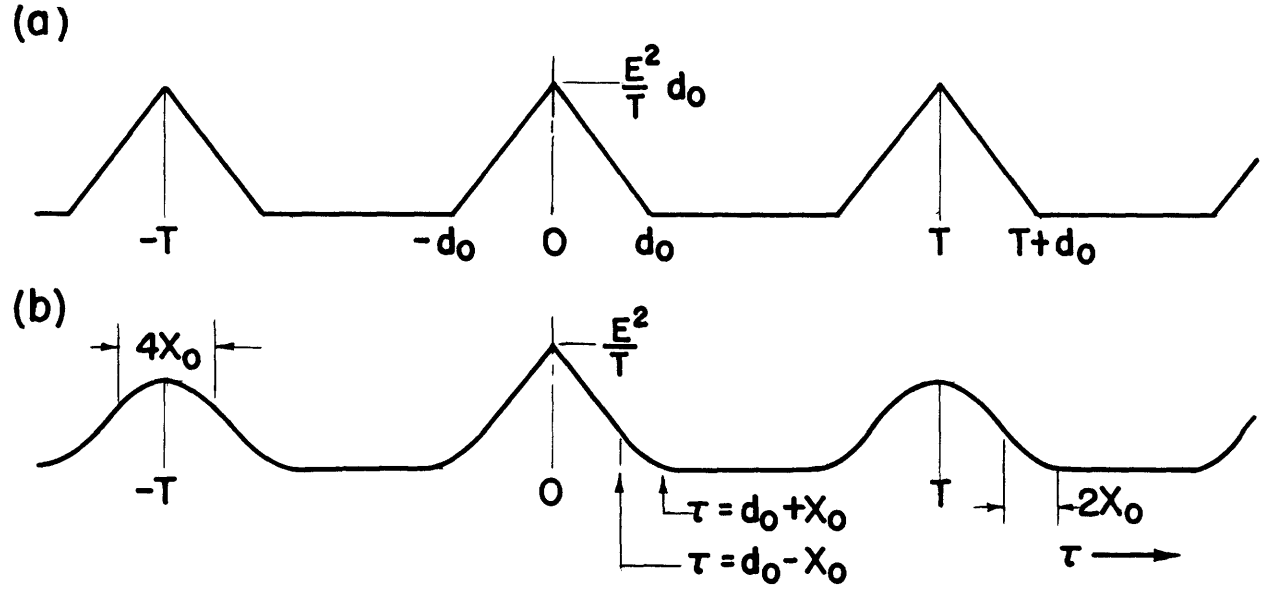

Fig.21 Auto-correlation of rectangular pulses
(a) no time shifts (b) one-edge random time shifts.

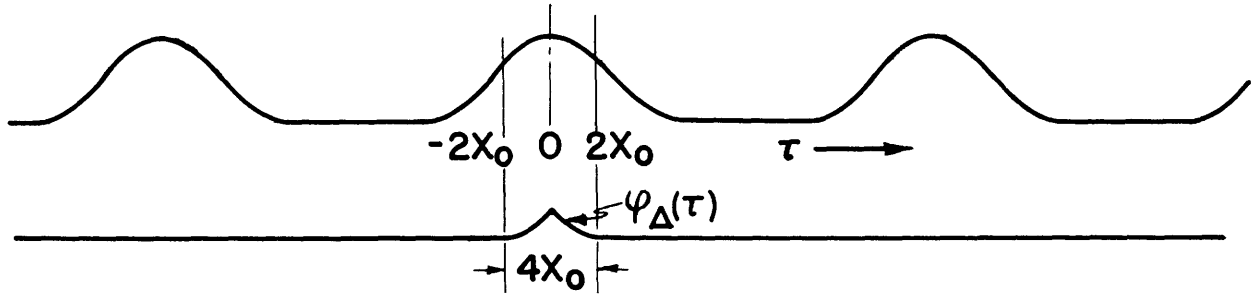

Fig.22 Periodic and aperiodic components of $\varphi_{11}(\tau)$.

more and more pulses cease to have overlap, so that their contribution to the linear decrease in overlap ceases. The slope in $\varphi_{11}(\tau)$ decreases, which accounts for the concave-upward curvature noted at the bottoms of the triangles in the lower half of Fig. 21. Partial overlap continues out to $\tau = d_o+x_o$, rather than just to $\tau = d_o$. The "bottom curvature" of the $\varphi_{11}(\tau)$ is therefore associated with the coincidence of the fixed leading edges and the uncertainty region of the trailing edges. Exactly the same phenomenon occurs also if the leading and trailing edges concerned do not belong to the same pulse (a pulse and its shifted replica) but, instead, to two different pulses which coincide for larger values of τ.

3. For $\tau = nT$, there is less total overlap than for $\tau = 0$, since none of the overlapping pulses are identical in duration, and the overlap for each pair is determined by the shorter one. As τ is changed from nT, the initial decrease in $\varphi_{11}(\tau)$ is small because, for the same reason, the overlap on most pulses does not change; as more and more overlaps begin their linear decrease, the total overlap decreases at an increasing rate, which accounts for the convex-upward curvature or "top curvature" of the $\varphi_{11}(\tau)$ triangles in the lower part of Fig. 21. This curvature is associated with the coincidence of the uncertainty regions of the trailing edges, and it occurs only if these edges belong to different pulses. When τ differs from nT by more than $2x_o$, the linear decrease in overlap has set in for all pulses, so that $\varphi_{11}(\tau)$ decreases linearly.

4. For $2x_o < \tau+nT < d_o-x_o$, $\varphi_{11}(\tau)$ varies linearly as if there were no time shifts. This linear region exists only if $2x_o < d_o-x_o$, or $x_o < d/3$, which is the reason for that assumption made at the beginning. Similarly, the reason for choosing $d_o+x_o < \frac{1}{2}T$ was to prevent the bottoms of adjacent $\varphi_{11}(\tau)$ triangles from blending into each other.

The preceding numbered paragraphs explain qualitatively why the auto-correlation has the appearance indicated in Fig. 21. Before beginning the quantitative part of the analysis, one can draw some important and useful conclusions from further consideration of the qualitative picture of Fig. 21. The auto-correlation of the periodic pulse train is also a perfectly periodic function, and the corresponding spectrum is obviously a discrete spectrum having lines at the pulse radian frequency p and its harmonics np. The auto-correlation of the second pulse train differs from that of the first

principally in that it is not periodic, the triangle about $\tau = 0$ being different from all the triangles about $\tau = nT$. As shown in Fig. 22, it can be split into two components, one of which is purely periodic (though somewhat different from that encountered previously), and the other a nonperiodic component extending only from $\tau = -2x_0$ to $\tau = +2x_0$. The periodic component again corresponds to a periodic time function, namely the periodic part of the pulse train with shifted trailing edges; associated with this is a line spectrum which is not of primary interest in the present problem The nonperiodic component is a direct consequence of the random part of the time function; associated with this nonperiodic component is a continuous spectrum -- the spectrum of the time-shift noise which is to be determined. The seemingly insignificant lone triangle in Fig. 22 is therefore the key to the solution. Being the difference between the entire auto-correlation and its periodic component, it will be denoted by $\varphi_\Delta(\tau)$, and the corresponding power spectrum by $\Phi_\Delta(\omega)$. Both the auto-correlation and the power spectrum are, of course, on a power basis, and the relations between them therefore apply equally to components such as $\varphi_\Delta(\tau)$ and $\Phi_\Delta(\omega)$. The power spectrum of the time-shift noise is the Fourier transform of the nonperiodic component of the auto-correlation, as expressed mathematically in (42).

$$\Phi_\Delta(\omega) = \frac{1}{2\pi} \int_{-\infty}^{\infty} \varphi_\Delta(\tau) \epsilon^{j\omega\tau} d\tau \ . \qquad (42)$$

Except for the following remarks which may be of general interest, attention will be focussed solely on the above quantities, since they are the sole representatives of the interference noise. It is of interest to note the changes in the overall spectral energy distribution of the pulse train as a result of the random pulse-edge time shifts. Without these time shifts, the power spectral lines at np have magnitudes which can be determined by expressing the triangular auto-correlation as a Fourier series. The same result is obtained by Fourier analysis of the square pulses and squaring the resulting coefficients. With the time shifts, the periodic component of the auto-correlation acquires rounded corners and can, in fact, be shown to be the auto-correlation of a new, totally periodic pulse train, in which the trailing edges have finite decay times ($= 2x_0$) instead of vertical edges. This means that, although the same type of line spectrum still exists, the magnitudes of the lines at the highest frequencies are

reduced. Since for a symmetrical time-shift probability distribution the total power must be unaffected by the time shifts, the power taken from the higher frequencies of the line spectrum is the same power now found spread continuously over the spectrum, its audio portion giving rise to the time-shift noise. The fact that the rectangular pulses with their random-edge time shifts have the same auto-correlation, in part, as differently shaped pulses without time shifts provides a valuable short-cut method for determining the entire auto-correlation function quantitatively.

Attention will now be focussed on the problem of determining quantitatively the aperiodic auto-correlation component, $\varphi_{\Delta}(\tau)$. According to Fig. 22, this requires only that one find the expression for the rounded tops of the triangles and subtract it from the straight triangle. The rounded bottoms do not enter the problem because they are identical for all the triangles; however this is not true in general, as will be seen later when both pulse edges are given shifts, and therefore the more general procedure will be used. It consists of finding the entire auto-correlation and taking the difference between the triangle centered about $\tau = 0$ and any other triangle, such as the one centered about $\tau = T$. These two "triangles" will be referred to frequently and they should therefore be given appropriate names. The one about $\tau = 0$ differs from all the others because it is the "self-correlation" of all the pulses; all the others are what one might call "cross-correlations" between different pulses, but this expression is generally reserved for correlations between different functions rather than those between different parts of the same function, so that the word "inter-correlation" will be used instead. The immediate problem, then, is to find the self-correlation and the inter-correlation. The writer has done this by a number of different methods which ultimately lead to identical results. Only the simplest and most efficient of these methods will be used in this chapter.*

From the comments on the periodic auto-correlation component (page 48), it follows that equivalent nonrandom, periodic pulses can be used to obtain the inter-correlation.** The self-correlation can be found by similar

---

* The formulas arrived at through other methods, as well as outlines of these methods, are given in Appendix I.

** The writer is indebted to Mr. T. P. Cheatham, who suggested the application of this property to the present problem.

methods, generally even simpler. Although the equivalent pulses no longer have the advantage of being rectangular, this is more than offset by the fact that the sloping sides contain all the necessary statistical information so that only a single pulse need be considered. A physical picture of the equivalence-replacement is shown in Fig. 23, where the shaded region represents a superposition of many pulse edges in all the possible positions, with the depth of shading indicating the distribution of the pulse edges. The latter is given by $P(x)$ discussed in some detail in Chapter 2. The shape of the equivalent sloping edge must be such that the area of the pulse from its leading edge to a vertical line erected a (time) distance d_o+x from the leading edge is the same as the average area, measured over the same range, of a very large number of the actual rectangular pulses.* Consequently the sloping edge is given by the simple expression

$$y(x) = E \int_{x}^{x_o} P(x)dx \ . \qquad (43)$$

In the particularly simple case of a constant (flat) probability distribution, for example, the equivalent pulse edge is obviously linear. To find the inter-correlation, it is necessary merely to determine the auto-correlation of a single one of the equivalent pulses with the period taken as the pulse repetition period, T, rather than infinity. The resulting function will be centered about $\tau = 0$, rather than about $\tau = nT$ as in the actual auto-correlation, which is helpful when it comes to subtracting this function from the self-correlation. Because of the complete symmetry about $\tau = 0$ (a property of all correlation functions), only positive values of τ need be considered. The mathematical development which follows is illustrated in Fig. 24, showing a sketch for the case of small τ, in which the curves to be multiplied can be split into three zones corresponding to three mathematical terms which give the rounded top of the inter-correlation. Also shown is the simpler case of larger τ, $(d_o-x_o < \tau < d_o+x_o)$, which gives the rounded bottoms for both the inter- and self-correlations.

---

* Note that the total area of the new pulse equals the actual average pulse area, Ed_o, which is also the pulse area in the absence of time shifts if $P(x)$ is symmetrical.

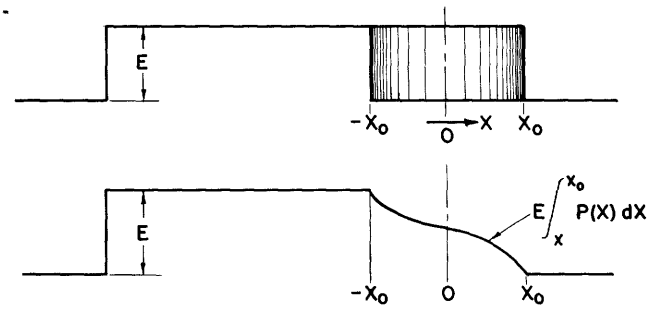

Fig.23 Equivalent nonrandom pulse

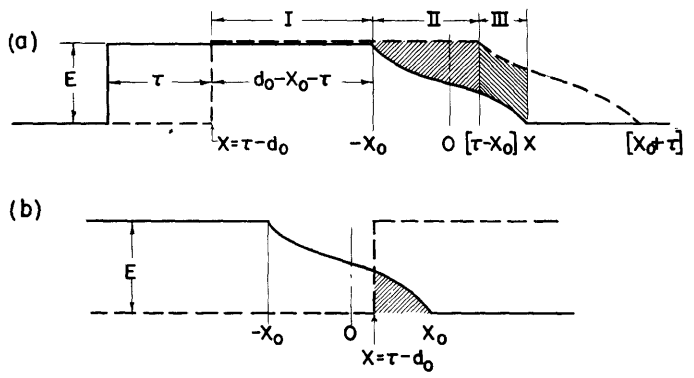

Fig.24 Determination of Inter-correlation (a) for $-2x_o<\tau<2x_o$ (b) for $[d_o-x_o] < \tau < [d_o+x_o]$.

$0 < \tau < 2x_o$. Inter-correlation = $\varphi_i(\tau)$. The expression for $\varphi_i(\tau)$ comprises the following three parts, corresponding to the three zones shown in Fig. 24. Each part is simply the product of the solid and the broken (shifted) curves, divided by T.

$$\varphi_{i_I} = \frac{E^2}{T}(d_o - x_o - \tau)$$

$$\varphi_{i_{II}} = \frac{E}{T}\int_{-x_o}^{-x_o+\tau} y(x)dx = \frac{E^2}{T}\int_{-x_o}^{-x_o+\tau}\int_{x}^{x_o} P(u)\,du\,dx \quad * \qquad (44)$$

$$\varphi_{i_{III}} = \frac{1}{T}\int_{-x_o+\tau}^{x_o} y(x)y(x-\tau)dx = \frac{E^2}{T}\int_{-x_o+\tau}^{x_o}\left[\int_{x}^{x_o} P(u)\,du\right]\left[\int_{x-\tau}^{x_o} P(u)\,du\right]dx$$

* In all double integrals involving x under both integral signs, x will be replaced by the symbol u in the inside integral.

$$\varphi_i = \varphi_{i_I} + \varphi_{i_{II}} + \varphi_{i_{III}}$$

$$= \frac{E^2}{T}\left\{ d_o - x_o - \tau + \int_{x_o}^{-x_o + \tau} \left[\int_x^{x_o} P(u)\,du \right] dx + \int_{-x_o + \tau}^{x_o} \left[\int_x^{x_o} P(u)\,du \right] \right.$$

$$\left. \left[\int_{x - \tau}^{x_o} P(u)\,du \right] dx \right\} \qquad (0 < \tau < 2x_o) \qquad (45)$$

$2x_o < \tau < d_o - x_o$. In this range, the inter-correlation, as well as the self-correlation, $\varphi_s(\tau)$, is the same as for rectangular pulses of duration d_o. This is readily understood when one remembers that the equivalent pulse has the same area, namely Ed_o, subject to the assumption of a symmetrical probability distribution. The correlations are therefore given by

$$\frac{E^2}{T}(d_o - \square\tau\square) \ , \qquad (41)$$

which is also the value of the self-correlation for τ between zero and $2x_o$.

$d_o - x_o < \tau < d_o + x_o$. In this range, both the inter- and self-correlations are obtained in accordance with the lower sketch of Fig. 24. A single term takes care of the product as follows.

$$\varphi_i(\tau) = \varphi_s(\tau) = \frac{E}{T} \int_{x = \tau - d_o}^{x = x_o} y(x)\,dx = \frac{E^2}{T} \int_{x = \tau - d_o}^{x = x_o} \left[\int_x^{x_o} P(u)\,du \right] dx \ . \qquad (46)$$

The nonperiodic auto-correlation component is now given by

$$\varphi_\Delta(\tau) = \varphi_s(\tau) - \varphi_i(\tau)\Big|_{0 < \tau < 2x_o} = \left[\frac{E^2}{T}(d_o - \tau) - (45) \right]$$

$$= \frac{E^2}{T}\left\{ x_o - \int_{-x_o}^{-x_o + \tau} \left[\int_x^{x_o} P(u)\,du \right] dx - \int_{-x_o + \tau}^{x_o} \left[\int_x^{x_o} P(u)\,du \right] \left[\int_{x - \tau}^{x_o} P(u)\,du \right] dx \right\} \qquad (47)$$

By making use of the relations

$$\int_{-x_o}^{x_o} P(u)\,du = 1 \ , \tag{a}$$

and

$$\int_{-x_o}^{x_o} \left[\int_{x}^{x_o} P(u)\,du \right] dx = x_o \ , \ ^{*} \tag{b}$$

(47) can be reduced to the relatively simple (50), as follows. First using the relation (b) on the first two terms, one obtains

$$\varphi_{\Delta}(\tau) = \frac{E^2}{T}\left\{ \int_{-x_o + \tau}^{x_o} \left[\int_{x}^{x_o} P(u)\,du \right] dx - \int_{-x_o + \tau}^{x_o} \left[\int_{x}^{x_o} P(u)\,du \right] \left[\int_{x - \tau}^{x_o} P(u)\,du \right] dx \right\} . \tag{48}$$

Next, factoring common terms gives

$$\varphi_{\Delta}(\tau) = \frac{E^2}{T} \int_{-x_o + \tau}^{x_o} \left[\int_{x}^{x_o} P(u)\,du \right] \left[1 - \int_{x - \tau}^{x_o} P(u)\,du \right] . \tag{49}$$

Finally, application of relation (a) to the second factor yields

$$\varphi_{\Delta}(\tau) = \frac{E^2}{T} \int_{-x_o + \tau}^{x_o} \left[\int_{x}^{x_o} P(u)\,du \right] \left[\int_{x_o}^{x - \tau} P(u)\,du \right] dx . \tag{50}$$

The expression for $\varphi_{\Delta}(\tau)$ as given by (50) is the most important general result of this chapter. Substitution of a specific function for P(u) results

---

* This relation is readily derived for any symmetrical probability distribution P(u).

in a specific function of τ, the Fourier transform of which is the desired power spectrum. However, before more specific results will be obtained, there are additional points in connection with the above result which call for further general considerations.

For the sake of simplicity, the above result was obtained on the basis of certain simplifying assumptions; it is of interest to show that the same result (50) is obtained even without these assumptions. Up to this point, x_o has been restricted to below one-third of d_o. This restriction assured that the curved top and bottom zones of the inter-correlation would never overlap, but would instead be separated by a linear zone, a remnant of the triangular auto-correlation of a rectangular pulse. The three zones extend from $\tau = 0$ to $2x_o$, $2x_o$ to d_o-x_o, and d_o-x_o to d_o+x_o.

Consider now the remaining possible values of x_o: 1/3 d_o up to d_o. The two curved zones of the inter-correlation now overlap so as to form a third curved portion, wiping out the linear portion. There are still three zones for which $\varphi_1(\tau)$ is given by different expressions and must be derived separately: $0 < \tau < d_o-x_o$, $d_o-x_o < \tau < 2x_o$, $2x_o < \tau < d_o+x_o$. If the two pictures of Fig. 24 are redrawn with larger x_o, it will be found that they are unchanged except for proportions and yield the same results (45) and (46) in the two end zones of τ. The situation for the middle zone, where τ is between d_o-x_o and $2x_o$, is shown in Fig. 25, and the product of the solid and broken

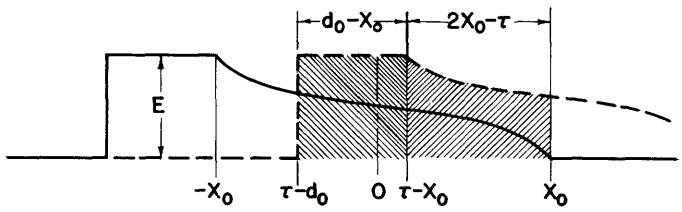

Fig.25 Determination of inter-correlation for $[d_o-x_o] < \tau < [d_o+x_o]$, $x_o > d_o/3$.

lines, averaged over one period to give the inter-correlation, is as follows:

$$\varphi_1(\tau) = \frac{E}{T}\int_{\tau-d_o}^{\tau-x_o} y(x)dx + \frac{1}{T}\int_{-x_o+\tau}^{x_o} y(x)y(x-\tau)dx$$

$$\frac{E^2}{T}\left\{\int_{\tau-d_o}^{\tau-x_o}\left[\int_{x}^{x_o} P(u)du\right]dx + \int_{-x_o+\tau}^{x_o}\left[\int_{x}^{x_o} P(u)du\right]\left[\int_{x-\tau}^{x_o} P(u)du\right]dx\right\}. \quad (51)$$

As for the self-correlation, this has changed only in that the curved portion at the bottom has expanded at the expense of the linear portion (see Fig. 25) and now extends over two of the τ zones, from $\tau = d_o - x_o$ to $d_o + x_o$. Since this includes the middle range $d_o - x_o < \tau < 2x_o$, this curved portion of $\varphi_s(\tau)$, given by (46), now figures in the evaluation of $\varphi_\Delta(\tau)$ which also extends over two of the τ zones instead of one. Since $\varphi_\Delta(\tau)$ also extends over two different τ zones, from $\tau = 0$ to $2x_o$ which is made up of 0 to $d_o - x_o$ and $d_o - x_o$ to $2x_o$, it must be determined separately in each of the two zones, but the result should check (50) in both regions. Consider the first zone, $0 < d_o - x_o$, in which $\varphi_i(\tau)$ is given by (45) and $\varphi_s(\tau)$ is still linear and equal to $(E^2/T)(d_o - \tau)$. Since both of the correlations are identically the same as in the previous development, the expression for $\varphi_\Delta(\tau)$, is also the same, namely (47), (48), (49), or (50). Next consider the second or middle zone, $d_o - x_o < \tau < 2x_o$, in which $\varphi_s(\tau)$ is given by (46) and $\varphi_i(\tau)$ by the new expression (51). Forming the difference $\varphi_s(\tau) - \varphi_i(\tau)$, one obtains

$$\varphi_\Delta(\tau) = \frac{E^2}{T}\left\{\int_{-x_o + \tau}^{x_o}\left[\int_x^{x_o} P(u)\,du\right]dx - \int_{-x_o + \tau}^{x_o}\left[\int_x^{x_o} P(u)\,du\right]\left[\int_{x-\tau}^{x_o} P(u)\,du\right]dx\right\}.$$

This is seen to be identical to (48), and this again leads to (50), which therefore proves that the same result is obtained for any physically possible value of maximum time shift x_o.

Another simplifying assumption made at the beginning of the analysis was the restriction that the maximum pulse duration $d_o + x_o$ be limited to less than half the period. The purpose of this was merely to prevent the adjacent lobes of the auto-correlation from overlapping, since their width is twice the maximum pulse duration but their spacing the same as the pulse-repetition period. Suppose this condition is no longer met; the pulse-overlap picture is now much more complex, many pulses overlapping more than one shifted pulse at a time. If, however, the pulse train is split into two new pulse trains, alternate pulses going to each one, then the result is two new functions each of which meets the original requirement and which add up to the original function. Now, it can be shown by simple substitution that the auto-correlation of the sum of two time functions is the sum of the individual auto-correlations

and twice the cross-correlation* between them. The cross-correlation between the two functions is wholly periodic, as can be appreciated easily when one remembers that there is no possibility of all the pulses overlapping their own shifted replicas which is the usual source of any aperiodicity, so that there is no self-correlation. Since we are concerned only with the aperiodic correlation components, it is clear that the cross term has no bearing on the problem and that $\varphi_\Delta(\tau)$ for the complete pulse train is simply the sum of the $\varphi_\Delta(\tau)$ functions. This proves that $\varphi_\Delta(\tau)$ as given by (50) is totally independent of the maximum pulse duration, even if the total auto-correlation no longer has the appearance of separate lobes.

The final assumption to be justified is that of the symmetrical probability distribution. If the pulse duration is d_o in the absence of any edge time shifts, then, in the presence of the time shifts, the average pulse duration is also d_o only if $P(x)$ is symmetrical. Suppose that it is asymmetrical, as shown in Chapter 2 (Fig. 10). The average pulse duration is now larger than d_o and may be denoted by d_o'. This makes both the self- and intercorrelations larger by equal amounts, leaving the difference or aperiodic component unchanged. In the original derivation of $\varphi_\Delta(\tau)$, d_o would be replaced by d_o' in certain instances, but would remain unchanged in others, as can be ascertained by a study of Figs. 24 and 25. While (45) remains unaffected, d_o changes to d_o' in (41), steepening the slope of the linear portions of the correlation lobes and raising $\varphi_s(0)$ by a factor of d_o'/d_o; $\varphi_i(\tau)$ is boosted in a different way, namely as a result of the fact that the relation (b) on page 53 no longer holds, the integral now being larger than x_o by the same amount by which d_o' exceeds d_o. It is clear, therefore, that in the subtraction and substitution process in (47) and (48), the increase drops out, so that (48), (49), and (50) are completely unaffected by the nature of $P(x)$. It should be pointed out, in this connection, that, because of the limits on the integrals in these expressions, $P(x)$ need be specified correctly only within the limits $-x_o$ to x_o. The function used to represent $P(x)$ need not be zero outside these limits, as $P(x)$ actually is, but may have any type of behavior.

---

* The cross-correlation between $f_1(t)$ and $f_2(t)$ is defined as

$$\varphi_{12}(\tau) = \varphi_{21}(\tau) = \lim_{T\to\infty} \frac{1}{2T} \int_{-T}^{+T} f_1(t) f_2(t+\tau)\,dt \ .$$

The general formula for the aperiodic auto-correlation component, repeated here for convenience, is

$$\varphi_{\Delta}(\tau) = \frac{E^2}{T}\int_{-x_o}^{x_o} + \left[\int_{\tau+x}^{x_o} P(u)du\right]\left[\int_{x_o}^{x-\tau} P(u)du\right]dx \ . \qquad (50)$$

This will now be applied to finding the power spectra for the more important probability distributions. In Chapter 2, some of the probability distributions for time shifts resulting from interference were derived and illustrated. Before applying these rather complex distributions, it is instructive to consider simpler distributions which are also of more than academic interest. Of particular interest is the "flat" or constant distribution, which gives no preference to any one pulse-edge position, each pulse edge having an equal probability of falling anywhere between the limits $-x_o$ and x_o. As previously noted, the equivalent nonrandom pulse edge is linear in this case, or the equivalent pulse trapezoidal in shape. Since $P(x)$ need not be specified correctly outside the limits of x, the simple expression $P(x) = C$ can be used, with C chosen so as to make

$$\int_{-x_o}^{x_o} P(x)dx = 1 \ ,$$

which means that the combined probability of all the possibilities in unity. The constant C is $1/2x_o$, so that

$$P(x) = P(u) = \frac{1}{2x_o} \ . \qquad (52)$$

Substituting (52) in (50), one obtains after evaluation of the integrals

$$\varphi_{\Delta}(\tau) = \frac{E^2}{T}\frac{1}{24x_o^2}(8x_o^3 - 12x_o^2\tau + 6x_o\tau^2 - \tau^3) = \frac{E^2}{T}\frac{1}{24x_o^2}(2x_o - \tau)^3;$$

$$\varphi_{\Delta}(\tau) = \frac{E^2}{T}\frac{1}{24x_o^2}(2x_o - |\tau|)^3 \ . \qquad (|\tau| < 2x_o) \qquad (53)$$

The absolute value sign has been placed on τ, since the function is known to be symmetrical about $\tau = 0$. The fact that $\varphi_\Delta(\tau)$ is a simple cubic curve, which is easily handled algebraicly, makes it a good illustrative example. Some of the important characteristics are easily determined: with the E^2/T factor omitted, the height or value at $\tau = 0$ is $1/3\ x_o$; the area, which will later be shown to be directly proportional to the audio-noise power, is $1/3\ x_o^2$. Plots of the positive-τ half of the function for this flat probability distribution, as well as of those obtained for other distributions will be found in Fig. 26. Before proceeding with the determination of the power spectrum, it is preferable to derive the aperiodic auto-correlation components for all of the other probability distributions to be considered.

A fact worth mentioning is that all probability functions between finite limits, such as $-x_o$ and x_o in the present case, can be regarded as amplitude distributions of periodic functions. Thus it was shown in Chapter 2 that constant-amplitude interference time shifts have a probability distribution which is the same as the amplitude distribution of a sinusoid, a half-wave rectified sinusoid or an intermediate waveform. One usually thinks in these terms only if $P(x)$ is such that the corresponding periodic function is a simple well-known function. In the case of the "flat" probability distribution considered above, the distribution is that of a triangular waveform, a sawtooth, and various other possible functions which spend equal amounts of time at all the amplitude limits of $-x_o$ and x_o. The mean-square value of such a function is known to be $1/3\ x_o^2$, the same as the area under the corresponding correlation curve. It will be seen that this is no coincidence, inasmuch as the same agreement exists for other probability distributions.

The second distribution to be considered is one which may be called "double-spike" probability distribution. It corresponds to the amplitude distribution of a square wave, having half of its possible values concentrated at x_o and the other half at $-x_o$. While it is impossible to represent $P(x)$ algebraically, it is clear that the two inside integrals in (50) are each equal to one-half. Consequently, the aperiodic auto-correlation component is given by

$$\varphi_\Delta(\tau) = \frac{E^2}{T} \int_{\tau - x_o}^{x_o} \frac{1}{4}\, dx = \frac{1}{4} \frac{E^2}{T}(2x_o - \tau) \ ,$$

and because of the symmetry about $\tau = 0$, this becomes

$$\varphi_{\Delta}(\tau) = \frac{1}{4}\frac{E^2}{T}(2x_o - |\tau|). \qquad (|\tau| < 2x_o) \tag{54}$$

This is a triangle the height of which is $\frac{1}{2}x_o$ and the area of which is x_o^2, omitting the E^2/T factor. The mean-square or power value of the square wave is x_o^2, again the same as the area under $\varphi_{\Delta}(\tau)$. To extend the parallelism between the probability distribution and the periodic function having the same amplitude distribution, the function's mean-square value minus its mean value squared equals the square of the so-called standard deviation of the probability curve, given by

$$\overline{x}^2 = \int_{-x_o}^{x_o} x^2 P(x)\,dx + \left[\int_{-x_o}^{x_o} xP(x)\,dx\right]^2 . \tag{55}$$

If one regards the periodic function as a voltage, then the square of the standard deviation corresponds to the total power minus the d-c power (the d-c component exists only for asymmetrical probability distributions). In the present case, it will become clear, when the power spectrum is derived, that, because of the equality between the square of the standard deviation of $P(x)$ and the area under $\varphi_{\Delta}(\tau)$, the low-frequency time-shift noise power must be directly determined by the standard deviation.

The two probability distributions considered so far have the time shifts distributed uniformly, and concentrated at the two extremes, respectively. It is logical, now, to consider a third distribution, in which most of the time shifts are concentrated near zero, the center of the probability curve. This is represented by a part of the Gaussian error function with constants so chosen as to make the function negligibly small (about 2 per cent of peak) at $-x_o$ and $+x_o$, and, of course, to make its area unity. It is given by

$$P(x) = \frac{2}{\sqrt{\pi}\,x_o}\,\epsilon^{-\left(\frac{2x}{x_o}\right)^2} . \tag{56}$$

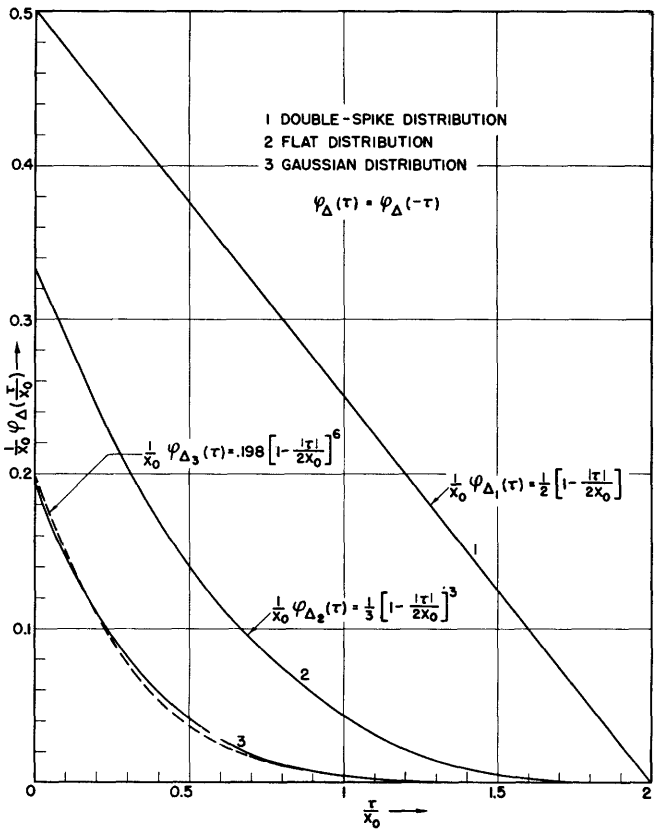

Fig.26 Auto-correlation functions, $\varphi_\Delta(\tau)$, of pulse-edge time-shift noise.
$\frac{1}{x_0}\varphi(\frac{\tau}{x_0})$ vs. $\frac{\tau}{x_0}$ for various probability distributions of time shifts; maximum time shift = x_0.
(Multiply all ordinates by E^2/T.)

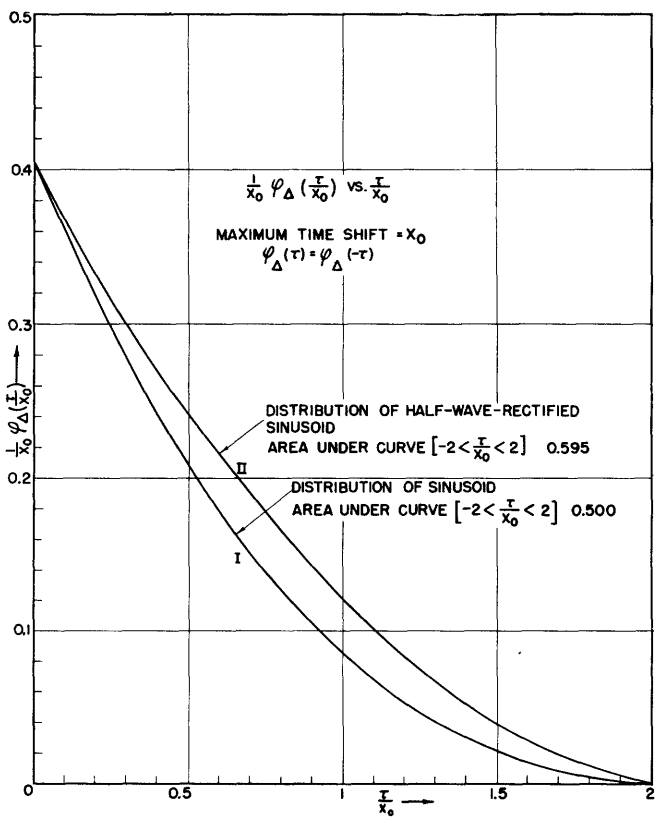

Fig.27 Auto-correlation functions, $\varphi_\Delta(\tau)$, of pulse-edge time-shift noise.
$\frac{1}{x_0}\varphi(\frac{\tau}{x_0})$ vs. $\frac{\tau}{x_0}$ for two different time-shift probability distributions.
(Multiply all ordinates by E^2/T.)

Substitution of (56) in (50) results in a double integral which cannot be solved analytically. The plot of $\frac{1}{x_o}\,\varphi_\Delta(\frac{\tau}{x_o})$ in Fig. 26 was obtained by numerical integrations. The area under the curve is approximately 1/9, corresponding to 1/9 x_o^2 under the curve of $\varphi_\Delta(\tau)$. By making a power-series approximation of this curve, one finds that it is fairly accurately given by (57), plotted in broken lines on the same figure, and again of the simple form found for the other probability distributions.

$$\varphi_\Delta(\tau) \approx \frac{0.0031}{x_o^5}\,(2x_o - |\tau|)^6 \,. \qquad (57)$$

A comparison of the three curves in Fig. 26 shows directly that their shape and the area under each one depends very much on the standard deviation of the corresponding probability distribution.

Before studying the distributions of the sinusoid and rectified sinusoid, it should be pointed out that the Gaussian distribution of time shifts is that actually obtained as a result of random noise, so that the power spectrum for this case should be of interest. The double-spike distribution of edge time shifts is actually another way of representing missing pulses or rather missing parts of pulses, namely the parts between $-x_o$ and x_o, which are present half of the time and absent half of the time. By adjusting the relative areas of the two spikes and letting $d_o = 2x_o$, the missing-pulse problem can be solved in general terms and gives the same result as obtained in the latter part of this chapter by a different method.

The two most important probability distributions as far as the interference characteristics of PTM are concerned are those derived and discussed in Chapter 2 and defined by (12) and (14), respectively. Again, the evaluation of (50) cannot be performed analytically, and the two plots in Fig. 27, on the preceding page, were obtained through point-by-point numerical integration. These curves have been approximated by power series to better than one per cent accuracy in order to facilitate the next step, namely the Fourier transformation leading to the power spectrum. For the "sinusoidal" distribution, the approximation is given by (58), and for the "half-wave rectified sinusoidal" distribution by (59).

$$\varphi_{\Delta}(\tau) = 0.0061(2x_o - |\tau|) + \frac{0.0615}{x_o}(2x_o - |\tau|)^2 + \frac{0.0184}{x_o^2}(2x_o - |\tau|)^3 . \quad (58)$$

$$\varphi_{\Delta}(\tau) = 0.0339(2x_o - |\tau|) + \frac{0.0919}{x_o}(2x_o - |\tau|)^2 - \frac{0.00404}{x_o^2}(2x_o - |\tau|)^3 . \quad (59)$$

The areas under the normalized curves, that is, the values of

$$\frac{1}{x_o}\int_{-1}^{1}\varphi_{\Delta}\left(\frac{\tau}{x_o}\right)d\tau ,$$

are 0.500 and 0.596, respectively. The former is equal to the mean-square value of the corresponding sine wave of unity amplitude, and the latter equals the mean-square value minus the square of the mean value of the corresponding half-wave rectified sinusoid. As is to be expected because these distributions favor the larger deviations over small ones, the resulting curves of $\varphi_{\Delta}(\tau)$ fall between the curves for the "flat" and the "double-spike" distributions. It is of interest to note that the plots of $\varphi_{\Delta}(\tau)$ do not show in any way whether or not the probability distribution of the pulse-edge time shifts is symmetrical.

3.3 Power Spectra of One-Edge Time-Shift Noise

It remains now to determine the power spectrum of the time-shift noise for the various probability distributions by obtaining the Fourier transforms of the various expressions for $\varphi_{\Delta}(\tau)$. All of these involve terms of the same form, namely

$$\frac{K_n}{x_o^{n-1}}(2x_o - |\tau|)^n , \qquad (|\tau| < 2x_o) ,$$

but none of them can be expressed by a single analytic function, since they end abruptly at $-2x_o$ and $+2x_o$ and since their derivatives are discontinuous at $\tau = 0$. Each term can, however, be broken up into three functions in accordance with the method of translation and sectioning used by Gardner and Barnes.* [21] Each of the three functions of t, or τ in the present case, are transformed individually by the Laplace transformation, and the individual transforms are

* Gardner and Barnes, "Transients in Linear Systems", page 238.

TABLE 1

AUTO-CORRELATIONS AND CORRESPONDING POWER SPECTRA

$\varphi_\Delta(\tau)$	$\Phi_\Delta(\omega)$	$\Phi_\Delta(\omega)$ for $(x_o\omega) < 1$
$K_1(2x_o - \lvert\tau\rvert)$	$K_1 \frac{2}{\pi} x_o^2 \left(\frac{\sin x_o\omega}{x_o\omega}\right)^2$	$K_1 \frac{2x_o^2}{\pi} [1 - \frac{1}{3}(x_o\omega)^2 + \ldots]$
$\frac{K_2}{x_o}(2x_o - \lvert\tau\rvert)^2$	$K_2 \frac{4}{\pi}\frac{1}{\omega^2}[1 - \frac{\sin 2x_o\omega}{2x_o\omega}]$	$K_2 \frac{8x_o^2}{3\pi} [1 - \frac{1}{5}(x_o\omega)^2 + \ldots]$
$\frac{K_3}{x_o^2}(2x_o - \lvert\tau\rvert)^3$	$K_3 \frac{12}{\pi}\frac{1}{\omega^2}[1 - (\frac{\sin x_o\omega}{x_o\omega})^2]$	$K_3 \frac{4x_o^2}{\pi} [1 - \frac{13}{120}(x_o\omega)^2 + \ldots]$
$\frac{K_6}{x_o^5}(2x_o - \lvert\tau\rvert)^6$	$K_6 \frac{192}{\pi}\frac{1}{\omega^2}[1 - \frac{5}{(x_o\omega)^2}$	$K_6 \frac{128\, x_o^2}{35\,\pi} [1 - \frac{315}{5680}(x_o\omega)^2 + \ldots]$
	$+ \frac{15}{2(x_o\omega)^4}(1 - \frac{\sin 2x_o\omega}{2x_o\omega})]$	

Note: $\lvert\tau\rvert < 2x_o$

P(x)	Values of Coefficients K_n (multiply all constants by E^2/T)		
double-spiked	$K_1 = \frac{1}{4}$		
flat	$K_3 = \frac{1}{24}$		
gaussian	$K_6 = 0.0031$		
sinusoidal	$K_1 = 0.0061$	$K_2 = 0.0615$	$K_3 = 0.0184$
rectified-sinusoidal	$K_1 = 0.0339$	$K_2 = 0.0919$	$K_3 = -0.00404$

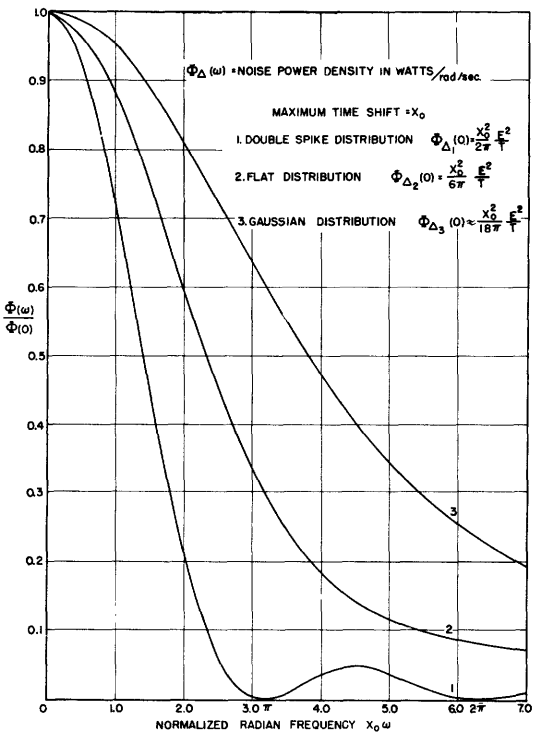

Fig.28 Normalized power spectra of pulse-edge time-shift noise for various probability distributions of time shifts.

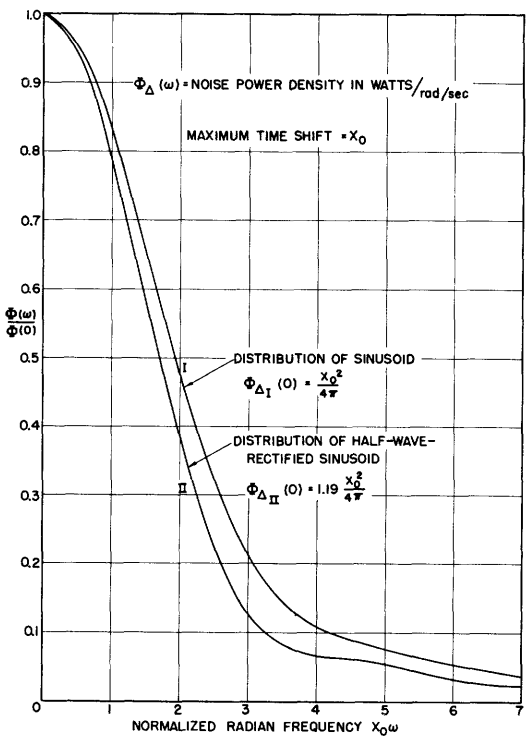

Fig.29 Normalized power spectra of pulse-edge time-shift noise for two different time-shift probability distributions.

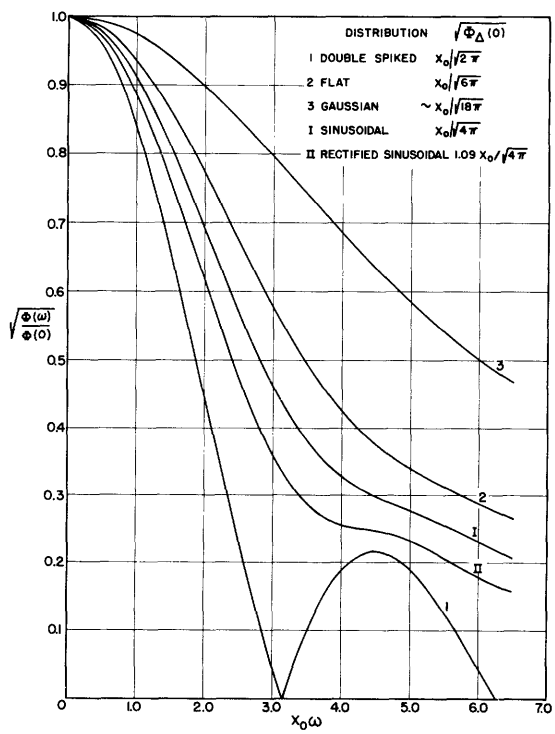

Fig.30 Square roots of normalized power spectra of pulse-edge time-shift noise for various probability distributions of time shifts;
maximum time shift = x_0.

then added to give the desired transform of $\varphi_\Delta(\tau)$. The details of the derivations will be found in Appendix III, and only the results will be listed here. Since the same type of terms occurs repeatedly with different coefficients in (53), (54), (57), (58), and (59), the transforms are given in Table 1 on the next page with the general coefficient K_n, and the various values of K_n for the different cases are listed below the transforms.

It is to be noted that at zero frequency, the Fourier or Laplace transform integrals reduce to the product of $1/2\pi$ and the simple integral

$$\int_{-x_o}^{x_o} \varphi_\Delta(\tau)\,d\tau$$

expressing the area under the function being transformed. For this reason, the power spectrum starts out at $\omega = 0$ with a magnitude equal to the area under $\varphi_\Delta(\tau)$ divided by 2π, from which it drops off in a manner indicated by the power-series approximations given in Table 1.

Graphical plots of the power spectra and the square-roots of the power spectra for all of the probability distributions considered will be found in Figs. 28, 29, and 30. In all of these plots the ordinate has been normalized with respect to the peak power density which always occurs at zero frequency, and the frequency has been normalized with respect to the peak time shift, x_o. The curves are symmetrical about $\omega = 0$, that is, they are mathematically the same for negative frequencies as for positive frequencies. Physically, this means that the actual power density at any actual frequency is twice as much as plotted. The noise represented by these spectra is referred to as one-edge time-shift noise, since only one edge of each pulse is subjected to the time shift, in contrast to two-edge noise to be considered later. Plotting the magnitude of the square root of the power density, though it does not have a direct physical meaning, helps spread the curves and accentuate some of their characteristics, such as the damped oscillations present to some degree in all of the curves. Table 1 shows that the $\sin x_o\omega/x_o\omega$ term, or its equivalent, which is responsible for this oscillation, is present in all of the spectra. This is to be expected of the transforms of all functions with definite limits; however, in the function $(2x_o - |\tau|)^n$, the higher n becomes, the smoother is the transition to zero at $|\tau| = 2x_o$, more and more derivatives become zero at this point, and the less noticeable is the oscillation in the transform.

It is of interest to note that, since the frequency appears as the

normalized variable $x_o\omega$ everywhere, the decrease of the spectra with increasing frequency as well as the location of the maxima and minima, are determined solely by the maximum time-shift excursion. Such factors as average pulse duration and pulse-repetition frequency have no bearing whatever on the noise power spectrum shape, but the magnitude of the spectrum is directly proportional to the pulse-repetition frequency. It is logical, of course, that the maxima and minima, being reflections of the time-shift limits, are most pronounced where the probability distribution favors the extremes, as in the case of the double-spike and the rectified-sinusoid distributions. As previously mentioned, time shifts which follow the double-spike probability distribution are equivalent to randomly missing pulses of a duration $2x_o$, which explains the nulls in the spectrum; these nulls are spaced at $1/2x_o$ cycles per second.

In order to evaluate the audible portion of the noise plotted in the graphs, some values will have to be assumed, such as the top audio frequency and the maximum edge time shift. In order to arrive at the largest audible values of $x_o\omega$ likely to be encountered, suppose that the top audio frequency is 15 kc ($\omega \approx 10^5$ sec^{-1}), and the peak time shift is one microsecond ($x_o = 10^{-6}$ sec). The spectrum is then of direct interest only over the range $0 < x_o\omega < 0.1$, since only the power in this range is audible and contributes to the total audio noise power. Inspection of all the noise spectra and their series approximations in Table 1 shows that the decrease in power density from the zero-frequency value is negligible at $x_o\omega = 1$; even in the "worst" case, that of the double-spike distribution, the drop is only about a third of one per cent, and with the simusoidal distributions, which occur in practice, it is still less. The conclusion is that, for all practical purposes, the audio-noise spectrum is entirely flat before being deformed by the transmission characteristic of the receiver audio system. After passage through this system, the power-density spectrum will therefore have the same shape as the square of the audio transfer characteristic. The total audio-noise power is the area under the final power-density curve, up to the highest audible frequency. Therefore, so long as the audio system characteristic is known, no matter what its shape may be, the output noise spectrum and total noise power can always be computed. They are given by (60) and (61), respectively, in which $H(\omega)$ is the audio-system function, and ω_o the highest audible frequency.

$$\text{Output-Noise Power-Density Spectrum} = H^2(\omega)\Phi_\Delta(\omega) \qquad (60)$$

$$\text{Total Audio-Noise Power } P = 2\int_0^{\omega_e} H^2(\omega)\Phi_\Delta(\omega)\,d\omega \ . \qquad (61)$$

The multiplying factor of two in (61) is required because the integration extends only over positive values of frequency. As shown above, $\Phi_\Delta(\omega)$ changes so little between 0 and ω_e that it can be treated as a constant in the above integral. This constant is $\Phi_\Delta(0)$, and the remaining integral is simply the area under the squared audio-frequency characteristic.

In the ideal pulse system the audio frequency characteristic is flat up to p/2, half the sampling frequency, and is nonexistent above p/2. This is the characteristic of an ideal low-pass filter with cut-off frequency p/2, which is physically unrealizable, but can be approached as closely as desired. With such an audio system, of unity gain, the output-noise power-density spectrum is, of course, substantially constant at the value $\Phi_\Delta(0)$ up to $\omega = p/2$. The exact value of the total output noise power is

$$P_{\text{ideal exact}} = 2\int_0^{p/2} \Phi_\Delta(\omega)\,d\omega \ . \qquad (62)$$

The approximate value, which is within a small fraction of a per cent in most practical cases, is given by

$$P_{\text{ideal approx.}} = 2\,\frac{p}{2}\,\Phi_\Delta(0) = p\Phi_\Delta(0) \ . \qquad (63)$$

It has been mentioned on page 65 that $\Phi_\Delta(0)$ is equal to

$$\frac{1}{2\pi}\int_{-x_o}^{x_o} \varphi_\Delta(\tau)\,d\tau \ ,$$

that is, the area under the correlation curve divided by 2π; also, it was found earlier that this area equals E^2/T times the square of the standard deviation of the time-shift probability distribution, which may be denoted by $\overline{\overline{x}}^2$ or $\overline{\overline{\Delta t}}^2$. Consequently, in this case of the ideal low-pass filter characteristic, the approximate noise power is given by

$$P_{\text{ideal approx.}} = p\Phi_{\Delta}(0) = \frac{p}{2\pi}\int_{-x_o}^{x_o}\varphi_{\Delta}(\tau)d\tau = \frac{1}{T}\int_{-x_o}^{x_o}\varphi_{\Delta}(\tau)d\tau = E^2\frac{\overline{\overline{\Delta t}}^2}{T^2}. \qquad (64)$$

Expression (64), from which it follows that the approximate effective noise voltage at a one-ohm resistance level is equal to $E(\overline{\overline{\Delta t}}/T)$, is a very interesting result. The quantity $\overline{\overline{\Delta t}}$ depends on the probability curve as given by (55). It is also the root-mean-square value of the alternating component of the periodic function $\Delta t(\phi)$, of which successive Δt values are random samples. Clearly, if this function were sampled in orderly fashion to obtain an orderly variation of successive time shifts with at least two samples per period of the function, then the output alternating voltage would have a peak value of $E(\Delta t_{max}/T)$ and an effective or r-m-s value $E(\overline{\overline{\Delta t}}/T)$. This is the same voltage as was obtained for the random noise above; it is the voltage obtained, if, for example, the pulse edge is time-modulated sinusoidally, at less than half the pulse-repetition frequency in which case $\overline{\overline{\Delta t}} = 0.707\ \Delta t_{max}$, and it is independent of the audio-frequency characteristic so long as the gain is unity at the modulating frequency and zero at and above half the pulse-repetition frequency.

The above discussion leads to the following conclusion: random pulse-edge time modulation with a certain mean-effective value produces random noise the total power of which is approximately the same as that produced by periodic modulation with the same mean-effective value, provided that the randomly modulated pulses are passed through an ideal low-pass filter with cut-off at half the pulse-repetition frequency. The periodic modulation is, of course, at a frequency less than half the pulse-repetition frequency, and the audio system through which the periodically modulated pulses are passed, while not necessarily an ideal low-pass filter, must have the same gain at the frequency or frequencies of the periodic modulation as the ideal filter in the random case.

The fact that this relation between the power produced by random and non-random time shifts is only approximate (though very close in all practical cases) is a result of the fact that pulse-time modulation, with the modulation and demodulation processes generally used, does not involve true periodic sampling. The relation would of course be exact if (63) and hence (64) were mathematically exact. This, in turn, would be possible only if $\Phi_{\Delta}(\omega)$ were constant at the value $\Phi_{\Delta}(0)$. In the case of true periodic sampling, it is

easily seen that these conditions are fulfilled. Imagine, for example, that the sequence of samples obtained by random sampling of some periodic function is represented by a succession of impulses of infinitesimal duration, infinite height, and area proportional to the sample value. The aperiodic auto-correlation component is then also necessarily an impulse (in the τ-domain), from which it follows that the noise-power-density spectrum is flat, and the relations described above as approximate are exact. Stated in another way, the samples of a signal produce an ideal low-pass filter response whose mean-square value is dependent only on their amplitude distribution. It is possible, also, to think of the perfect samples as finitely proportioned pulses of sin z/z shape, since such a pulse is the impulse response of the ideal low-pass filter. Rectangular pulses of finite though constant duration cannot represent true samples in the way that impulses or sin z/z pulses can; they are subject to the so-called aperture effect, which appears in the steady-state frequency characteristic as a gradual drop in response with increasing frequency.[23,24] A good treatment of the theory of sampling may be found in a recent publication.[25]

Pulse-time modulation, with the usual modulation and demodulation processes does not represent true sampling for reasons similar to but more complicated than the aperture effect in amplitude-modulated pulses. Not only is the time used to convey the instantaneous sample of finite duration, but the time interval taken to convey it is of variable magnitude and time position, depending on the sample values. As mentioned in Chapter 1, this departure from true sampling shows up as intermodulation distortion in the steady-state sinusoidal characteristic, and it appears in the peculiar drop-off of the power spectrum found in this chapter. In the limit as Δt_{max} approaches zero, all these "symptoms" disappear: the spectrum is stretched in inverse proportion to Δt_{max} or x_o and therefore becomes flat in the limit, showing that perfect sampling is approached with very small time shifts. This is true in spite of the fact that the pulse duration is finite and may in fact be nearly as long as the sampling or pulse-repetition period. That portion of the pulse, of duration $d_o - x_o$, which is never affected by the edge time shift has no effect whatsoever on the alternating component of the output.

The auto-correlation method of analysis thus proves itself a powerful tool in statistical problems in which the conventional approach would be very cumbersome and in which results obtained by logic are frequently unsatisfactory

because of lack of proof and preciseness.

3.4 Auto-Correlation of Two-Edge Time-Shift Noise

It is not difficult to extend the results thus far obtained to the more complicated cases of pulse-edge time shift, in which both pulse edges are involved. Results for two-edge time-shift noise will be directly applicable to various situations in which duration-modulated pulses are the desired signal, and the interfering signal is continuous or consists of pulses with fairly high duty factor. Without further explanation at this point, it suffices to state that three cases of two-edge time-shift noise should be analyzed, in which the time shifts are subject to the following conditions, respectively:

1. The individual time shifts of the two edges of each pulse are independent, as though they were shifts of edges belonging to different pulses. This case calls for very little additional mathematical work beyond that needed in the one-edge case.

2. The time shifts of the two edges of each pulse are equal in magnitude and sense, so that the entire pulse is shifted intact. The noise resulting from such time shifts may be called PPM noise.

3. The time shifts of the two edges of each pulse are equal in magnitude but opposite in sense, so that the duration of the pulse is changed. The noise which results in this case may be called PDM noise. The determination of its spectrum will be found more complicated than that of PPM noise.

Case 1

The simplest way of obtaining a clear picture of how the auto-correlation function differs from that obtained for one-edge time shifts if both edges are shifted independently, is to refer back to Fig. 21 and the four numbered paragraphs on pages 45 and 47. These explain qualitatively how and why the rounded tops and bottoms in the auto-correlation triangles occur. The rounded top of the inter-correlation results from the decreased total overlap when pulses overlap with the shifted replicas of other pulses, as explained in Section 3.2 on page 47. If both edges "wiggle" with the same maximum excursion previously experienced by only one edge, this decrease in overlap is simply doubled. Quantitative analysis by the equivalent nonrandom pulse, which now has two symmetrically sloping edges, instead of only one sloping edge,

confirms this. Inasmuch as the top of the self-correlation is unaffected, the aperiodic component of the auto-correlation, $\varphi_{\Delta}(\tau)$, is just twice as large as that given by (50). The rounded bottoms of the auto-correlation curves were shown to result when the fixed edges of the shifted* function coincide with the time-shift range of the moving edges. This phenomenon was found not to contribute to the aperiodic auto-correlation component, since it is common to both the inter- and self-correlations. In the present case of independent two-edge time shifts, curvatures at the bottoms of the auto-correlation triangles are again common to all of these and hence do not contribute. It is of importance to note, however, that the shape and extent of the curvature are different from those found before, since they are now caused by overlap of the leading-edge time-shift range of the function and the trailing-edge time-shift range of the shifted* function, and vice versa. It is readily seen that the partial overlap of these two regions or ranges, both of which have a width of $2x_o$, extends over $4x_o$, namely from $|\tau| = d_o - 2x_o$ to $|\tau| = d_o + 2x_o$. This is twice as much as the previous extent from $d_o - x_o$ to $d_o + x_o$. The curve, previously given by (46), is now the same shape as the top curve, as might have been expected from the fact that both curvatures are now caused by overlap of two sets of independently shifted edges. Consequently, the expression for the curvature at the bottom is such that if it is subtracted from the straight triangle obtained in the absence of time shifts and translated by an amount d_o to the origin, the result is precisely (50). While this has no effect on the aperiodic component of the auto-correlation in the present case of independent time shifts, it is of primary importance when the shifts of leading and trailing edges are related, as in Cases 2 and 3.

The conclusion, as far as Case 1 is concerned, is that $\varphi_{\Delta}(\tau)$ is the same as for one-edge time-shift noise, except doubled in magnitude. Consequently the power-density spectrum is also doubled in magnitude, but is otherwise unchanged, and the power in a given frequency band is doubled or the rms voltage raised by a factor of the square root of two. It is interesting to note that the effect of subjecting the previously fixed pulse edges to independent time shifts is identically the same as the effect of doubling the pulse-repetition frequency, regardless of the relative spacing between leading and trailing edges, that is, regardless of the average pulse duration.

---

* The word "shift" here refers to the parameter τ of the auto-correlation.

Case 2

Regardless of whether or not the time shifts of the leading and trailing edges are independent, the inter-correlation is determined entirely by the correlation between different pulses with independent time shifts, so that in Case 2, as well as in Case 3 and all other types of two-edge time shifts, the inter-correlation is exactly the same as in Case 1. The self-correlation, on the other hand, is very much dependent on the relation between the time shifts of the two edges of each pulse. The top of the self correlation (at $\tau = 0$) is of course never affected by any time shift, since every pulse completely coincides with its own replica; but the bottom portion (around $\tau = d_o$) is a direct measure of the correlation between the leading edge and trailing edge of the same pulse. In Case 2 the two edges of each pulse shift together, leaving the pulses intact, so that the entire self-correlation is identically the same as without any time shifts, namely a triangle. The quantity of interest is the difference between this triangle and the inter-correlation; as illustrated in Fig. 31. The three separate little "bumps" blend into a single curve if the maximum time shift x_o equals or exceeds one-fourth of the normal pulse duration d_o. The condition $x_o < 1/4\ d_o$ takes the place of the former condition $x_o < 1/3\ d_o$ required in order that there be no overlap between the curved top and bottom portions of the inter-correlation. As before (see 3.2 pages 54-57), it can be shown that the aperiodic auto-correlation component derived under this condition is nevertheless the general result.

From the discussion of Case 1, the expressions for the three "bumps" or lobes in Fig. 31 are already known. The center lobe is given by (50) multiplied by a factor of two.

$$\varphi_{\Delta}(\tau) = \frac{2E^2}{T} \int_{\tau - x_o}^{x_o} \left[\int_{x}^{x_o} P(u)du\right]\left[\int_{-x_o}^{x - \tau} P(u)du\right]dx \ . \qquad (65)$$

The two outside lobes, when inverted and transposed to the origin, are also each given by (50), as will now be shown. Subtraction of the inter-correlation from the straight auto-correlation triangle yields three lobes which are symmetrical about $\tau = 0$ as a group and each of which is symmetrical about its own center if $P(x)$ is symmetrical. The right-hand lobe, for example, is

symmetrical about $\tau = d_o$, extending from $d_o - 2x_o$ to $d_o + 2x_o$. Now, since the triangle (see Fig. 31) extends only as far as $\tau = d_o$, the half of the right-hand lobe between d_o and $d_o + x_o$ is identical to the inter-correlation with reversed algebraic sign. This makes a simple one-step derivation possible, as follows.

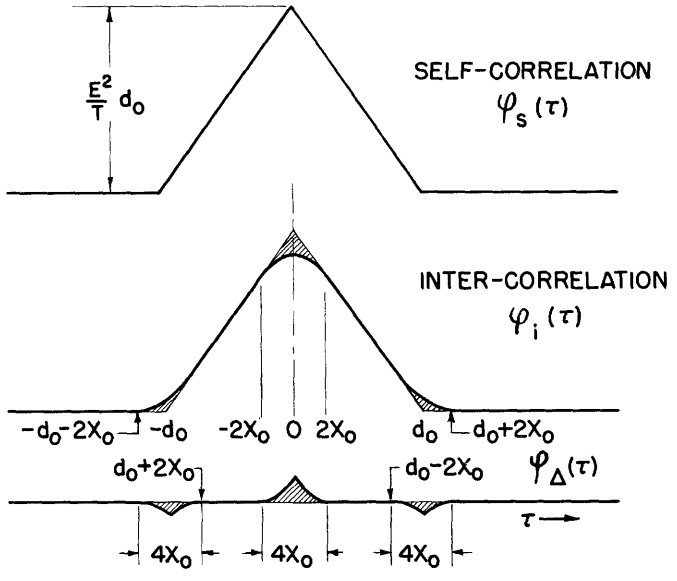

Fig.31 Auto-correlation of "PPM noise".

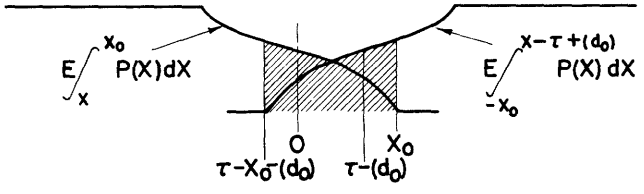

Fig.32 Derivation of inter-correlation of pulses with two-edge time shifts; $(d_o) < \tau < (d_o) + 2x_o$.

Figure 32 illustrates the derivation of the expression for the side lobe of the aperiodic auto-correlation component by the equivalent nonrandom pulse method. The diagram is drawn for the condition $d_o < \tau < d_o + 2x_o$, for which a single multiplication expresses the product of the two curves, and this product divided by T gives the desired correlation component.

With the origin for x chosen, as usual at the average position of the trailing edge, the equivalent trailing edge is given by

$$y_t(x) = E \int_{x}^{x_o} P(x)dx \ .$$

The leading edge of the shifted pulse is centered at $\tau - d_o$ and is therefore given by

$$y_\ell(x - \tau + d_o) = E \int_{-x_o}^{x - \tau + d_o} P(x)dx ,$$

or by

$$y_\ell(x - \tau) = E \int_{-x_o}^{x - \tau} P(x)dx$$

if it is desired to transpose the side lobe to the origin so as to make it symmetrical about $\tau = 0$. While its actual position at $\tau = d_o$ must of course be remembered, it is convenient to delete the d_o wherever it appears in connection with the shifted leading edge, making that edge centered at τ, rather than $\tau - d_o$. The term d_o, although it is included in parenthesis in Fig. 32 is therefore not included in the mathematical expressions below. Since the lobe is symmetrical about $\tau = 0$ if $P(x)$ is symmetrical, only the right half need be given.

$$\underset{\substack{\text{side lobe} \\ \tau \to (\tau \pm d_o)}}{\varphi_\Delta(\tau)} = -\frac{1}{T} \int_{\tau - x_o}^{x_o} y_t(x) y_\ell(x - \tau)dx \qquad (0 < \tau < 2x_o)$$

$$= -\frac{E^2}{T} \int_{\tau - x_o}^{x_o} \left[\int_{x}^{x_o} P(u)du \right] \left[\int_{-x_o}^{x - \tau} P(u)du \right] dx . \qquad (66)$$

The expression on the right-hand side of (66) is recognized as being identical to (50), except for sign, and the above is presumably the simplest possible derivation of this important function. The notation $\tau \to (\tau \pm d_o)$ indicates that, to get the actual positions, τ should be replaced by $\tau \pm d_o$.

Returning to Fig. 31, one finds, therefore, that the two negative side lobes have the same shape as the center lobe, but are each only half as tall and have half the area. The total area, if considered all positive, is exactly four times that under $\varphi_\Delta(\tau)$ as given for one-edge noise by (50); or, if the area of the negative lobes is considered as negative, then the net area

is zero. For a flat probability distribution of time shifts, the three lobes are composed of cubics, as in (53), with the center lobe given by

$$\varphi_{\Delta}(\tau)_{\text{center lobe}} = \frac{E^2}{T} \frac{1}{12x_o^2} [2x_o - |\tau|]^3 . \qquad (67)$$

Plots of $\varphi_{\Delta}(\tau)$ for four different relative values of x_o and d_o will be found on the following page, for the flat probability distribution, to show how the shape varies when the three lobes overlap; the conditions for which Figs. 35 and 36 are plotted cannot, in general, result from interference, since the peak time shift, x_o, cannot exceed the pulse rise or decay time. For asymmetrical probability distributions, the expressions for $\varphi_{\Delta}(\tau)$ are more complicated; the side lobes do not have the same shape as the center lobe and they are not generally symmetrical about their own centers; however their areas are still the same, each equal to one-half the center-lobe area (see Appendix II).

The determination of the power spectrum corresponding to the aperiodic auto-correlation component consisting of three lobes will be postponed until after the consideration of Case 3, which will be found to give three lobes also.

Case 3

Case 2, in which the two edges of each pulse shift in unison, was found to be characterized by a triangular self-correlation. Going to the extreme opposite, Case 3, in which the two edges of each pulse shift together but in opposite senses, one finds a certain departure from the triangular shape. The inter-correlation, as explained under Case 2, does not change. Therefore, that departure from the triangular shape must be solely responsible for changing the end result $\varphi_{\Delta}(\tau)$ of Case 2 to a new result for Case 3. The simplest procedure is therefore to determine the difference or departure of the self-correlation from the triangle, and then to add this to the three lobes obtained previously in Case 2.

The self-correlation departs from the triangular shape in the same general way as in the case of one-edge noise, that is, by the curvature extending to both sides of $|\tau| = d_o$. In the case of one-edge noise, as explained in Section 3.2 on page 47, this curvature is associated with the

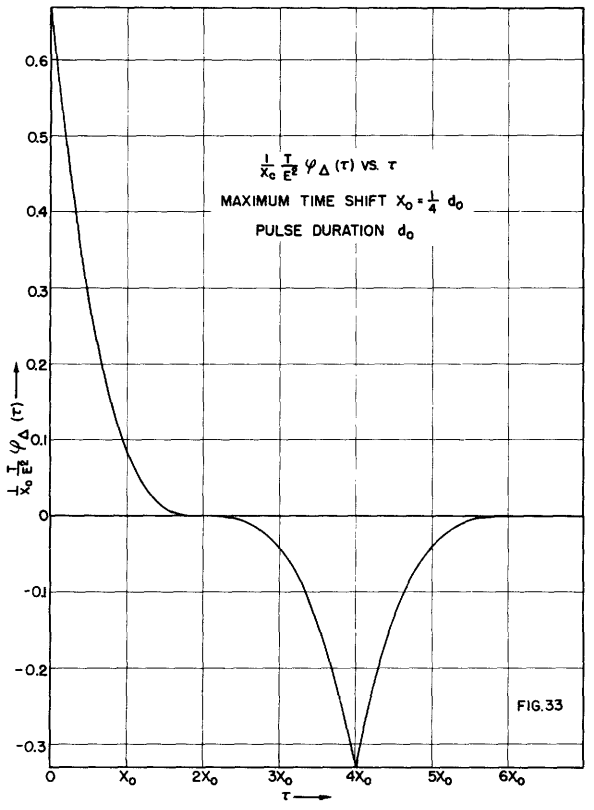

FIG.33

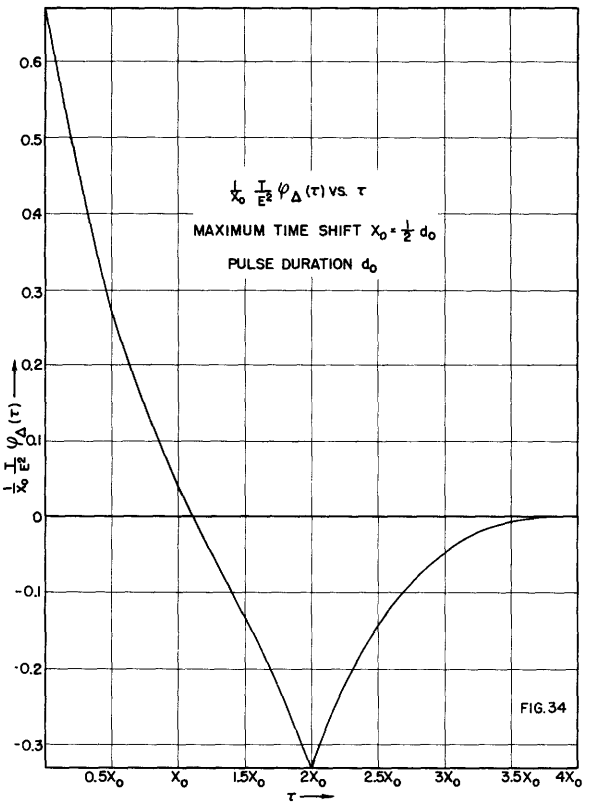

FIG.34

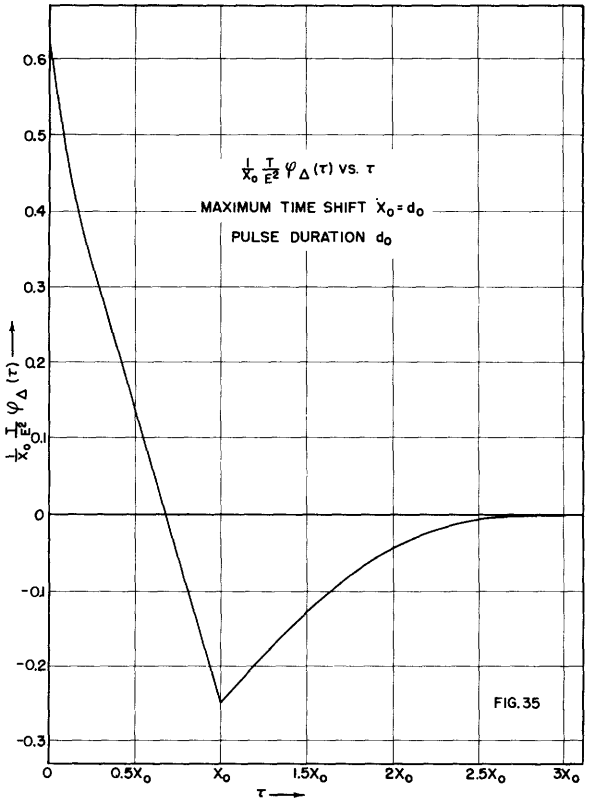

FIG.35

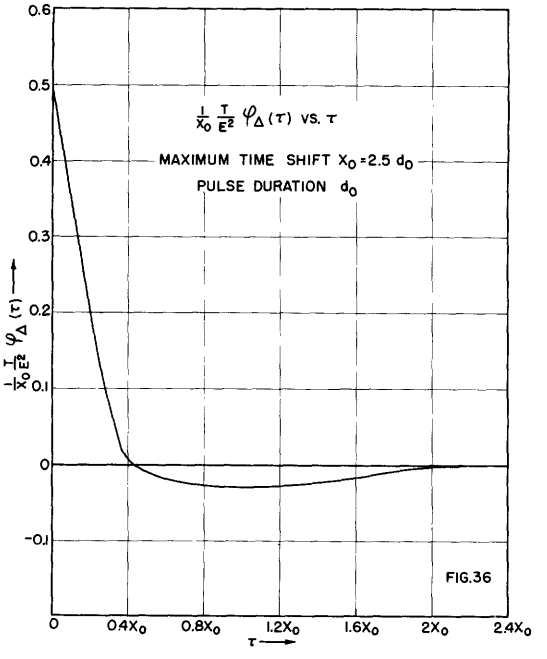

FIG.36

Figs.33-36 Auto-correlation of "PPM noise" for "flat" time-shift distribution; $P(x) = 1/2x_0$.

coincidence of the "shifty" trailing edges and the fixed leading edges, which means that some pulses have some partial overlap with their shifted replicas, and others do not. In the present case, the fixed edges are replaced by edges which are shifted from their normal positions by amounts equal and opposite to the shifts of the other set of edges with which they partially coincide. This is in sharp contrast to the situation associated with the bottom curvature of the inter-correlation, where the two sets of coinciding edges have independent shifts. In the present case, since the relative shifts between the two sets of edges under consideration (e.g., the trailing edges of the pulses and the leading edges of their shifted replicas) are just double the absolute shift of either, it is possible to consider one set of edges fixed and the other shifted twice as far. The equivalent nonrandom pulse principle can then be applied, as shown in Fig. 37, where the leading edge of the right-hand (shifted) equivalent pulse is vertical, and the trailing edge of the left-hand pulse extends symmetrically about the origin over twice the usual range, so that the equivalent maximum time shift is $\Delta t_{max} = 2x_o$. It is clear from Fig. 37 that the product of the two functions will give the entire curved portion of the self-correlation, extending from $\tau = d_o - 2x_o$ to $d_o + 2x_o$. If the triangle, which extends only to $\tau = d_o$, is subtracted out, as shown in Fig. 38, the resulting lobe (as well as its mirror image for negative τ) is symmetrical about its center at $|\tau| = d_o$, in the same way as in the inter-correlation (see Fig. 31) provided that $P(x)$ is symmetrical. The simplest procedure, therefore, is that used in determining the side lobe in Case 2: find the self-correlation in the range $d_o < \tau < d_o + 2x_o$, within which it is also the difference between the self-correlation and the triangle, and then transpose this to the origin. It is only necessary to carry out the multiplication of the overlapping curves in Fig. 37, with d_o deleted, that is with the vertical edge located at τ rather than $\tau - d_o$. The broken curve, therefore, is given by

$$y_\ell(x - \tau) = E \qquad \text{for } x > \tau ,$$

and the solid curve, representing the equivalent trailing edge, is given by

$$y_t(x) = \tfrac{1}{2} \int_x^{2x_o} P(\tfrac{x}{2})\,dx \qquad \text{(to be used for } 0 < x < 2x_o).$$

The expression for $y_t(x)$ differs from (43)(see page 50)by the various factors of two appearing in it; these have the effect of stretching the edge over the

required $\pm 2x_o$ time-shift range. The desired correlation component is given by (68).

$$\varphi_{\Delta}(\tau) \underset{\substack{\text{side-lobe comp.} \\ \tau \rightarrow (\tau \pm d_o)}}{} = \frac{1}{T} \int_{\tau}^{2x_o} y_t(x) y_{\ell}(x - \tau) dx \qquad (0 < \tau > 2x_o)$$

$$= \frac{E^2}{T} \int_{\tau}^{2x_o} \left[\tfrac{1}{2} \int_{x}^{2x_o} P(\tfrac{u}{2}) du\right] dx \qquad (68)$$

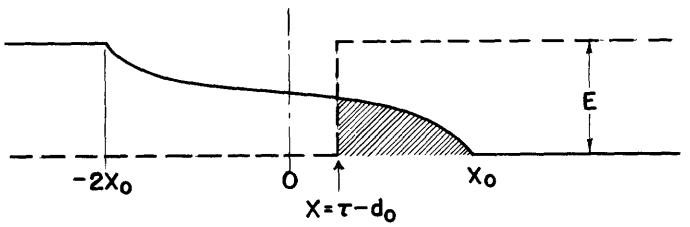

Fig.37 Determination of self-correlation for "PDM time shifts"; $d_o - 2x_o < \tau < d_o + 2x_o$.

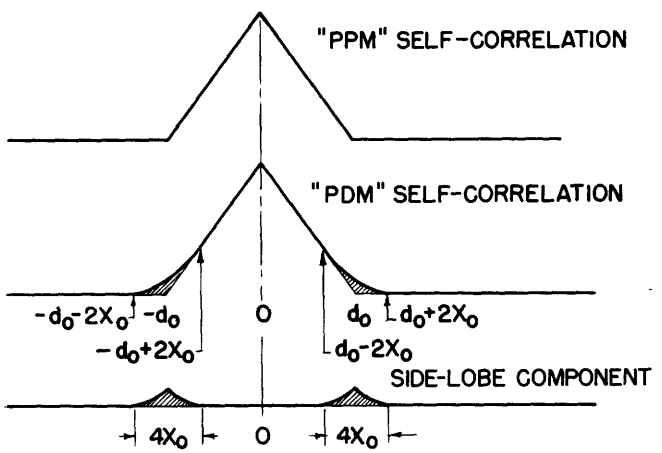

Fig.38 Determination of side-lobe component to be added to auto-correlation of "PPM noise" to give auto-correlation of "PDM noise".

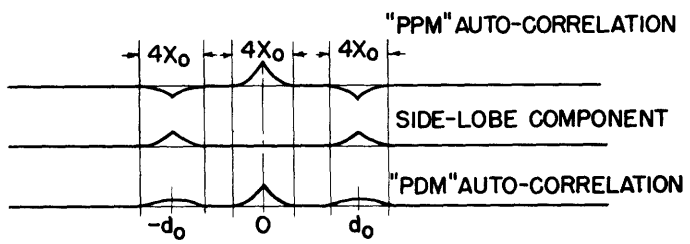

Fig.39 Determination of auto-correlation of "PDM noise".

Figure 39 illustrates how this expression is used to determine the overall aperiodic auto-correlation component for Case 3. Expression (68)

represents the departure of the self-correlation from the triangle; this departure or difference is a side lobe coinciding completely with the side lobe of Case 2, transposed to the origin. It is necessary only to add this side lobe component to the side lobe of Case 2, in order to convert the $\varphi_\Delta(\tau)$ for Case 2 to the $\varphi_\Delta(\tau)$ for Case 3.

The aperiodic auto-correlation component $\varphi_\Delta(\tau)$ for Case 3 consists of three lobes. The center lobe is identical to that obtained also in Case 2, given by (65), repeated here for convenience.

$$\varphi_{\Delta}(\tau)_{\text{center lobe}} = \frac{2E^2}{T} \int_{\tau - x_o}^{x_o} \left[\int_{x}^{x_o} P(u)du \right] \left[\int_{-x_o}^{x - \tau} P(u)du \right] dx \,. \qquad (65)$$

It will be remembered that this gives only the right half of the center lobe the left half (for negative values of τ)being identical. The side lobes are the same as those of Case 2, plus the new additional side-lobe component given by (68). Since the side-lobe expression (66) and the additional component (68) are both referred to the origin, they can be added directly. The resulting expression (69) gives the right half of the new side lobe for Case 3, the left half being identical; while (69) gives the side lobe as being centered about $\tau = 0$, it must be remembered that there are actually two such lobes centered at $\tau = d_o$ and $-d_o$, as indicated by the notation $\tau \rightarrow \tau \pm d_o$.

$$\varphi_{\Delta}(\tau)_{\substack{\text{side lobe} \\ \tau \rightarrow (\tau \pm d_o)}} = \frac{E^2}{T} \int_{\tau}^{2x_o} \left[\tfrac{1}{2} \int_{x}^{2x_o} P(\tfrac{u}{2})du \right] dx - \int_{\tau - x_o}^{x_o} \left[\int_{x}^{x_o} P(u)du \right] \left[\int_{-x_o}^{x - \tau} P(u)du \right] dx \,. \qquad (69)$$

The side lobes of $\varphi_\Delta(\tau)$, given by (69), generally have a different shape than the center lobe, given by (65). The center lobe is positive and generally concave upwards over its entire range, while each of the side lobes is now also positive and generally convex upward over part of its range. An exception occurs in the limiting case of the double-spike probability distribution which makes all three lobes triangular. In spite of the generally different shape, however, it can be shown that the area of each side lobe is exactly half that of the center lobe. The total area under $\varphi_\Delta(\tau)$ is therefore four times that

under the $\varphi_\Delta(\tau)$ lobe for one-edge noise given by (50).

The expressions and plots for the center lobe, which are the same as (50) for one-edge noise, have been previously given and plotted for the five different probability distributions. It will be of interest to evaluate the side-lobe expression (69) for some specific probability distributions. Here again, only the first term need be considered, since the second is the negative of (50) for symmetrical P(x). This first term of (69) is given by the following particular expressions for the double-spike, flat, and sinusoidal probability distribution, respectively:

$$\text{P(x): double-spike:} \quad \frac{E^2}{T}\,\frac{1}{2}[2x_o - |\tau|]$$

$$\text{P(x): flat:} \quad \frac{E^2}{T}\,\frac{1}{8x_o}[2x_o - |\tau|]^2$$

$$\text{P(x): sinusoidal:} \quad \frac{E^2}{T}\,\frac{1}{\pi}\left[2x_o\sqrt{1-\left(\frac{\tau}{2x_o}\right)^2} + \tau \sin^{-1}\left(\frac{\tau}{2x_o}\right) - \frac{\pi}{2}\tau\right]$$

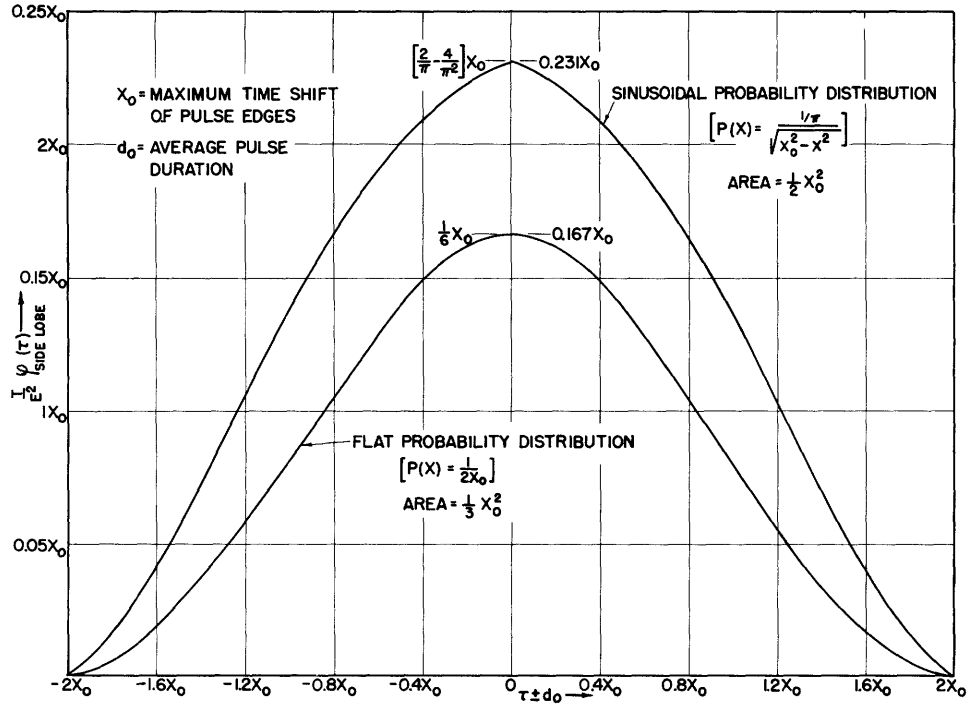

Fig.40 Side lobe of $\varphi_\Delta(\tau)$ for "PDM time shifts"; $\varphi_{\text{side lobe}}(\tau)$ vs. τ.

The second term of (69) to be subtracted from these three expressions is given by (54), (53), and (58), respectively. In the case of the double-spike distribution, the resultant expression for the side lobe (both terms of (69)) is given by $(E^2/T)\frac{1}{4}[2x_o - \square\tau\square]$, a triangle; for the flat distribution it is a quadratic curve minus a cubic, while it is still more complicated for the sinusoidal distribution. Graphical plots of one of the side lobes for the flat and sinusoidal probability distributions, respectively, are given in Fig. 40. The overall aperiodic component of the auto-correlation, $\varphi_\Delta(\tau)$, has the appearance of a center lobe, and two side lobes which generally have shapes different from that of the center lobe, are less than half as tall, but each have just half the area. If d_o is less than $4x_o$, they blend into a single curve. Plots of $\varphi_\Delta(\tau)$ for three different relative values of x_o and d_o will be found in Figs. 41, 42, and 43.

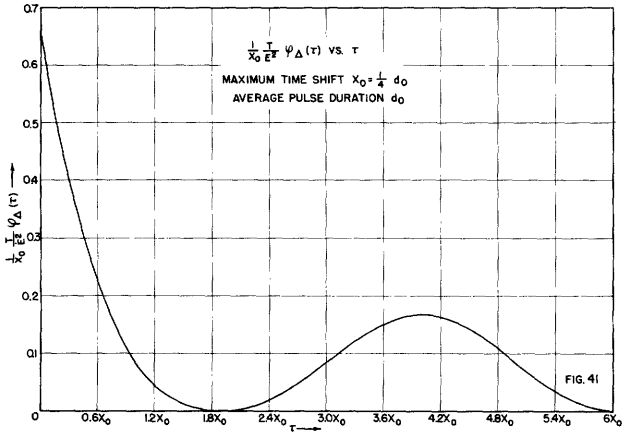

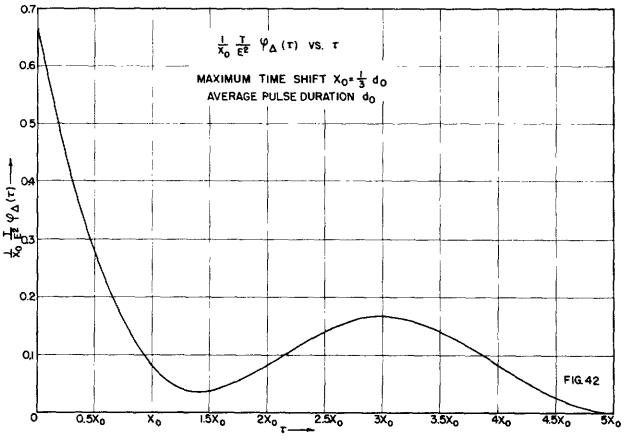

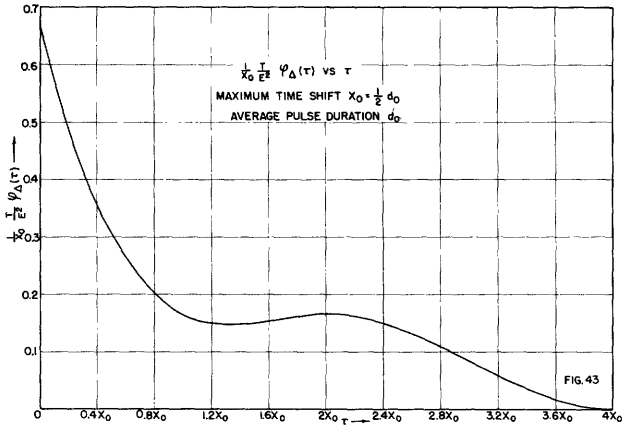

Figs.41-43 Auto-correlation of "PDM noise" for "flat" time-shift distribution; $P(x) = 1/2x_o$.

Before proceeding to the power-density spectra for two-edge time-shift noise, the findings of the preceding pages will be recapitulated. In Case 1

(see page 70), the aperiodic auto-correlation component, $\varphi_\Delta(\tau)$, was found to consist of a single lobe identical to that found for one-edge time shifts, except that it is twice as large in magnitude. Consequently, the power spectrum is simply multiplied by two. In Case 2, $\varphi_\Delta(\tau)$ was found to be composed of three lobes, a large center lobe identical to that of Case 1, and two negative side lobes each half as large in area. Finally, in Case 3, $\varphi_\Delta(\tau)$ is also composed of three lobes, the center lobe being the same as in Case 2, the two side lobes being positive and each having half the area of the center lobe.

3.5 Power Spectra of Two-Edge Time-Shift Noise

Since the power-density spectra have already been determined for one-edge time shifts with the various probability distributions, it will not be difficult to determine them for the various cases of two-edge time-shift noise. For Case 1, in which the edges of each pulse have independent time shifts, it has already been noted that the spectrum is the same as for one-edge time-shift noise, except multiplied by two. Certain facts can be seen by inspection for Cases 2 and 3 also. The zero-frequency power density, $\Phi_\Delta(0)$, is proportional to the algebraic total of the area under $\varphi_\Delta(\tau)$. In Case 2 ("PPM noise"), this total area is zero, since the side lobes just cancel the central lobe. In Case 3 ("PDM noise"), it is four times as large as for one-edge noise with the same time-shift distribution and same maximum time shift. The expressions for the complete spectra in Cases 2 and 3 can be found by using the previously obtained transforms and by applying the theorem of real translation to account for the "off-center" location of the side lobes. This theorem states that, if the Fourier transform of $f(t)$ is $F(j\omega)$, the transform of $f(t \pm a)$ is $\epsilon^{\pm ja\omega}F(j\omega)$, under certain conditions. In the present case, $f(t \pm a)$ will be replaced by the side lobes of $\varphi_\Delta(\tau)$, $\epsilon^{\pm ja\omega}F(j\omega)$ by the component of $\Phi_\Delta(\omega)$ corresponding to the side lobes, and the translation distance $\pm a$ will actually be $\pm d_o$.

Consider Case 2, where, if $P(x)$ is symmetrical, the side lobes are identical in shape to the center lobe, differing only in sign and in magnitude by a factor of two. The spectrum contribution of the center lobe is the same as for one-edge time-shift noise (see Table 1, page 6), multiplied by two, that is, $2\Phi_{\Delta_{\text{one-edge}}}(\omega)$. The spectrum contributions of the two side lobes are $-\Phi_{\Delta_{\text{one-edge}}}(\omega)\,\epsilon^{+jd_o\omega}$ and $-\Phi_{\Delta_{\text{one-edge}}}(\omega)\,\epsilon^{-jd_o\omega}$, respectively. The total side-lobe

contribution is therefore $-\Phi_{\Delta}(\omega)_{\text{one-edge}}\,[\epsilon^{jd_o\omega} + \epsilon^{-jd_o\omega}]$, and this is equal to $-2\Phi_{\Delta}(\omega)_{\text{one-edge}} \cos d_o\omega$. The power-density spectrum of the complete three-lobe combination will therefore be given by (70) as follows.

$$\Phi_{\Delta}{}_{\text{two-edge, Case 2}} = 2\Phi_{\Delta}(\omega)_{\text{one-edge}} \times [1 - \cos d_o\omega]. \qquad (70)$$

The spectrum is seen to have nulls at frequencies for which $d_o\omega$ equals zero and $2\pi n$ (where n is any integer), that is, it has nulls at zero frequency, at the frequency (expressed in cps) which is the reciprocal of the average pulse duration d_o, and at all multiples of this frequency. Between these nulls, the spectrum has maxima which reach four times the corresponding magnitude of the one-edge time-shift spectrum. This is correct regardless of whether or not the three lobes have partial overlap and blend into a single curve, since the law of superposition can be applied in either case. As an example of this spectrum in a typical case, a plot is shown in Fig. 44 for the flat probability distribution and $d_o = 4x_o$, the border-line case in which the three lobes just touch. The corresponding plot of $\varphi_{\Delta}(\tau)$ was given in Fig. 34. The audio-frequency portion of the spectrum is, of course, of primary interest; the low-frequency behavior is now governed principally by the average pulse duration, d_o, rather than by the peak-edge time shift, x_o. It will be of interest to compare the total audio-noise power with that obtained for one-edge noise in (64) on page 68, under similar conditions. The same ideal pulse system will be assumed, in which the audio system has an ideal low-pass filter characteristic with unity gain up to $\omega = p/2$, half the sampling frequency. The very good approximation introduced in (63) and (64) will again be used here, that is, $\Phi_{\Delta}(\omega)_{\text{one-edge}}$ will be assumed constant at $\Phi_{\Delta}(0)$ between $\omega = 0$ and $p/2$.

The total audio-noise power will then be given, in a manner analogous to (63), within close approximation, by (71).

$$P_{\substack{\text{two-edge}\\ \text{Case 2}}} \approx 2\Phi_{\Delta}(0)_{\text{one-edge}}\; 2\int_0^{\frac{p}{2}} (1 - \cos d_o\omega)\,d\omega\,. \qquad (71)$$

Then, in the same way in which (64) results from (63), and by carrying out the integration, the following relation can be derived from (71).

$$P_{\substack{\text{two-edge} \\ \text{Case 2}}} \approx E^2 \frac{\overline{\overline{\Delta t}}^2}{T^2} \frac{4}{p}\left[\frac{p}{2} - \frac{1}{d_o} \sin \frac{pd_o}{2}\right] . \tag{72}$$

The ratio of two-edge "PPM noise" to one-edge time-shift noise, under the conditions assumed, denoted by R_{ppm}, is therefore given by (73).

$$R_{ppm} = \frac{4}{p}\left[\frac{p}{2} - \frac{1}{d_o} \sin \frac{pd_o}{2}\right] . \tag{73}$$

This can be approximated by using the first two terms of the series expansion of sin $pd_o/2$, the first one of which cancels the $p/2$ term, yielding

$$R_{ppm} \approx \frac{\pi^2}{3} D^2 , \tag{74}$$

where D denotes the duty factor, d_o/T or $pd_o/2\pi$. The approximate expression for the two-edge Case 2 noise power then becomes

$$P_{\substack{\text{two-edge} \\ \text{Case 2}}} \approx E^2 \frac{\overline{\overline{\Delta t}}^2}{T^2} \frac{\pi^2}{3} D^2 . \tag{75}$$

The error in this approximate expression, which results from neglecting the other terms in the expansion is approximately plus twelve per cent in the worst case (duty factor $D = \frac{1}{2}$), and decreases rapidly with decreasing duty factor. It may be appreciated that such an error, giving a slightly higher result, is unimportant in view of the limited significance of the noise-power ratio R_{ppm}. This limited significance results from the fact that the two spectra being compared have radically different shapes. For the same total power, the "ppm-noise" with its emphasis on high frequencies is more annoying than the flat one-edge noise; on the other hand, this effect can be offset by de-emphasis of the high frequencies.

It is instructive to substitute some particular figures into (74) so as to obtain some numerical values of the ratio of "ppm-noise" power to one-edge noise power. Consider the two extremes likely to be encountered in practice in a PDM system (or any PTM system if demodulation consists merely of low-pass filtering).* A low duty-factor value may be 0.02, which makes the noise-power ratio given by (74) equal to approximately 0.0013, or little more than one-tenth of one per cent, corresponding to a difference of almost 49 decibels. On the other hand, a high duty factor may be D = 1/3, and in this case the noise-power ratio as given by (74) would be 0.35, which means that the two-edge noise is still approximately 9 decibels lower than one-edge noise.

The approximate expression (72) for the total audio-noise power can also be obtained without the use of auto-correlation analysis by heuristic methods, as will be shown in a later chapter (see Section 4.5).** Such methods, however, give rather incomplete pictures in general and frequently do not show whether or not a result is approximate or exact, or how large the error of approximation is. For this reason, the auto-correlation analysis is, of course, much to be preferred.

Case 3 is somewhat more complicated than Case 2, as indicated by the fact that the auto-correlation side lobes generally have different shapes than the center lobe. If one ignores the difference in shape momentarily, so that $\varphi_{\Delta}(\tau)$ for Case 3 differs from $\varphi_{\Delta}(\tau)$ for Case 2 only in that the side lobes are positive rather than negative. In this way, one quickly obtains a good idea of the appearance of the power spectrum. It is then easy to see that the resultant spectrum is derived exactly as in Case 2, except for the reversal in the algebraic sign of the side-lobe contributions to the spectrum. The approximate result is given by (76).

$$\underset{\substack{\text{two-edge}\\ \text{Case 3}}}{\Phi_{\Delta}(\omega)} \approx 2\underset{\text{one-edge}}{\Phi_{\Delta}(\omega)} [1 + \cos d_o\omega] . \qquad (76)$$

---

* The results of this chapter will also be applied to PPM systems.

** It is also shown how the above results are extended to cover the asymmetrical rectified-sinusoid time-shift distribution.

This spectrum is complementary to that given by (70) in that the zeros and the approximate locations of the maxima are interchanged. Its zero-frequency value is four times that of the one-edge time-shift noise spectrum, and the rate of decrease with increasing frequency depends primarily on the average pulse duration d_o. The approximate plot is superimposed on the exact plot shown on page 87, and the agreement is seen to be good at low frequencies.

The exact expression for the spectrum in Case 3 is obtained by adding to the spectrum of Case 2 the additional large spectrum contribution due to the side-lobe components given by (68) or the first term of (69). This additional spectrum contribution can be evaluated for any symmetrical probability distribution by substituting the particular P(x) in (68), taking the transform of the result by the method of translation and sectioning, and multiplying the result by cos $d_o\omega$ to account for the off-center side-lobe location. The particular side-lobe component expressions for three of the probability distributions considered earlier were given on page 80. Addition of one of these to the corresponding $\varphi_\Delta(\tau)$ for Case 2 gives the desired $\varphi_\Delta(\tau)$ for Case 3. With the double-spiked probability distribution this leads to a result which is identical to the approximate result of (76); with the flat distribution, for which various plots of $\varphi_{\Delta\,\text{two-edge, Case 3}}(\tau)$ have been given in Figs. 41, 42, and 43 and therefore serve as a good illustration.

If the transform or spectrum contribution of the side-lobe components (68) is denoted by $\Phi_{\Delta\,s.\ell.c.}(\omega)$, then a general expression for the composite spectrum in Case 3 can be written as follows.

$$\Phi_{\Delta\,\text{two-edge Case 3}}(\omega) = 2\Phi_{\Delta\,\text{one-edge}}(\omega) + 2[\Phi_{\Delta\,s.\ell.c.}(\omega) - \Phi_{\Delta\,\text{one-edge}}(\omega)]\cos d_o\omega \,. \qquad (77)$$

For the flat probability distribution, the corresponding auto-correlation components are as follows (see page 81).

$$\varphi_{\Delta\,\text{one-edge}}(\tau) = \frac{E^2}{T}\frac{1}{24x_o^2}[2x_o - |\tau|]^3$$

$$\varphi_{\Delta\,s.\ell.c.}(\tau) = \frac{E^2}{T}\frac{1}{8x_o}[2x_o - |\tau|]^2 \,. \qquad (53)$$

The transforms will be found in Table 1 on page 63; substituting them into (77) gives the following expression for the complete power spectrum.

$$\Phi_{\Delta}(\omega)_{\substack{\text{two-edge}\\ \text{Case 3}}} = \frac{E^2}{T}\frac{1}{\pi}\frac{x_o^2}{\omega^2}\left[1 - \left(\frac{\sin x_o\omega}{x_o\omega}\right)^2\right] + \frac{E^2}{T}\frac{1}{\pi}\frac{x_o^2}{\omega^2}\left\{\left[1 - \frac{\sin 2x_o\omega}{2x_o\omega}\right] - \left[1 - \left(\frac{\sin x_o\omega}{x_o\omega}\right)^2\right]\right\}\cos d_o\omega \ . \qquad (78)$$

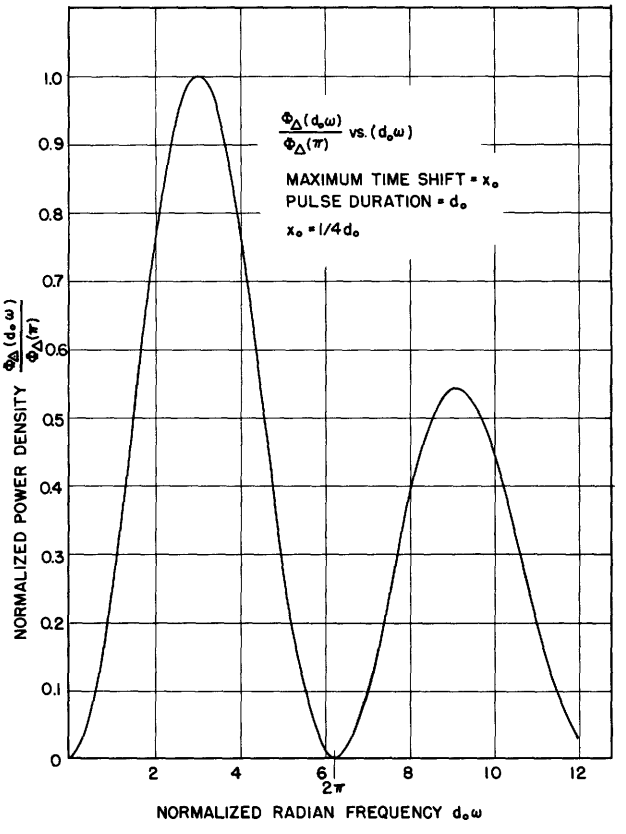

Fig.44

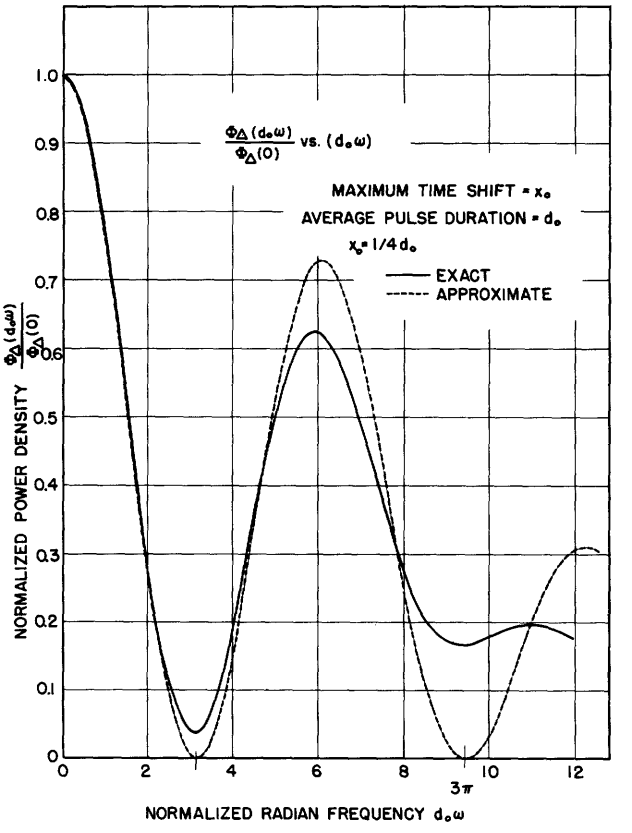

Fig.45

Figs.44-45 Normalized power spectra of two-edge time-shift noise for flat probability distribution of time shifts; Fig.44: Case 2 ("PPM"); Fig.45: Case 3 ("PDM").

A plot of this exact expression for the spectrum is shown in Fig. 45, with the plot of the appropriate expression (76) superimposed in broken lines, for the borderline case $d_o = 4x_o$ in which the three lobes just touch, the same condition for which the spectrum was plotted in Case 2 (Fig. 44).

The total audio-noise power will again be computed and compared to the results previously obtained in other cases. As a first approximation, it may be stated that this power is four times as great as for one-edge time-shift noise under similar conditions. This ignores the more rapid decrease with increasing frequency of the spectrum under consideration, and therefore gives too high a result, expecially for large duty factors. With a duty factor of 0.50, the error is about twenty-five per cent, while it is less than one per cent with a duty factor of 0.10, decreasing approximately as the square of the duty factor. The ideal low-pass filter characteristic with cut-off at half the pulse-repetition frequency is assumed.

A more accurate comparison can be obtained by integrating the approximate expression (76) over the audio band from $\omega = 0$ to $p/2$. since this is rather accurate within this low-frequency range (see Fig. 45). Assuming $\Phi_{\Delta}(\omega)_{\text{one-edge}}$ constant at $\Phi_{\Delta}(0)$ over this range, one obtains, in a manner analogous to (63) and (71), the following expression.

$$P_{\substack{\text{two-edge} \\ \text{Case 3}}} \approx 2\Phi_{\Delta}(0)_{\text{one-edge}} \, 2 \int_{0}^{\frac{p}{2}} [1 + \cos d_{o}\omega] d\omega \, . \tag{79}$$

By carrying out the integration and making use of (64), one arrives at the following two relations, which differ from the corresponding relations (72) and (73) for Case 2 only by the algebraic sign of the second term. R_{pdm} denotes the ratio of two-edge "PDM-noise" power to one-edge time-shift noise power.

$$P_{\substack{\text{two-edge} \\ \text{Case 3}}} \approx E^2 \frac{\overline{\Delta t}^2}{T^2} \frac{4}{p}\left[\frac{p}{2} + \frac{1}{d_{o}} \sin \frac{p d_{o}}{2}\right] . \tag{80}$$

$$R_{pdm} \approx \frac{4}{p}\left[\frac{p}{2} + \frac{1}{d_{o}} \sin \frac{p d_{o}}{2}\right] . \tag{81}$$

It is of interest to note that R_{ppm} and R_{pdm}, as given by (73) and (81), respectively, add up to a constant, four. This indicates that, in the low-frequency range, the power spectra for Cases 2 and 3 of two-edge time-shift

("PPM and PDM noise", respectively) are complementary; their sum is nearly constant at four times the one-edge noise-power density value. This fact has no great practical significance but may be found helpful in connection with the discussion of two-edge time-shift noise in the next chapter (4.5).

By using the first two terms of the series expansion of sin $pd_o/2$, and designating the duty factor $pd_o/2\pi$ by the symbol $\underline{D}$, the following approximate formula for R_{pdm} is obtained. It has a small negative error which reaches only a few per cent even at the highest duty factors.

$$R_{pdm} \approx 4 - \frac{\pi^2}{3} D^2 \ . \qquad (82)$$

To give a numerical example: with the low duty factor value 0.02, the ratio is 4.00, and with the rather high value 0.3, the ratio is approximately 3.7.

In the light of the discussion of true and approximate sampling, on pages 68 and 69, the following is readily seen: samples in the form of symmetrically duration-modulated pulses are still further from being true samples than those in the form of asymmetrically duration-modulated pulses. The limiting factor cannot be the finite pulse-edge time shift, but rather the finite pulse duration which is bound to be larger. It must be pointed out, however, that this would refer only to true symmetrical PDM in which each sample of a periodic sequence of samples advances the leading edge of a pulse by the same amount by which it retards the trailing edge, or vice versa. Such modulation is not generally used in practice, but a steady-state spectrum analysis of it has appeared in the literature.[10] The exact type of time modulation, of course, has no bearing at all on the results obtained for the interference noise; only the demodulation process, so far assumed to consist of ordinary low-pass filtering, is of importance.

In closing the present discussion of two-edge time-shift, one point should be made clear. As indicated, general formulas derived for the three-lobe aperiodic auto-correlation component and then for the noise-power density hold only for symmetrical probability distributions. While they are not radically different for asymmetrical distributions, such as the rectified-sinusoid distribution, they are more complicated, inasmuch as the auto-correlation side lobes are asymmetrical. The expressions for these asymmetrical side lobes can be derived in the same way as the simpler expressions for the symmetrical

side lobes, by the equivalent nonrandom pulse method. The Fourier transform giving the power-spectrum contribution of the asymmetrical side lobes can be found by the same method of translation and sectioning used previously. The difference in shape of the side lobes has relatively little effect on the end result, especially on the spectrum at low frequencies, since the area relations of the three auto-correlation lobes are preserved. In order to prove this, the exact solutions for two asymmetrical distributions are given in Appendix II. The general results for two-edge time-shift noise, although derived on the basis of symmetrical time-shift distributions, will give close answers also when asymmetrical distributions are substituted for P(x).

3.6 Auto-Correlation of Missing-Pulses Noise

As previously indicated, the so-called missing pulses effect can be treated as a special case of one-edge time shift with a double-spiked probability distribution, by adjusting the relative spike areas in accordance with the fraction of missing pulses F, and letting $d_o = 2x_o$. The spike areas, which, of course, always add up to unity, will be F and 1 - F, respectively, and these will therefore be the respective values of the two integrals in (50). The quantities F and 1 - F are seen to be interchangeable inasmuch as only their product appears in (50), which means that the aperiodic auto-correlation component is the same for 30 per cent missing pulses as for 70 per cent missing pulses. Expression (50) thus adapted to give $\varphi_\Delta(\tau)$ for the missing pulses effect becomes

$$\varphi_\Delta(\tau) = \frac{E^2}{T} \int_{-d_o + \tau}^{d_o} (F)(1 - F)dx \,. \qquad (-d_o < \tau < d_o) \qquad (83)$$

Evaluating this integral yields the expression for the aperiodic component of the auto-correlation, a triangle of height $(E^2/T)2d_o(F - F^2)$ and width $2d_o$.

$$\varphi_\Delta(\tau) = \frac{E^2}{T}(F - F^2)(d_o - |\tau|) \,. \qquad (-d_o < \tau < d_o) \qquad (84)$$

The same result can also be obtained more directly (rather than by way of (50)) by considering the missing-pulses effect as a separate phenomenon

rather than a special case of the time-shift effect. This direct derivation will now be given. The value of the auto-correlation at $\tau = 0$ is equal to the mean power of the function, since there is complete overlap between f(t) and f(t + τ). This value is $(E^2/T)(d_o)$ for the perfectly periodic sequence of rectangular pulses, and if a fraction F of these pulses is missing, then $\varphi_\Delta(0)$ is equal to $(E^2/T)d_o(1 - F)$. As $|\tau|$ increases, the overlap decreases linearly, reaching zero at $|\tau| = d_o$, forming a triangle just as in the case of the periodic pulse train, except with all ordinates multiplied by (1 - F). This is the portion of the auto-correlation which has been designated by the title "self-correlation", since it contains only the correlation of every pulse with itself. Figure 46 shows the pulse train with randomly missing

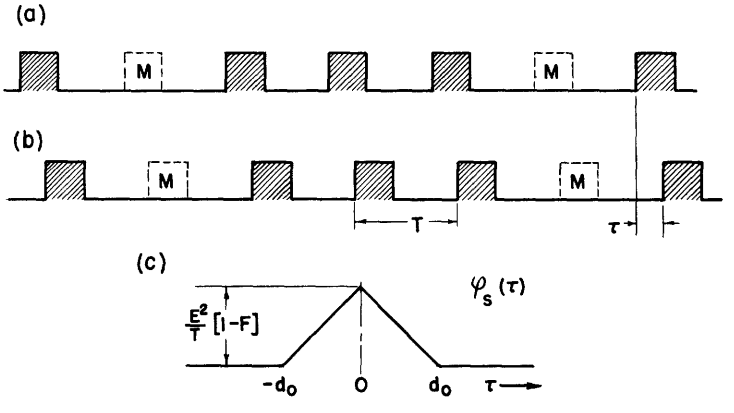

Fig.46 (a) Pulse train with randomly missing pulses; (b) shifted replica of (a) for $-d_o < \tau < d_o$ (τ = shift); (c) self-correlation of pulse train.

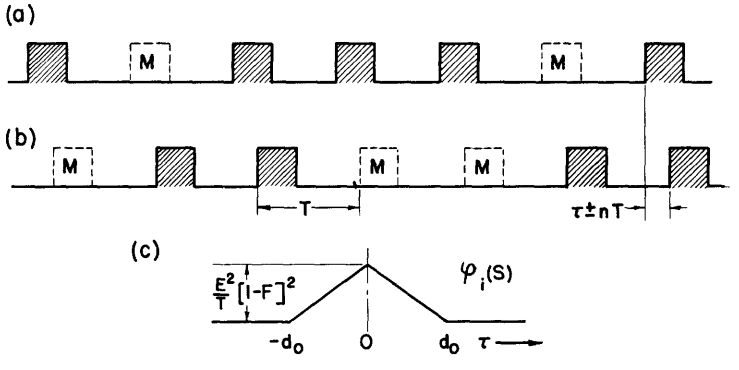

Fig.47 (a) Pulse train with randomly missing pulses; (b) shifted replica of (a) for $-d_o < \tau+nT < d_o$ [$n \neq 0$]; (c) inter-correlation of pulse train.

pulses, as well as its shifted replica, and the resulting self-correlation. Figure 47 shows how the inter-correlation is obtained (for the auto-correlation values of $|\tau|$ large enough so that pulses overlap with the shifted replicas of other pulses). It is readily seen that the overlap must still change linearly with τ and form triangles of width $2d_o$, but the maximum overlap or height of each triangle is decreased by a larger factor than in the case of the

self-correlation. The probability that a certain pulse is present is 1 - F, but the probability with which the partially overlapping pulse is present is also 1 - F. Since the presence of both is required to produce the overlap, the probability of this overlap is $(1 - F)^2$, and this is the factor by which the height of the inter-correlation triangle is reduced from the maximum $(E^2/T)(d_o)$. The inter-correlation is therefore given by $(E^2/T)d_o(1 - F)^2$ $(2d_o - |\tau|)$. Subtraction of this from the self-correlation, $(E^2/T)d_o(1 - F)$ $(2d_o - |\tau|)$ yields the aperiodic component of the auto-correlation

$$\varphi_\Delta(\tau) = \frac{E^2}{T}\left\{[1 - F] - [1 - 2F + F^2]\right\}(d_o - |\tau|) = \frac{E^2}{T}[F - F^2](d_o - |\tau|). \qquad (85)$$

This result is identical to that obtained by the time-shift method, from (50). It applies, of course, only if pulses are missing from an otherwise unimpaired pulse train; if time shifts of the edges are also present, the correlations of the two effects can not be simply superposed, as will be shown in the next chapter.

3.7 Power Spectrum of Missing-Pulses Noise

The power spectrum of missing-pulses noise can be obtained from Table 1 (page 63), which lists the Fourier transform of $K_1(2x_o - |\tau|)$, $[-2x_o < \tau < 2x_o]$. In the present application, $2x_o$ is replaced by d_o, and K_1 is equal to $(E^2/T)[F - F^2]$, so that the power-density spectrum is given by the following expression.

$$\Phi_\Delta(\omega) = \frac{E^2}{T}\frac{2}{\pi}[F - F^2]\left(\frac{d_o}{2}\right)^2\left[\frac{\sin\left(\frac{d_o\omega}{2}\right)}{\frac{d_o\omega}{2}}\right]^2 . \qquad (86)$$

A plot of this spectrum is shown on the following page in Fig. 48, and, except for scale factors, this is seen to be identical to the spectrum plotted in Fig. 28 for the time-shift noise with the double-spike distribution. Nulls occur at $d_o\omega = 2\pi, 4\pi, \ldots 2n\pi$, corresponding to frequencies $f = 1/d_o$, $2/d_o, \ldots n/d_o$, and the general variation is quite similar to that found in the approximated spectrum for Case 3 of two-edge time-shift noise ("PDM noise"), which has nulls at the same frequencies.

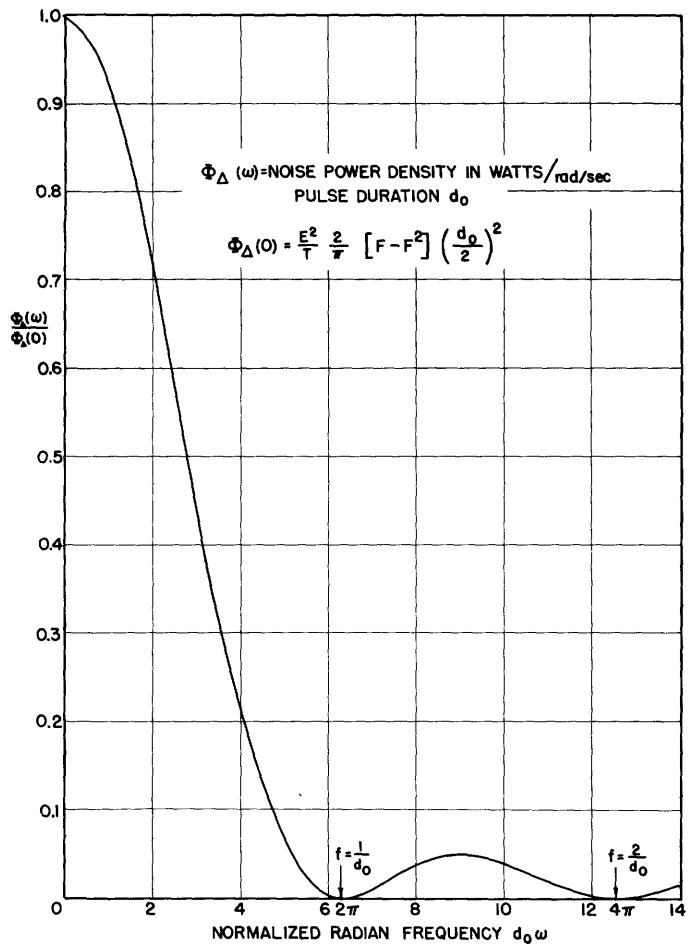

Fig.48 Normalized power spectrum of missing-pulses noise.

The total audio-noise power can be roughly approximated by assuming $\Phi_\Delta(\omega)$ constant at $\Phi_\Delta(0)$ for $\omega = 0$ to $p/2$. Remembering the factor of two to account for the mathematically negative frequencies, one obtains (87), in which the subscript "mp" denotes missing pulses, and $D = d_o/T$.

$$P_{mp} \approx p\Phi_\Delta(0) = E^2D^2[F - F^2]. \qquad (87)$$

A more accurate expression can be obtained by approximating the frequency dependent $[(\sin z)/z]^2$ (see (86)) by the first two terms of its series expansion $1 - (z^2/3)$.

$$P_{mp} \approx 2\Phi_\Delta(0)\int_0^{\frac{p}{2}} [1 - \frac{d_o^2}{12}\omega^2]d\omega = p\Phi_\Delta(0)[1 - \frac{\pi^2}{36}D^2] = E^2D^2[F - F^2][1 - \frac{\pi^2}{36}D^2]. \quad (88)$$

Expression (88) is accurate within one per cent for all values of the duty factor D, and it differs from (87) appreciably only for large values of D. The error in (87) is less than eight per cent at D = 0.50, and less than a third of one per cent at D = 0.10.

Because of the small number of variables involved, the missing-pulse phenomenon in its basic form, that is, with complete pulses rather than parts of pulses missing, is seen to be considerably simpler than the time-shift effect. Certain interference situations in two-station PDM interference involve the missing-pulses effect in somewhat more complicated form, as will be seen in the next chapter.

CHAPTER 4

NOISE FORMULAS FOR SPECIFIC INTERFERENCE SITUATIONS

In order that the results of the preceding chapter may be properly applied to the great variety of possible situations involving interference, these situations must be examined in sufficient detail to allow the problem to be stated in terms of the interference effects discussed and analyzed in the preceding two chapters. In the simplest situations -- simplest, that is, from the viewpoint of simplicity of analysis -- the time-shift effect can be applied directly without any further modifications of the basic results obtained in Chapter 4; in others the missing-pulses effect applies directly in its basic form. These simple situations, although not the most important from a practical point of view, will be considered first, giving an opportunity to consolidate some of the ideas of the last chapter.

4.1 One-Edge Time-Shift Noise in PDM

It has been stated previously that, with interference ratios less than one-half, time-shift noise is the only manifestation of the interference. This presupposes, of course, that the slicing level is above the interference level a, usually adjusted to one-half the height of the desired pulses. In certain cases, in which the interference consists of a train of pulses repeating synchronously or almost synchronously with the desired pulses, this interference overlaps only, say, the leading edge of each desired pulse. This condition may persist for several seconds or minutes, after which it will shift to the other pulse edge, or it may persist indefinitely. Two-path transmission might result in just such a situation, as is shown in Fig. 49, where

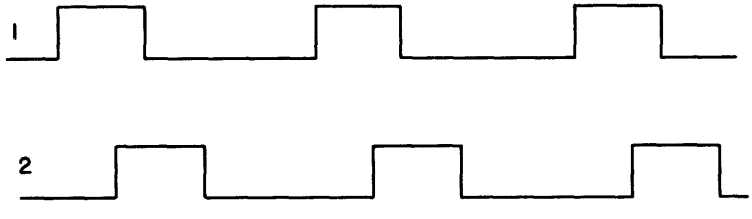

Fig.49 Partial overlap of synchronous pulse trains causing one-edge time shifts.

the path-2 pulse train, with a relative delay of several pulse-repetition periods, coincides partially with the path-1 pulse train. Such a situation

might also be the result of two-station interference, provided the pulse rates are identical or similar enough to cause this situation to persist for several seconds or more.

The power of the random noise which the interference causes in the output at a one-ohm resistance level is given by the approximate expression (64), which is based on an ideal low-pass filter audio characteristic. In practice, the audio characteristic, in order to have sufficient attenuation at half the sampling frequency, begins to roll off at a considerably lower frequency, so that the area under the squared transfer characteristic from $\omega = 0$ to $p/2$ is lower than the ideal area $p/2$ assumed in (64). If the factor by which this area differs from the ideal value is denoted by k_f^2, then the noise power is given by (89), and the corresponding noise voltage by (90).

$$P_n = k_f^2 E^2 \frac{\overline{\overline{\Delta t}}^2}{T^2} \tag{89}$$

$$V_n = k_f E \frac{\overline{\overline{\Delta t}}}{T} \tag{90}$$

In these relations, E is the pulse height at the output of the video stages or input to the audio system multiplied by the low-frequency gain of the audio system; in other words, it is the peak voltage of the pulses that would appear at the output if the audio gain did not drop from its low-frequency value with increasing frequency. $\overline{\overline{\Delta t}}$ denotes the root-mean-square deviation of the time-shift values from their mean value, which is equal to the square root of the mean-square value minus the mean value squared of the periodic function $\Delta t(\phi)$. This function is given, for linear pulse edges, by (7) in Section 2.1; with the slicing level at $s = \frac{1}{2}$, it is given by (91), below.

$$\Delta t(\phi) = \delta[\tfrac{1}{2} + a \cos \phi - \sqrt{(\tfrac{1}{2})^2 - (a)^2 \sin^2 \phi}\,] \qquad (0 < a < \tfrac{1}{2}) \tag{91}$$

The positive and negative peak values of $\Delta t(\phi)$ are $\underline{a}\delta$, no matter whether $\underline{a}$ is close to zero or close to $\frac{1}{2}$. However, the shape of the variation changes from that of a sinusoid to that of a half-wave rectified sinusoid, as shown in the graphical plots on page 17, as $\underline{a}$ increases from zero to $\frac{1}{2}$. For small

values of $\underline{a}$, it therefore follows that $\overline{\overline{\Delta t}} = 0.707\delta a$, since the r-m-s value of a sinusoid is 0.707 times its peak value, and the mean value is zero. By carrying out the appropriate integrations, it can be found that the mean-square value of the half-wave rectified sinusoid is $(2\pi-4)/\pi$ or 0.727, and the mean value squared $[(\pi-2)/\pi]^2$ or 0.132. The difference between these two figures is 0.595, which is analogous to the mean-square value of 0.500 of a sinusoid. From $\sqrt{0.595} = 0.771$, it follows that $\overline{\overline{\Delta t}} = 0.771\delta a$ for $\underline{a}$ near $\frac{1}{2}$, which represents an increase of just ten per cent over the above formula for $\overline{\Delta t}$. More generally, $\overline{\overline{\Delta t}}$ is given by the slowly convergent series given in Appendix IV; for $\underline{a}$ considerably smaller than $\frac{1}{2}$, say $\underline{a} = 0.30$, $\overline{\overline{\Delta t}}$ exceeds $0.707a\delta$ by less than two per cent, that is, most of the ten per cent total increase is crowded just below $\underline{a} = 0.5$. This ten-per-cent increase in the effective time shift can occur also for small values of $\underline{a}$, if the slicing level $\underline{s}$ is decreased so that a/s approaches unity, which is the third of the three reasons quoted on page 28 for keeping $\underline{s}$ at one-half when the interference ratio $\underline{a}$ is below one-half.

More important than the ten per cent deviation from the linear relation $\overline{\overline{\Delta t}} = 0.707\delta a$ (which results from the increase in the mean-square value of the time-shifts) is a much larger increase in $\overline{\overline{\Delta t}}$ resulting from a different cause, namely from the nonlinearity of the pulse edges. This factor is unimportant for $\underline{a}$ less than 0.3, but may cause an increase of more than 30 per cent at $\underline{a} = 0.4$, and more than 100 per cent at $\underline{a} = 0.49$. It becomes necessary, then, to find $\overline{\overline{\Delta t}}$ for the leading and trailing exponential edges, respectively, from (20A) and (20B) derived in Section 2.1. The results are considerably different for the two edges, particularly when a/s is not much less than unity, which might have been predicted from inspection of the plots of $\Delta t(\phi)$ for exponential pulse edges, in Figs. 13 and 14. An analytical determination of $\overline{\overline{\Delta t}}$ is not possible in this case, but numerical integrations of (20A) and (20B) to determine the mean-square values and the squares of the mean values give the desired results. For small values of $\underline{a}$, these results are the same as those obtained from the linear relation $\overline{\overline{\Delta t}} = 0.707\delta a$, provided that the rise time $\underline{\delta}$ of the linear pulse edge is twice as large as the time constant $\underline{\lambda}$ of the exponential pulse edge, ($\delta = 2\lambda$), so that the slope at $s = \frac{1}{2}$ is the same for the exponential edges as for the linear edges. As $\underline{a}$ increases beyond 0.3, the effective time shifts for the exponential edges depart noticeably from $0.707\delta a$. At $\underline{a} = 0.40$, the value of $\overline{\overline{\Delta t}}$ for the leading edge exceeds $0.707\delta a$ by the

factor 1.32, and for the trailing edge, the corresponding factor is 1.42. At $\underline{a} = 0.49$, the corresponding factors are 1.98 and 2.64, respectively. These of course, are exact results, obtained by numerical integration, but rather good approximations giving only one value for both edges are obtainable from the following formula.

$$\overline{\overline{\Delta t}} \approx 0.35\,\lambda\,\ell n\left[\frac{1+2a}{1-2a}\right] \qquad (92)$$

This relation is simply the two-edge peak-to-peak time shift given on page 27 in Section 2.1, divided by two to give an average value for one edge, and multiplied by 0.7 to give an approximate effective value. The factors by which this expression exceeds $0.707\delta a$ are 1.37 and 2.47 for $\underline{a} = 0.40$ and 0.49, respectively, which compare favorably with the values given above.

Returning to (90), one may therefore state that, for the exponential pulse generally used in practice, the effective time shift for small values of $\underline{a}$ is $\overline{\overline{\Delta t}} = 0.71\delta a$ or $\overline{\overline{\Delta t}} = 1.42\lambda a$. At $\underline{a} = 0.2$, this is approximately 5 per cent low. A good approximation, which is within about three per cent for $\underline{a} < 0.4$, is given by (92). Above $\underline{a} = 0.4$, the effective time shifts of the two edges become so noticeably different that only the exact solution by numerical integration of (20A) and (20B) will give accurate values. The computed factors, given above, by which $\overline{\overline{\Delta t}}$ exceeds $1.42\lambda a$, constitute sufficient additional information to fix $\overline{\overline{\Delta t}}$ within a few per cent over the entire range from $\underline{a} = 0$ to 0.49. Approximate and exact plots of $\overline{\overline{\Delta t}}/\lambda$ vs $\underline{a}$ are shown in Fig. 50. The output noise voltage, given by (90), is directly proportional to the ordinate of this curve. With some of the approximations for $\overline{\overline{\Delta t}}$ substituted into (90), one obtains, for exponential pulse edges with time constant λ, with the slicing level assumed at $s = \frac{1}{2}$,

$$V_n = k_f E\,\frac{1.42\,a\lambda}{T} \qquad (a < 0.2,\ 5 \text{ per cent low at } a = 0.2) \qquad (93)$$

$$V_n = k_f\,\frac{E}{T}\,0.35\,\lambda\,\ell n\left[\frac{1+2a}{1-2a}\right] \qquad (a < 0.4,\ 3 \text{ per cent error at } a = 0.4) \qquad (94)$$

In order to give a practical significance to these expressions for the output noise, they should be compared to the signal voltage. With sinusoidal

modulation effecting a maximum time shift Δt_m^*, the r-m-s signal output voltage is

$$V_s = E \frac{0.71\ \Delta t_m}{T} \quad . \tag{95}$$

Using expressions (93) and (95), one obtains the following formula for the signal-to-noise voltage ratio, which, of course, is subject to the same limitation as (93).

$$\frac{V_s}{V_n} = \frac{\Delta t_m}{2ak_f\lambda} \quad . \qquad (a < 0.2) \tag{96}$$

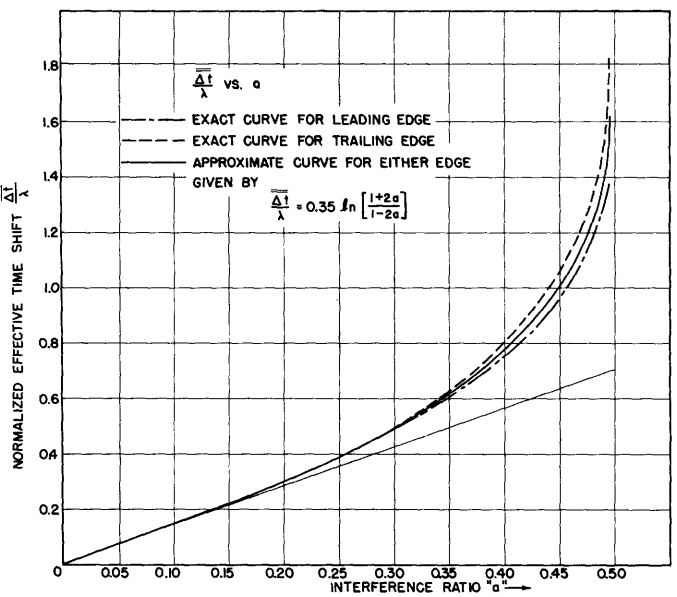

Fig.50 Normalized time shift (effective value) for exponential pulse edges vs. interference ratio obtained by accurate computation and by approximate formula.

For larger values of a, the signal-to-noise ratio is somewhat smaller than (96) indicates, by roughly 6 db when a is 0.48 or 0.49. In a typical situation, with the interference ratio equal to one-third, the signal-to-noise ratio approximately equals the ratio of peak modulation time shift to the rise or decay time constant of the pulses, $\Delta t_m/\lambda$, if k_f is assumed to be near unity

* In the case of "symmetrical" PDM, Δt_m is twice the time-shift of either pulse edge.

(actually it is usually closer to 0.6, favoring higher S/N). The magnitude of this ratio depends on the particular system, of course. For example, Δt_m may range from 1 microsecond to as much as 50 microseconds, and λ may be between 0.05 and 2 microseconds depending only on the available bandwidth. Typical values in a ten-megacycle-bandwidth multi-channel PPM system are $\lambda = 0.05$ and $\Delta t_m = 2$, giving a signal-to-noise ratio of forty.* In a single-channel 250 kc-bandwidth PDM system, possible values are $\lambda = 2$ and $\Delta t = 40$, giving a signal-to-noise ratio of twenty. These are typical signal-noise values; they decrease, of course, in direct proportion to bandwidth if this is reduced from the above values. If it were desired, for example, to design a PDM system to compete with an FM system having a bandwidth of 150 kc and an audio-frequency response good up to 15 kc, then the time constant λ would exceed 3 microseconds, and the maximum excursion Δt_m would be only 15 microseconds. In this case, still with an input interference ratio of approximately one-third, the signal-to-noise ratio would be poorer than five. It must be remembered, of course, that the case of one-edge noise is severe in that each and every pulse is affected.

The present discussion and results may apply to PPM systems, as well as PDM systems, under certain conditions, depending principally on the type of demodulator used in the PPM system. The pulse position may be detected or measured by utilizing the timing of only the leading or perhaps only the trailing edge of each pulse, or it may be detected by way of the timing of the center of the pulse. The former is the usual practice, and therefore, even if the interference overlaps the entire pulse, only the mean effective time shift of one edge will be of interest. The time position of that edge is generally compared to that of the corresponding edge of an unmodulated time-reference or synchronizing pulse; if this is free of interference, the situation is completely analogous to one-edge interference in PDM as discussed above; otherwise the resulting noise would be 3 db higher. The details of PPM detection schemes will be discussed in Chapter 5, but a few more pertinent facts will be mentioned here. It is the time difference, of course, between, say, the leading edge of the position-modulated pulse and the leading edge of the reference pulse which is converted into a voltage amplitude at the output.

---

* The exact relationship between time constant and bandwidth depends, of course, on the definition of bandwidth.

This can be done in two fundamentally different ways. In the first and oldest method, the time difference is converted into the duration of a pulse which, as in PDM, is passed through a low-pass filter to the output; needless to say, all time shifts are thus directly passed on to the final duration-modulated pulse and have precisely the same effect as in a PDM system. In the second method, the time differences are directly converted into amplitude samples by a nonlinear circuit. No duration-modulated pulses are involved, and the time-shift noise spectrum is therefore different from the spectra derived in Chapter 4. However, the low-frequency portion and hence the audio-noise power relative to the signal power is the same, regardless of the method of demodulation.

4.2 Missing-Pulses Noise in PDM

While the missing-pulses effect usually occurs in combination with the time-shift effect, there are certain interference situations in which it may occur in its simplest basic form, the time-shift noise being relatively negligible or absent altogether. The situations mentioned at the beginning of this chapter in connection with one-edge time shift noise will also cause "simple" missing-pulses noise if the interference ratio is more than one-half. The qualification "simple" is used to convey the fact that the identical portion of each pulse, if not each complete pulse, is subject to the effect. In other words, either all pulses are completely overlapped by interference as would be true with continuous interference, or the same portion of succeeding pulses would be overlapped by interfering pulses, which would generally happen in the case of two-path interference. In either event, time-shifts will also be present, but may have relatively negligible effect if the pulse rise or decay time is very short, as will be seen later in this chapter. Interfering pulses shorter than the desired pulses, having the same repetition rate, and timed so as to coincide completely with a portion of each desired pulse, will cause missing pulses without any time shifts.

It was shown in the previous chapter that the power of the noise caused by randomly missing pulses is given approximately by (87). It can be readily shown that the same formula applies, if, instead of the entire pulse only a portion is susceptible to cancellation, provided that the duration of the missing pulses is replaced by the duration of the susceptible portion of the pulse. This portion is determined by the amount of overlap between the

desired and interfering pulses. This overlap, divided by the pulse-repetition period, T, will be denoted by the letter U, the upper limit of which is the duty factor D_1 of the desired pulses. (The subscripts 1 and 2 refer to the desired and undesired signals, respectively.) With D in (87) replaced by the more generally applicable U, and with the filter constant k_f first introduced in (89) to account for the departure of the audio characteristic from its ideal shape, the expression for the noise power becomes

$$P_{mp} = k_f^2 E^2 U^2 (F - F^2) \quad . \tag{97}$$

Since the above is the power normalized to a one-ohm resistance, the corresponding rms missing-pulses noise voltage is given by (98).

$$V_{mp} = k_f E U \sqrt{F - F^2} \quad . \tag{98}$$

It will be recalled that F is the fraction of missing pulses, or more generally the probability that any one of the susceptible portions will actually be missing. It is given by (34) and plotted as a function of interference ratio a in Fig. 18. The rms signal output voltage is given by (95). In order to obtain an estimate of the output signal-to-noise ratio under certain typical conditions, it is convenient to write an expression for the approximate maximum rms signal in a PDM system; the maximum modulation time shift Δt_m is limited to an amount somewhat less than the pulse duration; it may be approximately 0.7 d_o in a typical case. The approximate expression for the maximum rms signal is therefore

$$V_s = 0.5\, E D_1 \quad . \tag{99}$$

The maximum signal-to-noise ratio is given approximately by (100), if it is assumed that the signal itself is not affected by the missing-pulses effect.

$$\frac{V_s}{V_{mp}} = \frac{D_1}{2 k_f U} (F - F^2)^{-\frac{1}{2}} \quad . \tag{100}$$

At worst, U is equal to D_1, as would be the case if the interference is continuous or if it is a result of two-path transmission with the delay difference equal to an integral number of pulse-repetition periods. Since the highest possible value of F is one-third, $\sqrt{F - F^2}$ is 0.47 at most, and assuming $2k_f$ slightly more than unity, the signal-to-noise ratio in this worst possible case of missing pulses turns out to be only two. The conditions are severe in that the interference overlaps each pulse completely, and the interference ratio is close to unity. The improvement with decreasing interference ratio is very slow, inasmuch as F decreases very slowly (see Fig. 18), and $\sqrt{F - F^2}$ therefore decreases still more slowly. On the other hand, the noise voltage decreases linearly with the interference overlap, U, which improves the signal-to-noise ratio over the minimum value of two in many actual situations. In order to give a greater significance to the various figures of signal-to-noise ratio being quoted, the writer has determined experimentally that the lowest tolerable value is of the order of ten. This relatively high value is required for fair intelligibility because the crest factor of speech is much lower than that of a sinusoid. In other words, the definition of signal-to-noise ratio could be improved or be made more meaningful by using the average crest factor of speech or music, as the case may be, rather than that of a fictitious sinusoidal signal.

The missing-pulses interference effect, although manifesting itself primarily in the form of random noise, also has certain other consequences affecting the signal. (Conversely, the signal modulation also affects the missing-pulses noise to some extent, tending to reduce it.) Consider first the simplest case of missing pulses, in which entire pulses are susceptible; this happens, for example, when the interference is a continuous wave. Since the pulses carry the signal, loss of a fraction F of the total number of pulses means a loss in signal, aside from the noise which results. This loss in signal appears as a reduction in output-signal strength, further reducing the signal-to-noise ratio below the figure given by (100). Elementary considerations would show the reduced signal voltage to be proportional to 1-F, the fraction of remaining pulses. Experimentally it is found that the reduction may be somewhat greater in certain instances; but then the noise is generally so great that the signal-to-noise ratio is well below the useful limit even without the signal reduction.

In the cases in which only a portion, say the first half, of each pulse

is susceptible, as a result of partial overlap with an interfering pulse train, the effect on the signal modulation may be quite different, depending on the circumstances. With only one edge of each pulse susceptible to being lost there will be no signal loss if the susceptible edge happens to be the fixed edge of an asymmetrically modulated pulse train, but if it is the modulated edge, the signal loss will be just as great as if the entire pulse were susceptible to being "missing"; in the case of "symmetrical" PDM, with both edges modulated, the signal reduction will be only one-half as great.

The signal-reduction effect is generally accompanied by a complementary effect which transfers some of the time modulation of the interfering pulse train to the desired pulse train. Obviously, wherever one side of a pulse is missing, its true edge is replaced by another edge, the timing of which may be determined in part by the modulation of the interfering pulse train. Such fragmentary transfer of modulation gives rise to a small amount of cross talk which is masked sufficiently by the missing-pulses noise to be quite negligible for most practical purposes. Various special circumstances may arise: for example, in the case of two-path interference, a pulse edge may be replaced by another edge carrying the same modulation, though delayed and reversed in polarity.

4.3 Combination of Time-Shift and Missing-Pulses Effects

With interference ratios between one-half and unity, one usually deals with both time-shift and missing-pulses noise. While the former may be negligible compared to the latter in some cases, this is not generally true, so that it becomes necessary to determine the combined effect of the two phenomena. Although each effect alone produces a random output, the total output noise power is not simply the sum of the individual values. The cross-correlation between the two effects causes it to be larger by an amount generally intermediate to the two individual values. This cross-correlation results from the fact that any one portion of a pulse is generally subject only to one effect or the other, that is, the two effects are mutually exclusive.

The problem of finding the total noise power can be solved in two radically different ways which lead to identical results. First, the missing-pulses effect may be considered as a special type of time shift which, in combination with the ordinary time shift, gives a new time shift with a different probability distribution. In order to evaluate the approximate audio-noise

power it is then necessary only to find the standard deviation of the new probability distribution. This is the simpler of the two ways and will therefore be used here. In the second method, the time shifts and the missing pulses are regarded as two different effects, and their cross-correlation* is found by methods similar to those used to find auto-correlation in Chapter 3. The Fourier transform of the aperiodic component of this cross-correlation is the continuous component of the so-called interaction power spectrum, which, when added to the time-shift and missing-pulses power spectra, gives the total power spectrum. Only the area of the aperiodic cross-correlation component need be found in order to evaluate the audio-noise power connected with it. This method requires a greater number of steps, principally because, with a larger than one-half, the time-shift distribution is modified even without inclusion of the missing-pulses effect.

The following analysis, for the sake of clarity, is based on linear pulse edges. An analysis based on exponential pulse edges cannot be carried out completely by analytic methods and would be rather cumbersome. The linear-pulse-edge analysis shows the principles involved, and with the knowledge of exponential-edge time shifts given earlier in this chapter, one can modify the results to apply to pulses with exponential edges.

It is necessary, at this time, to reconsider (7), which gives the relation between the edge time shift Δt and the radio-frequency phase difference angle ϕ. It was shown in Section 2.2, in the analysis of the missing-pulses effect, that, with $s = a$, there is no solution for Δt over a certain range of values of ϕ, extending an amount θ on each side of $\phi = \pi$, θ being equal to $\cos^{-1}(1/2a)$. Within this range, the pulse edge does not pierce the slicing level, and if the entire pulse fails to reach the output, this is equivalent to a time shift of magnitude equal to the pulse duration, d. Therefore, the function $\Delta t(\phi)$, ordinarily subject to the restriction $0 < a < \frac{1}{2}$, can be extended by relaxing this restriction to permit values of a up to one, and noting that $\Delta t = d$ for $\phi = \pi - |\theta|$ to $\phi = \pi + |\theta|$, if $a > \frac{1}{2}$, where $|\theta| = \cos^{-1}(1/2a)$. A qualitative plot of this modified function $\Delta t(\phi)$ is shown in Fig. 51 for a somewhat less than unity, so that θ is slightly less than 60 degrees. Successive values of the pulse-edge time shift are random samples of this function;

---

*Cross-correlation has been defined on page 56.

their probability distribution curve is shown in the lower part of Fig. 51.

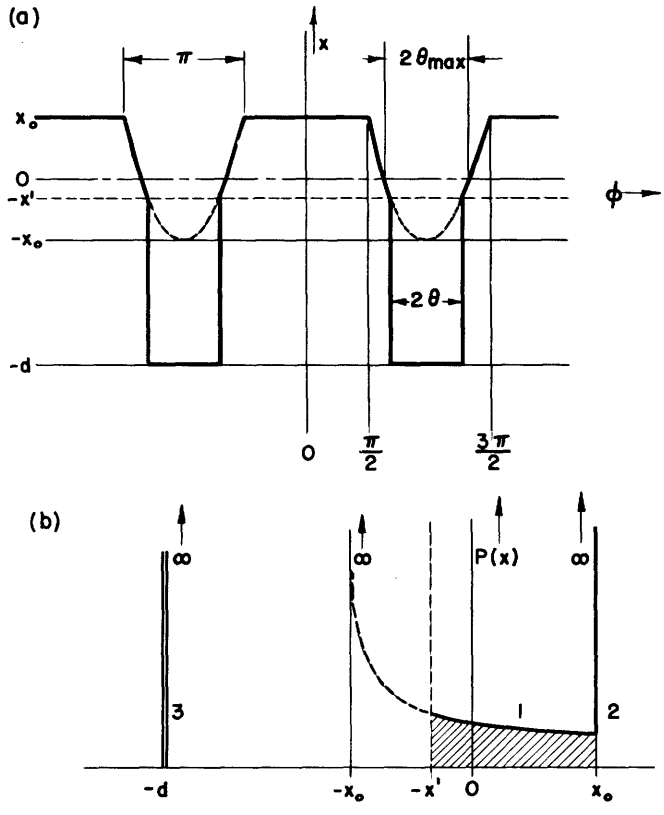

Fig.51 Pulse-edge time shift for $0.5 < a < 1.0$; (a) time shift vs. r-f phase difference ϕ (b) time-shift probability distribution.

$x' = x_0(1 - 2\cos\theta)$
$\theta = \cos^{-1}(1/2a)$
$\theta_{max} = \pi/3$

This distribution is the same half-wave-rectified sinusoid distribution shown in Fig. 10, with part of its area removed and replaced by the spike at $\Delta t = x = -d$. Finding the standard deviation of the distribution amounts to determining the mean-square and squared mean values of the new $\Delta t(\phi)$ shown in Fig. 51, but it can also be found directly from the distribution curve by applying the following relation.

$$\bar{\bar{x}}^2 = M(x^2) - M^2(x) = \int_{-\infty}^{\infty} x^2 P(x)\,dx - \left[\int_{-\infty}^{\infty} xP(x)\,dx\right]^2 . \qquad (101)$$

In this relation, $M(x)$ and $M(x^2)$ denote the mean of x and x^2, respectively. To apply this, the probability-distribution curve is broken into three parts, numbered 1, 2, and 3, respectively, in Fig. 51. Parts 1 and 2 are given by (14) in Chapter 2, although Part 1 extends only from x_0 to $-x'$. It can be shown that $-x' = x_0(1 - 2\cos\theta)$, and that the "lost" area between $x = -x'$

and x_o is equal to θ/π or F, the fraction of missing pulses. This area is instead found in the infinitely high and infinitesimally narrow spike at $\Delta t = x = -d$, part 3 of the distribution curve. Part 2 is the usual spike corresponding to the flat portion of the half-wave-rectified sinusoid; its area is one-half, the total area of all three parts being one, of course. Evaluation of the three individual sets of $M(x)$ and $M(x^2)$ involves carrying out the integrals appearing in (101), which is trivial for parts 2 and 3, but somewhat involved for part 1. In terms of x_o ($x_o = a\delta$) and θ ($\theta = \cos^{-1}[1/2a]$), the results appear as follows.

$$M_1(x) = \frac{x_o}{\pi}\left[-2 + 2\sin\theta - \theta + \frac{\pi}{2}\right]$$

$$M_1(x^2) = \frac{x_o^2}{\pi}\left[4(\sin\theta - 1) - \sin 2\theta - 3\theta + \frac{3\pi}{2}\right]$$

$$M_2(x) = \tfrac{1}{2} \qquad M_3(x) = \frac{\theta}{\pi}(d_1)$$

$$M_2(x^2) = \tfrac{1}{2} \qquad M_3(x^2) = \frac{\theta}{\pi}(d_1^2) \tag{102}$$

In terms of the same parameters, the final answer for the square of the total effective time shift, $\overline{\overline{\Delta t}}^2$, is obtained as follows.

$$\Delta t^2 = x^2 = M_1(x^2) + M_2(x^2) + M_3(x^2) - [M_1(x) + M_2(x) + M_3(x)]^2$$

$$= x_o^2\ 2 + \frac{1}{\pi}[4(\sin\theta - 1) - \sin 2\theta - 3\theta] + \frac{1}{\pi^2}[\pi - \theta + 2(\sin\theta - 1)]^2$$

$$+ 2x_o\left(\frac{\theta d_1}{\pi^2}\right)[\pi - \theta + 2(\sin\theta - 1)]$$

$$+ (d_1)^2\left[\frac{\theta}{\pi} - \left(\frac{\theta}{\pi}\right)^2\right] \quad . \tag{103}$$

Note: $x_o = a\delta$, $\theta = \cos^{-1}(1/2a)$; $\frac{1}{2} < a = s < 1$.

The total noise power is obtained by substituting (103) in (89). The three terms in (103) are the time-shift term, the cross term, and the missing-pulses term, respectively. The latter, on multiplication by $\bar{T}^2$, becomes identical to the missing-pulses noise power found previously and given by (87). Since the terms and factors associated with the time-shift effect and missing-pulses effect can be identified, those associated with the time shifts can, if desired, be modified to conform more closely to the true shape of the pulse edges. In this connection, it should be noted that the line of demarcation which exists between the time-shift and missing-pulses effects if the pulse edges are assumed linear is not nearly so sharp in the case of pulses which have a gradual transition from edge to flat-top. It follows, therefore, that the transition from pure time-shift noise to the combination of time-shift and missing-pulses noise is generally more gradual than is indicated by the analysis. That portion of the transition which lies below $a = \frac{1}{2}$ has already been treated in this chapter (see Fig. 50). Above $a = \frac{1}{2}$, the effect is essentially one of raising the time-shift contribution by a rather large factor. If (103) is used without such a correction to check experimental results, the principal discrepancy will be found in the insufficiently large time-shift contribution, as will be seen in the next chapter.

4.4 Discontinuous Interference: More Complicated Interference Situations

The general situation which results from interference between two pulse trains with different pulse-repetition rates involves the same principles discussed up to this point, but it is complicated by the fact that successive desired pulses experience different degrees of overlap with the interfering pulses. As far as the time shift is concerned, this means that some desired pulses may suffer one-edge time shift, some two-edge time shift with or without some dependence between the two shifts, and others may not be subjected to time shifts at all. As regards the missing pulses, the process is more complicated inasmuch as each pulse may have a different portion susceptible to being missing. This situation obtains in the most general case of two-station PDM interference, so that one or both sets of pulses are generally time-modulated. As a result, the variation in overlap from pulse to pulse is neither perfectly systematic nor perfectly random, and can therefore not easily be treated precisely, particularly in the case of missing-pulses noise. Instead, results are obtained by approximate methods which are sufficiently

accurate for engineering purposes.

As regards the time-shift effect, it is necessary first to find the fraction of pulses that suffer two-edge and one-edge time shifts, as a function of the average durations and repetition rates of the two sets of pulses. The problem can be simplified by assuming the repetition rates close enough at the outset to have approximately the same ratio between the desired-pulse duty factor D_1 and the interfering-pulse duty factor D_2, as between the corresponding pulse durations d_1 and d_2. D_1 and D_2 can then be regarded as normalized pulse durations. Of course, if the interference had a perfectly random time distribution with duty factor D_2, then the most one would be able to say is that the probability of two edges of the same desired pulse both being overlapped is D_2^2, that of just one edge being overlapped $D_2(1 - D_2)$, and that of neither edge being overlapped $(1 - D_2)^2$.[18] In the present case, however, the available information about the two pulse trains is such that the problem can be formulated more precisely, as follows. The effect of modulation on both or either of the two pulse trains can be neglected without appreciable error, as is confirmed experimentally, because the symmetry of the modulation tends to cancel the effect on the average overlap over a period of time, and also because the modulation crest factor is generally so low as to make the effective modulation small.

In determining the individual probabilities of a given pulse having zero, one-edge, and two-edge overlaps, respectively, one has to distinguish between the two cases $D_1 > D_2$ and $D_1 < D_2$. Both cases are illustrated in Fig. 52. It is assumed that both D_1 and D_2 are less than one-half, so that any one pulse of either signal can overlap no more than one pulse of the other signal. By sliding pulse 1 along the entire extent of one repetition period of pulse train 2, which is unity on the normalized basis, one notes that over a certain range there is no coincidence with pulse 1; over another range only the leading edge of pulse 1 is overlapped, and so forth. The extent of each of these ranges represents the relative frequency with which the corresponding situation will occur. Considering first the case $D_1 > D_2$, one finds that it is impossible for both edges of pulse 1 to be overlapped by pulse 2 simultaneously, but that either the leading or the trailing edge is overlapped with probability D_2. (The word "probability" is being used here in the sense of relative frequency with which a certain condition is encountered in examining a large number of pulses, or it may be regarded as the probability of finding

the condition in question on a single pulse chosen at random.) The total "one-edge probability" is therefore given by $2D_2$, which leaves $1 - 2D_2$ for the probability of finding no time shift at all, the "two-edge probability" being zero. Considering next the case $D_1 < D_2$, illustrated in the lower half of Fig. 52, one finds, in sliding pulse 1 over the complete range of one

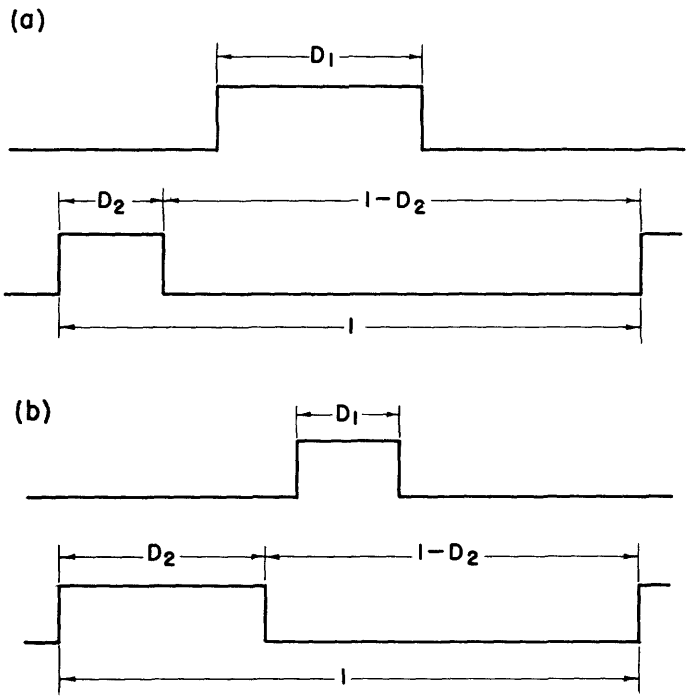

Fig. 52 Determination of probabilities of overlaps between two pulse trains with nearly equal repetition frequencies; (a) $D_1 > D_2$ (b) $D_1 < D_2$.
Note: if the repetition periods, T_1 and T_2 are not approximately equal, replace D_1 by d_1/T_1 and D_2 by d_2/T_2.

period, that both its edges coincide with portions of pulse 2 over a range $D_2 - D_1$, and that each edge individually experiences overlap over a range D_1. The total "one-edge probability" is therefore $2D_1$, and the "two-edge probability" $D_2 - D_1$, leaving $1 - D_1 - D_2$ for the probability of finding no overlap. The probability of finding either a one-edge or a two-edge overlap is accordingly $D_1 + D_2$. The various probabilities are repeated below.

	$D_1 > D_2$	$D_1 < D_2$		
No-overlap probability	$1 - 2D_2$	$1 - D_1 - D_2$	$(1 - \frac{d_1}{T_2} - \frac{d_2}{T_2})$ *	
One-edge probability	$2D_2$	$2D_1$	$(\frac{2d_1}{T_2})$	
Two-edge probability	0	$D_2 - D_1$	$(\frac{d_2 - d_1}{T_2})$	(104)

* The expressions in parentheses are more general, applying if the pulse-repetition rates are not approximately equal; see pages 111-112.

The total time-shift audio-noise power is found by weighting the one-edge and two-edge contributions in accordance with the above probabilities. One-edge time-shift noise has been treated in detail in the first part of this chapter. Expression (89) for the noise power need only be multiplied by $2D_1$ or $2D_2$, whichever is the smaller, to yield the one-edge contribution to the total time-shift noise. If D_1 exceeds D_2, this is the only contribution, but if D_2 exceeds D_1, there is the additional two-edge noise contribution, obtained by multiplying the proper expression for two-edge noise by the probability $D_2 - D_1$. The form of the expression for two-edge noise depends, of course, on the relation which may exist between the shifts of the two edges of a given pulse; for example, the two-edge audio-noise power has been shown (3.4) to be exactly twice as large as the one-edge audio-noise power if the shifts are independent, and nearly four times as large if they are equal and opposite. In the former example, the two-edge contribution would be $(2P_{\text{one-edge}})(D_2 - D_1)$, which, when added to the one-edge contribution, $(P_{\text{one-edge}})(2D_1)$, yields $(P_{\text{one-edge}})(2D_2)$. This is the same total noise power which is obtained in the simpler case in which D_1 exceeds D_2, showing again that independent time-shifts, though on the two edges of the same pulse, can be regarded separately as one-edge time shifts. In the latter example, letting $P_{\text{two-edge}} = 4P_{\text{one-edge}}$ leads to the result $(P_{\text{one-edge}})(4D_2 - 2D_1)$. Other results are obtained with the other possible types of two-edge noise, which will be considered in Section 4.5 of this chapter. In the simplest case, the total time-shift audio-noise power equals the one-edge power multiplied by $2D_2$, regardless of which duty-factor is the larger. If this is applied to (89), the basic expression for one-edge audio-noise power, the result is

$$P_n' = 2D_2 k_f^2 E^2 \frac{\overline{\overline{\Delta t}}^2}{T^2} . \qquad (105)$$

Similarly, all the noise-voltage formulas following (89) would be multiplied by $\sqrt{2D_2}$.

The initial assumption of nearly identical pulse-repetition frequencies of the two pulse trains may of course be unfounded, and the results given by (104) will therefore be generalized. The pulse-repetition periods will be denoted by T_1 and T_2, respectively. With the aid of Fig. 29, it is easily verified that, for $d_1 > d_2$, the probabilities as given by (104) remain

unchanged. With T_1 considerably smaller than T_2, it is possible, of course, for both edges of a single pulse to be overlapped by different interfering pulses. However, because of the incoherence between pulses, the two resulting time-shifts are independent and can therefore be regarded separately as one-edge time shifts, and they are in fact taken care of as such by the same probability factor $(2D_2)$. For $d_2 > d_1$, the probability factors will be modified, but the net result in the special case discussed above is again the same, the multiplying factor being $2D_2$. More generally, the "two-edge probability" $D_2 - D_1$ is replaced by $(d_2 - d_1)/(T_2)$, and the "one-edge probability" $2D_1$ is replaced by $(2d_1)/(T_2)$, as indicated in parenthesis in (104).

Missing-pulses noise is modified more radically by the intermittent nature of the interference noise than time-shift noise. Because of the varying overlap from pulse to pulse, different portions of successive pulses are susceptible to being "missing", so that, strictly speaking, a new auto-correlation analysis is required to find the audio-noise power. This is not simple, however, because of the partly systematic, partly random overlap variations, and is therefore not carried out here. An acceptable formula for audio-noise power can be obtained by modifying the result for the simple type of missing-pulses noise given, for example, by (97), repeated below.

$$P_{mp} = k_f^2 E^2 U^2 (F - F^2) \quad . \tag{97}$$

The most direct approach is to find the average fractional overlap per desired pulse, and to substitute this for U in (97). Such a procedure ignores the fact that actual successive overlaps depart from periodicity in both duration and time position. However, a similar result is obtained by other arguments involving different errors. For example, a limiting case may be considered, in which the interfering pulses are so much longer in duration than the desired pulses $(d_2 >> d_1)$ that the missing-pulse phenomenon takes place in its simplest form, that is, for the most part, whole pulses rather than portions of pulses are susceptible to being "missing". The fraction of missing pulses is then the variable which is modified; F is replaced by FD_2, and U is equal to D_1 as in the original derivation in (87). The error lies in the fact that the probability FD_2 of any pulse not reaching the output is no longer necessarily totally independent of whether or not the previous pulse was

missing, inasmuch as the probability corresponding to the factor D_2 is not a true probability, but rather the relative frequency with which a certain situation is encountered. The same end result can also be obtained by other arguments involving similar errors; this result is given by (106).

$$P'_{mp} = k_f^2 E^2 D_1^2 [FD_2 - (FD_2)^2] \quad . \tag{106}$$

In order to find the corresponding result for the other method, mentioned at the beginning of this paragraph, the average fractional overlap between the two pulse trains must be determined. This is the fraction of the total time during which the two pulse trains overlap, which is in fact equal to the cross-correlation* obtained for any value of τ if both pulse amplitudes are assumed equal to one. It is a simple matter to show that it is equal to the product of the two duty factors, $D_1 D_2$, regardless of their relative magnitudes and of the time distribution of the pulses. Consequently, the resulting expression for the missing-pulses audio-noise power becomes

$$P''_{mp} = k_f^2 E^2 D_1^2 D_2^2 (F - F^2) \quad . \tag{107}$$

The experimental results presented in the next chapter conform more closely to (106) than to (107), and the former is therefore to be preferred.

Expression (103), which gives the equivalent effective time shift for $a > \frac{1}{2}$ and hence the total audio-noise power, can now be modified to apply to intermittent interference, e.g., two-station PDM interference, by using the time-shift and missing-pulses modifications derived above. The change merely amounts to multiplying the first line of (103) by $2D_2$ (assuming the most general type of two-edge noise), the second line by $2D_2\sqrt{D_2}$, and replacing θ in the third line by θD_2. If these changes are made, and if the new expression for $\overline{\Delta t}^2$ is substituted in (89), the following expression results. (Here, x_0 has been replaced by its value, $a\delta$, and in some instances, θ/π has been replaced by its equivalent, F.)

---

* For definition of cross-correlation, see page 56

$$P_{\substack{\text{total}\\ \text{audio noise}}} = \left(\frac{k_f E a\delta}{T_1}\right)^2 (2D_2)\left\{f_1(\theta) + [f_2(\theta)]^2\right\}$$

$$+ \left[\frac{(k_f E)^2 2a\delta}{T_1}\right](D_1 D_2 \sqrt{D_2})(F)[f_2(\theta)]$$

$$+ (k_f E)^2 D_1^2 D_2 (F - D_2 F^2) \quad . \qquad (108)$$

Note: $\frac{1}{2} < a = s < 1$

$\theta = \pi F = \cos^{-1}(1/2a)$

$f_1(\theta) = 2 + \frac{1}{\pi}[4(\sin\theta - 1) - \sin 2\theta - 3\theta]$

$f_2(\theta) = \frac{1}{\pi}[\pi - \theta + 2(\sin\theta - 1)]$.

The discussion which follows (103), dealing with the gradual transition from time-shift noise to missing-pulses noise, applies also to the situation corresponding to (108), but in a still more complicated way. Some interference overlaps around the leading edge of a desired pulse may be of such short duration that the resultant does not reach the slicing level during the overlap, although it would if the overlap persisted for a longer time. This example shows that the demarcation line between time shift and missing pulses is still further blurred if the interference is of the more complicated intermittent type.

The treatment of the noise resulting from this type of interference is not complete without discussion of the periodic component which may be contained in the noise, as a result of a beat phenomenon between the two different pulse-repetition frequencies. Clearly, if the duty factors of both pulse trains are considerably less than one-half, and the repetition rates differ by a fairly small percentage, then periods of repeated overlaps will alternate with longer periods of no overlaps at all, and the alternation will take place at a frequency equal to the difference between the two pulse-repetition frequencies. Unlike the pulse-repetition frequency and its harmonics, this

frequency and some of its harmonics may be low enough to be passed by the audio system; generally, however, there is no actual component at this frequency, or it is quite small. Rather, the output noise, instead of being continuous, consists of bursts of noise repeating at this frequency, or, in other words, the noise is off-on modulated at this frequency. In the case of pure time-shift noise ($a < \frac{1}{2}$), with $d_1 > d_2$, there are in fact separate bursts of noise corresponding alternately to groups of leading and trailing-edge time shifts. The extent to which this noise periodicity is audible depends essentially on the following two factors: first, the actual beat-frequency component which may be present in addition to the noise modulation for reasons given below, and second, the property of the human ear to distinguish a pitch in repeated bursts of noise, even though the spectrum has no intensification at the repetition frequency.[26]

A principal reason for a small beat-frequency component in the case of time-shift noise is the somewhat asymmetrical probability distribution of the time shifts. It was shown in Chapter 2 that, even with linear pulse edges, the time-shift distribution becomes increasingly asymmetrical as the interference ratio a approaches one-half. The fact that the leading pulse edge, for example, is more likely to be advanced than delayed (making the average pulse duration slightly longer in the presence of time shifts than the original pulse duration) gives the output noise bursts a tendency to prefer positive values over negative values. In other words, the noise bursts have an alternating component. In the case of the exponentially shaped pulse edges used in practice, an additional asymmetry in time-shift distribution appears for large interference ratios, as was shown in Chapter 2 (Fig. 14). The leading edge, for example, while still being advanced more often than delayed, suffers much larger shifts in the delay direction than in the advance direction. This opposes the other factor, tending to equalize the areas under the two halves of the time-shift probability distribution, and can in fact cancel it. The practical details of the subject will be further discussed in the next chapter in connection with experimental results.

In the case of missing-pulses noise, the beat-frequency component can be accounted for in a different way, along with the signal-reduction and cross-talk effects previously discussed for different conditions, on pages 103 and 104. Successive overlaps vary in accordance with the difference between the repetition frequencies of the two pulse trains and the time modulation on the

edges bounding the overlaps. Only a fraction F of these overlaps prevents the corresponding portion of the desired pulse from reaching the output. These portions may be regarded as another pulse train which has been subtracted from the desired pulse train. Some or all of the pulse edges of this new pulse train are time-modulated by the difference between the pulse-repetition rates, and by the modulating signals of the two original pulse trains. Signal 1 may modulate the leading edge, and signal 2 the trailing edge of a given pulse in the new pulse train. The fact that these pulses contain three different fragmentary time modulations (and, of course, the large random component causing missing-pulses noise) has the following consequences. The "corrupted" desired pulse train contains its own modulation but diminished by a certain amount evaluated below, it contains the modulation of the interfering pulses to a small degree, and it is modulated to some degree by the pulse-repetition frequency difference and its harmonics. (Also, of course, it contains the random component which becomes the missing-pulses noise.) The first of the three effects can be evaluated approximately by a simple method, namely by assuming that the relative signal reduction is proportional to the fraction of modulated pulse edges lost. This is generally equal to FD_2, so that one would expect the signal to be reduced from 1 to $1 - FD_2$. The actual reduction tends to be somewhat greater. The second effect, transfer of modulation from the interfering to the desired pulses, is not correctly estimated by assuming it equal to the original modulation multiplied by the fraction of modulated pulse edges transferred, which is also generally equal to FD_2; it is usually much smaller, and completely masked by the noise, presumably because of the fragmentary nature of the transfer of modulation. The beat modulation is also a rather complex phenomenon; it decreases, of course, with decreasing duty factors of both pulse trains and it may, in fact, be hardly noticeable with duty factors less than ten or fifteen per cent.

4.5 Two-Edge Time-Shift Noise

Expressions for the noise-power spectra and for the audio-noise power resulting from so-called two-edge time shifts were derived in the last part of Chapter 3. Three different cases were considered: (1) "Independent two-edge noise", in which there is no relation between the shifts of the two edges of each pulse; (2) "PPM noise", in which these shifts are identical, and (3) "PDM noise", in which they are equal in magnitude but opposite in sense. The

first case received some attention in the preceding analysis of the more complicated interference situations. For PDM, it occurs only in these situations, if it is possible for two interfering pulses to have partial overlap with the two sides of a desired pulse, or if the interference is continuous but incoherent (for example, a heavily modulated FM wave). For PPM, it can occur with any type of interference, if demodulation is performed by conversion to PDM, since the marker pulse and the position-modulated pulse are not generally coherent with one another and therefore suffer independent time shifts which are passed on to the two edges of the duration-modulated pulses.

The two other cases, as well as any number of intermediate cases in which there is a definite relation between the two time shifts in each pulse, can occur in a PDM system if the interference is a continuous unmodulated carrier, or if relatively long coherent pulses overlap both edges of some or all of the desired pulses. If they overlap only some of the pulses in this manner, there will be a component of the corresponding type of two-edge noise, while the remaining noise may be of the one-edge time-shift variety. However, attention will first be focussed on the simpler possibility, in which each pulse is completely overlapped. Case 3, that is, "PDM noise", is the more important of the two extreme Cases (2 and 3), inasmuch as it is more common and causes much stronger audio noise (see Section 3.5). The time shifts of the two edges will be equal in magnitude and opposite in sense if the r-f phase difference, ϕ, is the same at both edges, which it will be if the radio frequencies of the two signals are identical, or if they differ by an integral multiple of the reciprocal of the pulse duration. The statement that the time shifts are equal and opposite under these conditions is strictly true only if each edge has the same time-shift distribution, as in the case of linear pulse edges. Case 2, "PPM noise", is obtained, if the r-f phase difference, ϕ, changes by 180° from the leading to the trailing edge, or if ϕ changes by any odd multiple of 180°. Such a change in phase angle will take place if the radio frequencies of the two signals differ by $n/2d_1$, where n is any odd integer, and d_1 is the duration of the desired pulses. In the presence of modulation, d_1 is not constant, so that the 180-degree relationship can not be maintained exactly. As Case 3, Case 2 requires that the two pulse edges have identical probability distributions, but, in addition, these distributions must be symmetrical; more specifically, the function $\Delta t(\phi)$ must be symmetrical in such a way that $\Delta t(\phi) = -\Delta t(\phi \pm \pi)$. This condition is

nearly fulfilled for small interference ratios with linear or exponential pulse edges. Otherwise, the time shifts are not generally equal, and may even be opposite in sense for certain values of ϕ. For example, $\Delta t(\phi)$ for linear pulse edges with (a/s) = 1 (see Fig. 8) is so asymmetrical that $\Delta t(\phi) = \Delta t(\phi + \pi)$ for $\phi = \pm \pi/2$, and the condition for pure "PPM noise", namely, $\Delta t(\phi) = -\Delta t(\phi + \pi)$, is fulfilled only for $\phi = 0$ or π. Nevertheless, the approximate audio-noise power can be computed under these conditions, by resolving the time shift into a Case 2 (PPM) and a Case 3(PDM) component.

Case 2 and Case 3 represent extreme conditions, resulting in near-minimum and maximum noise, respectively. As will be seen from the experimental curves in the next chapter, there is a smooth transition from one to the other as $\Delta\phi$, the change in r-f phase difference ϕ from the leading to the trailing edge, goes from 0° to 180°, 180° to 360°, and so on. For all intermediate values of $\Delta\phi$, the two-edge time shifts can be resolved into pure "PPM" and "PDM" time shifts. Attention will therefore be focussed on the limiting cases, first on $\Delta\phi = 2n\pi$ (Case 3) and then on $\Delta\phi = (2n - 1)\pi$, (Case 2) where n is any integer including zero. With regard to the first, Case 3, the complete story is already known from Chapter 3, and no new results will therefore be obtained here. This, of course, is the type of two-edge noise obtained for true common-channel interference, in which the difference in radio frequencies, Δr-f, is quite small compared to the reciprocal of the pulse duration. Case 2, on the other hand, results only when there is a frequency difference of $1/2d_1$, $3/2d_1$, ... and so on. In a typical PDM system, the average pulse duration might be 10 microseconds, so that the first noise minimum would appear at Δr-f = 50 kc, the next one at 150 kc, and so forth.

Case 3 is characterized by the fact that the shifts of the two edges of each pulse reinforce each other completely, thereby producing almost four times as much noise power as either would produce alone. More accurately, the ratio is somewhat smaller than four, especially when the duty factor is not much smaller than 0.5, and it is given by (82), which was deduced from the approximated power-density spectrum (76). Heuristic reasoning can lead to exactly the same result: the same expression for the approximated low-frequency power spectrum can be obtained by reasoning on a voltage basis, assuming sinusoidal time modulation. The modulation corresponding to Case 3 is true symmetrical PDM, without the quotation marks around the word symmetrical, because the movements of the two edges are really "geared". (This,

as explained in Chapter 1 and illustrated by Fig. 3, is not true in the case of the actual signal modulation generally used.) Complete reinforcement between the movements of the two edges of a pulse, which results in exactly twice as much output voltage, occurs only if the modulating frequency is so low that the instantaneous modulating voltage does not change during the time between leading and trailing edges. If it does change, then the co-operation between the two edges becomes imperfect, since their movements should actually differ in phase by the same amount by which the modulating-voltage phase changes. For example, in the extreme case in which the phase changes by 90 degrees (duty factor $D = \frac{1}{2}$, modulating frequency $q = p/2$), the contributions of the two edges add in quadrature rather than in phase. The output voltage is then only 0.707 of that obtained at low frequencies. More generally, the voltage drops off as the resultant of two vectors of equal, say unity, magnitude, differing in phase angle by $d_o q$, the angle by which the phase changes from leading to trailing edge. (See vector diagram, Fig. 53.) The square of this resultant, giving the power relative to one-edge modulation power, is $1^2 + 1^2 + 2 \cos d_o q$, or $2(1 + \cos d_o q)$, which is recognized as the ratio of the approximated power spectrum (76) to the one-edge noise-power spectrum. The same approximate, but quite adequate, expressions for the total audio-noise power derived at the end of Chapter 3 can therefore be obtained from the above result. However, the heuristic method which led to this result does not reveal the presence of an error, much less its nature and magnitude.

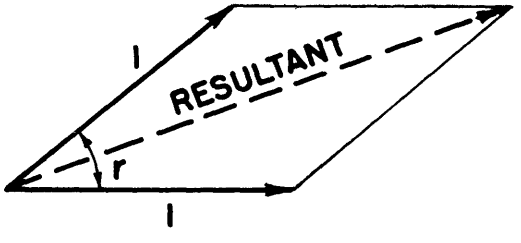

Fig.53 Vectorial combination of sinusoidal time shifts of leading and trailing pulse edges; for "PDM time shift" (Case 3), $r = d_o q$; more generally, $[r] = d_o q - \Delta\phi$.

Case 2 is characterized by the fact that so far as audio noise is concerned, there is almost perfect cancellation between the shifts of the two edges, especially if the pulse duration is small compared to the period of the highest audio frequency, - in other words, if the duty factor is small. The same heuristic reasoning employed in the preceding paragraph again provides a short-cut method of duplicating a result obtained in Chapter 3.

With sinusoidal modulation, the motions of the two edges can be represented by vectors differing in phase angle by $\pi + d_o q$, and the square of the resultant is given by $2(1 - \cos d_o q)$. This is the ratio of the exact power spectrum for "PPM noise", given by (70), to the power spectrum of one-edge time-shift noise. The same reasoning which previously led to approximate results now gives exact results. This can be explained physically by noting that, although both "PDM and PPM noise" are special limiting cases in which there is a particularly simple relation between the shifts of the two edges of each pulse, the latter has the distinction of having constant-duration pulses. The self-correlation, as determined in Chapter 3, is unaffected by the time shifts only in this particular case, which causes the auto-correlation side lobes to have the same shape as the central lobe, thus in turn resulting in the simple power spectrum (70). Evidently, the same heuristic method which gives exact results in Case 2, and approximate results in Case 3, can be applied to the intermediate cases with equal ease. Only the angle between the two vectors representing the two edges is affected: it is simply $r = d_o q - \Delta\phi$. The square of the magnitude of the resultant is $2(1 + \cos r)$, and the resultant magnitude itself, which corresponds to the output voltage, is $2 \cos r/2$. The latter is more convenient if one desires to think in terms of a complex two-edge time shift denoted by $2(\cos r/2 + j \sin r/2)$; the real part of this is the noise output voltage (relative to the corresponding one-edge noise voltage), and the imaginary part corresponds to the noise that is cancelled because of the particular relation between the time shifts of the two edges.

The preceding discussion of Case 2 ($\Delta\phi = \pi$) and the intermediate cases applies strictly only so long as the interference ratio is small enough to make $\Delta t(\phi)$ sinusoidal. Only Case 3 ($\Delta\phi = 0, 2\pi n$) permits asymmetry, inasmuch as the requirement $\Delta t(\phi) = \Delta t(\phi + 2\pi n)$ is always met. The requirement characterizing Case 2, $\Delta t(\phi) = -\Delta t(\phi + \pi)$, is, as previously explained (page 118, top), not generally met when a/s is near unity. In other words, the relation $\Delta t(\phi) + \Delta t(\phi + \pi) = 0$ no longer holds, and the pulses are therefore no longer of constant duration. While the "PPM noise" component is unchanged as will be shown, there is now in addition a "PDM noise" component. The low-frequency power of this component can be evaluated by finding the mean-square value minus the squared mean value of $\Delta t(\phi) + \Delta t(\phi + \pi)$. More generally, π would be replaced by $\Delta\phi$. The evaluation of $\overline{\Delta t(\phi)}$ (the effective value of

$\Delta t(\phi))^*$, leading to a power series in a/s, was discussed earlier in this chapter (see page 97), and is given in Appendix IV A (for linear pulse edges). The effective value of $\Delta t(\phi) + \Delta t(\phi + \pi)$ is found in the same way, and is given in Appendix IV B. The series resulting in this case converges so slowly that, for (a/s) = 1, even the first thirteen terms of the series give a result which is too low by seven per cent. The function $\frac{\Delta t}{s\delta}(\phi) + \frac{\Delta t}{s\delta}(\phi + \pi)$, by direct substitution of (8), is found to be equal to (109).

$$\frac{\Delta t}{s\delta}(\phi) + \frac{\Delta t}{s\delta}(\phi + \pi) = 2\left[1 - \sqrt{1 - \left(\frac{a}{s}\right)^2 \sin^2\phi}\,\right] \quad . \tag{109}$$

This function, like $\frac{\Delta t}{s\delta}(\phi)$, becomes sinusoidal for small values of a/s, but it approaches this form in a different manner, and the period of the sinusoid is half as great, that is, the function is periodic in 2ϕ; the latter is true for all permissible values of a/s. In the limiting case, (a/s) = 1, (109) becomes (110), which describes a full-wave-rectified sinusoid, varying between amplitude limits 0 and +2, but inverted, as shown in Fig. 54.

$$\frac{\Delta t}{s\delta}(\phi) + \frac{\Delta t}{s\delta}(\phi + \pi) = 2(1 - |\cos\phi|) \quad . \tag{110}$$

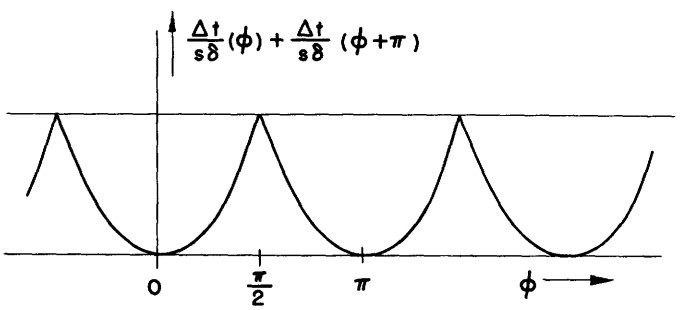

Fig.54 "PDM time shift" component of two-edge noise for $a = \frac{1}{2}$, $\Delta r\text{-}f = (2n\text{-}1)/2d_1$.

The expression for $\frac{\Delta t}{s\delta}(\phi)$ under the same condition, (a/s) = 1, was found to describe a half-wave-rectified sinusoid in Chapter 2, given by (13).

$$\frac{\Delta t}{s\delta}(\phi) = 1 + \cos\phi - |\cos\phi| \quad . \tag{13}$$

---

* This is intended to mean the effective value of the alternating component only.

In the same way in which (13) was found to have an effective value 0.771, just ten per cent higher than that of a sinusoid (see top of page 97), the effective value of (110) is found to be 0.693, just two per cent lower than 0.707. This means that, in this particular case of two-edge time-shift noise, the "PDM component" alone gives about as much noise as is caused by one-edge time shift-noise. However, it decreases rapidly as a/s decreases from unity. It should be remembered that the above method of combining the time shifts of the two edges into a single quantity and operating on this quantity is approximate in that it neglects the time elapsed between the two pulse edges. The approximation is of the same nature as that in the statement that the two-edge audio-noise power in Case 3 is four times the corresponding one-edge time-shift noise power. Of greater importance is the error resulting from the assumption of linear pulse edges, which becomes considerable when a/s approaches unity. This is not serious, however, so long as the two-edge noise is expressed in terms of one-edge noise, which has been determined for nonlinear pulse edges as well.

In addition to the "PDM component", there is of course the "PPM component", which is characteristic of Case 2. Contrary to what one might expect, this component is unaffected by the asymmetry of $\Delta t(\phi)$; this can be shown by again combining the shifts of the two edges, this time by forming half the difference, $\frac{1}{2}[\Delta t(\phi) - \Delta t(\phi + \pi)]$. By direct substitution of (8), the following simple result is obtained.

$$\tfrac{1}{2}\left[\frac{\Delta t}{\delta}(\phi) - \frac{\Delta t}{\delta}(\phi + \pi)\right] = a \cos \phi \quad . \tag{111}$$

The "PPM component" of the two-edge noise in Case 2 is therefore the same as that given in Chapter 3 in the analysis of Case 2. The approximate values of the total audio-noise power is obtained by adding the two components. Addition on a power basis is more nearly correct than addition on a voltage basis, because the two components have completely different spectra.

The preceding discussion of two-edge noise shows a wide variety of possible effects, with the resulting noise power ranging anywhere between $\frac{1}{3}(E\pi D\overline{\Delta t}/T)^2$, obtained from (74) (which may be almost negligible) and four times the noise power resulting from one-edge time-shift noise. With $\Delta\phi = 2\pi n$, it is always close to four times as large, but for $\Delta\phi = (2n - 1)\pi$, it may be much

smaller than the corresponding one-edge noise power if the interference ratio $\underline{a}$ and the duty factor $\underline{D}_1$ are both small; on the other hand it may be of the same order of magnitude as the one-edge noise power, for larger values of $\underline{a}$ and $\underline{D}_1$. The change in the r-f phase difference from leading to trailing edge, $\Delta\phi$, changes continuously with the radio-frequency difference, Δr-f, and the pulse duration, d_1, that is, it is equal to Δr-f $\times$ d_1. Consequently, the noise power exhibits a series of maxima and minima as a function of these variables. The effect of modulation, which causes d_1 to vary, is to blur these maxima and minima (except the maximum at Δr-f = 0). The blurring effect is, of course, directly proportional to Δr-f; when it is large enough to cause the variation of d_1 to sweep $\Delta\phi$ over 360 degrees or more, the minima and maxima are lost completely, and the result is similar to "independent two-edge noise", which has twice the power of one-edge noise.

As mentioned at the beginning of this section dealing with two-edge time-shift noise, this discussion applies only to PDM. Although duration-modulated pulses are also usually obtained in PPM systems in the demodulation processes, the time shifts on the two edges are independent. There are, however, methods of demodulation,* in which the position of a pulse is detected as the position of the center of the pulse - that is, the point half-way between the two edges, rather than by the position of either edge alone. Where such methods are used, the relation between the shifts of two edges of each position-modulated pulse is of great importance. With Δr-f = 0, for example, the shifts are equal and opposite, so that the effective position of the pulse does not change, and no time shift is therefore detected. For Δr-f = $1/2d_0$, which may be as large as 1 Mc, with the short pulses used in PPM, the pulse edges shift more or less together, and the center of the pulse shifts by the same amount. There may therefore be more time-shift noise under certain conditions of adjacent-channel interference than with common-channel time-shift interference; but with the interfering signal differing by 1 Mc from the frequency to which the receiver is tuned, the interference ratio (always measured at the detector), is generally much smaller than in the case of common-channel interference. Also, of course, it must be remembered that the two-edge type of time-shift noise is only one of the possibilities which may exist only if entire pulses are overlapped by the interference, as explained at the beginning of this section.

---

* See Appendix V.

In the general case of two-station PDM interference, discussed in the preceding section, which deals with the more complicated interference situations, it was shown that, with the interfering pulses longer than the desired pulses ($d_2 > d_1$), there is a probability $(d_2 - d_1)/T_2$ of obtaining two-edge overlaps, in addition to the probability $2d_1/T_2$ of obtaining one-edge overlaps. Theoretically, therefore, the total audio-noise power is obtained by combining the expressions for one-edge and two-edge time-shift noise power with their respective weighting factors, as follows.

$$P_{total} = \frac{2d_1}{T_2} P_{one\text{-}edge} + \frac{d_2 - d_1}{T_2} P_{two\text{-}edge} \qquad (d_2 > d_1) \quad . \qquad (112)$$

Depending on the relative difference between d_2 and d_1, the two-edge component may or may not be a significant portion of the total power. Experimentally, the two components can be distinguished by virtue of the fact that the two-edge component varies periodically with Δr-f, while the one-edge component remains constant. In practice, the simpler relation $P_{total} = 2D_2P_{one\text{-}edge}$ gives sufficiently close results under many conditions. However, if, for example, $P_{two\text{-}edge}$ is much smaller than $P_{one\text{-}edge}$, and d_2 is twice as large as d_1, then (112) should be used to avoid a considerable error. These relations will be discussed further in the next chapter, in connection with experimental observations and measurements.

Since the effect of radio-frequency difference, Δr-f, on time-shift noise has been covered in the above discussion, a few remarks about its effect on missing-pulses noise are in order. It was shown in Chapter 2 (see Fig. 19) that the missing-pulses effect loses its characteristics if Δr-f departs sufficiently far from zero to make the r-f phase difference change through several multiples of 360 degrees during the longest desired pulses. This may mean a radio-frequency difference of a few hundred kilocycles, or less, in systems using fairly long pulses, and a difference of a megacycle or more if short pulses are used. A mathematical formulation of the problem is difficult, but a qualitative analysis of the effect of increasing Δr-f from an initial value of zero can be given, as previously indicated in Chapter 2, pages 38 and 39. The audio-noise power rapidly decreases, because the randomness disappears, giving way to a periodic variation of frequency Δr-f. Since this difference

is well above the audio range before the missing-pulses effect degenerates into the beat phenomenon, most of the noise energy is inaudible. There remains only the effect of the random phase difference at the beginning and end of a desired pulse, which combines with the time-shift effect, varying the time at which the edge crosses the slicing level by as much as half a beat period. This effect decreases, of course, with increasing radio-frequency difference. Experimental measurements are plotted and discussed in the next chapter.

CHAPTER 5

EXPERIMENTAL MEASUREMENTS AND OBSERVATIONS

5.1 Experimental Setups

The interference characteristics of pulse-time modulation can be determined experimentally by duplicating or simulating as closely as necessary the various interference situations likely to be encountered in practice. The experimental results presented in this chapter were obtained in this manner, while the theoretical results are found by means of the expressions developed in the preceding chapter. The presentation is divided into four parts, two dealing with two-station interference in which the desired signal is pulse-duration modulated and pulse-position modulated, respectively, and the remaining two dealing with two-path interference in PDM and PPM systems, respectively. Circuit details are given in Appendix V and need not be discussed here; however, the over-all system setups will be described with the aid of block diagrams. The general setups are identical for the PPM tests and the PDM tests, except that different transmitters and receivers are used. Consequently, there are only two different block diagrams; one for two-station interference and the other for two-path interference.

The essential components needed to investigate two-station interference are two complete transmitters, operating on similar radio frequencies, and a receiver. In the present case, at least one of the two transmitters is a PTM transmitter, and the other one may be a pulse-modulated or continuously modulated transmitter, depending on what type of interfering signal is being considered. A PTM receiver is obviously required, inasmuch as the desired signal always consists of time-modulated pulses. In addition to this essential equipment, certain auxiliary components are useful. Cables connecting each of the two transmitters with the receiver are preferable to wireless paths, since they facilitate control of the relative magnitudes of the two signals at the receiver. In addition to the loudspeaker and the human ear as a means of perception, an output meter giving quantitative indications of the r-m-s output voltage is useful, as is also a cathode-ray oscilloscope for observing waveforms at various points in the receiver.

The block diagram of the setup used to study two-station interference is

shown in Fig. 55. The large number of variables involved in this study requires that numerous controls be incorporated in the equipment, or that certain changes can be readily made where controls are impractical. The following is a list of these variables, most of which have been encountered in the theoretical work of the preceding three chapters; the corresponding controls used in the equipment are also listed below and indicated in Fig. 55.

Variable	Equipment Control
1. Radio-frequency difference $\Delta r\text{-}f$:	Both transmitters adjustable over a range of 10 Mc or more
2. Pulse-repetition-frequency difference..... Δprf: (if interference is pulsed)	The prf of one or both of the pulsed transmitters adjustable over a range of 15 kc
3. Duration, in a PPM system, or average duration in a PDM system, of the desired pulses....d_1 and corresponding duty factor.....D_1	In PDM transmitters, pulse duration adjustable from 2δ to well over $\frac{1}{2}T$, corresponding to duty factors of $2\delta/T_1$ to more than $\frac{1}{2}$. In PPM transmitters, pulse duration 0.02 T to 0.05 T.
4. (Average) duration of interfering pulses..... d_2 and corresponding duty factor..... D_2	[T = pulse-repetition period]
5. Coherence or incoherence of the time-modulated pulses with respect to each other	PTM transmitters designed to operate as pulsed oscillators or as pulsed amplifiers
6. Interference ratio..... $\underline{a}$	Adjustable attenuators inserted between the two transmission cables and the receiver input
7. System bandwidth.....BW (this determines the pulse rise and decay times, δ)	Receiver bandwidth variable from 3 Mc down to 150 kc. (Narrow bandwidths achieved by positive feed-back)
8. Audio bandwidth	Audio-filter cut-off frequency (response down 17 db from midband value) either 5 kc or 10 kc, normally 10 kc
9. Slicing level.....$\underline{s}$	Slicing level in receiver continuously adjustable from zero to well above the level of the strongest pulse signals, with additional fine adjustment.

The following additional variables occur in the investigation but do not enter the results as directly as the above nine variables.

10. The absolute values of the radio frequencies: between 30 Mc and 40 Mc.

11. The absolute values of the pulse-repetition frequencies: 15 kc to 30 kc.

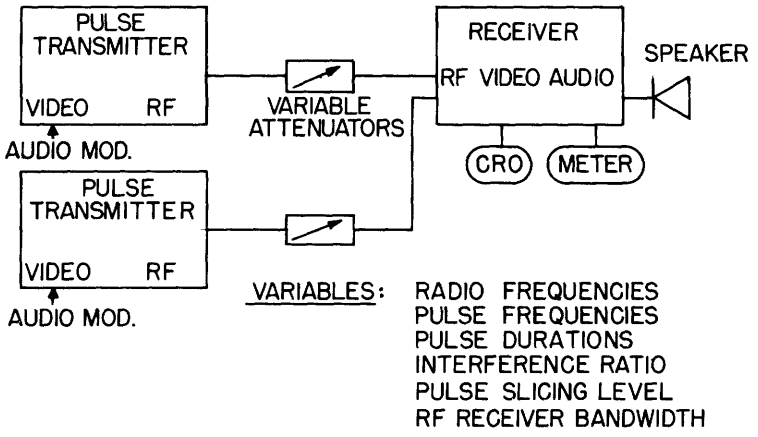

Fig.55 Block diagram of experimental setup for two-station interference.

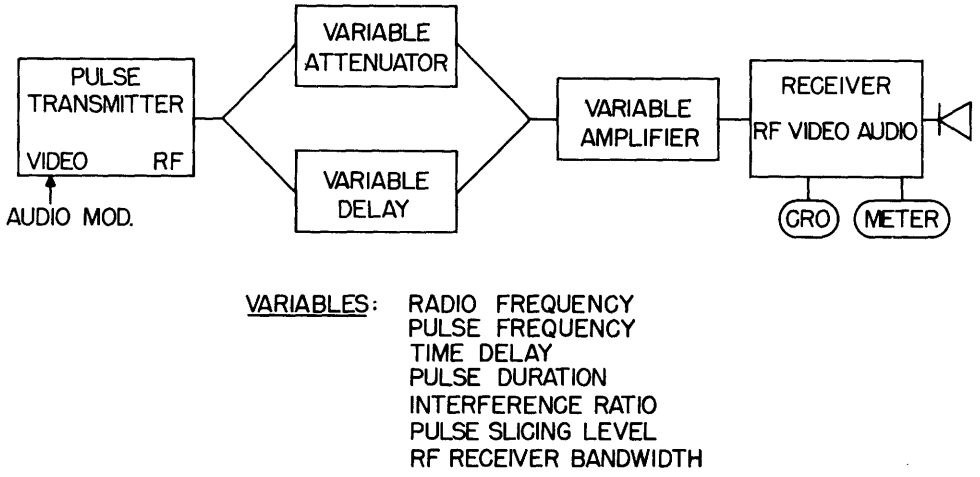

Fig.56 Block diagram of experimental setup for two-path interference.

Another variable, which exists only in the case of PPM systems, is the method of demodulation: the results are dependent, for example, on whether the pulse position is determined from one edge or from the center of the pulse. Essentially two different PPM demodulation schemes have been used in this investigation, with each one adjustable so as to permit various modes of operation. They will be discussed in this chapter only insofar as they affect the results, while the circuits are shown and discussed in Appendix V.

It should be mentioned that the system bandwidth, while normally determined by both transmitter and receiver is determined by the receiver r-f stages alone in the present study. Since the system is linear from the transmitter output to the receiver detector, it is immaterial at which point the

filtering is performed.

The equipment for the investigation of two-path interference differs from that used for two-station interference in two respects: the transmitter producing the interfering signal is eliminated and a time delay is introduced in one of the two transmission paths, both of the transmission paths now leading from the same PTM transmitter to the receiver. A block diagram of the experimental setup used to study two-path interference is shown in Fig. 56. The delay element is a mercury column capable of transmitting radio-frequency signals by means of ultrasonic propagation through the mercury.[25] The electric signal is converted into an ultrasonic beam by a quartz crystal at one end of the delay line, and is reconverted by the same means at the other end. The line used has a delay of approximately one-half millisecond, which is adjustable over a range of several per cent, and its attenuation is in the order of magnitude of 80 decibels.

Fewer variables are involved in the study of two-path interference than in the study of two-station interference, since only a single signal source is involved. Both Δr-f and Δprf (variables 1 and 2) are fixed at zero, and the interference duty factor or pulse duration (variable 4) becomes the same as the duty factor or pulse duration, respectively, of the desired pulses (variable 3). A new variable is the delay difference between the two transmission paths, but the effects of changing the delay difference can also, within limits, be achieved by varying the pulse-repetition frequency and the radio frequency. The question of whether the r-f pulses are coherent or incoherent with each other is more important for two-path interference than for two-station interference, since coherence within one signal means coherence also between the two signals. All remaining variables listed on pages 127 and 128 are the same for two-path interference.

The degree of realism attainable is limited principally by the fact that the laboratory transmission paths do not have the propagation characteristics which actual paths may have at certain frequencies. However, in most cases, the actual situation can be simulated with sufficient accuracy. In the case of two-station interference, only possible variations in the relative attenuations of the two paths would be of importance; however, these generally occur at sub-audio rates and therefore present no problem. In the case of two-path interference resulting from reflections from the ionosphere, airplanes, or other moving objects, the delay difference varies with considerable speed.

This variation has no important effect if the pulses are incoherent, but if they are coherent with each other, it may destroy the otherwise fixed r-f phase relation between the delayed and undelayed signals. The latter is an important effect, which can be simulated at a limited rate by manual adjustment of the delay line, or by modulating the radio-frequency at the transmitter. A great deal of multi-path interference caused by reflections from buildings and other fixed objects is encountered at ultra-high frequencies; in such cases the delay difference is fixed, and the mercury column simulates the actual situation perfectly. The fact that the simulated delay difference is always approximately one-half millisecond need not detract from the generality of the results in spite of the wide range of values which it may have in practice, and the same is true of the radio frequency which is not varied by more than a few megacycles from its nominal value of 30 Mc. Of course, keeping these two parameters nearly fixed in this manner eliminates extreme situations which would occur for very much different values: for example, very small delay differences (smaller than the pulse duration) which cause the overlapping pulses to be coherent with each other; and very high radio frequencies which may make coherence unattainable because of insufficient oscillator stability. However, the results obtained with the present equipment are readily modified to apply to such cases.

Another point with regard to the realism of this investigation of PTM interference is the question of its applicability to multi-channel systems. Although all equipment used in the experimental research is of the single-channel type, the most important situations likely to be encountered with time-division multiplex systems can nevertheless be simulated. For example, two-path transmission may cause the pulses of channel A arriving by way of path 1 to overlap partially with the pulses of channel B arriving by way of path 2; this differs from the single-channel situation in that the two overlapping pulses are modulated by different signals. This situation may be simulated by using two separate transmitters with the same radio frequencies and with pulse-repetition frequencies synchronized. The problem of synchronization, which is of paramount importance in time-division multiplex systems, is outside the scope of this paper, although two different schemes are used in the experimental work. The use of automatic phase and frequency control has already proved its value in television and is definitely indicated also in pulse-communication systems.[26] The conclusions reached for multi-channel PTM systems

assume that synchronization is maintained; loss of synchronization would, of course, result in complete failure of the system.

5.2 Two-Station Interference in PDM Systems

The greater part of this section will be devoted to two-station PDM interference in which the interfering signal is also PDM or at least consists of pulses similar to those of the desired signal. As a starting point, the special case in which the two-pulse-repetition frequencies are equal ($\Delta prf = 0$) will be considered, with each of the interfering pulses overlapping either one edge or both edges of each desired pulse.* This case is simpler than the more general case and has possible application also to other interference situations - notably interference by a continuous signal, and two-path interference between two channels of the same multi-channel PTM system, as explained on page 130.

5.21 Two-Station Interference with Synchronous Pulse-Repetition Frequencies

With one or both of the two pulse trains of the usual incoherent type, the first manifestation of the interference as its magnitude is gradually increased from zero is random background noise. This is the so-called time-shift noise; although it is random in character and is not readily distinguished from ordinary fluctuation noise, some of its characteristics differ from those of fluctuation noise. The following observations and measurements can be made:

(1) Observation of the pulse waveform ahead of the slicer, at the detector output, with the slicer inoperative. Such an observation can give a great deal of information about the pulse rise and decay times, the peak value of the interference time shifts, the interference ratio, and possibly even the radio-frequency difference.

(2) Observation of the pulse waveform after slicing. This shows the time shifts quite clearly and provides a good check on the slicing operation.

(3) Observation of the noise waveform at the receiver output (after filtering), and measurement of the r-m-s voltage of the noise. It is a simple matter to measure the r-m-s signal output for full modulation, and the above measurement therefore gives the signal-to-noise ratio.

---

* The other possibility is that there is no coincidence between the two pulse trains, in which case perfect reception is possible.

5.21(1) Detector Output

Figure 57 is an oscillogram of the detector output in the absence of any modulation; a long interfering pulse overlaps a somewhat shorter desired pulse, producing a resultant which depends on the r-f phase difference. The oscillogram is a superposition of approximately 100,000 such occurrences, each one with a different resultant. The shaded area is produced by the many different resultants, and the gradation of the shading is indicative of the probability distribution of the resultant. The interference ratio can be scaled directly off the oscillogram, as indicated in Fig. 57, in which it is approximately one third. Similarly, the peak time-shift values relative to the pulse durations can be scaled off directly at various slicing levels. (The pulse durations are 20 and 30 microseconds, respectively.) The lateral uniformity and smooth gradation of the shaded area indicate complete incoherence of at least one of the two pulsed carriers. A good method of ensuring total incoherence is afforded by slight noise modulation of either pulse train (preferably the interfering pulse train, since its edges need not be observed). The degree of time modulation needed to ensure incoherence is so slight that the modulation is not visible in Fig. 57. The oscillogram of Fig. 58, on the other hand, exhibits some degree of coherence. Again, this

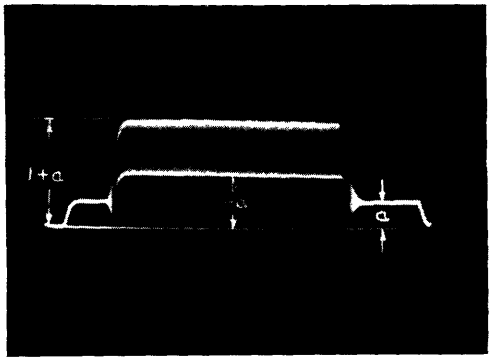

FIG. 57

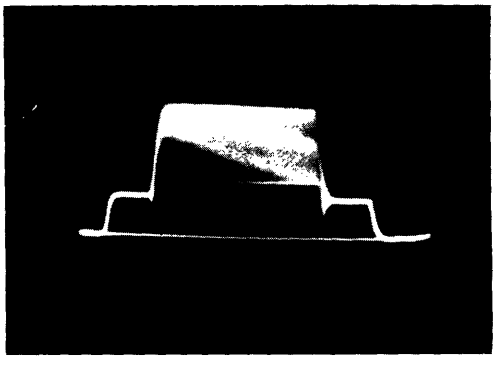

FIG. 58

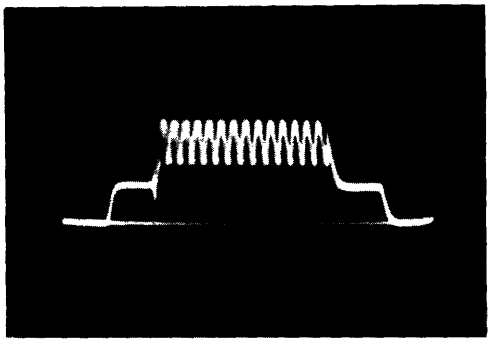

FIG. 59

Figs. 57-59 Detector output showing various degrees of coherence; interfering pulses of longer duration than desired (taller) pulses.

picture is the superposition of nearly 100,000 successive pulses but, in the great majority of these, the r-f phase difference favors certain values. This is particularly evident near the leading pulse edge, where ϕ favors values between approximately -90° and +90°. During the time of the desired pulse, ϕ changes by approximately 90°, favoring 0° to 180° (or 0° to -180°) at the trailing edge. This accounts for the greater concentration of resultants at the leading edge. The change in ϕ of approximately 90°, corresponding to a quarter-cycle of the beat between the two radio frequencies, indicates a radio-frequency difference equal to approximately one-fourth of the reciprocal of the desired-pulse duration, about 15 kc in the present case.

Almost complete coherence is illustrated by the oscillogram of Fig. 59, in which Δr-f is much larger, approximately $14/d_1$ or nearly 1 Mc, since there are fourteen beat cycles in somewhat more than fourteen microseconds. One important consequence of the larger radio-frequency difference is to be noted. The separation between the extreme values of the resultants, which is equal to $\underline{2a}$ if Δr-f is small (see Fig. 57), decreases rapidly as Δr-f is increased above a certain value. This is simply a result of the limited high-frequency response of the detector (due to shunt capacity), and the beat amplitude therefore decreases with increasing beat frequency directly as the detector response. In the case of Fig. 59, the beat amplitude is only $\underline{1.2\ a}$ instead of the usual value $\underline{2a}$. The important consequence is the fact that it is no longer necessary to slice between $\underline{a}$ and $\underline{1-a}$ in order to avoid interference effects other than edge time shifts ($a < s < 1-a$) the limits being $\underline{a}$ and $\underline{1-0.6\ a}$ in the present case. As a result, the maximum value of $\underline{a}$ which still permits slicing with no defects, other than edge time shifts, will be larger than the usual $a = \frac{1}{2}$, namely $a = 1/1.6$. This effect combines with the two effects already discussed at the end of the previous chapter (Section 4.5) to reduce high-interference- ratio noise still further for fairly large frequency separations between the desired and interfering signals. The video bandwidth should therefore not be made any larger than is necessary to prevent the pulse buildup and decay times from being lengthened; these should be determined by the system bandwidth and not affected appreciably by the video bandwidth, which must therefore be somewhat larger than one-half the double-side-band r-f system bandwidth.

In all of the above oscillograms (Figs. 57-59), the interfering pulses (of smaller amplitude than the desired pulses) have longer duration than the

desired pulses and overlap all their edges. If the pulse durations d_1 and d_2 are interchanged, without changing the respective amplitudes 1 and a, none of the desired-pulse edges will be affected by the interference. The oscillogram in Fig. 60 illustrates this for completely incoherent interference; it gives an expanded view of the "tail end" of the interference overlap and shows the completely unimpaired trailing edges of the 100,000 superposed desired pulses. It is possible to detect the position of these edges without any error resulting from the interference, for all interference ratios smaller than one, by keeping the slicing level below $1-a$ ($0 < s < 1-a$). In fact, reviewing Figs. 57-59, one finds that even when the longer pulses have smaller amplitude than the shorter pulses, they can be detected without disturbance by setting the slicing level low enough. This is therefore one of the unusual situations in which the weaker signal is favored; moreover, either signal can be chosen at will by merely adjusting the slicing level, the weaker signal being completely free of noise and the stronger signal virtually so if the interference ratio is small enough. (Of course, the weaker signal will be more susceptible to other noise or interference entering the system.) A second illustration of interference with d_1 larger than d_2 and none of the desired-pulse edges overlapped by interfering pulses is given by Fig. 61, in which both r-f carriers are coherent and Δr-f is approximately 600 kc. In spite of the superficial resemblance to Fig. 59, this waveform is radically different inasmuch as the interference beat does not have a d-c component as in Fig. 59.

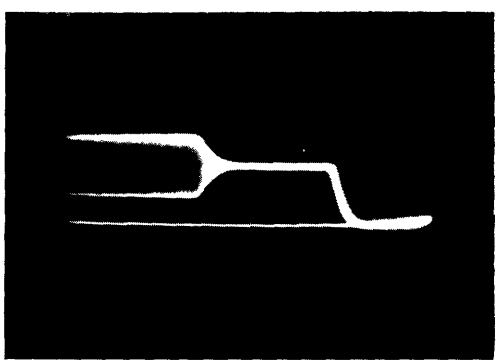

FIG. 60

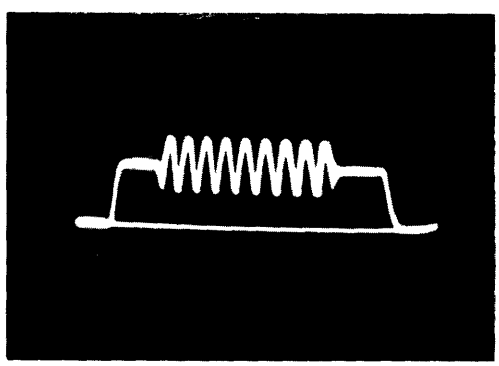

FIG. 61

Figs. 60-61 Detector output for incoherent (Fig. 60) and coherent (Fig. 61) interference. Interfering pulses are of shorter duration than desired (taller) pulses.

The observation of the preceding paragraph, showing that it is possible to select either of two signals by merely adjusting the slicing level, suggests a simple method of selecting any one out of a number of signals transmitted on a single r-f carrier. A pyramid of duration-modulated pulses, each one modulated by its own signal, can be transmitted as shown in Fig. 62, and

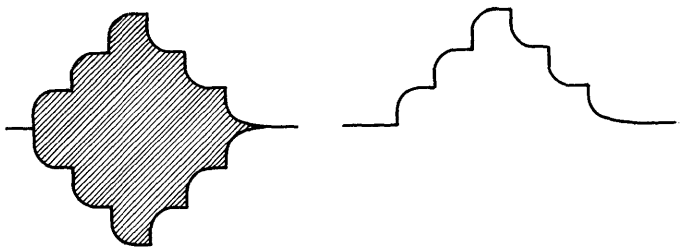

Fig.62 "PDM pyramid".

the individual "stories" can be separated by using different slicing levels. In contrast to the so-called frequency-selection and time-selection methods, this may be called amplitude selection. As is evident from Fig. 62, the degree of modulation of each "story" of the pyramid is strictly limited, which means reduced signal-to-noise ratio. The system bandwidth need not be larger than that required for any one of the "stories" alone, except insofar as long rise and decay times reduce the allowable time modulation by greater relative amounts. The noteworthy feature of the system is the extreme simplicity of the selection scheme at the receiver, particularly if only one "channel" at a time is to be selected. Neither variable tuning nor synchronization nor timing circuits are required. The transmitter, too, can be quite simple.

5.21(2) Slicer Output

Next, the waveform of the slicer output will be considered. Oscillograms of the slicer output are shown in Figs. 63 and 64 for one-edge and two-edge time shifts, respectively. In the first case, the interference was so phased as to overlap only the trailing edge; in the second case, it overlaps both edges of each desired pulse. Since attention is to be focussed on the edges, the pulses shown are shorter than those in the preceding oscillograms, namely seven to eight microseconds at the half-amplitude level. The time shifts, obtained with interference ratios between 0.4 and 0.5, therefore appear relatively large. Ordinarily, because of the wide-band response of the slicer and video-amplifier stages, these pulses have shorter rise and decay

times. These had to be lengthened, however, in order to make the edges clearly visible without excessive over-exposure on other parts of the pulse. These oscillograms not only show the peak-to-peak time shift, but also confirm the theoretical predictions with regard to the time-shift distribution.

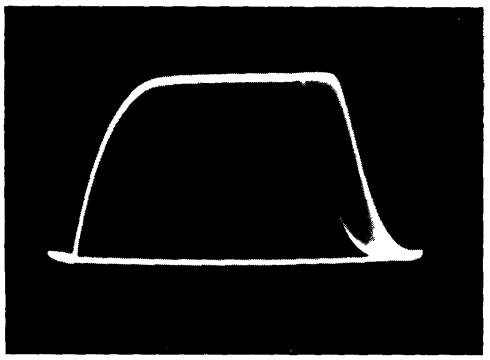

FIG.63

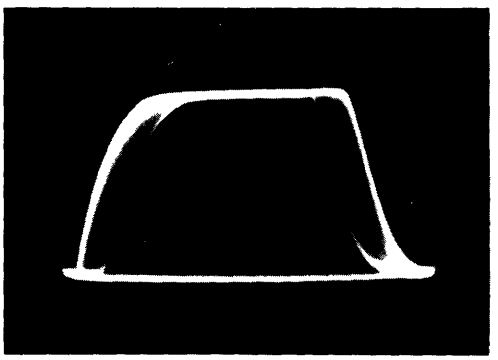

FIG.64

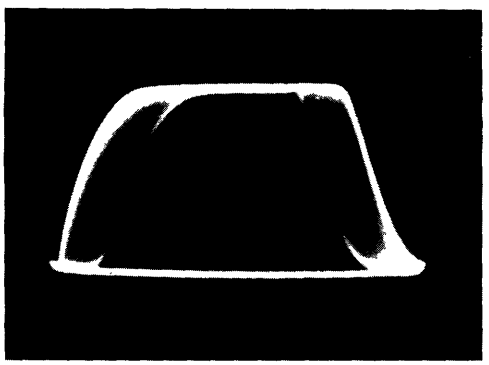

FIG.65

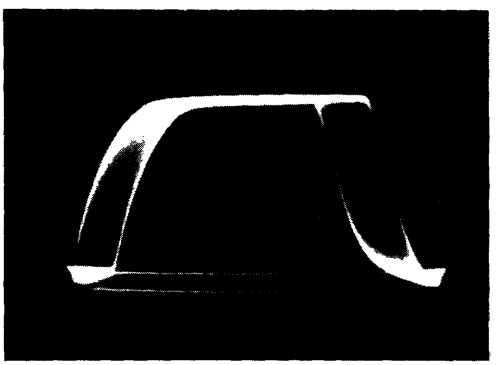

FIG.66

Figs.63-66 Slicer output showing one-edge random time shift (Fig.63), two-edge random time shift (Figs.64-65), and sinusoidal two-edge time modulation shown for comparison (Fig.66).

Since the interference ratio is nearly one-half, the peak advance of the leading edge and peak delay of the trailing edge are strongly favored over other shifts, as confirmed by the brightness distribution or gradation of the shaded areas. Figures 65 and 66 show a comparison between the random time shifts caused by interference and nonrandom time shifts caused by sinusoidal time modulation, respectively. The difference in time-shift distribution is quite apparent, as is the finer "texture" of the shaded areas. (Nonuniformities such as the apparently unequal modulation of the two edges are caused by CRO-sweep nonlinearity.)

5.21(3a) Observation of Audio Output

Information about the audio output is, of course, more directly pertinent to the interference problem, since the ultimate effect is of principal interest.

Appreciation of such information, however, is greatly facilitated by the other two observations discussed under 1. and 2. in the preceding pages. The most important item is the measurement of the audio-noise power or voltage as a function of variables such as the interference ratio; but first a small investigation of some characteristics of the audio noise is in order. Oscillograms of time-shift audio noise are shown in Figs. 67 and 68 with long and relatively short exposures, respectively. The appearance of the noise in Fig. 67 is the layman's conception of noise: the voltage variations are too rapid (relative to the sweep period) to be resolved, and so many incoherent superpositions of successive sweeps compose the oscillogram that the resulting picture gives little suggestion of the fact that the noise is nothing more than a single-valued function of time. However, Fig. 67 does convey some information: it shows, in a qualitative way, the amplitude distribution of the noise. It is apparent that this distribution is quite different from the distribution of the time shifts, favoring the average rather than the extremes. The oscillogram of Fig. 68, though still a superposition of several successive sweeps, shows the point-to-point variations of the noise voltage.

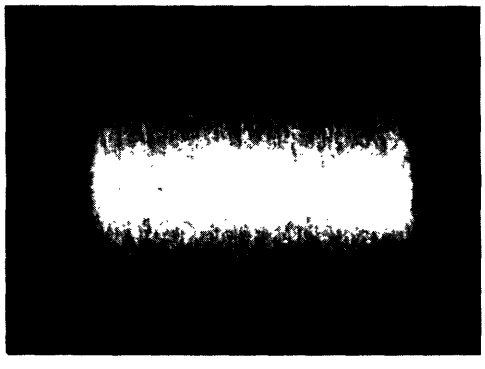

FIG. 67

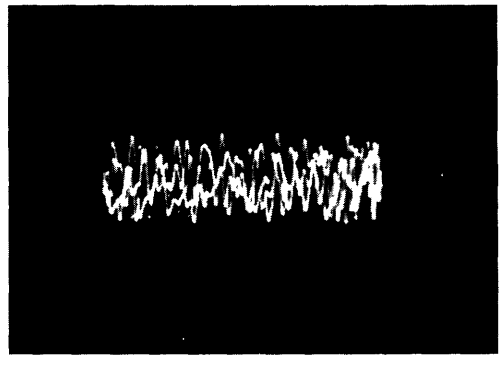

FIG. 68

Figs. 67-68 Oscillograms of random time-shift noise with 5-second exposure (Fig. 67) and with 1/100-second (Fig. 68).

It can be seen that there is no relation between the noise occurring during the successive sweeps. An average frequency can be determined by counting zero-axis crossings or using a frequency meter, and this turns out to be approximately at the "center" of the audio characteristic, approximately 5 kc for the 10-kc filter and 2.5 kc for the 5-kc filter.

Although the audio-noise power resulting from any time shift of specified distribution through an audio system of known characteristics is completely

defined by (89) (page 96), it is nevertheless of interest to consider the noise power in terms of the instantaneous voltage, at least in a qualitative manner. The following facts are known: if the audio system had the ideal low-pass filter characteristic, the audio-noise power would be the same as the audio power resulting from sinusoidal modulation within the pass band (on the assumption that the interference time-shift distribution is sinusoidal). This means that the output noise voltage would have the same peak amplitude as the sinusoidal output, and also the same amplitude distribution; for the peak amplitude can obviously not be any larger, nor can the crest factor (ratio of peak value to r-m-s value) become smaller than the original value of $\sqrt{2}$ in a linear system. Therefore, in the limiting case of the ideal low-pass filter, both the peak value and amplitude distribution of the time shifts are preserved in the output voltage. (Preservation of the peak value is intended to mean that $V_{max} = E(\Delta t_{max}/T)$, see Section 4.1.) The noise voltage obtained with the actual nonideal audio characteristic obviously does not have the sinusoidal amplitude distribution. Inspection of Fig. 67 shows that the crest factor is considerably larger than that of a sinusoid and also larger than that of a sawtooth ($\sqrt{3}$) with its flat amplitude distribution. Furthermore, measurement of the peak-to-peak time shift and the peak-to-peak noise voltage shows that the peak time-shift value is not preserved in the output noise voltage. The maximum time shift is now given by

$$V_{max} = g_1 E^{\frac{\Delta t_{max}}{T}} , \qquad (113)$$

in which g_1 is smaller than unity and may be termed the peak-reduction factor. It depends on the audio characteristic; for example, its value is approximately 0.9 for the 10-kc filter and 0.8 for the 5-kc filter. The peak-reduction effect can be readily explained by physical reasoning: the transient response of the audio system is too slow to permit the output voltage to follow the sample values, and for the same reason the amplitude distribution is altered in favor of the smaller instantaneous voltage values. The crest factor can be evaluated by peak and r-m-s noise measurements, which has led to values between 2.0 and 3.0, depending on the audio characteristic. The approximate value of 2.2 obtained with the 10-kc filter represents an increase over the original value 1.4 by a factor of somewhat more than 1.5,

or a reduction in r-m-s value by that factor for a given peak value. The reciprocal of this factor may be called the r-m-s reduction factor, g_2, and is defined as follows:

$$g_2 = \frac{\text{crest factor of samples}}{\text{crest factor of output}} \quad . \tag{114}$$

Multiplication of the two reduction factors g_1 and g_2 should give the factor by which the r-m-s noise voltage is smaller than the ideal-filter output voltage, namely k_f defined in Section 4.1. It is the square root of the ratio of the area under the actual squared filter characteristic to the area of the ideal squared filter characteristic. With the above figures, one obtains $k_f = g_1 g_2 = (0.9)(0.64) = 0.58$. The value of k_f as obtained from the filter-characteristic area is also approximately 0.6 for the 10-kc filter. It should be pointed out that this is by far the more reliable and direct method of obtaining k_f; accurate experimental determinations of g_1 and g_2 are difficult, and a mathematical formulation of these factors is not attempted; their purpose and the purpose of the preceding discussion is merely to show as much as can be readily seen about the characteristics of the time-shift noise by making some simple observations and measurements.

5.21(3b) Measurement of Audio-Noise Power

As mentioned previously, the measurement of greatest importance is that of the audio-noise power or r-m-s voltage as a function of the variables involved. Inasmuch as this section is a treatment of the special case $\Delta prf = 0$, there are not so many variables involved, particularly for interference ratios less than one-half. The pulse-edge time-shift noise can be either of the one-edge or of the two-edge type, depending on whether the interfering pulses are so phased as to overlap one set of desired-pulse edges or whether they are long enough and so phased as to overlap both sets of edges. Missing-pulses noise depends directly on the amount of overlap relative to the pulse-repetition period. Of principal interest is the variation of the total noise, or noise-to-signal ratio, as a function of the interference ratio, a. This is shown in Fig. 69 for the conditions indicated, and theoretical curves obtained in part by computation from (103) (see Section 4.3) are superimposed in broken lines.* The quantity plotted is r-m-s volts for

* All plots are for the 10-kc audio filter ($k_f \approx 0.60$); for the 5-kc filter

100-volt pulses (E = 100); to obtain the noise-to-signal ratio one need only remember that the peak signal is $100(\Delta t_{max}/T)$ or approximately 100 D_1, corresponding to ideal peak-signal voltages of 10 and 30 volts, respectively, for the two curves. The actual peak-signal values are several volts lower because the finite rise and decay times limit Δt_{max} to somewhat less than d_1.

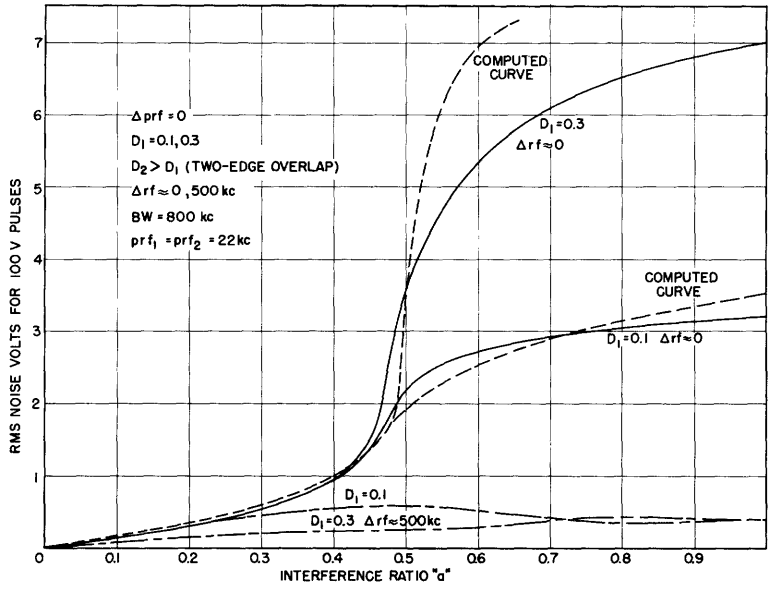

Fig.69 Interference noise voltage versus interference ratio.

The outstanding feature of these curves is the knee at a = 0.5, caused by the rather sudden appearance of the missing-pulses effect. It is particularly outstanding if the duration of the missing pulses is much larger than the pulse rise time and hence the peak time shifts, and it becomes almost unnoticeable when these quantities are of the same order of magnitude, as will be shown later.

The discrepancy between the experimental and computed curves can largely be accounted for. Expression (103), based on linear pulse edges, was used to give the computed results, except for the values for a = 0.40 and 0.49, which were obtained from computations based on exponential pulse edges (see Section 4.1). However, as pointed out in Section 4.3, the time-shift noise component included in (103) and in (104) is too small, and this presumably accounts for the most serious discrepancy in Fig. 69, namely the excessive

---

($k_f \approx 0.42$), all experimental and theoretical values of noise are approximately 3 db lower. The filter characteristics are given in Appendix V.

difference between the two computed curves for D_1 = 0.1 and 0.3, respectively. Since the same time-shift noise component is common to both curves, an increase in this component will raise the lower curve while hardly affecting the upper curve, inasmuch as this component is added to the remaining (larger) components on an r-m-s basis. Although both curves will be somewhat high, the ratio of their ordinates will be more nearly that expected.

The data for Δr-f = 500 kc are included in Fig. 69 as typical curves for adjacent-channel interference. In the case of the smaller duty factor (D_1 = 0.10), the two-edge time-shift noise is more or less of the PDM type (Case 3, $\Delta\phi = 2\pi m$, see Section 4.5), while in the case of the larger duty factor (D_1 = 0.30), it is of a type intermediate to PDM and PPM (Case 2) and is consequently smaller than the Δr-f = 0 value. In either case, the important feature is the relatively small noise increase, if any, with increasing a, for values of a above 0.4 or 0.5. A complication occurs for relatively large values of Δr-f as the interference ratio a is changed (between 0.5 and 1.0): the value of $\Delta\phi$ (see Section 4.5) also changes, because the slicing level s is varied with a and the effective pulse duration, d_1, consequently also varies somewhat. This accounts for the slight drop in the noise voltage for D_1 = 0.1 and Δr-f = 500 kc.

The variation of the r-m-s noise voltage with the radio-frequency difference, Δr-f, is shown in Fig. 70, for one particular set of values, a = 0.3 and d_1 = 2 microseconds. The plot is normalized with respect to the one-edge

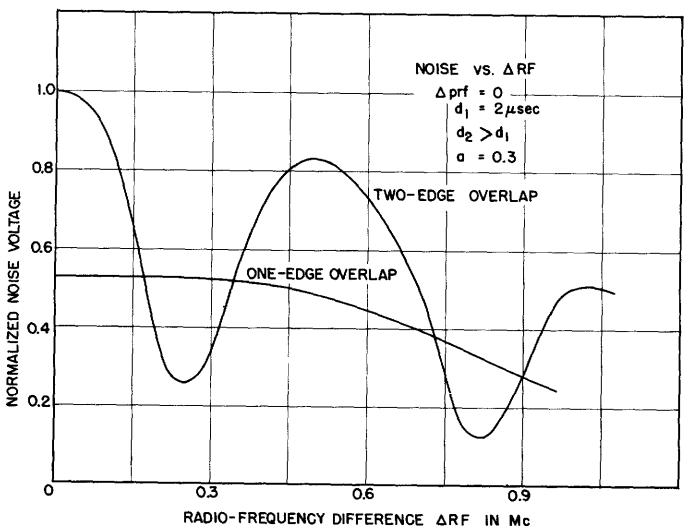

Fig.70 Interference noise voltage vs. radio-frequency difference.

noise value. Theoretically, the one-edge time-shift noise is independent of the r-f difference, while the two-edge noise oscillates in accordance with

the principles discussed in detail in the last section of the preceding chapter (Section 4.5). The highest value of the two-edge noise voltage is nearly twice that of the one-edge noise voltage, as predicted, while the lowest value is somewhat less than one-half the one-edge noise voltage. This minimum value, occurring for $\Delta\phi = \pi, 3\pi, \ldots$, is composed of a PPM and a PDM component: the former is given by (74) in Section 3.5, and with the duty factor just under 0.05 it amounts to less than ten per cent of the one-edge noise voltage. The PDM component, resulting from the asymmetry of $\Delta t(\phi)$, is given by (109) and by the series expansion included in Appendix IV B. For $\underline{a}$ = 0.3, the interference ratio in Fig. 70 , it equals slightly more than one-third of the one-edge noise. The two components combined on a power basis amount to somewhat less than forty per cent of the one-edge noise voltage, as compared to forty to fifty per cent in Fig. 70. The somewhat higher experimental values can readily be accounted for by the additional asymmetry in $\Delta t(\phi)$ due to the exponential shape of the edges which begins to be noticeable at a = 0.3 and exerts an increasing influence at larger values of $\underline{a}$. Curves of noise voltage for longer pulse durations (d_1) have a similar appearance but exhibit proportionately more oscillations in a given range of r-f difference.

A similar plot of r-m-s noise voltage, with the duty factor (D_1) or pulse duration (d_1) larger than in Fig. 70, is shown in Fig. 71. The important difference, however, is the larger interference ratio, a = 0.8 instead of a = 0.3, For Δr-f = 0, the noise consists mostly of the missing-pulses component, which decreases rapidly with increasing r-f difference, leaving essentially only the two-edge time-shift noise.

The cross-talk and signal-reduction effects have been discussed in the preceding chapter (Section 4.2, pages 103-104). Since they occur only in the presence of strong missing-pulses noise ($\frac{1}{2} < a < 1$, Δr-f $\ll 1/d_1$), any cross-talk is generally lost in the noise. In the most extreme cases, with $\underline{a}$ almost unity, the signal-voltage reduction amounts to thirty to fifty per cent when the interference overlaps both sets of edges of the desired pulses, and fifteen to twenty per cent if one set of edges is overlapped.

5.22 Continuous-Wave Interference in PDM Systems

Continuous-wave interference in PDM systems is similar to the type of interference discussed in Section 5.21. The only difference is that the

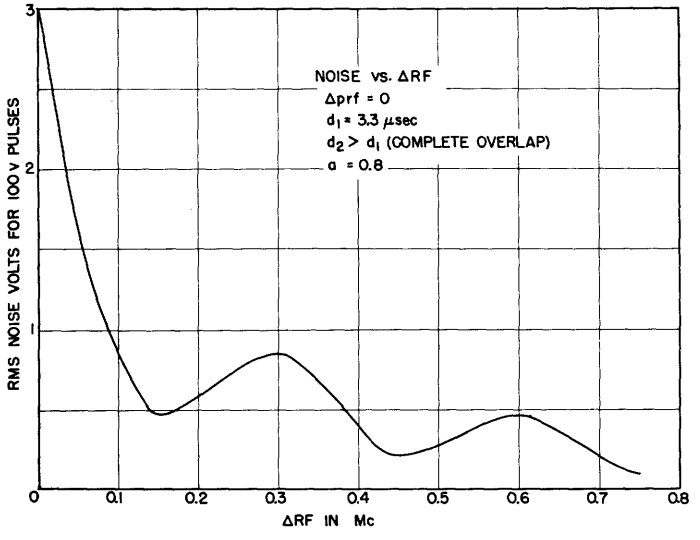

Fig.71 Interference noise voltage vs. radio-frequency difference.

interference necessarily overlaps both edges of each desired pulse, and that there is a greater chance of coherence. Continuous signals, unless frequency-modulated, are generally coherent. The desired signal, even though it originates from a pulsed oscillator, has enough coherence in the absence of time modulation to make the normally random interference noise (resulting from either time shifts, missing pulses, or both) take on a semi-random character. This means that, in the absence of modulation, the sound resembles that of frying eggs or sometimes that of a Bunsen burner but reverts to the usual hiss noise as soon as a slight amount of time modulation is imposed on the leading pulse edges. The results are then exactly the same as those of Section 5.22 (when the synchronized interfering pulses overlap the desired pulses completely); even when the noise is of the semirandom type, its r-m-s voltage is generally within ten per cent of that of the perfectly random noise. It is likely that at radio frequencies higher than 30 to 40 Mc (used in this study) the tendency toward nonrandomness becomes increasingly smaller. There is always some slight time modulation or "jitter" on the pulse edges (caused by power-frequency pickup and fluctuation noise) which spoils the possibility of perfect coherence. Such time modulation would have to be in the order of magnitude of 1/30 microsecond at carrier frequencies of approximately 30 Mc, but only about 10^{-4} microsecond at X-band frequencies.

Gating the output of an oscillator*, instead of pulsing the oscillator

* See Appendix V, Fig. 146.

itself, theoretically results in r-f pulses which are coherent with each other regardless of their time modulation. In practice, at 30 Mc, this is found to be true provided that the oscillator frequency is stabilized by use of a crystal. As a result, the time-shift and missing-pulses noise are not random; instead they assume the character of beat notes between the interfering carrier on the one hand and the carrier and side bands of the desired pulses on the other hand. With large interference ratios (close to unity), the noise is prohibitively strong only if Δr-f is in the audio range, so that the beat between the two carriers is audible. The actual noise voltage is larger than in the random case by the factor $H(\omega)/k_f$, where $H(\omega)$ is the audio gain at the frequency of the beat, Δr-f, and k_f the audio-filter constant defined in Section 4.1. This factor is larger than one over most of the audio range, except at the extremities where the response decreases well below its midband value, and the beat note is correspondingly weaker. When Δr-f is outside the audio range, there is generally a multitude of beat notes; like the random noise voltage in the incoherent case, the voltage of the beats has a series of maxima and minima as Δr-f is increased, but the noise is considerably less offensive to the average listener.

The effect of the slightly imperfect coherence which may be attained if the oscillator is not crystal-controlled is to give rise to "corrupted" beat notes instead of the clean beat notes. This may occur, for example, as a result of some sixty-cycle frequency modulation of the oscillator. It is improbable, though not impossible, that the practically perfect coherence attainable at 30 Mc through use of quartz crystals is readily attainable at very much higher radio frequencies. It must be remembered that the absolute, not the relative, stability must be the same in order to give the same degree of coherence; only the short-time stability is involved (a few seconds or less).

Regardless of whether the interference noise is random or nonrandom, the missing-pulses noise is accompanied by the signal-reduction effect. With pulse durations less than approximately twenty per cent of the pulse-repetition period, the signal voltage at any audio frequency is reduced to (1-F) of its normal value; this means a decrease of $3\frac{1}{2}$ decibels for F = 1/3 (interference ratio about 0.9 or higher). For longer pulse durations, however, the reduction is somewhat larger, especially in the incoherent case, in which the intense random missing-pulses noise appears to have a masking effect. Reductions as large as seven decibels have been measured for duty factors of

fifty per cent.

If the continuous interference is amplitude-modulated, the modulation does not reach the output so long as the peak interference is less than one-half the pulse amplitude. However, for larger interference ratios, it does reach the output and the PDM signal cannot be properly received, unless Δr-f is large.

5.23 Two-Station Interference with Asynchronous Pulse-Repetition Frequencies

If one or both of the two pulse trains are of the usual incoherent type, the first manifestation of the interference, as the interference ratio is increased from zero, is random time-shift noise. The quality of this noise may or may not differ appreciably from that of the time-shift noise discussed in Section 5.22, depending on the relative pulse durations and repetition frequencies. The noise in the present, more general, case generally consists of bursts of the continuous noise obtained in the situations treated in Section 5.21. As in that section, the experimental study is broken down into several distinct types of observations and measurements (see pages 131-132), which will be discussed in turn.

5.23(1) Detector Output

Oscillograms of the detector output under various conditions are shown in Figs. 72 through 75. As in similar oscillograms shown in Section 5.21, the shaded area is produced by the many different resultants of the desired and interfering pulses. The CRO sweep is synchronized with the repetition frequency of the desired pulses; consequently the interfering pulses are not stationary and therefore not visible on these oscillograms, which are superpositions of between 50,000 and 100,000 successive sweeps. However, the heavy white line of height a (see Fig. 72) represents the tops of the interfering pulses. All the various possible relative phase positions between the two pulse trains are encountered in at least a few of the many superposed pictures: the heavy white line (see Fig. 72) starting from the bottom (zero line) and then passing through the shaded region is the desired pulse; it appears on these oscillograms because many of the desired pulses (out of the 100,000 composing the oscillogram) are partially or totally undisturbed by the interfering pulses. On the other hand, every part of the desired pulse is sooner or later affected by the interference, with every possible value of the r-f phase difference ϕ, and the result is the uniform interference

envelope. The gradation of the shaded area is indicative of the probability distributions of the time shifts at the pulse edges and of the pulse amplitudes at the pulse tops. Furthermore, Figs. 72 and 73 show the peak positive and negative time shifts of both the leading and trailing edges at any slicing level $\underline{s}$, between $\underline{a}$ and $\underline{1-a}$. In spite of the relatively small difference in interference ratios for these two oscillograms, the peak-to-peak time shifts differ by a factor of approximately two, which substantiates the logarithmic relation (92) and the plot of Fig. 50 in Section 4.1. The same oscillogram

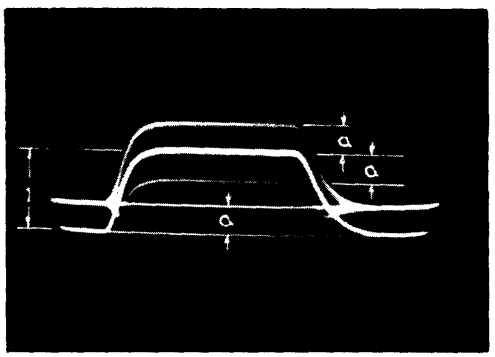

FIG. 72

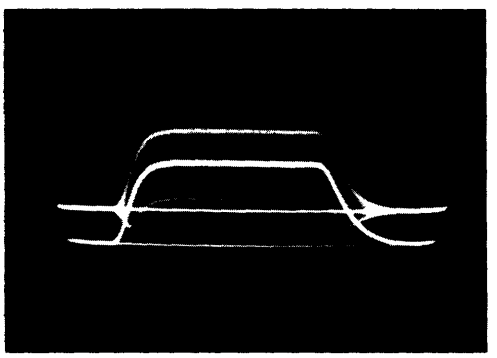

FIG. 73

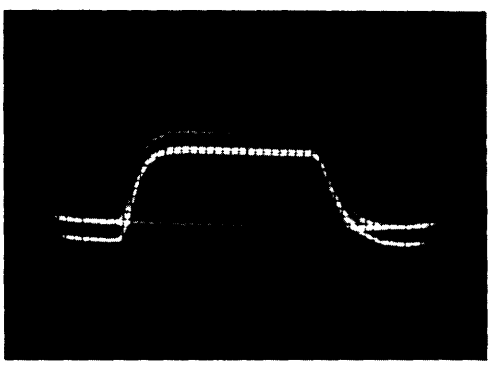

FIG. 74

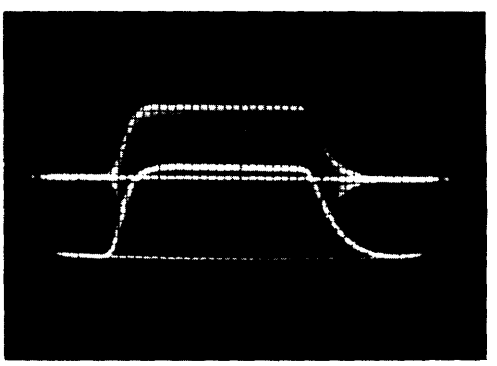

FIG. 75

Figs. 72–75 Oscillograms of detector output for interference ratios $\underline{a}$ = 0.35, 0.42, 0.20, 0.90, respectively.

as that of Fig. 72 was shown in Fig. 13 (Chapter 2) as a comparison against Fig. 12, the theoretical superposition of the desired and interfering pulses. Apart from differences in pulse shape, there is only one noticeable discrepancy between the theoretical and actual resultant envelopes: in the oscillograms, the two little negative peaks at the leading and trailing edges, respectively, should actually reach zero. This theoretical zero value occurs at the instant of time when the desired-pulse edge passes the value "a", only on those occasions on which the r-f phase difference ϕ is within a few degrees of 180°.

Since it lasts only an infinitesimal time and is near zero for a small fraction of the pulse rise or decay time, the video transient response is insufficient to follow the actual envelope at the points in question.

Figure 74, which is also an oscillogram of the detector output, illustrates the larger choice in slicing level ($a < s < 1-a$) when a is relatively small. It is evident, nevertheless, that the optimum slicing level is at about one-half the height of the desired pulse; at higher levels, the leading edge is subject to larger time shifts, and at lower levels, the trailing edge has larger shifts. The other extreme, large interference ratio, is illustrated by the oscillogram of Fig. 75. The optimum slicing level is just above the heavy white line of height a, but below the desired-pulse height, unity. The resultants which compose the lower half of the shaded area are those which never reach the slicing level and are responsible for the missing pulses in the output. The great majority of those resultants which do pierce the slicing level are seen to have large positive time shifts (leading edge advanced, trailing edge retarded). The brightness distribution of the shaded area checks with the mathematical fact that two nearly equally large vectors have a probability of 2/3 of yielding a resultant larger than either vector, the remaining 1/3 being the probability that the resultant is smaller (therefore causing a missing pulse). In fact, the bright rim along the upper border of the interference envelope indicates a distribution approaching that of the half-wave-rectified sinusoid, with the rim corresponding to the flat (zero-slope) portions.

The effect of increased radio-frequency difference on the interference envelope is the same as in the case of synchronous pulse-repetition frequencies, discussed in some detail on page 133. The separation of the extreme resultant values decreases from its peak value of $2a$ in accordance with the video-response characteristic, making it possible to avoid the missing-pulses effect even for interference ratios larger than 0.5.

Unlike the special cases discussed in Section 5.21, the present, more general, case never permits discrimination in favor of the weaker (interfering) signal, regardless of whether its pulse duration is longer or shorter than that of the desired-pulse signal. So far as the appearance of the detector output (Figs. 72-75) is concerned, the duty factor of the interfering pulses has only one easily noticeable effect: if it is very small, the shaded regions and the horizontal line of height a (the interference level) are scarcely visible,

while the desired pulse appears perfectly normal. As the interference duty factor is increased, the dim regions become brighter, and the zero base line and the outlines of the desired pulse become dimmer; they disappear completely when the interference duty factor is unity, as in the case of continuous interference.

5.23(2) Slicer Output

The oscillograms in Figs. 76 - 79 differ from those of Figs. 64 and 65 in that, of the 50,000 to 100,000 pulses superposed to form each oscillogram, only a fraction have shifted edges. This fraction is large, well over one-half in the case of Fig. 76, as a result of a large interference duty factor, but it is considerably smaller in the other three oscillograms. The rise and decay times of the pulses had to be lengthened by reducing the high-frequency response of the video stages, in order to make the shaded regions visible.

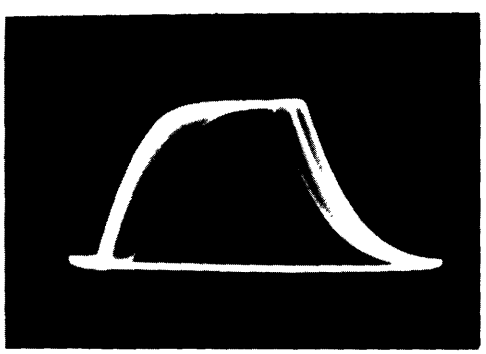

FIG. 76

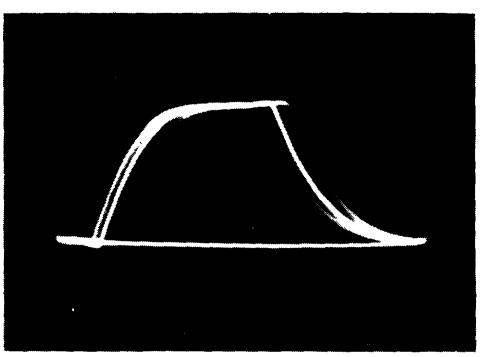

FIG. 77

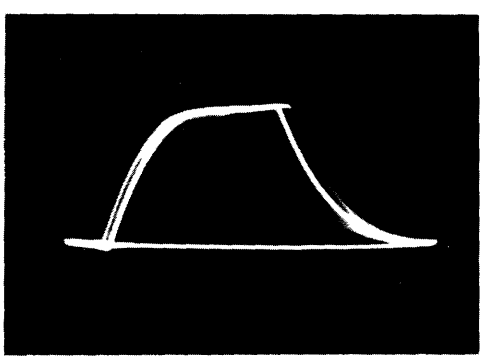

FIG. 78

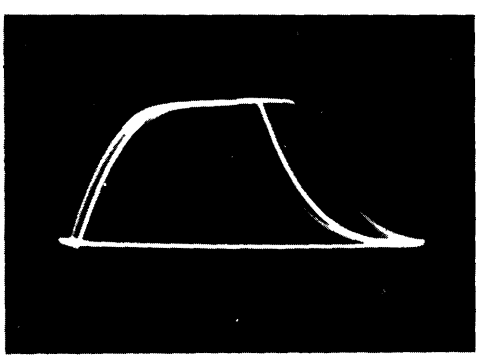

FIG. 79

Figs. 76-79 Oscillograms of slicer output for large interference duty factor (Fig. 76) and for small interference duty factor with various slicing levels.

Figures 77 - 79, obtained under identical conditions except for slicing level (interference ratio, a = 0.4), illustrate the effect of varying the slicing level, s. Figure 77 represents the optimum condition ($s \approx 0.5$) as confirmed

by the fact that the peak-to-peak time shifts of the two sets of edges are approximately equal. In the case of Fig. 78, and also Fig. 76, the slicing level is too high, so that some of the leading edges are delayed excessively; in the case of Fig. 79, the slicing level is too low, so that some of the trailing edges are delayed excessively. It will be noticed that the trailing edges with the largest delays in Fig. 79 are much more clearly visible than the leading edges with the largest delays in Fig. 78. This is not the result of different photographic exposures; it is the result of the asymmetrical time-shift probability distributions which always favor positive time shifts (leading edges advanced, trailing edges delayed); consequently, the fraction of the total number of trailing pulse edges which are delayed excessively when the slicing level is below one-half by a certain amount is larger than the corresponding fraction of leading pulse edges when the slicing level is above one-half by the same amount. A high slicing level is therefore less harmful, in general, than a low slicing level. An additional reason causes a slightly high slicing level to be preferable; this is the desirability of having little or no "direct component" in the time shifts, in order to minimize the Δprf beat note (see Section 4.4, pages 114 and 115). Thus, for example, comparison of Figs. 78 and 79 shows that, while the total effective time shift is definitely smaller in the former, the direct component may be smaller in the latter, particularly for the trailing edge. In other words, it is desirable to counterbalance the asymmetry of the time-shift distributions by a different, opposite asymmetry: the preference for positive time shifts is offset by making the negative time shifts larger so as to compensate for their smaller number. This will be further illustrated in the next section, dealing with the direct observation of the output-noise bursts.

5.23(3a) Observation of Audio Output

The audio noise is considerably more complex in the general case of asynchronous pulse-repetition frequencies than in the special case of synchronous pulse-repetition frequencies. The essential feature is that the noise is generally discontinuous or at least nonuniform as a function of time. This can be readily explained and illustrated by oscillograms of the output noise. Time-shift noise will be considered first. Suppose that neither of the two pulse trains are modulated, that the interfering pulses are of shorter duration than the desired pulses ($d_2 < d_1$), that the pulse-repetition

frequencies differ by a sub-audio frequency, 1 cps, for example, and that the interference ratio is less than one-half. A sequence of four events, lasting a total of one second, will then repeat periodically at the difference frequency, 1 cps (Δprf). The following events take place during the one-second period: (1) during a fraction D_2^* of this period, the interfering pulses overlap only the leading edges of successive desired pulses, causing one-edge time-shift noise; (2) next, if $T_2 > T_1$, there will be an interval $(d_1 - d_2)/T_2$ during which the interfering pulses coincide with the central portions of successive desired pulses without overlapping either edge. No time-shift noise results during this second interval. (3) During the third interval, which lasts a fraction D_2 of the one-second period, the interfering pulses overlap only the trailing edges of successive pulses, causing one-edge time-shift noise as during the first interval. (4) Finally, during the fourth interval, which lasts a fraction $1 - [(d_1 + d_2)/T_2]$ of the beat period, the interfering pulses coincide with the spaces between desired pulses, and no noise results. With $T_1 > T_2$, the order of these four events is simply reversed. If the two pulse-repetition frequencies differ by more than 1 cps, the four intervals, while still occupying the above respective fractions of the total beat period, last for a shorter absolute duration. In terms of the beat period T_{12} corresponding to the difference between pulse-repetition frequencies, Δprf, the respective durations of the four intervals are

$$W_1 = D_2 T_{12} \qquad \text{(leading edges shifted)}$$

$$W_2 = (d_1 - d_2)\frac{T_{12}}{T_2}$$

$$W_3 = D_2 T_{12} \qquad \text{(trailing edges shifted)}$$

$$W_4 = (T_1 - d_1 - d_2)\frac{T_{12}}{T_2} \qquad T_{12} = \left[\frac{T_1 T_2}{T_1 - T_2}\right], \quad d_1 > d_2 \ . \qquad (115)$$

---

* The following symbols will be recalled:

d_1 = duration, D_1 = duty factor, T_1 = repetition period, of desired pulses

d_2 = " , D_2 = " , T_2 = " " , of interfering pulses.

Two complete beat periods, each lasting approximately 33 milliseconds (Δprf = 30 cps), are shown in the oscillogram of the audio output in Fig. 80. Because of the long duration of W_1 and W_2 (4 milliseconds), each noise burst is composed of a large number (approximately 100) of successive shifted edges. Consequently, with such low values of Δprf, the voltage variations within the individual noise bursts are not distinguishable. The oscillogram, which consists of the superposition of several successive sweeps, is intended merely to show the sequence of events. It is to be noted that the leading-edge and trailing-edge noise bursts are distributed along the time axis in the same way as the leading and trailing edges of the desired pulses. By measuring the relative durations of the various intervals, one can infer that D_2 is approximately 1/8 and D_1 about 1/4, or possibly 3/4. It is important to remember, however, that the absolute time durations are quite different from the corresponding intervals of the desired pulse train; they differ by the factor T_{12}/T_2, as can be seen by inspection of (115) and the dimensions given in Fig. 80.

The oscillogram of Fig. 81 was obtained under somewhat different conditions (Δprf = 200 cps), with a faster CRO sweep. It is not a superposition of a number of successive sweeps, but shows merely a single beat period. The interference ratio in both Figs. 80 and 81 is between 0.4 and 0.5, and a trace of missing-pulses noise resulting from imperfect slicing is visible during "interval 2", between the leading- and trailing-edge noise bursts. In these oscillograms, and also in subsequent ones, T_2 is kept larger than T_1, so that the interfering pulse train "slides through the desired pulse trains from left to right (in the positive time sense)". In Fig. 81, the leading-edge noise burst is considerably larger than the trailing-edge noise burst, mostly because the slicing level is high. This will be discussed in more detail later. The individual samples (successive pulses with edge-time shifts) forming each noise burst can be distinguished.

A somewhat different sequence of events occurs during each beat period if the interfering pulses are of longer duration than the desired pulses ($d_2 > d_1$). The four intervals correspond to (1) interfering pulses overlapping leading edges of the desired pulse, (2) interfering pulses overlapping the leading and trailing edges of each desired pulse,(3) the trailing edges only, and (4) not coinciding with any part of the desired pulses. This can also be interpreted as another form of the case discussed above, in which

intervals (1) and (3) (see page 150) overlap and form interval (2) in the sequence outlined above. The respective durations of the four intervals are now

$$Y_1 = \frac{d_1}{T_2} T_{12} \qquad \text{(leading edges shifted)}$$

$$Y_2 = (d_2 - d_1) \frac{T_{12}}{T_2} \qquad \text{(all edges shifted)}$$

$$Y_3 = \frac{d_1}{T_2} T_{12} \qquad \text{(trailing edges shifted)} \qquad T_{12} = \left[\frac{T_1 T_2}{T_1 - T_2}\right]$$

$$Y_4 = (T_2 - d_1 - d_2) \frac{T_{12}}{T_2} \qquad d_2 > d_1 \qquad (116)$$

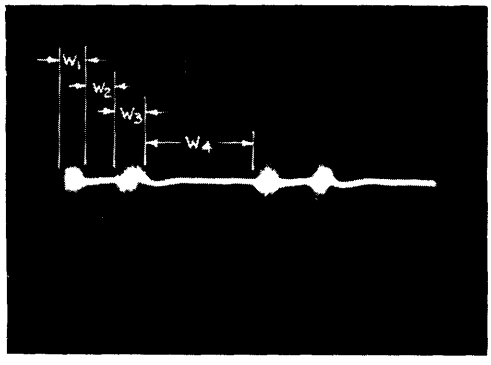

FIG. 80

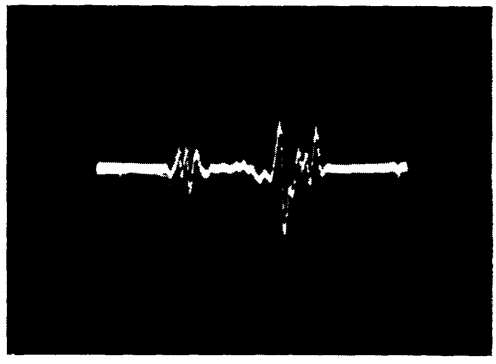

FIG. 81

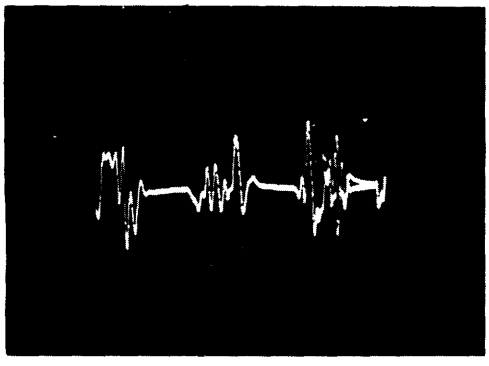

FIG. 82

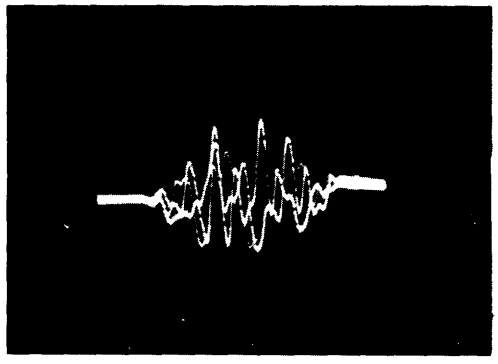

FIG. 83

Figs. 80-83 Oscillograms of time-shift noise bursts under various conditions.

For $d_2 > d_1$ there is only a single burst of noise per beat period; it extends over the intervals Y_1, Y_2, and Y_3, and may or may not be noticeably different during the interval Y_2, depending on Δr-f and the duration Y_2 relative to Y_1 and Y_3. Figures 82 and 83 are oscillograms for $D_2 = 0.5$, $D_1 = 0.1$, and Δprf = 250 cps. The first shows three successive beat periods in a single sweep, while the latter also shows three beat periods superimposed on successive sweeps. Both figures bring out the fact that successive noise bursts differ a great deal from each other, which is to be expected since relatively few random "samples" compose each noise burst. Figure 83 exhibits a tendency towards higher noise peaks in the central portion (during the interval Y_2) than at either end (intervals Y_1 and Y_3), resulting from the fact that the two-edge noise composing the central portion of each noise burst is larger than the one-edge noise at the beginning and end of each noise burst.

It will be of interest, at this point, to resume the discussion of the relation between slicing level and time-shift distribution, illustrated in the preceding section by Figs.76-79. The audio-noise outputs corresponding to Figs. 77, 78, and 79 are shown in Figs. 84, 85, and 86, respectively.

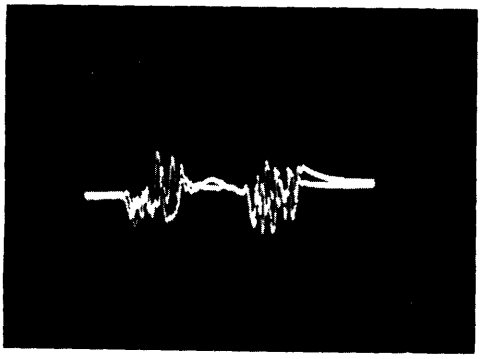

FIG.84

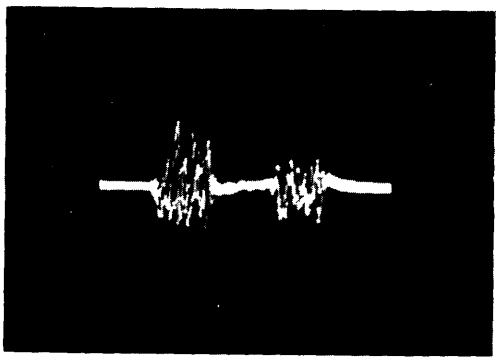

FIG.85

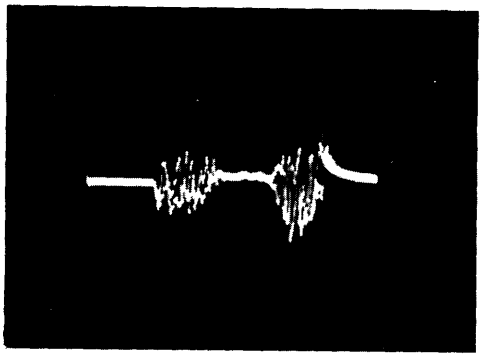

FIG.86

Figs.84-86 Oscillograms of time-shift noise bursts, showing effect of slicing level (medium, high, and low, respectively).

Because of the phase reversal in the odd number of amplifier stages used, positive time shifts (leading-edge advances or trailing-edge delays) give negative (downward) noise peaks; this must be kept in mind in the observations which follow. Figures 84 - 86 are oscillograms showing the two noise bursts occurring in one beat period for the case $d_1 > d_2$ ($D_1 = 0.15$, $D_2 = 0.30$, $\Delta prf = 200$ cps, $a = 0.33$). A noticeable difference between these oscillograms and those shown in the previous figures is the greater average frequency (number of zero-axis crossings) of the noise within each burst in Figs. 84 - 86, resulting from the fact that the 10-kc low-pass filter was used instead of the 5-kc filter. However, the important effect which Figs. 34 - 86 are intended to show is the effect of the slicing level, s, on the d-c and a-c components of the noise, and hence on the audibility of the beat frequency, Δprf.

The output noise shown in Fig. 84 corresponds to the slicer output in Fig. 75, obtained for $s = 0.5$. The fact that positive time-shift values are favored over negative values is reflected in Fig. 84 by the definite downward tendency of both noise bursts, which in turn results in a weak beat note distinctly audible in addition to the random noise. The total r-m-s noise voltage is near its minimum for this condition.* The noise in Fig. 85, on the other hand, is several decibels stronger but contains no audible beat component and may therefore be less offensive than the weaker noise containing the beat component (depending on the value of Δprf). Figure 85 was obtained with a slicing level $s = 0.65$ and corresponds to the slicer output shown in Fig. 76. The opposite extreme is illustrated by the oscillogram of Fig. 86, in which the preference in favor of positive time shifts (corresponding to "downward" noise") is enhanced by a low slicing level ($a = 0.35$). This results in a strong beat note, and in still higher noise power. The close correspondence between the trailing pulse edges in Fig. 79 and the second noise burst in Fig. 86 is noteworthy. Two asymmetry effects are added here to make the beat component especially strong: the prevalence of trailing-edge delays is enhanced by making the delays larger than the advances. Just the opposite is true in the case of the leading edge in Figs. 78 and 85; the two

---

* The exact theoretical location of the minimum is slightly above $s = 0.5$, since, for $s = 0.5$, the effective time shift of the trailing edge is somewhat larger than that of the leading edge. (See Section 4.1)

asymmetry effects oppose each other and cancel. The first noise burst is more "crowded" in the downward direction but has larger peaks in the upward direction.

Although the preceding discussion was illustrated by noise oscillograms obtained for $d_1 > d_2$, it applies equally for $d_1 < d_2$. The oscillogram of Fig. 83, for example, was obtained for the condition of "beat cancellation" ($s > 0.5$). The greater density in the downward direction and higher peaks in the upward direction are distinctly visible, particularly if the figure is turned sideways, or if it is inverted.

The bursts of noise resulting from the missing-pulses effect ($a > 0.5$) exhibits fewer drastic variations with varying parameters than those caused by time shifts. Each burst lasts as long as there is any coincidence between the two sets of pulses, that is, its duration is $[d_1 + d_2][(T_{12}/T_2)]$. It consists of three intervals; the first one, during which the noise power is increasing approximately linearly, is of duration $d_1(T_{12}/T_2)$ or $d_2(T_{12}/T_2)$, whichever is the smaller; the second interval, during which the noise power is at its peak, has a duration $[d_1 - d_2][(T_{12}/T_2)$; and the third interval, during which the noise decreases to zero, is of the same duration as the first one.*

Although complete elimination of the beat (Δprf) component is not generally possible for $a > 0.5$, it can be approached very nearly in most cases by adjusting the slicing level to a value just above $\underline{a}$. The adjustment is more critical than for $a < 0.5$, and the remaining beat note is very much weaker for fairly small duty factors ($D_1 = D_2 = 0.1$) than for large values ($D_1 = D_2 = 0.5$).

5.23(3b) Measurement of Audio-Noise Power

The measurement of the output noise voltage and hence the signal-to-noise ratio as a function of the numerous variables involved is of great practical significance, inasmuch as it reveals in simple terms the quality of communication attainable through a given system under certain conditions. The most important variables are the interference ratio, the pulse duration or duty factor of each of the two pulse trains, and the system bandwidth; these are included as parameters in the graphs to be discussed in this section. Certain other variables are also of importance and will be considered first.

---

* It can easily be shown that the average fractional overlap between the two pulse trains is D_1D_2.

They are the slicing level, s, the difference between the two pulse-repetition rates, Δprf, and the audio bandwidth which, together with the repetition rate of the desired pulses, determines the filter constant, k_f.

The slicing level has already received prominent mention in this chapter and in preceding chapters. Experimental findings show that, for small interference ratios ($\underline{a} < 0.1$) $\underline{s}$ is not critical over most of its permissible range. As $\underline{a}$ is increased, the noise minimum at approximately $a = 0.5$ becomes more and more noticeable; it is quite sharp for $\underline{a} = 0.4$. At the same time it is observed that the beat tone (Δprf), which is distinctly audible for these larger values of $\underline{a}$, can be made inaudible by raising $\underline{s}$ somewhat above 0.5, as discussed in Sections 5.23(2) and (3a). If the interference ratio exceeds one-half ($0.5 < a < 1.0$), the optimum slicing level is always just above $\underline{a}$ ($s = a+$). This condition is found to be optimum not only from the view point of minimizing the total noise power, but a critical minimum for the Δprf beat component also exists; in addition, the cross-talk and signal-reduction effects are minimized by keeping $\underline{s}$ close to $\underline{a}$. This is simply a result of the fact that F, the fraction of missing pulses, is minimized under this condition. An important fact which naturally follows from the principles and observations being discussed will bear repeating here: as the interference ratio is raised above unity, the rôles played by the desired and interfering signals, respectively, are interchanged, so that the output signal switches abruptly from one to the other. This so-called capture effect is particularly striking if the duty factors of both pulse trains are small, for example 0.1 or less, since the missing-pulses noise is then too weak to obscure the signal, and the signal-reduction and cross-talk effects are imperceptibly small. Increasing the r-f difference between the two transmissions also reduces these interference effects and enhances the capture effect. Only the finite thickness of the "slice" selected by the slicer appears to impose a limit, which makes the transition tend to be gradual rather than extremely sudden. In the case of the best slicer used in this study, the transition extended only from pulse-amplitude ratios of 0.97 to 1.03. The ideal and actual slicer characteristics are shown in Fig. 87. It may also be pointed out in this connection that the simple slicer used* is self-adjusting within limits, maintaining the condition $s = a+$ with sufficient accuracy if $\underline{a}$ is changed by as much as 0.05,

* See Appendix V, Fig. 148.

or possibly more if certain modifications are made.

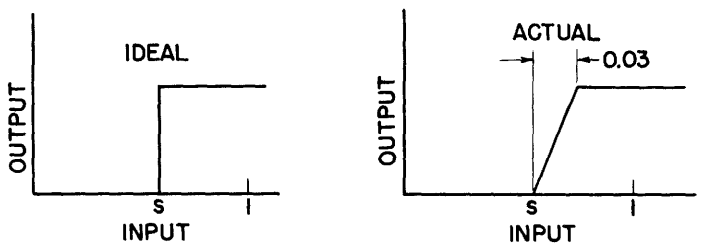

Fig.87 Ideal and actual slicer characteristics.

The difference between the two pulse-repetition rates, Δprf, determines, to some extent, the nature of the interference noise as perceived by the ear. If the noise contains an appreciable beat component (generally caused by improper slicing), this is most offensive for Δprf between approximately 200 and 2000 cps. Even if no such component is present, the ear is capable of differentiating the pulsed or intermittent noise from continuous noise.[25] Of course, if Δprf is less than 1 cps, the beat periods are long enough to be resolved individually so that the various noise bursts discussed in Section 5.23(3b) are heard individually as a series of "ssshhh" sounds separated by silent intervals. As Δprf is increased to low audio-frequency values, the individual sounds fuse into a continuous sound which is not so smooth or uniform as continuous one-edge or two-edge noise and is slightly more offensive than continuous noise of the same average power. The smaller the "duty factor" of the noise bursts, the "thinner" the noise sounds. The same is true also if Δprf is in the mid-audio range, except that one obtains the impression that the noise spectrum might have a peak at the frequency Δprf, even though this is not true* and no measurable beat component is present. However, the impression is generally so vague that one cannot readily learn the value of Δprf without purposely changing s to introduce an actual beat component. If this is done, the resulting beat tone consists not only of a component at frequency Δprf, but also of its harmonics which are relatively weak. It might be supposed that the second harmonic is the major contribution if $D_1 = 0.5$ and $D_2 < D_1$ $(a < 0.5)$, inasmuch as there are then two noise bursts per beat period, and they are spaced half a beat period apart. Actually, the

* It can be shown that if noise having a spectrum which is flat up to a certain frequency is pulsed on and off periodically, the spectrum of the resulting pulse noise is flat over the same range.

fundamental predominates decidedly even in this special case; this is a result of the fact that one of the two sets of noise bursts generally contributes almost all of the a-c component. If Δprf is several kilocycles or more, the discontinuous or pulsed nature of the noise becomes much less noticeable. The noise bursts are no longer well defined, since each one may consist of only two or three "samples" (defective pulses), and the intervals between the bursts may be so short that the noise at the filter output is more or less continuous, depending on D_1 and D_2. If an appreciable Δprf beat note is present, it weakens and disappears before Δprf reaches the upper cutoff frequency, but other sum and difference components, though much smaller in magnitude, appear in its place. For interference ratios larger than 0.5, the unavoidable beat component diminishes rapidly with decreasing values of D_1 and D_2.

The audio bandwidth, or more precisely the audio-system frequency characteristic, determines the total audio-noise power, other parameters being constant. Experimental tests confirm the theoretical result which states that the noise power is proportional to the area under the squared transfer characteristic, supporting the finding that the noise spectrum (previous to filtering) is flat within the audio range. The 5-kc low-pass filter yields less noise by about three decibels than the 10-kc filter; the areas under the squared characteristics differ by a factor of two. This means that the signal-to-noise ratio can be improved by reducing the audio bandwidth, a well-known fact in all communication systems in which random noise reaches the output along with the signal. In the case of pulse systems, with a given amount of noise introduced by a given number of pulses, decreasing the repetition frequency of the desired pulses similarly improves the signal-to-noise ratio. The controlling factor is the filter constant k_f, involving both the filter characteristic and the pulse-repetition frequency (see Section 4.1, page 96). The ideal value of k_f is unity, and while reducing this factor increases the signal-to-noise ratio, it also decreases the system utilization in that a narrower signal-frequency band is conveyed. All of the noise plots shown in this section were obtained with the 10-kc filter* which has an equivalent noise bandwidth of 4.8 kc. At a pulse-repetition frequency of approximately 24 kc, used in most of the tests, $k_f^2 = (2)(4.8)/24 = 0.4$, and $k_f = 0.64$.

*See Appendix V, Fig. 155.

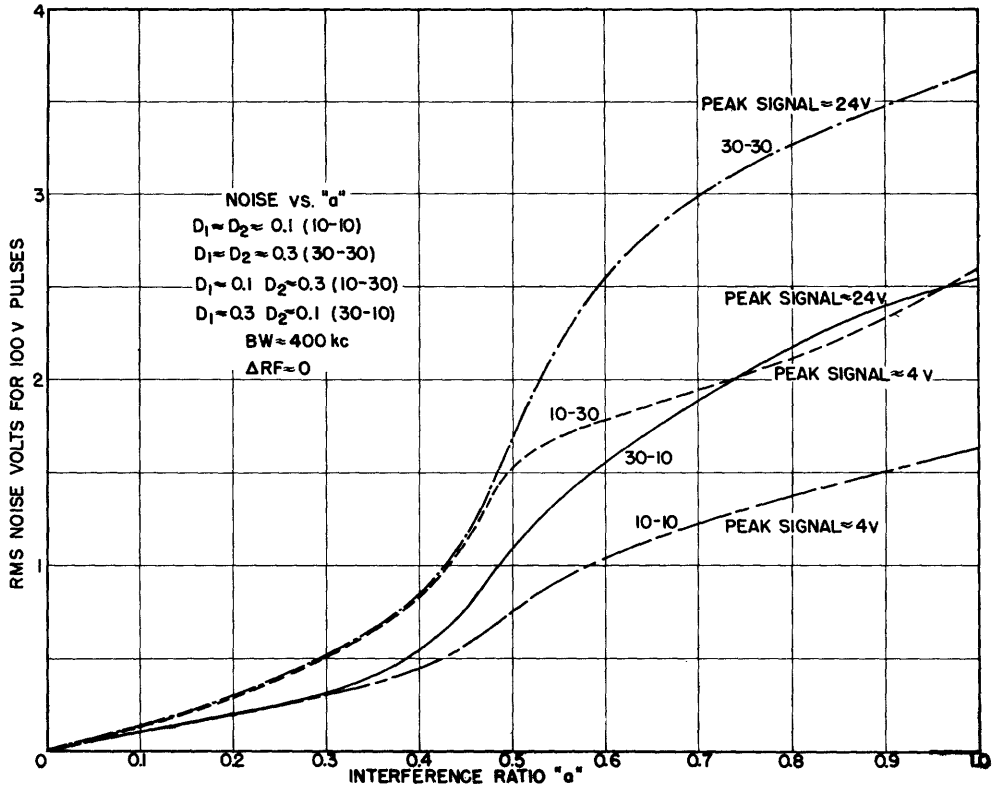

Fig.88

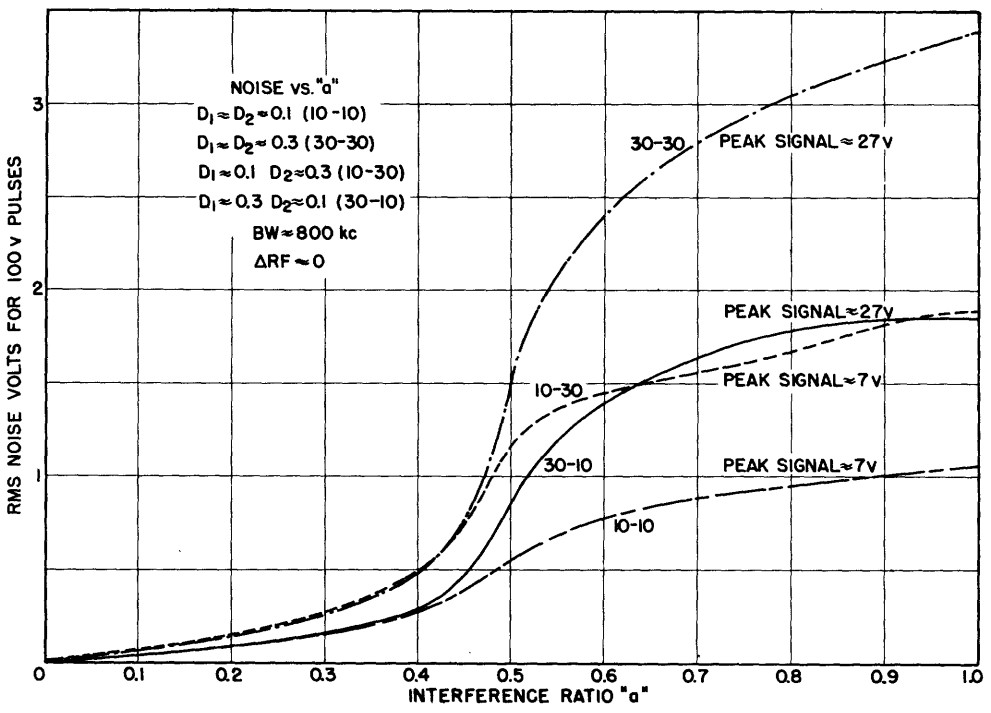

Fig.89

Figs.88-89 Interference noise voltage vs. interference ratio for various values of the desired-pulse and interfering-pulse duty factors.

The relations between the r-m-s voltage on one hand, and the interference ratio a, the interference duty factor D_2, the desired-pulse duty factor D_1, and the system bandwidth BW on the other hand are plotted in various forms in Figs. 88 - 92. The variation of the noise with the interference ratio is shown in Figs. 88 and 89 for two different values of system bandwidth and various values of the two duty factors. The salient features can be summarized as follows: the system bandwidth affects the noise seriously only for $a < 0.5$, where the noise voltage is twice as large for BW = 400 kc as for BW = 800 kc. This is a result of the larger pulse rise and decay times caused by narrower bandwidth, which has the additional important result of reducing the peak-signal modulation. This reduction in signal becomes an important factor for small values of D_1 if the average pulse duration is not very much larger than the rise and decay times. The ideal maximum signal modulation is $\Delta t_{max} = d_1$, while the actual value permissible (without exceeding a certain amount of distortion) is $\Delta t_{max} = d_1 - (k/BW)$, where k is in the order of magnitude of unity. The noise for $a > 0.5$ is not appreciably affected by the system bandwidth except for small duty factors, that is, if the time-shift contribution to the total noise is large enough to be of influence. As for the effect of D_1 and D_2, the noise voltage is proportional to D_2 but related to D_1 in a more complicated manner.

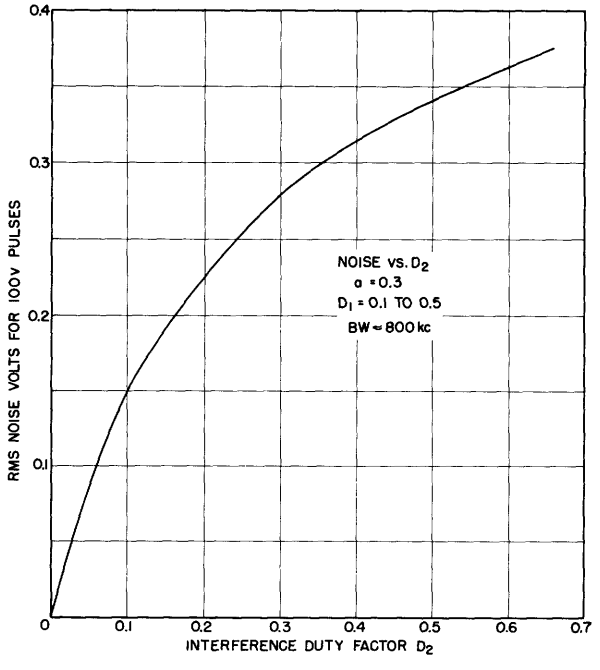

Fig.90 Interference noise voltage vs. interference duty factor for interference ratio less than one-half.

Figures 90 - 92 show the dependence of the noise voltage on the duty factors. The value a = 0.3 (Fig. 90) is used as a typical example for a < 0.5, while a = 0.8 (Figs. 91 and 92) serves as a typical value for a > 0.5. The noise voltage is seen to be approximately proportional to the square root of D_2 and nearly directly proportional to D_1 plus a constant which depends on D_2.

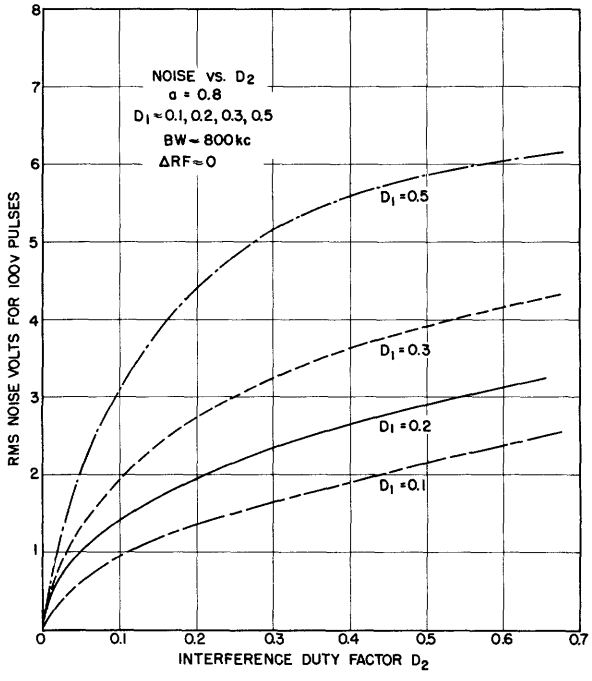

Fig.91 Interference noise voltage vs. interference duty factor for various desired-pulse duty factors; large interference ratio.

Theoretical curves computed from the results of the analysis in Section 4.4 are shown in Figs. 93, 94, 95, and 96, which correspond to the experimental curves in Figs. 88, 89, 91, and 92, respectively. For small values of D_1 the computed results check the experimental results perfectly for all values of the other variables. However, there is one discrepancy for a > 0.5 which is in evidence in each of the four figures and causes errors as large as 80 per cent when both D_1 and D_2 are large (0.5 or more), and 30 per cent for moderately large values of D_1 and D_2 (0.3). The discrepancy is a result of the fact that the missing-pulses component of the noise given by (106) and contained in (108) does not actually vary as rapidly with D_1 as these formulas indicate. Nevertheless, the computed variation of noise voltage vs. D_1 (see Fig. 96) is of the same form as the actual variation (see Fig. 92), namely "constant plus proportional". The discrepancy is principally in the computed

values of the constant and the proportionality factor, the former being too small and the latter too large. The constant component is the time-shift noise, which is not dependent on D_1 (see Fig. 90). Increasing the time-shift contribution for a < 0.5 is, therefore, a step in the right direction. However, the root of the discrepancy is in the approximate method of derivation of (106), which places too much weight on the parameter D_1. The alternate formula, (107), which is a still cruder approximation, places equal but excessive weight on both D_1 and D_2.

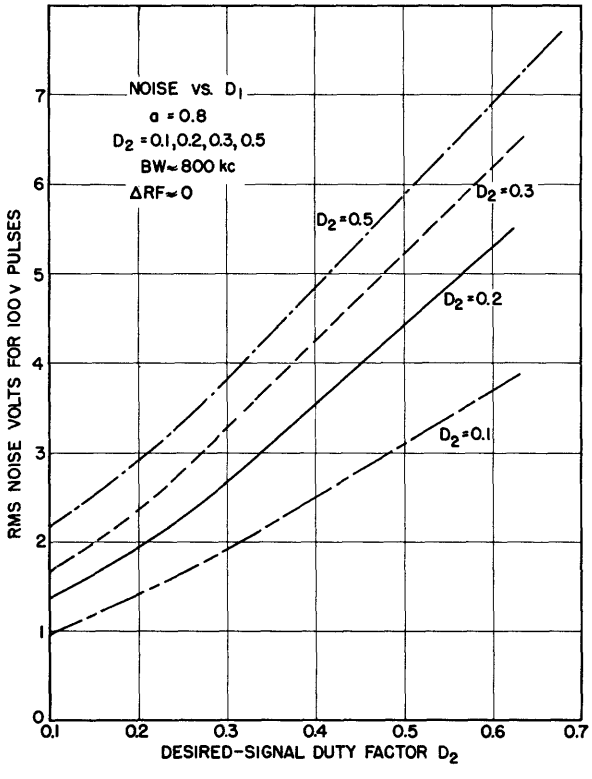

Fig.92 Interference noise voltage vs. desired-signal duty factor for various values of interference duty factor; large interference ratio.

Another discrepancy between experimental observations and theoretical results is found in Fig. 90, which shows that, for a < 0.5 and $\Delta r\text{-}f = 0$, D_1 has no measurable effect on the noise voltage. Some dependence on D_1 should be expected, since there is an increasing component of two-edge time-shift noise if d_1 is made smaller than d_2. This effect is unnoticeable, however, so that the simple expression (105) (derived on page 111) holds generally with sufficient accuracy for $\Delta r\text{-}f = 0$, regardless of the relative magnitudes of D_1 and D_2, and as though the time shifts of the two edges of each pulse were independent. For other values of $\Delta r\text{-}f$, the varying

contribution of the two-edge noise component does have a decided effect on the total noise voltage, as the following results will show.

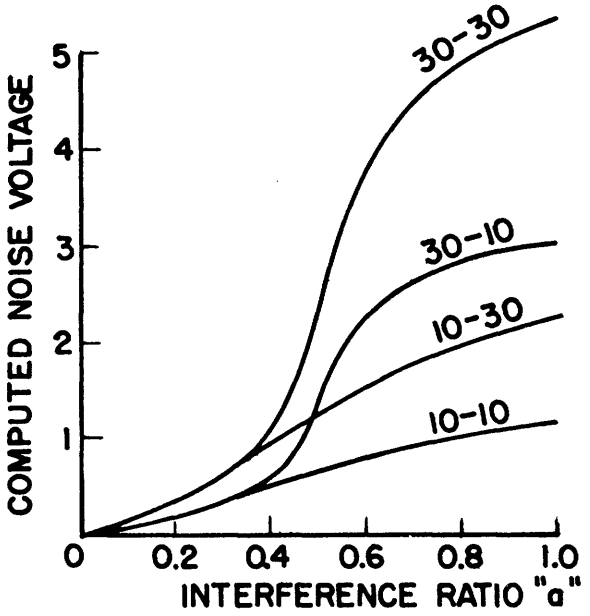

Fig.93 Computed results corresponding to experimental data of Fig.88

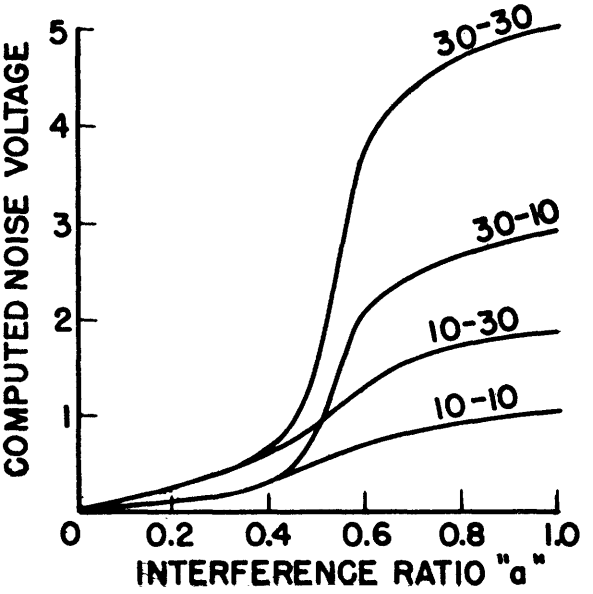

Fig.94 Computed results corresponding to experimental data of Fig.89

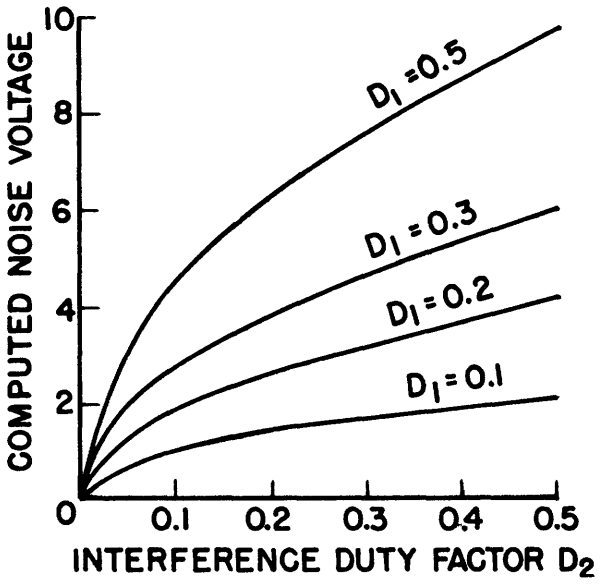

Fig.95 Computed results corresponding to experimental data of Fig.91

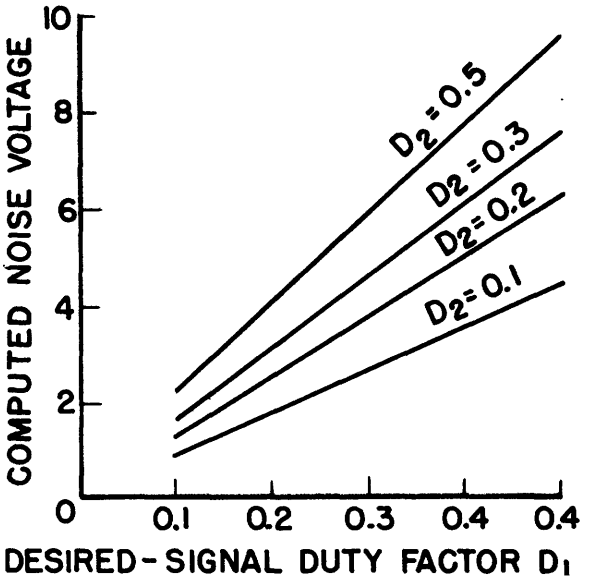

Fig.96 Computed results corresponding to experimental data of Fig.92

The variation of the total r-m-s normalized audio-noise voltage as a function of Δr-f is shown in Figs. 97 - 99 for three different values of D_1

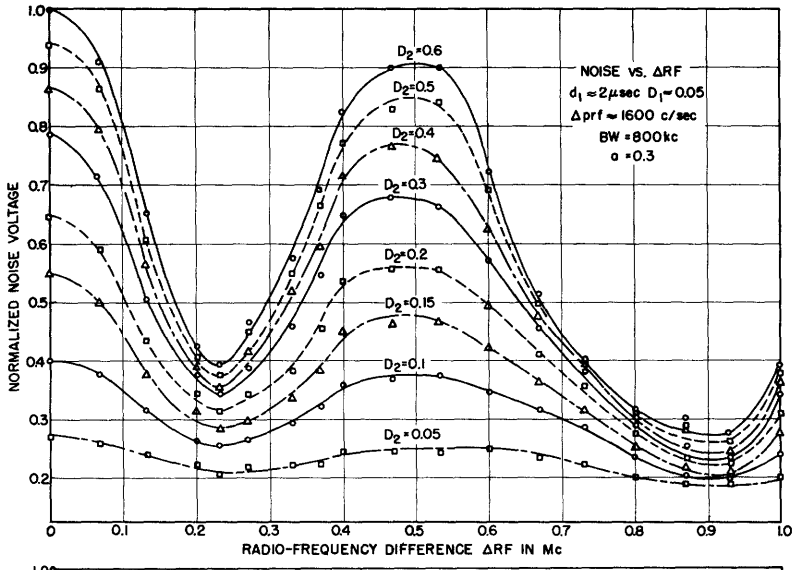

Fig.97

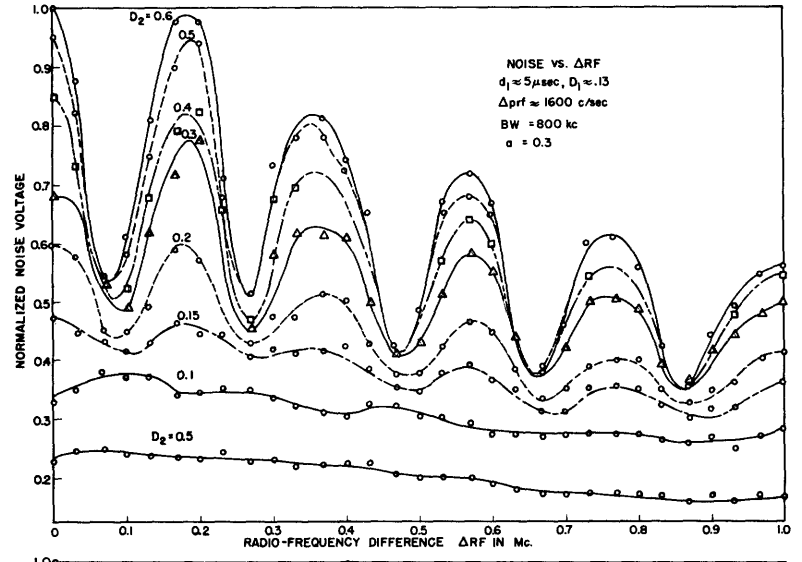

Fig.98

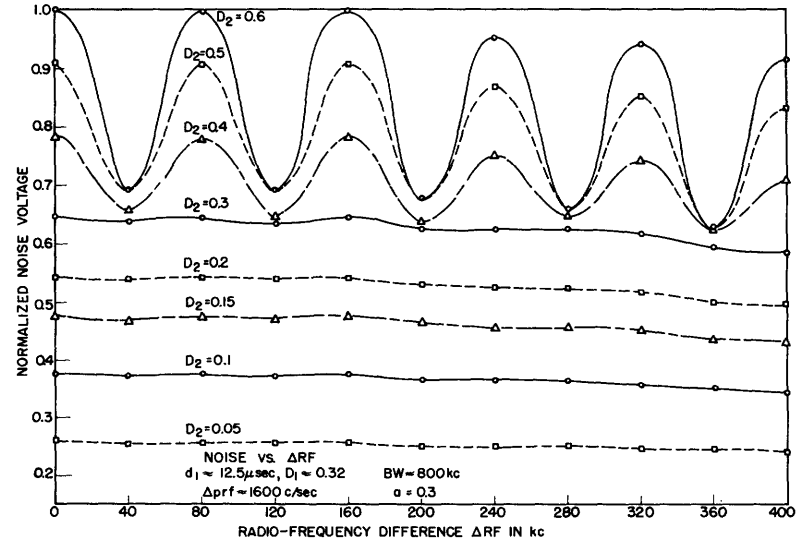

Fig.99

Figs.97-99 Normalized interference-noise voltage vs.r-f difference for various duty-factor values.

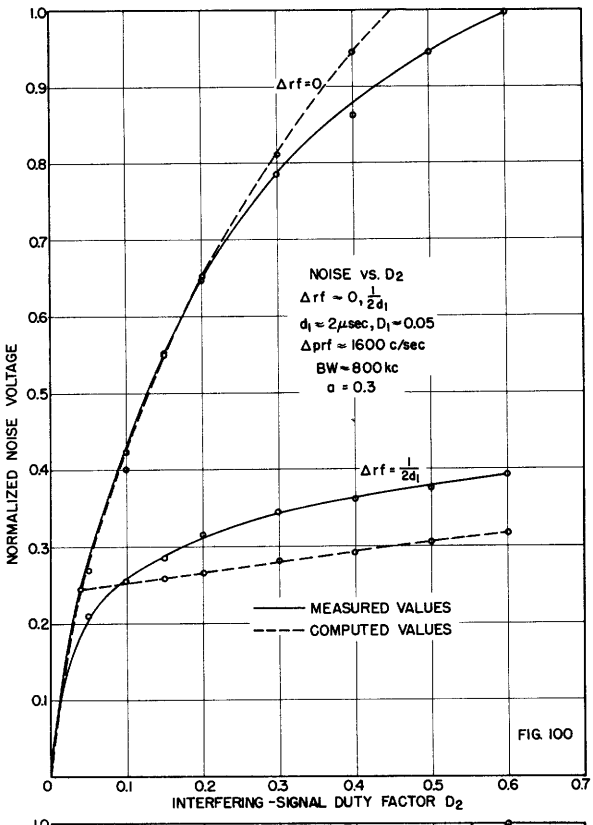

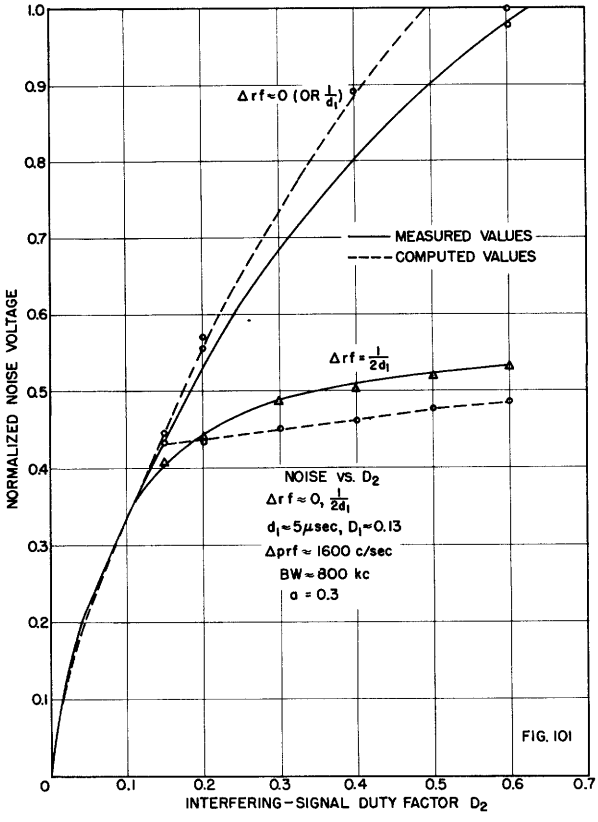

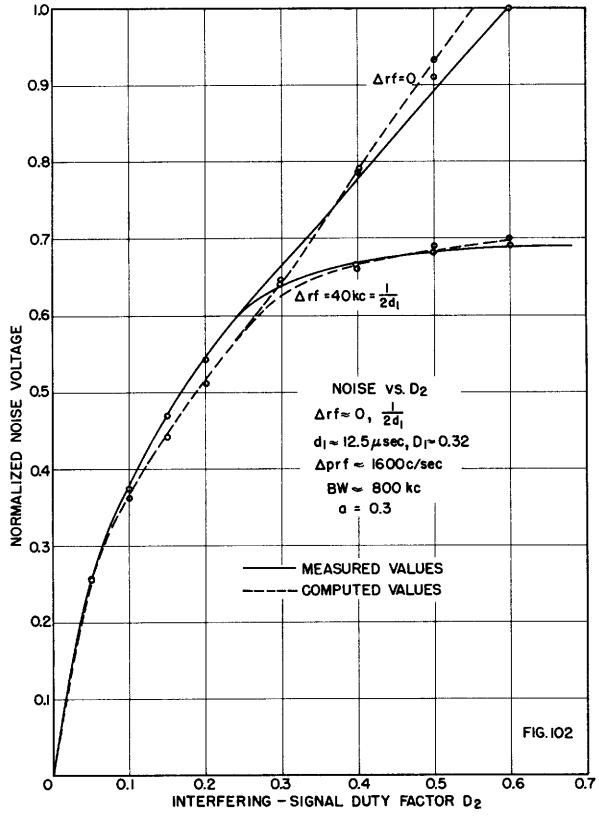

Figs.100-102 Normalized interference-noise voltage vs. interference duty factor D_2 for $\Delta r\text{-}f = 0$ and $\Delta r\text{-}f = 1/2d_1$.

and many values of D_2 (a < 0.5). Figures 100 - 102 show part of the same data (only the noise maxima and minima corresponding to $\Delta r\text{-}f = 0$ and $1/2d_1$, respectively) plotted as a function of D_2 for the three different values of D_1. These six curves demonstrate the effect of the two-edge noise component which causes the cyclic variation. As expected from theory (see (112)) this effect exists only when d_2 exceeds d_1 and becomes more pronounced the greater the difference $d_2 - d_1$ becomes. However, as found on several previous occasions, the difference between the maxima and minima (or the ratio of the maxima to the minima) is not quite so large as the theory predicts. The theoretical values are indicated in dashed lines on Figs. 100 - 102. The actual maximum values are somewhat lower, showing that the two-edge noise contribution is not so large as computed (though somewhat larger than the values obtained if the shifts of the two edges of each pulse are assumed independent). The experimental minimum values are higher than the computed values, which can be accounted for by the exponential shape of the edges, as explained in connection with Fig. 68 [Section 5.21(3b)]. The abrupt change in slope in the computed curves for $\Delta r\text{-}f = 1/2d_1$ (Figs. 100 and 101) results from the fact that as soon as d_2 exceeds d_1, the one-edge noise contribution becomes constant and only the relatively small two-edge contribution increases with D_2. Since Δprf is less than seven per cent of either of the two pulse-repetition frequencies, the abrupt change occurs within seven per cent of $D_2 = D_1$. Referring to Fig. 97, the departure from periodicity for $\Delta r\text{-}f >$ 500 kc is a result of changes in slicing level which alter the small effective pulse duration by a large percentage. Thus, the second noise minimum, which is normally expected to be at $\Delta r\text{-}f = 2d_1/3 = 750$ kc, has been displaced in the opposite direction, and for smaller values of $\underline{a}$ (permitting a wide range of slicing level, $\underline{s}$) one can generally minimize the noise for $\Delta r\text{-}f \neq 0$ by taking advantage of this effect. However, this is true only for pulse durations not much longer than the combined rise and decay times of the pulse.

The final plot of this section, Fig. 103, shows the r-m-s interference noise voltage as a function of $\Delta r\text{-}f$ for $d_2 < d_1$ and for two typical values of $\underline{a}$ below and above 0.5, respectively. The decrease in the noise for a = 0.8 results from the decrease in the missing-pulses component as $\Delta r\text{-}f$ is increased (see Section 4.5, page 124); the asymptote which the noise approaches for $\Delta r\text{-}f >$ 1 Mc is the time-shift component of the noise. The maximum signal amplitude is approximately 26 volts, thirteen times the maximum r-m-s noise

voltage for a = 0.8, and 150 times the r-m-s noise voltage for a = 0.3. It must be remembered, of course, that the effective signal voltage is generally far below the peak value.

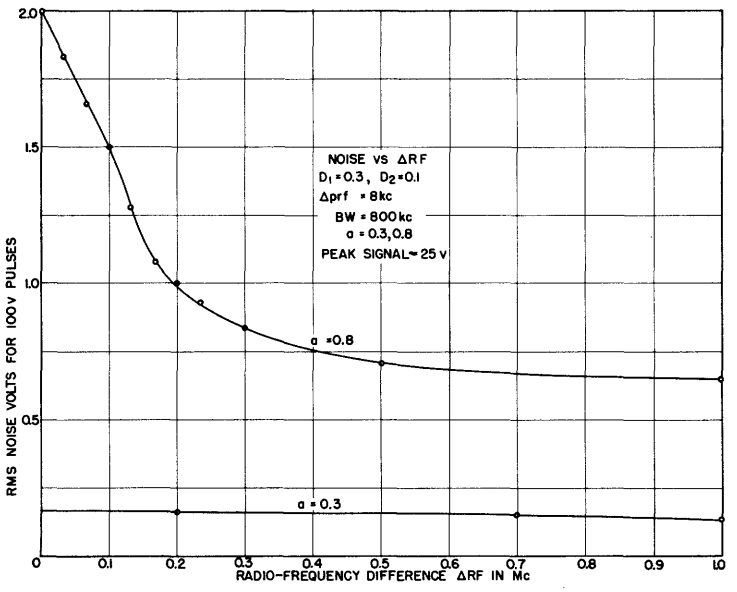

Fig.103 Interference-noise voltage vs. r-f difference for $d_1 > d_2$, $a < \frac{1}{2}$; $d_1 > d_2$, $a > \frac{1}{2}$.

5.24 Summary and Conclusions for Two-Station PDM Interference

The results presented thus far in this chapter will now be summarized, with emphasis on the important points previously obscured by the numerous details. If two single-channel PDM signals simultaneously reach the detector of a PDM receiver, the receiver output generally consists essentially of the modulating signal of the "taller" pulses and random noise.

If the interference ratio is less than one-half, the noise voltage is inversely proportional to system bandwidth, proportional to the square root of the interference duty factor, and independent of the radio-frequency difference between the two signals. It is nearly proportional to the interference ratio, a, for $a < 0.2$, while the relation becomes exponential for larger values; but the noise is generally not large enough to impair the signal intelligibility, especially if the duty factor of the desired pulses is close to 0.5, permitting the largest possible signal.

For interference ratios larger than one-half, the noise depends on a larger number of variables. If both pulse trains have large duty factors (0.3 or greater), and the radio-frequency difference is zero, the noise is

generally so severe as to make the signal unintelligible. This is aggravated by the so-called signal-reduction effect which may reduce the signal output by a few decibels, and, in addition, a weak but objectionable beat note may be present. When both pulse trains have duty factors in the order of magnitude of 0.1 or less, the situation is much improved: the latter two effects are negligible, and the noise is not strong enough to overshadow the signal. The noise voltage is decreased as the square root of the interference duty factor and, like the signal, in approximately direct proportion to the desired-pulse duty factor. Consequently, subject to the assumption that similar PDM systems interfere with each other, the duty factors should be as small as possible without unduly curtailing the maximum signal modulation. The latter is possible only if the combined pulse rise and decay times occupy no more than two to four per cent of the pulse-repetition period, assuming ten per cent as a suitable duty-factor value. A certain minimum system bandwidth (for a 10-kc audio band generally 500 kc or more, double-side-band) is therefore required to prevent the capture effect from being obscured by noise; increasing the bandwidth above this value makes further improvement of the signal-to-noise ratio possible. If the radio frequencies of the two signals are not alike but differ by a sizable fraction of the system bandwidth, 200 kc, for example, the noise ($0.5 < a < 1$) is generally much smaller and the signal is intelligible, even when both duty factors are large.

Special cases of two-station PDM interference, in which the two-pulse-repetition frequencies are synchronous (Section 5.21) serve as an introduction to the more general case summarized above, and they will be found useful in connection with the studies reported in the next section (two-path interference). However, if the possibility of synchronism between the desired and interfering pulse train is real, the conclusion is that the disturbance caused by the interference may be as bad as in the worst case mentioned above, or it may be much less severe or completely absent. While the two duty factors have no effect on the magnitude of the maximum possible disturbance, the probability of partial coincidence of the two pulse trains and hence the probability of obtaining any disturbance diminishes rapidly with decreasing duty factors.

An important conclusion from the viewpoint of equipment design is that the slicer must operate correctly, taking the thinnest possible "slice" out of the pulse, and that the slicing level should be adjustable in order to make optimum reception possible under all conditions.

As for interference between two multichannel PDM systems, the same general results summarized above are applicable provided that synchronization between transmitter and receiver is not lost. The fact that each channel is selected by means of time gating does not cause any improvement, since the interference is excluded from the spaces between pulses by the slicing process. However, the fact that many channels of one system interfere with every single channel of the other system means that the effective interference duty factor is much larger than the effective desired-pulse duty factor. This means prohibitive noise for interference ratios higher than one-half (for which synchronism is likely to be lost anyway), but in view of the large system bandwidth generally used in such systems, intelligibility will generally be good for interference ratios smaller than one-half.

5.3 Two-Path Interference in PDM Systems

One of the important characteristics of two-path interference is the fact that, except under certain conditions in time-division multiplex systems, the interfering signal has the same modulation as the desired signal. The modulation of one is delayed with respect to that of the other, but this is not generally of serious consequence in the case of speech or music. It is therefore not necessary to suppress the modulation of the weaker signal, unless, for some special reason, the original modulating signal must be reproduced exactly even at the expense of signal-to-noise ratio, or if a multichannel system is involved. Two cases will therefore be considered: the special case in which it is necessary to suppress the modulation of the weaker signal (this will be considered first because of its similarity to two-station interference), and the more important case in which the modulating signals may be combined.

5.31 Two-Path Interference with Modulation of Weaker Signal Suppressed (Time-Division-Multiplex Systems)

One case which obviously belongs under this classification has been explained on page 130 (Section 5.1). If the two-path signals from a time-division multiplex system arrive in such phase relation that there is partial overlap between pulses belonging to different channels, cross talk will result if no attempt is made to discriminate against the smaller signal. The necessary discrimination is effected by keeping the relative slicing level, s, above the interference ratio, a, as in all cases of two-station interference.

If the pulses are incoherent with respect to each other the result is therefore exactly the same as in the case of two-station interference with synchronous pulse-repetition frequencies. The problem is even simpler than in that case, inasmuch as the two radio frequencies are exactly alike and the average durations and duty factors of the two sets of pulses are the same. If there is no overlap between the two pulse trains, the presence of the interfering signal has no effect whatever other than imposing the restriction $s > a$. However, the probability of encountering this favorable condition is generally low, if not zero, in a multichannel system because of the high duty factor; for a single-channel system, it is given by $1 - 2D$, where D is the duty factor or the normalized pulse duration* (the maximum modulated pulse duration if there is to be no partial overlap during modulation peaks).

The situation of principal concern is that in which the relative time delay between the two pulse trains reaching the receiver is such that there is partial coincidence between them. Two cases must be considered, incoherent interference and coherent interference. Two conditions must be fulfilled to make the interference incoherent: first, there must not be any coherence between different r-f pulses, which, as explained in Chapter 2, is generally true; second, the delay difference between the two paths should be larger than the maximum pulse duration in order to prevent the pulses from overlapping their own delayed replicas. Either or both of two conditions will make the interference coherent: (1) coherence between the r-f pulses; (2) a delay difference small enough so that each pulse can overlap only its own delayed replica (since each r-f pulse is coherent within itself).

Consider first the incoherent case; the interfering (smaller) pulse overlaps one edge of the desired (taller) pulse, as well as a portion of the desired pulse itself. The overlap, expressed as a fraction of the pulse-repetition period, has been denoted by U and can have any value from 0 to D. The result is simple (continuous) one-edge time-shift noise for $a < 0.5$, and for $a > 0.5$ there is, in addition, missing-pulses noise in its very simplest form (see Section 4.2). The theoretical results applicable to this situation are contained in the first three sections of Chapter 4, and the experimental

---

* The subscripts 1 and 2 for the durations and duty factors are not used in this section, since $d_1 = d_2 = d$

$$D_1 = D_2 = D$$

study of 5.21 also covers this situation. Similar observations (oscillograms of detector output, slicer output, and audio output) and measurements can, of course, be made by means of the two-path setup. Only the most important measurement, that of the audio-noise voltage, will be discussed here. The interference simulated by the delay-line setup produces the same type of random noise as that produced by the two separate transmitters with synchronized pulse-repetition frequencies; since $\Delta r\text{-}f$ equals zero exactly, the missing-pulses noise ($a > 0.5$) is always very severe and masks the signal except for very small overlaps. Experimental and computed plots of audio-noise voltage as a function of the interference ratio, a, for various values of average overlap, U, and for two widely different values of system bandwidth, BW, are shown in Figs 104 and 105. The duty factor, of course, has no effect on the noise for a given degree of overlap, but it determines the maximum signal. It is evident, from inspection of Figs. 104 and 105, that only the very smallest overlaps yield usable signal-to-noise ratios for large interference ratios. In the case of the narrower system bandwidth (150 kc), even the time-shift noise alone is large enough to lower the signal-to-noise ratio to a generally unacceptable value (12 db) for $a = 0.45$. The agreement between experimental and computed results is better than that obtained in similar plots shown in earlier parts of this chapter; the precision of the measurements is greater, and the theoretical curves have, in part, been accurately corrected for the exponential shape of the pulse edges [theoretical curves computed from (103)].

This brief investigation leads to the conclusion that any attempt to receive only the modulation of the stronger of two overlapping pulse trains is generally futile for large interference ratios ($a > 0.5$), while it is generally successful for smaller ratios if a random-noise background is permissible.

The coherent case of two-path PDM interference is radically different from the incoherent case. The exact result depends on the behavior of the delay difference as a function of time. In the experimental equipment, the delay difference is normally constant at approximately 500 microseconds but can be varied over a sufficiently wide range and with sufficient speed to simulate conditions under which the delay difference is constantly changing at a low rate. Greater rates of change can readily be simulated by slight manual frequency modulation of the transmitter. The simplest possibility,

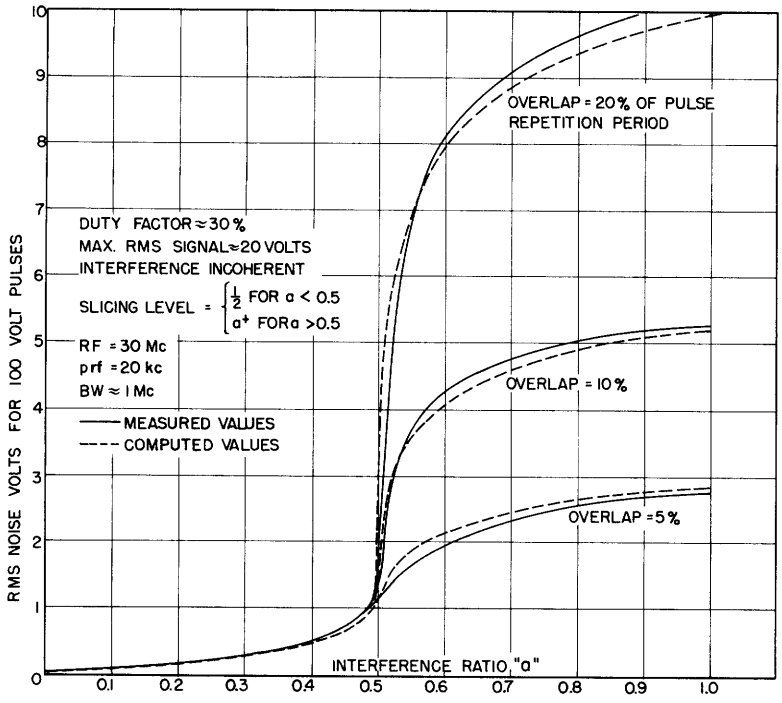

Fig.104 Noise due to two-path PDM interference vs. interference ratio a for various degrees of overlap; large bandwidth.

that of constant delay difference will be considered first. In practice this may be encountered as a result of reflections from fixed objects. The r-f phase difference ϕ, instead of changing randomly from pulse to pulse, remains fixed at some value which depends critically on the radio frequency and the delay difference. Any value is equally likely, as in the random case, and consequently the probability distribution of the resultant of the two pulses is the same as in the incoherent case.

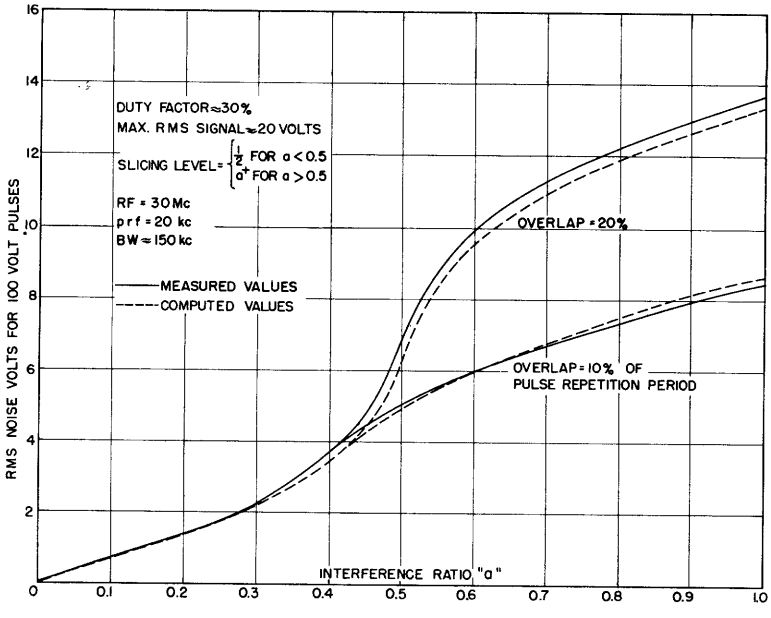

Fig.105 Noise due to two-path PDM interference vs. interference ratio a for two degrees of overlap; small bandwidth.

For interference ratios less than one-half, there are time shifts, but they are the same from pulse to pulse and therefore amount to nothing more than a change in average pulse duration and have no effect on the output. However, with delay differences of the order of magnitude of audio periods, it may happen that, in the presence of audio modulation, not all pulses have overlap, inasmuch as normally overlapping pulses may be modulated in opposite senses and miss each other. The result is that not all edges undergo the "d-c" time shift, but this is of no noticeable consequence as far as the audio output is concerned. Other special conditions which may tend to cause some distortion and increase the effect of random noise are possible: for example, if $\phi = 180°$ and $a = 0.49$, the effective pulse duration may be shortened to such an extent as to cause overmodulation, and the height of the resultant exceeds the slicing level by so little that other noise or interference, if present, may easily reach the output. Both theory and experiment show the probability of such conditions to be low, so that little or no disturbance generally results from interference ratios less than one-half.

Interference ratios larger than one-half give rise to the missing-pulses phenomenon, though in a form quite different from that encountered before. Instead of occasional pulses (or portions of pulses) failing to reach the output with a probability F, there is a probability F that all of them fail to reach the output. Since the overlap between the two pulse trains is generally partial rather than complete, only one set of edges is generally lost (with probability F), but even if the remaining edge is time-modulated, distortion will result if the larger part of the pulse is lost. Complete loss of intelligibility results only in case of complete coincidence between the two pulse trains, or if asymmetrical PDM is used and the modulated edge happens to be overlapped. The remaining probability (always at least two-thirds) is that of obtaining a resultant which exceeds the height of the smaller signal and hence the slicing level. Apart from inconsequential effects caused by occasional large changes in overlap resulting from signal modulation, reception is perfect (with probability 1-F).

Oscillograms of the detector output are shown for various interference ratios and for several r-f phase-difference values, ϕ, in Figs. 106 - 113; oscillograms are shown also for incoherent interference. The exposures are several seconds in all cases, but the value or level of the resultant persists indefinitely in the coherent case, while it is different from pulse to pulse

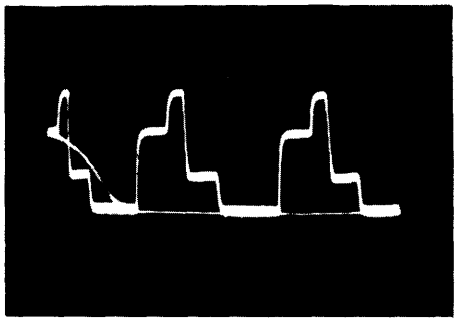

FIG.106
a = 0.4
ϕ = 0°

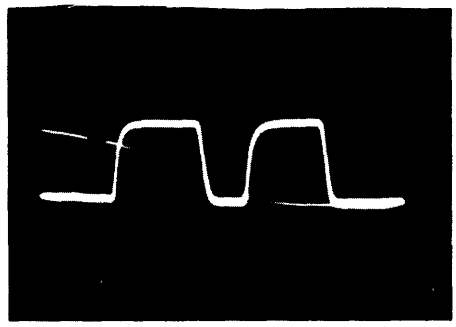

FIG.107
a = 1.0
ϕ = 180°

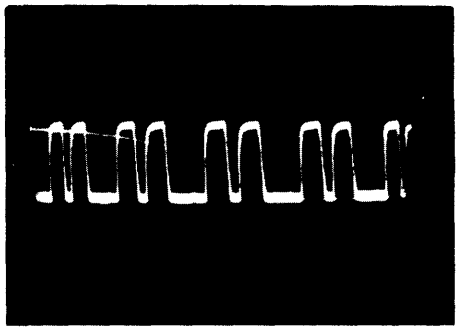

FIG.108
a = 1.0
ϕ = 180°

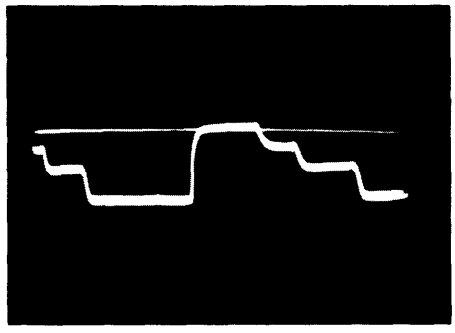

FIG.109
a = 0.45
ϕ = 130°

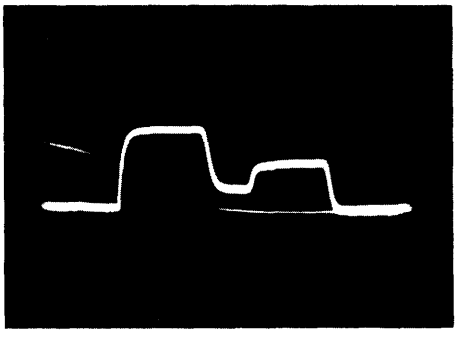

FIG.110
a = 0.65
ϕ = 180°

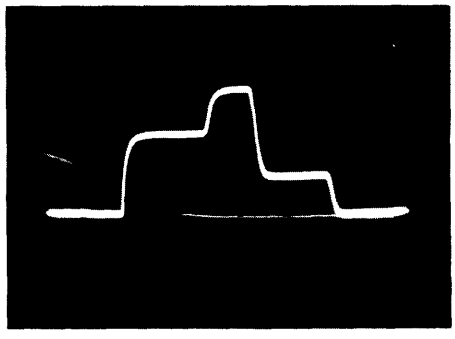

FIG.111
a = 0.5
ϕ = 0°

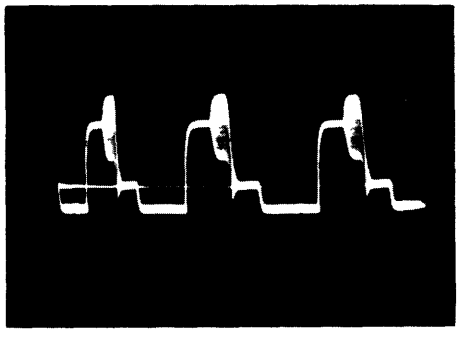

FIG.112
a = 0.3

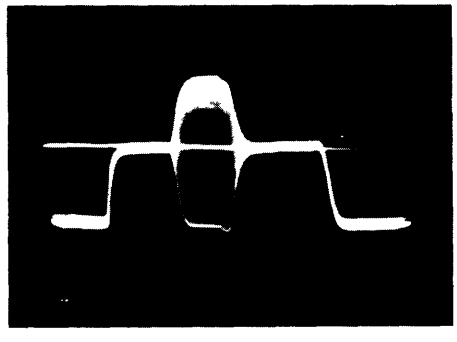

FIG.113
a = 1.0

Figs.106-111 Detector output showing partial overlap of two coherent pulse trains.

Figs.112-113 Detector output showing partial overlap of two incoherent pulse trains.

(each 1/20,000 second) in the incoherent case. In the extreme case, in which $\underline{a} = 1$ and $\phi = 0°$, each pulse is, in effect, split into two separate parts, consisting of parts of both pulse trains. Such situations (occurring with probability F, never exceeding 1/3) do not permit reception under the conditions stated at the beginning of this section (5.31), but it will be found in the next section (5.32), that good reception is generally possible if it is permissible to mix the modulating signals of the two pulse trains. Under the present conditions, the conclusion is that there is a probability equal to two-thirds or more of obtaining perfect reception, while the remaining third may mean poor or unacceptable reception. For a given delay difference between the two paths, the precise value of the radio frequency alone determines whether reception is good or bad. In the case of a point-to-point time-division multiplex system, it is conceivable that slight adjustments in the radio frequency be made to keep any multipath interference "in phase" ($\phi = 0$) or at least within the limits required to make the resultant of the desired and interfering pulses exceed the slicing level. This can even be done automatically through a narrow-band control link from the receiving station back to the transmitter. The discussion of the next paragraph will show that the required changes in frequency may be extremely small.

In order to change the r-f phase difference by 180°, the two-path delay difference need change by an amount equal to only half the r-f period, generally a very small fraction of one microsecond. Conversely, the radio frequency need change only the same relative amount in the opposite sense; this follows from the relation

$$\phi = 360°(1-n) \times \frac{\text{delay difference}}{\text{radio frequency}} , \qquad (117)$$

in which the integer n may be so chosen as to yield a value of ϕ between 0° and 360°. Therefore the relative change in radio frequency required to change ϕ by 180° is half the r-f period ($1/2f_{r-f}$) divided by the delay difference. In the case of the equipment used in this study (radio frequency = 30 Mc, delay difference = 0.5 ms), this change amounts to one part in 3×10^4, and the stability over short periods can readily be kept high enough to prevent even changes amounting to only one part in 10^6 (corresponding to a 5-degree change in ϕ). At S-band frequencies, for the same delay difference,

these relative changes would be one-hundred times smaller, and the oscillator would not generally be stable enough to keep ϕ substantially constant. However, at these high frequencies, the delay differences, especially those which are constant, are generally much smaller than 500 microseconds, namely a fraction of a microsecond to ten or twenty microseconds. Therefore a stability of one part in 10^6 is still sufficient to prevent ϕ from changing enough to destroy the coherence.

In multipath interference caused by reflections from moving objects, the delay difference may be changing rapidly over extended periods of time. Conditions of perfect reception and unacceptable reception may then alternate continuously, and it is of interest to estimate the possible frequencies of these alternations. A path involving a reflection from aircraft may change at a rate as high as 1000 feet per second, which means that the delay difference changes at a rate of one microsecond per second. At a frequency of 100 Mc, at which aircraft reflections are common, this means that during every second the vector describing ϕ makes 100 complete revolutions. In other words, the frequency of alternation is so great that, although the signal may be intelligible at all times, an audio-frequency beat note results; its frequency in cps is approximately equal to the radio frequency in Mc in an extreme case of rapid change in path length. In the case of ionospheric reflections, both the radio frequency and the rate of change in path length are generally smaller, and the alternation is expected to be at a sub-audio frequency. It should be pointed out that an alternation at an audible frequency will produce a beat note even at low interference ratios ($a < 0.5$) for which reception would otherwise be perfect, since the edges will be time-modulated periodically. This is simply another example of the well-known Doppler effect.

Comparing the results of coherent two-path interference with those of incoherent two-path interference, subject to the condition of this section (5.31), one is led to the conclusion that coherent interference is preferable since it permits good reception under conditions permitting only noisy reception in the incoherent case, and with a known probability may permit good reception where incoherent interference does not allow acceptable reception. The overall conclusion from the study of this section, while somewhat more optimistic than that given for the incoherent case alone (page 171), must still emphasize the fact that, while acceptable reception of the stronger signal is generally possible for interference ratios less than one-half, it cannot be

guaranteed for larger interference ratios.

5.32 Two-Path Interference in Single-Channel (Audio) PDM Systems

Consideration of the oscillograms of Figs. 106 - 113 shows that, regardless of whether the interference is coherent or incoherent, both the time-shift and missing-pulses effects can be avoided by lowering the slicing level sufficiently. To avoid these effects under all conditions, it must be lowered below a or 1-a whichever is the smaller. The condition $s < a$ ensures that the edge overlapped by interference and therefore subject to the time-shift effect is "bypassed" by the slicer, and the condition $s < 1-a$ ensures that all resultants exceed the slicing level . The respective conditions cannot be fulfilled in practice if a is very nearly zero ($a < 0.03$) or very nearly unity ($0.97 < a < 1$). In the former case, the slicing level can be set at 0.5, since the resulting time-shift noise will be small (or generally nonexistent if interference is coherent). In the latter case a slight amount of missing-pulses noise results from the disability to bring the slicing level completely below the smallest resultants; this will be discussed later.

The presence of appreciable input noise may make it impracticable to lower the slicing level below a certain minimum, since this would cause excessive noise at the output. In the experimental study of this section, the input signal-to-noise ratio exceeded 40 db and the slicing level could be lowered to 0.01 without causing appreciable output noise.

The principal result of lowering the slicing level below the interference level is that the smaller signal is no longer treated as unwanted interference. There is no discrimination in favor of either of the two pulse trains, and if they were time-modulated by different signals, both of these would generally reach the output. Since both pulse trains are modulated by the same signal, separated by a small time delay, this signal reaches the output, but not without certain modifications, from its original form. The exact nature of these modifications depends principally on the degree of overlap between the two pulse trains. These signal-distortion effects are common to both the coherent and incoherent cases of interference. (Certain additional disturbing effects which occur only in the incoherent case will be discussed later.)

For the purpose of this discussion, it is convenient to distinguish between three different degrees of overlap in the absence of modulation: no overlap, partial overlap, and precise coincidence. In the presence of modulation, the

borderline between the first two conditions may not be clearly defined, but one or the other generally prevails. Precise coincidence means that both sets of edges of each pair of pulses coincide exactly, or, in the presence of modulation, occur at equal instants on the average.

1. No Overlap between the Two Pulse Trains

The probability of obtaining no overlap even on modulation peaks is 1-4D, subject to the assumption that the peak pulse duration is twice the average pulse duration d (d = DT). However, experiment shows that occasional partial overlaps on modulation peaks are unnoticeable, so that a probability of 1-3D is sufficiently conservative. This probability, of course, is correct only if the delay difference can have a wide range of values (at least as large as the pulse-repetition period). If small values are favored, as at microwave frequencies, the "no-overlap probability" increases even more rapidly with decreasing duty factor. As previously mentioned, no overlap between the two pulse trains is, of course, the most favorable situation; there is no reason for slicing below the interference level unless this is extremely close to the desired-signal level or the no-overlap condition is only transitory. Perfect reception results if the slicing level is above the interference level; if the slicing level is below the interference level, both pulse trains reach the output unimpaired and the result is that their modulation signals are added linearly and both reach the output with full strength. Since the two signals are identical except for the delay difference, the resultant output is a linear superposition of the original signal, f(t), and the same signal delayed by an amount T_{dd}(delay difference). The output signal is

$$\text{Output (no overlap)} = f(t) + f(t - T_{dd}) \ . \qquad (118)$$

Alternately, the signal may be considered in the frequency domain instead of the time domain. At any given frequency, the sinusoidal components of both signals must be added vectorially, since they differ in phase. The phase angle, in radians, is simply ωT_{dd}. The two components to be combined are equal in magnitude which may be assumed unity. The resultant is

$$\text{Output (no overlap)} = 2(1 + \cos \omega T_{dd}) = \left[2 \cos \frac{\omega T_{dd}}{2}\right] \ . \qquad (119)$$

This means that the modulation-signal voltage spectrum is multiplied by a function which has maxima at zero frequency and all frequencies which are integral multiples of the reciprocal of the delay difference. More important, this function has nulls at all frequencies which are odd integral multiples of half the reciprocal of the delay difference. The maximum and null frequencies may, for brevity, be referred to as reinforcement frequencies and cancellation frequencies, respectively.

The actual result, so far as perception of speech and music is concerned, depends on the delay difference. If the delay difference is fifty microseconds or somewhat less, only the first cancellation frequency will fall within the audio band (10 kc), and the effect will simply be loss of high-frequency components. For smaller delay differences, there will be no noticeable effect. In the case of the 555-microsecond delay difference used in the experimental tests, there are nulls at approximately all multiples of 900 cps. With both speech and music, the listener obtains an impression of a change in quality, quite noticeable if he switches abruptly from one-path to two-path reception, but not so obvious after prolonged listening. Although a definite defect in the signal, this condition, which may be called spectrum distortion, is not offensive in any way for ordinary communication purposes. As regards high-fidelity reproduction of music, the maxima and minima in the frequency characteristic are obviously intolerable if the original energy-versus-frequency distribution is to be maintained.

The overall PDM-system frequency characteristic with and without two-path interference is shown in Fig. 114. Theoretical and experimental results coincide exactly and are therefore not shown separately. If plotted with a linear abscissa and ordinate scale, these curves are full-wave-rectified cosine functions.

2. Partial Overlap between the Two Pulse Trains

If there is partial overlap between the two pulse trains, and the slicing level is below the smallest possible resultant, each overlapping pair of pulses emerges at the output of the slicer as a single longer pulse. The leading edge of this new pulse carries the time modulation of the leading edge of one of the pair, while the trailing edge carries the time modulation of the trailing edge of the other pulse. Therefore, the presence of the second pulse train has no effect on the signal output if asymmetrical PDM is used; the signal of

one or the other of the two paths will be recovered, and the only change is the lengthening of the average pulse duration. In the case of symmetrical PDM, however, the result is similar to that described for the condition of no overlap. The leading edge of the new, longer pulse carries half of the modulation of one path, and the trailing edge carries half the modulation of the other path. The resulting signal output is one-half the sum of the signal and the same signal delayed by the delay difference. This differs from the result described for "no overlap" only by a factor of two, and hence the second curve with minima and maxima (Fig. 114) is exactly six decibels lower than the first one.

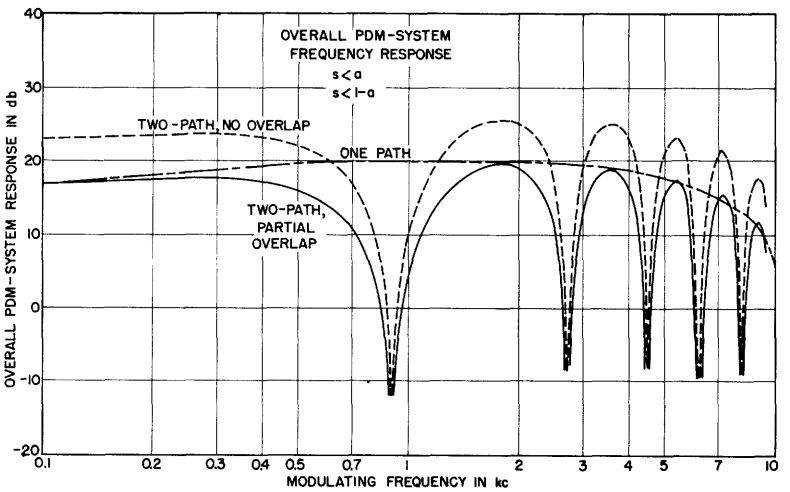

Fig.114 Overall PDM-system frequency characteristics with and without two-path interference (measured and computed).

A condition intermediate between no overlap and partial overlap is possible, of course, and may result in rapid back-and-forth switching of the output level. For example, the output may be six decibels higher on negative modulation peaks than on positive peaks. Consequently, distortion results, but this is not sufficiently severe to impair the intelligibility of speech, and it is noticeable only if there is almost exact coincidence between the leading edges of one pulse train and the trailing edges of the other. More serious distortion results in the case of slight partial overlap or no overlap if the duty factor is not much less than 0.5 and reaches peaks not much less than unity. The two pulse trains then momentarily (on positive modulation peaks) blend into a continuous signal, so that no edges are detected and no output is obtained. This difficulty is never encountered for duty factors

less than thirty per cent.

3. Precise Coincidence

If the edges of the two pulse trains occur at the same instants (in the absence of modulation), or if their separation in time is small compared to the effective modulation time shift, severe distortion results unless the delay difference is very small.

In the absence of modulation, the two sets of pulses overlap each other completely and emerge as a single pulse train from the slicer; they do not differ from the pulse train obtained from one-path reception. In the presence of modulation, this is still true only if the modulation of the two sets of overlapping pulses is the same; it is the same or nearly the same if the delay difference is small compared to the period of the highest modulating frequency. Consequently, for delay differences of the order of one microsecond or less, the effect of the two-path interference is virtually unnoticeable. The next lowest delay difference which results in precise coincidence is one pulse-repetition period, which is generally not much less than half the period of the highest-frequency-signal component. The effects of the two-path interference analyzed below are then present only at the high end of the audio-frequency band and are therefore not serious.

For delay differences comparable to periods corresponding to midband audio frequencies, the modulation on the coinciding pulses is generally different. Unlike "no overlap" and "partial overlap", "precise coincidence" does not result in a linear superposition of the two modulation signals. Consider, for example, the detection of the leading pulse edge. In the absence of modulation, the leading edge of pulse A (arriving by path 1) coincides with that of pulse B (arriving by path 2). In the presence of modulation, the edge of pulse A may precede or follow that of pulse B; these two conditions alternate on successive pulses, depending on the instantaneous values of the modulating signal. However, regardless of the order of arrival of the two edges, only that arriving first is detected by the slicer. Similarly, the trailing edge arriving last, regardless of whether it belongs to pulse A or pulse B, is the only one detected. The distortion resulting from this phenomenon is illustrated for a random signal in Fig. 115 under two different conditions: precise coincidence and partial overlap. It is seen that the distortion rapidly diminishes as the coincidence becomes less precise, inasmuch as the "damage"

is more and more confined to the signal peaks.

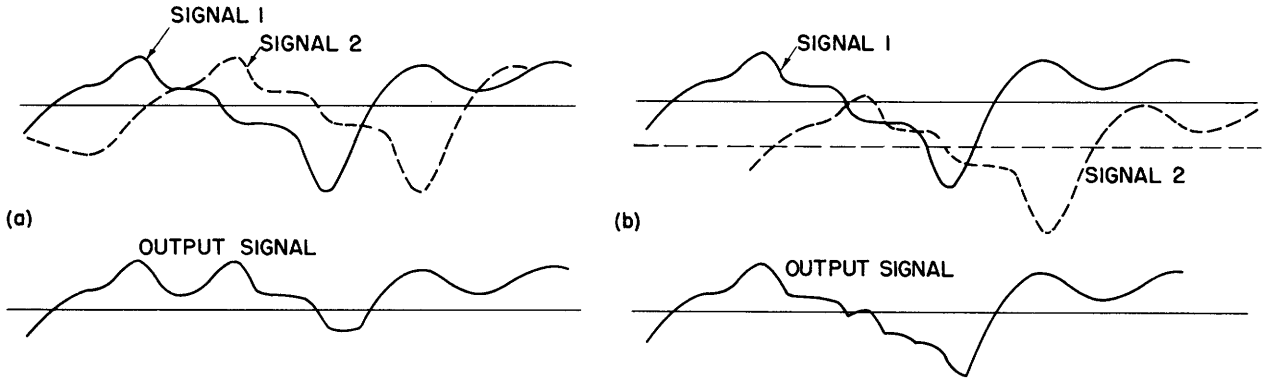

Fig.115 Distortion for (a) precise coincidence (b) partial overlap.

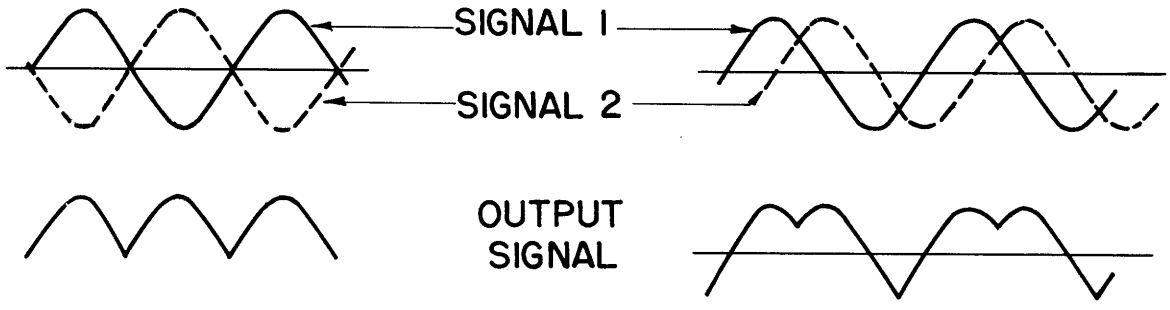

Fig.116 Precise-coincidence distortion for sinusoidal modulation.

While Fig. 115 completely shows and defines the type of distortion resulting from the condition being discussed, this can be readily formulated mathematically only on the basis of sinusoidal signal components. At "reinforcement" frequencies (see page 179), there is no distortion, since the modulation time shifts of the coinciding pulse edges are identical. On the other hand, at "cancellation" frequencies (see page 179), there is a maximum of distortion: it amounts to simple full-wave rectification of the signal. This, as well as the distortion obtained in an intermediate case (frequency between cancellation and reinforcement frequencies), is shown in Fig. 116.

Experimental verification of the theoretically predicted waveforms of Fig. 116 is found in the oscillograms of Fig. 117. These oscillograms show the PDM receiver output for four different modulation frequencies at the transmitter obtained under the conditions being discussed; superimposed on the same photographs are the outputs obtained from normal one-path reception. The

distortion ranges from complete rectification at cancellation frequencies (eliminating the fundamental and substituting mostly second harmonic) to zero distortion at reinforcement frequencies. Over a twenty-per-cent range on either side of a reinforcement frequency the distortion is not serious.

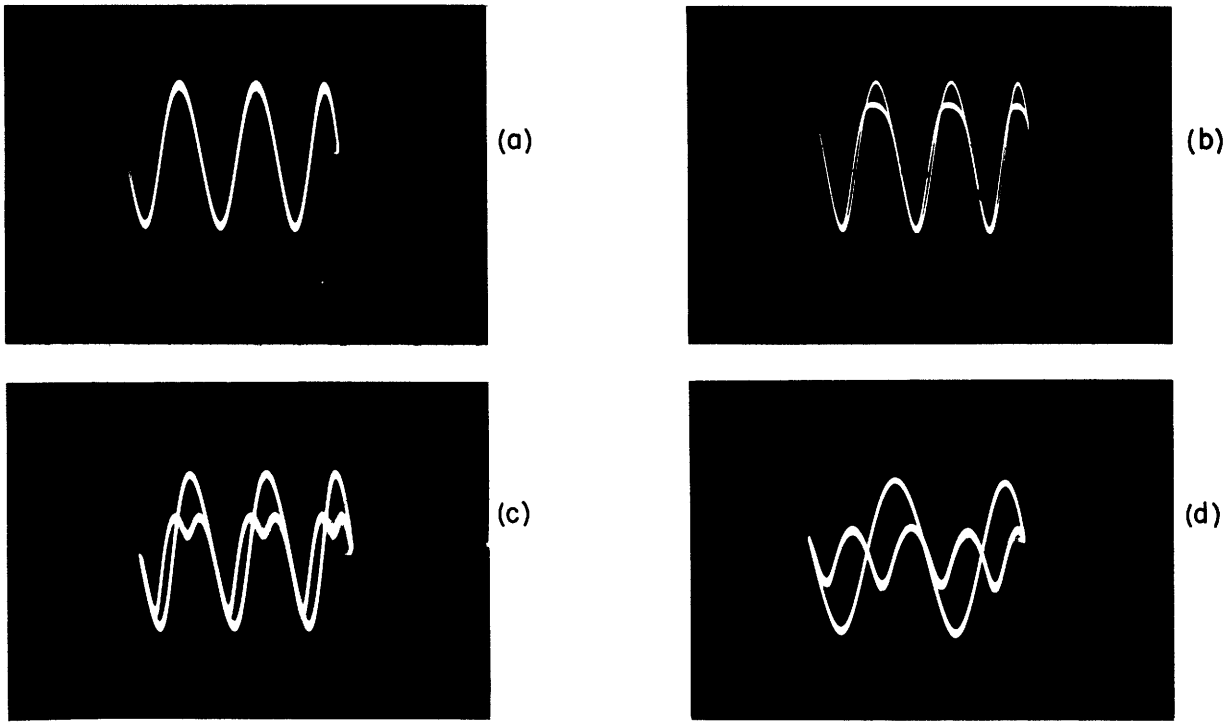

Fig.117a-d Precise-coincidence distortion for sinusoidal modulation; distorted output superimposed on undistorted output. Modulation frequency (a) 1800 cps (b) 1500 cps (c) 1200 cps (d) 900 cps.

Harmonic-analyzer measurements of the output as a function of modulation frequency describe the nature and extent of the distortion exactly. Such measurements are plotted in Fig. 118; computed magnitudes of the fundamental and its harmonics, obtained by Fourier-series analysis of the complex waveform, are also shown. Since the delay difference is 555 microseconds, the first cancellation frequency with its attendant heavy second-harmonic distortion occurs at 900 cps. This is not far from the most severe condition possible, inasmuch as the ear is most sensitive to distortion in this frequency range. The precise-coincidence distortion for this large delay difference is such as to make music unacceptable and speech very unpleasant though still intelligible. A departure from precise coincidence amounting to a few tenths of the peak-modulation time shift is sufficient to all but remove the distortion.

The discussion up to this point in Section 5.32 will be briefly summarized.

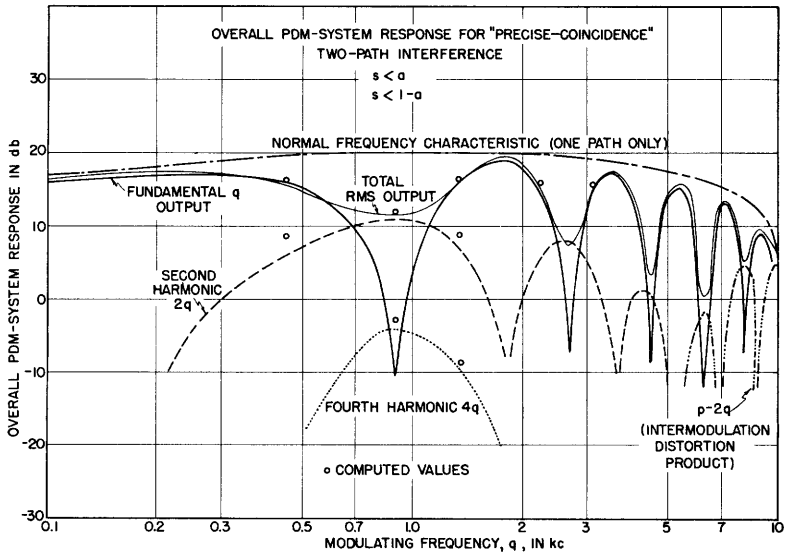

Fig.118 Overall PDM-system frequency characteristic showing distortion obtained for the condition of "precise coincidence" of the two pulse trains.

So-called spectrum distortion results if there is no coincidence or partial coincidence between the two pulse trains. This is generally harmless so far as speech or music are concerned; however, if there is no overlap between the two pulse trains, this effect can be avoided completely by raising the slicing level s above the interference level ($s > a > 1$). Some linear distortion, in addition to the spectrum distortion, occurs in the borderline case between no overlap and partial overlap, but this is not serious. Severe distortion results from precise coincidence, but the probability of precise coincidence is small. Neither this severe distortion nor the spectrum distortion mentioned above are encountered if the two-path delay difference is small compared to the periods of the highest frequency audio component.

The distortion effects described above are the most common manifestation of two-path interference if the slicing level is set below the interference level. In the coherent case (pulsed amplifier), these effects are the only manifestation of the interference; in the incoherent case (pulsed oscillator), additional effects are noticeable under certain conditions. These additional effects will now be discussed.

If the two pulse trains overlap each other partially or completely and the interference ratio is extremely close to unity, the missing-pulses effect cannot be entirely avoided since practical reasons make it impossible to satisfy the condition $s < 1-a$. A certain amount of missing-pulses noise therefore results, given by (97), (page 102), where F is, in turn, found from (32) (page 36). Expression (32) gives F as a function of both s and a. The noise power

varies approximately linearly with slicing level if the interference level is unity or within a few per cent of unity; this follows from (33) (page 36) and is shown in the computed plot of Fig. 119. On the other hand, Fig. 120 shows the noise to be nearly constant as a function of a over most of the range (1-s < a < 1) within which any missing-pulses noise is produced; this is seen to be true regardless of the value of s. The relation between noise voltage and overlap of the two pulse trains is linear.

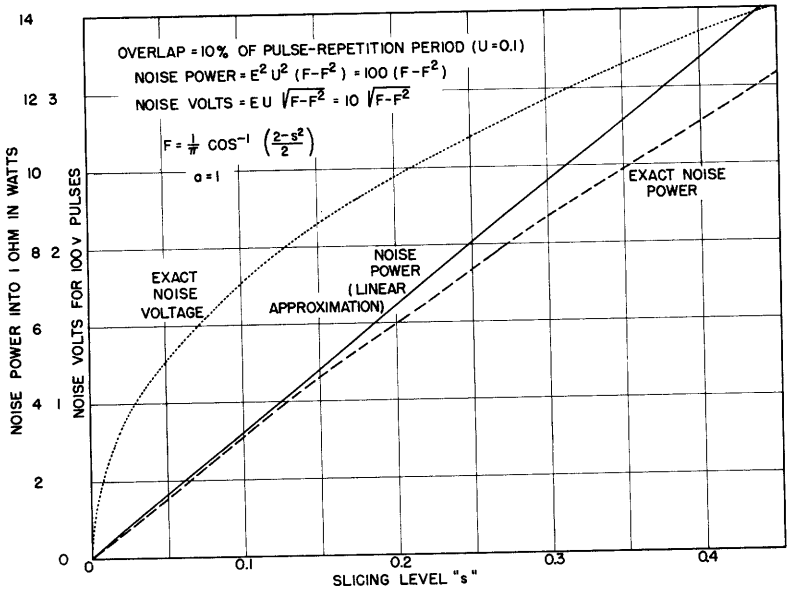

Fig.119 Two-path interference noise versus slicing level s for interference ratio a equal to unity.

If the two pulse trains coincide precisely, the missing-pulses noise discussed above has a maximum. It should be emphasized that this noise need exist only for interference ratios so close to unity that the slicing level s cannot be set below 1-a. Under the condition of precise coincidence a special type of time-shift noise also appears, which is not confined to large interference ratios, although it does increase rapidly with increasing interference ratio and is generally unnoticeable for small values. The noise is of a special type in that it is produced only under the condition of precise coincidence and disappears when time modulation of the pulse edges wipes out the precise coincidence. The coinciding pulse edges produce resultants with variable rise and decay times depending on the r-f phase difference, ϕ. Consequently there is a random departure from periodicity in the pulse-edge positions (the instants at which the slicing level is crossed). This is smaller than that associated with the ordinary edge-time-shift effect discussed earlier

in this paper; it decreases with decreasing slicing level and, theoretically, it goes to zero when the infinitesimally thin slicing level approaches zero. Experimentally obtained plots of the total noise as a function of overlap are shown in Fig. 121 for unity interference ratio and two different duty-factor values. In the case of the large value (D = 0.4), the missing-pulses noise almost completely masks the time-shift noise, but in the case of the smaller value (D = 0.1) the time shift noise is quite definitely in evidence.

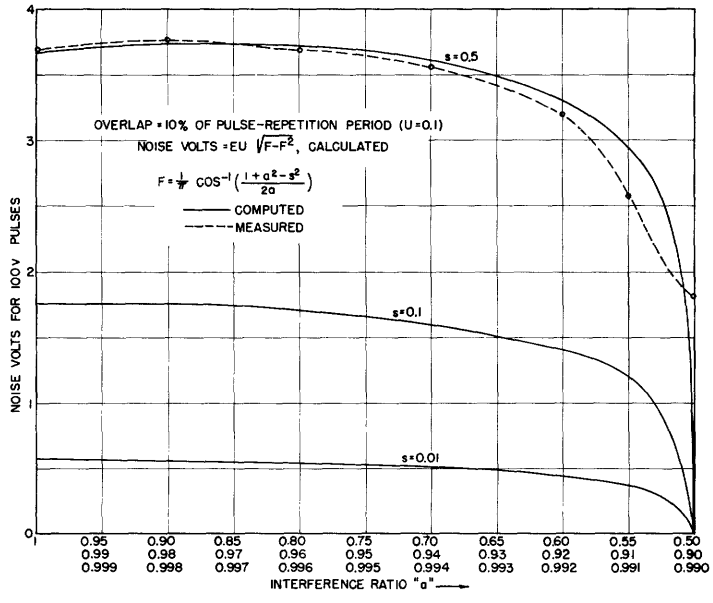

Fig.120 Two-path interference noise versus interference ratio a for various low slicing levels s.

Knowing the missing-pulses noise power obtained for a = 1, one can calculate from (33) (page 36) and (97) (page 102) the exact value of the slicing level which, theoretically, must have been used to produce this noise power. For data like those of Fig. 121, such calculations lead to values in the order of magnitude of 0.01.

The coherent type of two-path interference is completely free of the noise effects discussed above and is therefore noticeably "superior" to the incoherent type. In addition, the coherent case permits perfect reception, free even of the distortion effects discussed above, for interference ratios less than one-half ($s = \frac{1}{2}$). For larger interference ratios, there is a certain amount of freedom in the choice of slicing level. The two essential possibilities, namely high slicing level and low slicing level, have been covered in Sections 5.31 and 5.32. There are also some intermediate possibilities not previously discussed, and a summary of all the possibilities and associated

effects is therefore in order. This can readily be done with the aid of Fig. 122 which shows two partially overlapping pulses and indicates the possible values of the resultant.

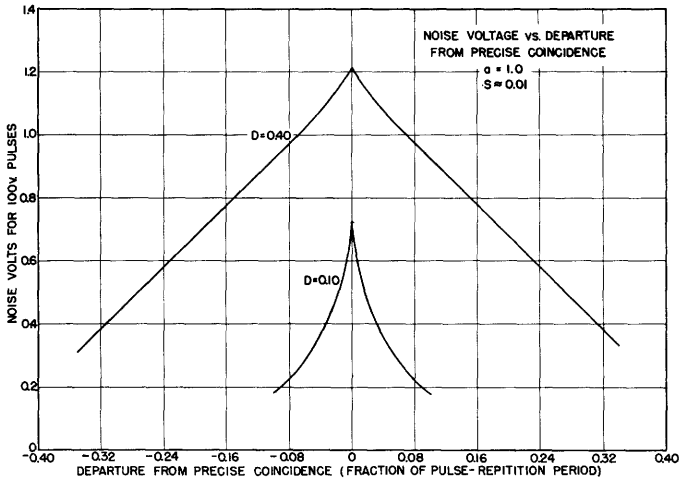

Fig.121 Two-path interference-noise voltage vs. departure from precise coincidence expressed as a fraction of the pulse-repetition frequency (experimental plots).

First, setting the slicing level below the smallest possible resultant ($s < 1-a$) gives reliable reception which is marred only by the spectrum distortion (for "symmetrical" PDM).

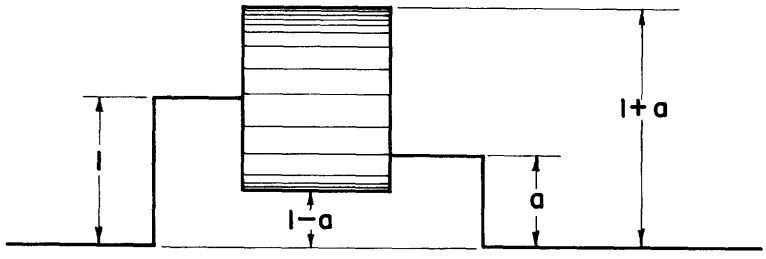

Fig.122 Partially overlapping pulses and the possible values of their resultant.

The second possibility, already discussed in Section 5.31, is that of setting the slicing level just above the interference level ($s = a+$). This means perfect reception with a probability 1-F (which is never less than two-thirds). This is the probability that the resultant of the overlapping pulses exceeds a and hence s, so that both edges of the desired pulse cross the slicing level. Some degree of intelligibility may still be obtained even if the resultant is less than a (probability = F) so long as the overlap is only partial. The pulse at the slicer output is a new pulse whose leading edge is that of the pulse arriving through path 1 and whose trailing edge is actually

the leading edge of the pulse arriving by way of path 2. Consequently, the output signal is proportional to the difference between the signals modulating these two edges; the result is spectrum distortion complementary to that found previously, with a null instead of a maximum at zero frequency. This will be discussed in somewhat greater detail in connection with PPM two-path interference, Section 5.43. If asymmetrical PDM is involved, the signal may be lost completely since there is an even chance that the two edges comprising the slicer-output pulse are the unmodulated edges of the original pulses.

A third possibility of interest is that of setting the slicing level at some intermediate value. Evidently, the condition $s = a+$ does not guarantee reliable reception, nor is it always possible or practicable to satisfy the condition $s < 1-a$. Consider, therefore, the possibility of $s = \frac{1}{2}$, which is optimum so far as the suppression of low-level interference is concerned. If the resultant of the overlapping portions of the two pulse trains exceeds one-half, the output consists of the superposition of the two signals as though the condition $s < 1-a$ were fulfilled. The probability of this happening is 1-G (see Fig. 123), which never drops below five-sixths. If the resultant of the overlapping portions is less than one-half, reference to Fig. 122 shows that two separate pulses appear at the slicer output. Both physical reasoning and experiment show that these pulses contain no usable signal components, inasmuch as almost complete cancellation takes place. The probability of this happening is G, which has been plotted together with F in Fig. 123. It never exceeds the relatively low value of one-sixth.

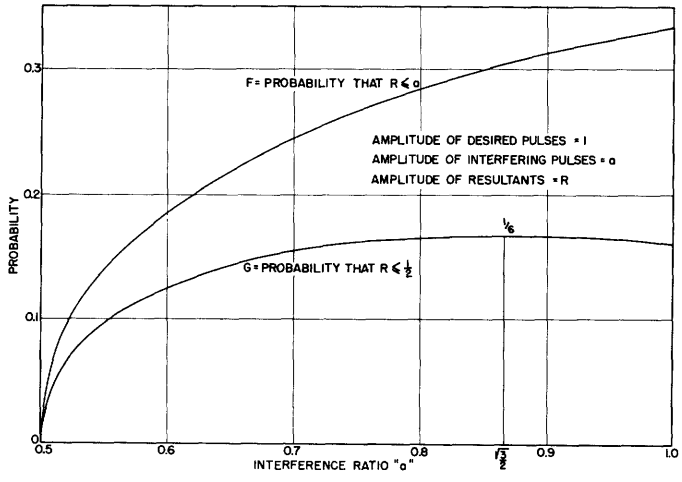

Fig. 123 Probability that resultant of overlapping pulses exceeds a and $\frac{1}{2}$, respectively, vs. interference ratio a.

Based on the most important condition, $s < 1-a$, the conclusion for the present section is that relatively good reception is generally obtainable in the presence of severe two-path interference, particularly if the transmitted pulses are coherent with each other. The spectrum distortion, unavoidable if the interference ratio exceeds one-half, is not generally serious for communication purposes, and the probability of obtaining the severe precise-coincidence distortion is sufficiently small to be fairly unimportant. Further conclusions can be reached only with knowledge of the actual conditions causing the two-path interference, or by means of actual field tests.

5.4 Two-Path Interference in PPM Systems

5.41 Outline of PPM Systems

The investigation of the interference characteristics of PPM is necessarily less complete and less precise than the corresponding investigation for PDM. The reason for this is the somewhat less fundamental nature of PPM, the more complex methods of demodulation needed, and the greater number of such methods. In order to facilitate the presentation of the experimental measurements and observations, general descriptions (without circuit details which can be found in Appendix V) of the PPM systems tested will be given.

The basic interference effects are the same for PPM as for PDM; they are the time-shift effect and the missing-pulses effect. However, the manner in which they manifest themselves depends to a large extent on the manner in which the PPM system operates. Two radically different systems are considered here. They differ in the following three respects: (1) the method of conveying the synchronizing information from transmitter to receiver; (2) the maximum permissible modulation time shift; (3) the method of demodulation. The method of demodulation is perhaps the most important of these differences, inasmuch as it is partially responsible for determining some of the parameters, for example, the maximum modulation. It is therefore convenient to distinguish the two systems by their method of demodulation or detection and to call them coincidence-detection and flip-flop-detection systems, respectively. The systems described below are not the only possible ones belonging under the two respective classifications; they are the particular systems used for the purpose of this study.

Coincidence-Detection System

In the coincidence-detection system, the maximum peak-to-peak time shift of the pulses is limited to the pulse duration measured at the slicing level actually used. (It is possible to modify the system so as to remove this limitation, but this is not always desirable; for example, in a time-division multiplex system having many closely-spaced channels, the need for prevention of cross-talk imposes a similar requirement.) At the receiver, the time-modulated pulse train is compared to two unmodulated (periodic) pulse trains; as shown in Fig. 124, one of these is phased so as to lead the modulated pulse train by d/2 (d = pulse duration) on the average, while the other one lags by the same amount. The result is that, on the average or in the absence of modulation, there is an equal amount of overlap or coincidence between the modulated pulse train and either of the two reference pulse trains. However, modulation alters the individual overlaps and causes the short-time average overlap to vary in accordance with the signal. The varying overlap between the modulated pulse train and either of the reference pulse trains is sufficient for recovering the original signal, but by utilizing both sets of overlaps (taking their difference) certain advantages are realized. The overlaps are converted into the output signal by means of coincidence detectors. The method of using two staggered reference pulse trains instead of one, whereby the positions of both sets of pulse edges have equal parts in determining the output, may be referred to as either balanced-coincidence, double-coincidence, or two-edge-coincidence detection.

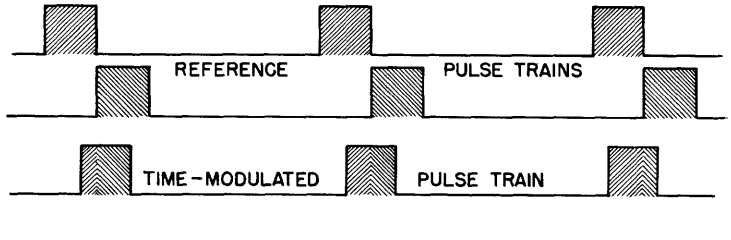

Fig.124 Double-coincidence detection of position-modulated pulses (pulse duration exaggerated).

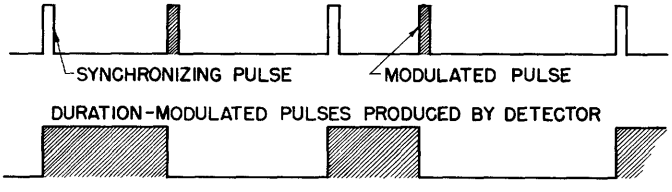

Fig.125 Flip-flop detection of position-modulated pulses.

Synchronizing information must, by some means, be available at the receiver in order to establish the frequency and phasing of the reference pulses. The most common method is to transmit so-called synchronizing pulses together with the modulated pulses, but this is wasteful of time and energy unless the synchronizing pulse train takes care of a number of channels simultaneously. The two methods used here in conjunction with the coincidence-detection system do not involve the use of synchronizing pulses. In one system, the synchronizing information is transmitted separately by means of a continuous sinusoid (which requires zero bandwidth in theory); in the other system, advantage is taken of the fact that all the synchronizing information needed is actually contained in the modulated pulse train. The long-time average of the modulation time shifts is zero, so that the time-modulated pulses need only be passed through a narrow bandpass filter to yield an unmodulated sinusoid from which a periodic pulse train can be formed. This method of synchronization may be referred to as self-synchronization, and the former method may be called external synchronization.

Flip-Flop Detection System

The flip-flop scheme, although not described by this name, was the earliest PPM system described in the literature.[2] For each sampling period, a "fixed" and a time-modulated pulse are transmitted. At the receiver, the sequence of alternating fixed and modulated pulses triggers a so-called flip-flop circuit, producing a duration-modulated pulse train, as shown in Fig. 125. In a time-division multiplex system, where several time-modulated pulses are transmitted per synchronizing pulse, it is obviously necessary to distinguish the latter from the modulated pulses; this is not the case in the single-channel system tested in this study, since it is immaterial whether the duration-modulated pulses are formed from the spaces between fixed and modulated pulses or the spaces between modulated and fixed pulses.

Either the leading or trailing edges can be used to trigger the flip-flop, and it is even possible to utilize both sets of edges simultaneously.* Unlike the coincidence-demodulation method described above, the flip-flop method does not impose a limit on the maximum modulation time shift. The maximum peak-to-peak time shift may approach a value equal to the pulse-repetition

*See Appendix V

period. In the case of this system and also the coincidence system, the all-important slicer precedes the demodulator. Its function is fully as essential in PPM systems as it was shown to be in PDM systems.

5.42 Two-Path Interference in Coincidence-Detection PPM Systems

As in the case of PDM two-path interference, there may or may not be overlap between the two PDM pulse trains. Since the pulses used in PPM systems are generally of considerably shorter duration, the probability of obtaining overlap is correspondingly smaller. The coincidence-detection scheme is "self-gating" in that it inherently ignores any undesired pulses which do not coincide with the desired pulse or fall in its immediate vicinity, regardless of whether or not they pierce the slicing level. With external synchronization (which is assumed to be undisturbed), the two-path interference therefore has no effect under the no-overlap condition. Self-synchronization without gating is disturbed if the interfering pulses reach the slicer output, inasmuch as the a-c component of the combined pulse trains is phased differently than that of one pulse train alone. (If the delay difference and the interference ratio are constant, a simple adjustment compensates for the synchronization phase shift.) If the received pulses are time-gated before being used as a time base, perfect synchronization can be obtained from one pulse train without any disturbance from the other, so long as there is no overlap or "near overlap" between the two pulse trains. Under this condition, therefore, two-path interference does not impair reception. The probability of obtaining no overlap is slightly less than 1-4D, which was approximately ninety per cent in the system tested.

The condition of partial or total overlap, though much less probable than no overlap, is of greater interest, since the results obtained under this condition show the limitations of the system in the presence of two-path interference. The results are considerably different, depending on whether the r-f pulses are coherent or incoherent with each other. Noise and distortion occur in the incoherent case, while only distortion is encountered in the coherent case. In either case, these effects are noticeable only if the two pulse trains are within one to two pulse durations of exact coincidence. The pulse duration used in most of the tests was 1 μsec at the half-amplitude level, and the system bandwidth such as to make the pulses "minimum-duration pulses" (approximately 1 Mc). As a result, the pulse shape is between a gaussian and

triangular shape (see Fig. 126), and the separation between leading and trailing edge is strongly dependent on the level at which it is measured. Inspection of Fig. 124 will make it clear that the double coincidence detection system operates satisfactorily only if the slicer-output pulse duration does not depart materially (more than 20 per cent) from the value for which the system was designed -- 1 μsec in the present case. Therefore, for technical reasons, a substantial departure from a slicing level of one-half is generally not desirable.

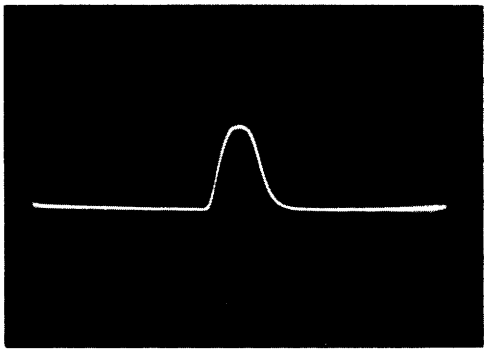

FIG. 126

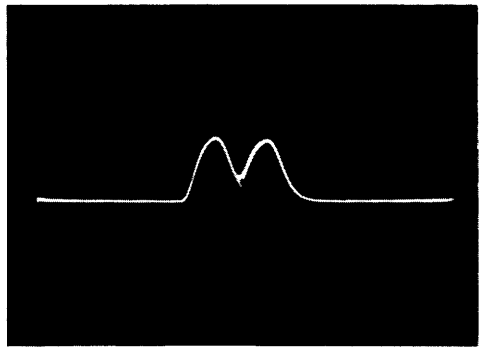

FIG. 127

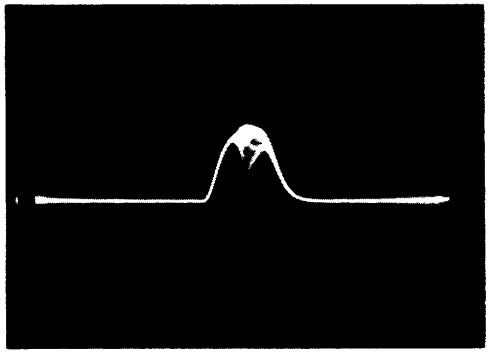

FIG. 128

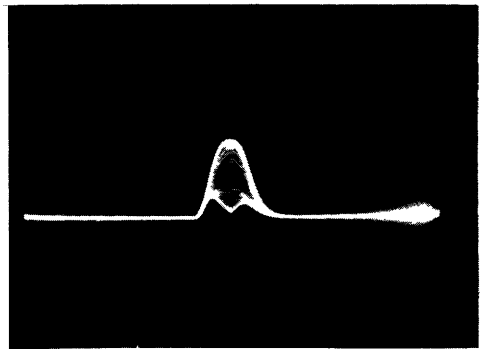

FIG. 129

Figs. 126-129 Detector output showing PPM-system pulses (two-path interference, a = 1); Fig. 126 one pulse, no interference; Fig. 127 two pulses spaced 1.5 μsec apart; Fig. 128 two pulses spaced 0.5 μsec apart; Fig. 129 two pulses coinciding.

Consider first the noise encountered in the incoherent case in the absence of modulation. The most severe condition, interference ratio close to unity, is illustrated for various degrees of overlap by oscillograms taken at the detector output, ahead of the slicer (see Figs. 126 - 129). As in similar oscillograms for PDM, the shaded white area represents successive random resultants of the overlapping voltages.

Noise measurements are conveniently referred to the maximum signal level, corresponding to the peak-to-peak time shift of one microsecond. The condition

shown in Fig. 127 does not give rise to any disturbance, since there is insufficient overlap to produce resultants exceeding the slicing level (one-half the pulse height). Strong, though not prohibitive, noise results from considerable overlap (Fig. 128), but the noise becomes weaker again as exact overlap is approached. The r-m-s noise voltage relative to the highest peak signal voltage is plotted as a function of overlap in Fig. 130. This experimentally obtained plot holds approximately for all values of interference ratio a between one-half and unity, provided the slicing level is held constant at one-half. Figure 131 shows the same noise as a function of interference ratio for partial overlap deviating from exact coincidence by approximately half the pulse duration ($\frac{1}{2}$ μsec). Computed results are superimposed on this plot.

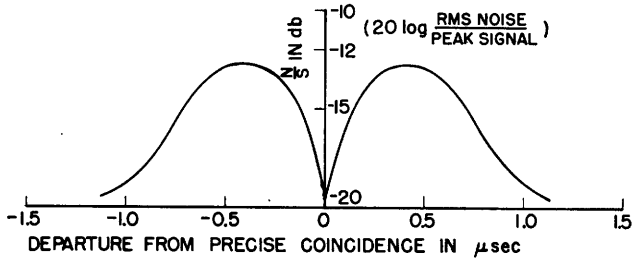

Fig.130 Two-path interference noise vs. pulse overlap (experimental); pulse duration at half-amplitude d = 1 μsec; double-coincidence PPM detection.

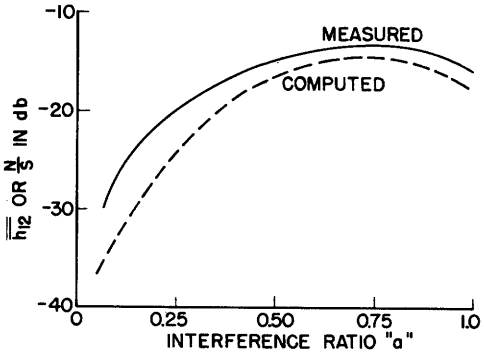

Fig.131 Two-path interference noise vs. interference ratio; partial overlap producing maximum noise; slicing level s = $\frac{1}{2}$; double-coincidence PPM detection.

The following two points may seem somewhat surprising at first sight: (1) the fact that the noise has a minimum for exact coincidence; (2) the fact that the noise tends to decrease when a is increased above one-half. The explanation for (1) is that symmetry between the time shifts of the two edges of each pulse causes the time-shift noise to cancel; while, on the other hand, $\frac{1}{2}$ μsec off exact coincidence, the peak of the interfering pulse coincides with the half-amplitude point of one of the edges of the desired pulse, which

consequently undergoes a large time shift while the other edge is hardly affected. The explanation for (2) is in a feature of the particular circuit used which prevents missing pulses from affecting the output.* When the interference ratio exceeds one-half and occasional pulses fail to reach the slicer level and hence the slicer output, the demodulator output is the same as though a pulse (identical in timing to the preceding pulse) were actually present. Only time-shift noise therefore reaches the output.

In Chapter 2 the time-shift expressions for interference between two gaussian pulses were derived. Equation (29) (page 33) does not have explicit solutions, but trial-and-error solutions have been obtained for numerous values of r-f phase difference, ϕ, normalized shift from exact coincidence, ℓ, and interference ratio, a. By carrying out the appropriate averaging processes over the entire range of ϕ, the effective time shift, and hence the r-m-s noise voltage, has been found. In this way, the theoretical curve of Fig. 131 as well as the curves in Figs. 132 and 133 were obtained. The curves of Fig. 132 give the noise obtained when two-edge detection is used; the curves in Fig. 133 give the noise obtained with one-edge detection, e.g., if one side of the balanced detector is made inoperative. These curves are shown for comparison; they prove that there is a considerable advantage under some conditions in using the balanced (two-edge) detector.

Additional experimental data pertaining to the subject under discussion have been obtained in connection with two-station PPM interference (Δprf = 0). The bandwidth of 1 Mc is somewhat larger than that theoretically required of a gaussian filter to form a gaussian pulse of 1-μsec duration at the half amplitude level. Measurements for other bandwidths indicate that the noise voltage changes approximately in inverse proportion to the bandwidth if the interference ratio is below one-half, and that the change is progressively smaller for larger interference ratios. The noise minimum at exact coincidence is found to be a perfect null for a bandwidth of 3 Mc and interference ratios smaller than one-half. This relatively wide bandwidth permits a perfectly symmetrical trapezoidal pulse shape instead of the slightly asymmetrical gaussian shape (see Fig. 126). Experimental values obtained with BW = 1 Mc for a = 0.9 agree closely with computed values plotted in Fig. 132; for smaller interference ratios, the noise measured with the 1-Mc bandwidth is several

---

* See Appendix V.

decibels higher than the computed values, while measurements for BW = 2 Mc check closely with computed values (a = 0.2 and 0.4). Measurements made with only one half of the detector operative (leading edge detected only) agree within experimental accuracy with the computed plots of Fig. 133.

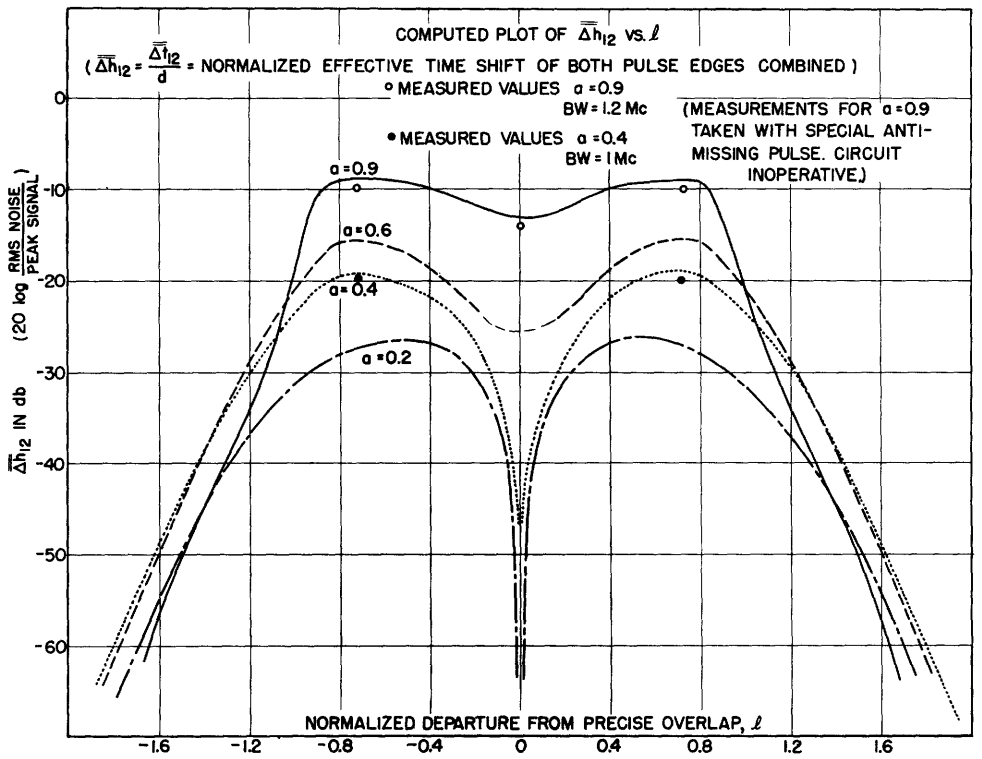

Fig. 132 Computed two-path interference noise vs. pulse overlap for various values of interference ratio; ℓ is the departure from precise overlap in μsec if the pulse duration d = 1 μsec.

The above data show that, in the worst cases, the noise is approximately 10 db below the peak signal. Nevertheless, intelligibility is maintained, inasmuch as modulation generally decreases the noise by varying the degree of overlap between the two pulse trains. For both two-station and two-path interference this decrease may be as large as 10 db. As a result, speech and music remain intelligible even under the most severe conditions of overlap and interference ratio, but reception cannot generally be considered acceptable under these conditions because of the distortion which will be discussed below. It should be mentioned that all of the above observations were made with external synchronization. Ideally, the same performance can be attained with self-synchronization, but the self-synchronization scheme used is not sufficiently perfect to prevent additional noise from being introduced by the timing pulses.

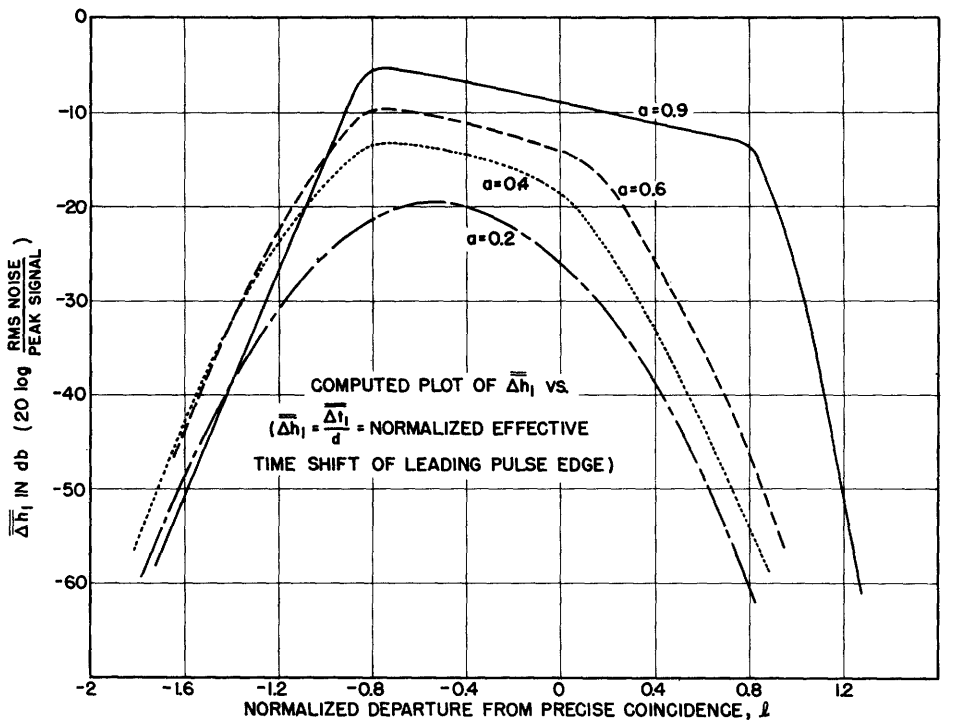

Fig.133 Computed two-path interference noise vs. pulse overlap for various values of a; ℓ = departure from precise overlap in μsec if pulse duration d = 1 μsec; single-edge detection.

For interference ratios less than one-half, the increase in noise from this cause does not exceed 3 db, but for larger interference ratios the noise increases, especially for exact coincidence due to the missing-pulses effect. Unlike the demodulation circuit, the self-synchronization scheme has no protection (other than the narrow-band filter*)against missing pulses, which are most common for exact coincidence. Consequently, with exact coincidence, for interference ratios close to unity, the r-m-s noise is approximately equal to the peak signal. This represents an increase in the lowest noise-to-signal ratio by 10 decibels and makes the modulation unintelligible. As in two-path PDM interference, lowering the slicing level reduces the noise, but, unless the pulses are trapezoidally shaped (large bandwidth), excessive distortion may result.

In addition to the noise discussed above (produced only in the incoherent case) partial or total coincidence interference (two-path) produces distortion

* See Appendix V, Fig. 149.

which will now be briefly considered. With the slicing level at one-half, no distortion is produced for interference ratios less than one-half. However, for exact coincidence and interference ratios larger than one-half, there is some distortion which is not serious under most conditions. If one side of the double-coincidence detector (see Fig. 124) is made inoperative so that the position of only one edge is detected, then the distortion is of exactly the same type as the "precise-coincidence" distortion (mostly second harmonic) encountered in two-path PDM interference.(see Figs. 115 - 118). If both pulse edges are detected, then, if the detector is perfectly balanced, this distortion cancels out (since it is equal and opposite for the two edges), leaving only the relatively harmless "spectrum distortion" encountered in two-path PDM interferecne (partial coincidence, see Fig. 114). This can be shown by simply adding the signals corresponding to the leading and trailing edges, respectively. Since the actual detector is never perfectly balanced, the output generally has a small remnant of second-harmonic distortion. This may be large enough to measure with sinusoidal modulation (at "cancellation" frequencies: 900 cps, 2700 cps, etc.), but it is hardly noticeable with speech or music, provided that the detector is well adjusted.

The distortion discussed in the preceding paragraph is encountered in the incoherent case, where it may be largely overshadowed by noise, and also in the coherent case for most values of the r-f phase difference, ϕ. The possibility of various values of ϕ makes the coherent case somewhat more complex than the incoherent case, in which all values of ϕ occur in rapid succession. Readjustment of the slicing level is necessary for optimum reception if ϕ changes from near 0° to near 180°, as is to be expected since the size of the resultant pulse depends drastically on whether the two overlapping pulses add in phase or out of phase. Distortion is small for all values of ϕ except those within approximately 30° of 180°. For these values, a complex type of distortion (harmonics and combination tones) results from the fact that at "cancellation" frequencies the overlapping pulses shift in opposite directions and the exact-coincidence condition is passed twice during each modulation cycle. Consequently the resultant falls below the slicing level momentarily during each audio cycle. All distortion (like the noise discussed above) disappears approximately 1 μsec (one pulse duration) off exact coincidence.

5.43 Two-Path Interference in Flip-Flop-Detection PPM System

The most important conclusions of this section may be stated as follows: The effects of interference are generally negligible in the presence of full modulation for interference ratios smaller than one-half; for larger interference ratios, on the other hand, acceptable reception is not always possible.

As in the detection system discussed in the previous section, time-shift noise occurs in the incoherent case if the two pulse trains overlap each other. The only important differences are that overlap between modulated pulses can be only a transitory condition (since the modulation time shift is larger than the pulse duration), and that detection normally occurs through the timing of only one edge of each pulse. In addition, the synchronizing pulses are capable of introducing noise if they are overlapped by interference. Maximum noise occurs in the absence of modulation with partial overlap such that the peaks of the interfering pulses coincide with the leading edges of the desired pulses (if the leading edges are used to trigger the flip-flop). Equal amounts of noise are then contributed by the channel pulses and the synchronizing pulses. Experimental plots of the noise as a function of interference ratio are shown in Fig. 134 for exact coincidence, and for partial overlap giving maximum noise. The maximum r-m-s noise is nearly 40 db below maximum peak signal; the maximum signal is that which corresponds to the largest possible time shift in a single-channel system -- that is, slightly less than half the repetition period or approximately 20 μsec. This is roughly 30 db higher than the maximum time shift usable in the coincidence system. Knowing the noise relative to the 20-μsec deviation, one can readily compute the signal-to-noise ratio for smaller peak time shifts by subtracting the appropriate number of decibels. In order to compare these results with the computed plots of Fig. 133, approximately 30 db must be added, since the noise in the computed plots is referred to a peak-to-peak time shift of one pulse duration (1 μsec). If this is done, it is found that in most cases the experimental signal-to-noise ratios are approximately 4 db lower than the computed values. This agrees with the observation of Section 5.42 to the effect that noise measured for BW = 1 Mc and $\underline{a}$ = 0.2, 0.4 was several decibels higher than computed values, while measurements for BW = 2 Mc agreed more closely.

It should be mentioned that any audible noise in the absence of modulation or in the presence of a small amount of modulation is not perfectly random, particularly if there is overlap between the synchronizing pulses of both

signals. Since the synchronizing pulses are perfectly periodic and not subject to appreciable jitter in a well-designed system, there is a considerable degree of coherence, and the noise is of the "frying-egg" type. If the two pulse trains are so phased that the synchronizing pulses of one overlap the modulated pulses of the other, and vice versa, a small amount of modulation (e.g., $\frac{1}{2}$ μsec peak-to-peak time shift) causes the noise to become perfectly random. There is, of course, no noise of any kind in the coherent case of two-path interference.

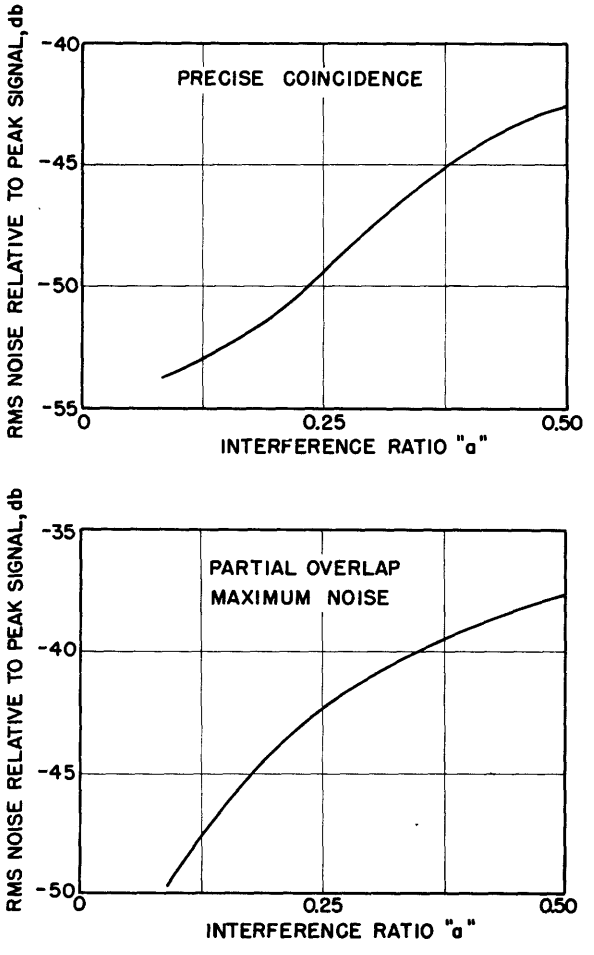

Fig.134 Two-path interference noise versus interference ratio for exact coincidence and partial overlap; flip-flop detection.

For interference ratios close to one-half, a small amount of distortion is detectable for very low-level modulation (time shift smaller than pulse duration) may be noted under partial-overlap conditions. This distortion is negligible at normal modulation levels.

No disturbance of any type results for interference ratios smaller than

one-half, if there is no overlap. If there is no overlap in the absence of modulation but the overlap condition is frequently passed during modulation, no disturbance generally results in the case of speech or music. The reason for this is the fact that the amplitude distribution of speech or music favors no values other than zero, so that overlap occurs only during a small fraction of the total time. In the case of sinusoidal modulation this is not true (the distribution favors the peaks), and it is consequently possible to observe noise which, for a given phasing of the two pulse trains, is audible only at a certain modulation level. This is the level for which the modulation time shifts are such that, at one of the two modulation peaks, the overlap condition is just reached. It is of interest to note the behavior of the system under this condition for sinusoidal modulation as compared to its behavior for speech or music modulation.

Interference ratios larger than one-half will be discussed only briefly, since the flip-flop system or any triggered demodulation system does not perform adequately in the presence of large interference. Acceptable performance is possible only if the two pulse trains never overlap, even in the presence of modulation. The exact results depend, of course, on the setting of the slicing level. If this is set above the interference level ($s = a+$), even a very small percentage of missing pulses is sufficient to produce intolerable noise. In a triggered system, even a single missing pulse causes a loud click. If no overlap occurs — a situation which is likely to occur only if full modulation is not used — then the interference has no effect, and reception is perfectly normal.

The possibility of missing pulses may be avoided by lowering the slicing level sufficiently ($s < 1-a$). However, since both desired and interfering pulses then pierce the slicing level, there are four pulses instead of two per sampling period. If any two pulses are very close to coincidence during part of the modulation cycle, intolerable noise again results since the flip-flop is uncertain whether the two pulses should be resolved into separate triggers or whether they should act as a single trigger. This condition need exist for only a small part of the time to make the noise intolerable. Two noteworthy situations may arise if the two pulse trains are so phased and modulation sufficiently low that near-coincidence does not occur with sufficient frequency to be of consequence.

First, it is possible that the two pulse trains overlap sufficiently

closely to be treated as a normal pulse train by the flip-flop. However, the modulated pulses will "stay together" only if the delay difference is small compared to the highest important modulating frequencies -- that is, no larger than one or two pulse-repetition periods. If this condition is fulfilled, reception is perfectly normal, as verified experimentally by modulating at frequencies for which the pulses "stay together" (reinforcement frequencies).

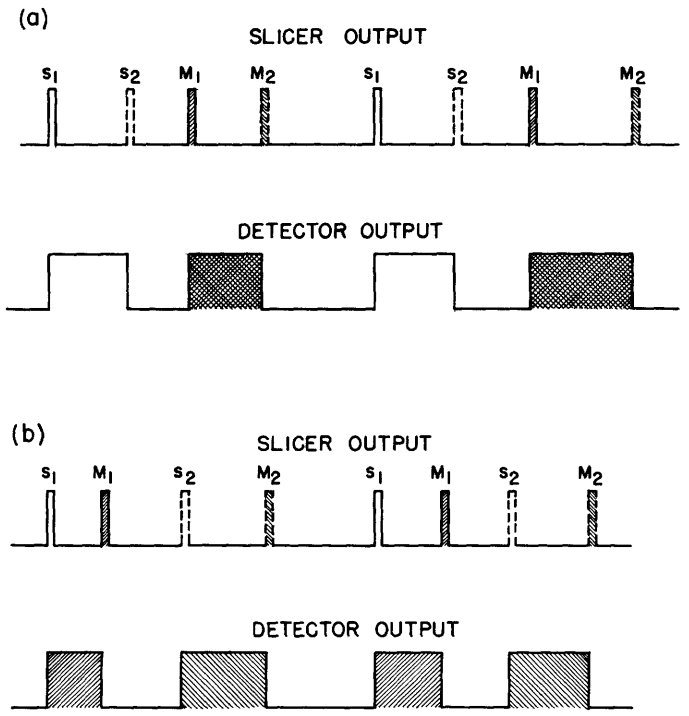

Fig.135 Two-path interference in PPM flip-flop system (a>s): two ways in which the desired and interfering pulse trains may become interleaved.

The second possibility is that the two pulse trains become interleaved in the manner shown in Fig. 135 (a) and the third possibility is that they are interleaved in the manner shown in Fig. 135 (b). In (a) two synchronizing pulses are followed by two modulated pulses which are, in turn, followed by two synchronizing pulses, and so on. Two pulses per sampling period are formed by the flip-flop, one of constant duration and the other of duration proportional to the difference of the modulation of the two pulses. The output is therefore the difference between the delayed* and undelayed* modulation

* The words "delayed" and "undelayed" are used for simplicity to identify the signals arriving by the longer and shorter routes, respectively.

signals. In (b), which is possible only if the synchronizing and modulated pulses are not spaced evenly, synchronizing and modulated pulses alternate. The flip-flop forms two duration-modulated pulses per sampling period, one carrying the delayed signal and the other carrying the undelayed signal. The result is the same as in two-path PDM interference: the output consists of the sum of the two signals.

The effect of obtaining the sum of the delayed and undelayed signals has been discussed in some detail in Section 5.32. The second effect, yielding the difference between the two signals, is more serious, since the difference approaches zero if the delay difference is sufficiently small. Considering the phenomenon in terms of "frequency-spectrum distortion" one finds that this distortion is complementary to that plotted in Fig. 114. The positions of the maxima and zeros are interchanged, the most important interchange being the replacement of the maximum at zero frequency by a zero. With the delay of approximately one-half millisecond used in the tests, the only noticeable effect with speech or music is a considerable reduction in bass response. Figure 136 shows the overall-system frequency characteristic (obtained both experimentally and by computation) together with the "sum" frequency characteristic and the normal characteristic. If plotted with linear scales, the "difference curve" is a full-wave rectified sine wave, while the "sum curve" is a full-wave rectified cosine wave.

It is clear that the conclusions which can be drawn for two-path interference in single-channel PPM systems cannot be so definite as in the case of PDM systems. This is a result of the greater complexity and variety of PPM systems. The smaller duty factor used in PPM makes overlap between the two pulse trains less probable, but this is the only factor tending to make the performance of PPM systems superior to that of PDM systems; however, it is more than offset by the poorer PPM performance when overlap does occur. On the whole, therefore, PPM performance is poorer than PDM performance for both of the systems tested. It is possible to devise more complicated PPM systems without the principal disadvantages of each of the two PPM systems tested -- that is, the limited modulation swing in the double-coincidence system and the trigger action in the flip-flop system. Such systems do not serve well for the determination of basic interference characteristics which tend to be obscured by the nonideal performance of the numerous circuit components. Moreover, they involve all the features required for time-division multiplex

systems and should be used only in such systems. The performance of multi-channel PPM systems is not inferior to that of multi-channel PDM systems (with regard to two-path interference); on the contrary, PPM performance is expected to be better than PDM performance, if the number of channels is ten or more. Both systems have the same synchronization problem, and modulation time shifts are limited equally. Neither system will give acceptable performance for interference ratios larger than one-half, and both will generally perform adequately for interference ratios less than one-half; the PPM system is, on the average, less affected by the interference because of the smaller duty factor.

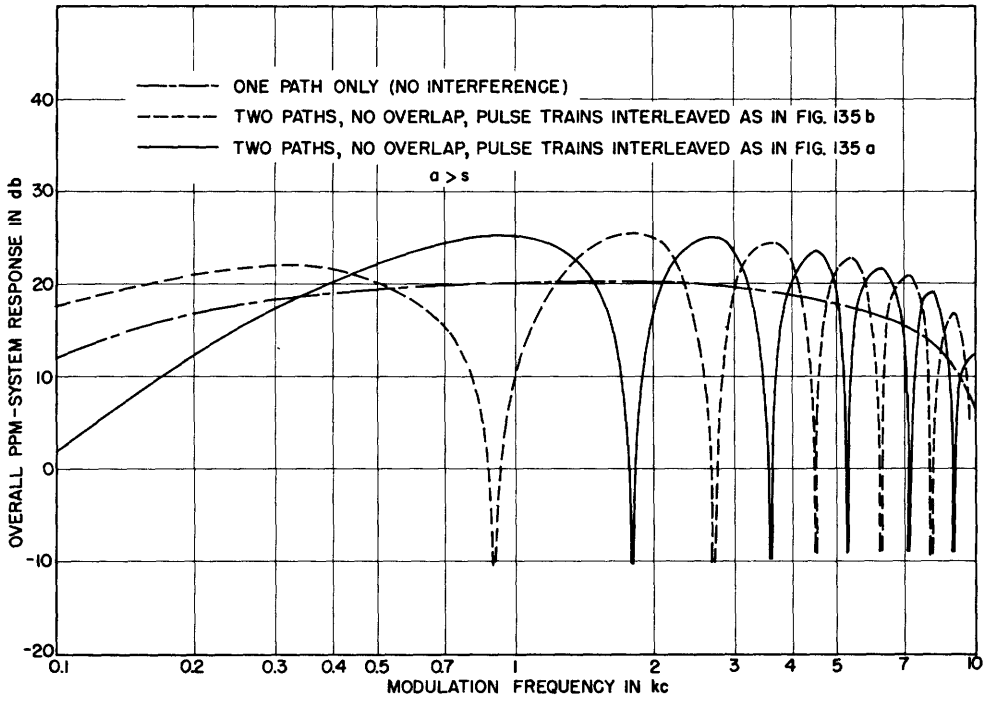

Fig.136 PPM system (flip-flop detection) overall frequency characteristics, one-path and two-path (measured and computed).

The main conclusion is that the multi-path-interference characteristics of PPM as a single-channel system are inferior to those of PDM as a single-channel system. This is in agreement with the general belief that there is generally no advantage in using PPM in other than time-division multiplex applications.

5.5 Two-Station Interference in PPM Systems

The final part of this chapter comprises a summary of the characteristics of the two previously discussed PPM systems with regard to interference from other similar services -- PPM, PDM, and CW. As in the preceding section, the results for the two PPM systems are sufficiently different from each other to justify separate discussions for each.

5.51 Two-Station Interference in Coincidence-Detection PPM System

Interference caused by a second PPM system will be considered first. The essential difference between this case and two-path interference is the fact that the repetition rates of the two pulse trains are not generally identical. The special case in which they are identical need not be considered here, since the results are the same as for two-path interference; there is, of course, the additional variable Δr-f, but this has little effect so long as the interfering pulses are not of longer duration than the desired pulses.

In the general case (Δprf $\neq$ 0), interference reaches the output only during a small fraction of the total time; one may picture the interfering pulse train "sliding" through the desired pulse train and causing a burst of noise at the output each time the two sets of pulses overlap. The fraction of the total time during which this occurs is slightly larger than the sum of the duty factors of the two pulse trains. In the present case (pulse-repetition frequencies approximately 20 kc and pulse durations 1 μsec), it is roughly five-hundredths. The repetition rate of the noise bursts is Δprf, the difference between the two pulse-repetition frequencies.

If at least one of the r-f pulse trains is incoherent from pulse to pulse (as is generally the case), the noise caused by the presence of the interfering pulse train has a random character, though not to the extent of resembling fluctuation noise. Because of the very short duration (relative to the repetition period) of the noise bursts, the ear perceives them as a buzzing sound unless their repetition frequency is below the audio range (in which case a succession of smooth "swishes" can be distinguished). The buzzing sound contains a small Δprf component which is hardly audible if the slicing level and other variables in the detector are correctly adjusted: (a small misadjustment or misdesign, such as insufficient video bandwidth at the slicer input, may increase the loudness of this beat note to such an extent that reception is impossible.) With external synchronization, for interference ratios not

exceeding 0.8, the noise is not sufficiently strong to affect seriously the entertainment value of music or to lower the intelligibility of speech; good reception is generally possible up to a = 0.9. Results obtained with "self-synchronization" are poorer; good reception is possible only for a < 0.5 and tolerable reception for a < 0.6. However, there is theoretical and experimental evidence that the performance of the self-synchronization system can be improved considerably.

The audio-noise power produced by the interference has been measured for various values of Δr-f, Δprf, d_2 and $\underline{a}$. The effect of Δr-f is negligible. The value of Δprf affects only the quality but not the power of the noise. The duration of the interfering pulses affects the noise power to a relatively small extent: changing it from 1 μsec (the duration of the desired pulses) to 2 μsec increases the noise 1 to 2 db. The only important remaining variables are the system bandwidth and the interference ratio. Experimental plots of the ratio of r-m-s noise to peak signal expressed in db are shown in Fig. 137. The peak signal to which the noise values are referred corresponds to maximum pulse time shift permitted by the coincidence detector, that is, a peak-to-peak time shift equal to d_1 -- 1 μsec. However, for interference ratios larger than one-half, the effective pulse duration (at the slicer output) is smaller, since the condition s = a+ must be maintained. The higher the interference ratio and hence the slicing level, the greater the reduction in pulse duration; also, the wider the bandwidth and hence the "squarer" the pulse shape, the smaller the reduction in effective duration. This reduction necessitates a proportionate decrease in peak modulation. For a = 0.9 and BW = 3 Mc this decrease is less than 1 db, but for a = 0.9 and BW = 1 Mc it is slightly more than 3 db. This is a correction to be subtracted from the signal-to-noise ratio obtained from Fig. 137.

The theoretical ratio of r-m-s noise voltage to peak signal voltage is equal to the effective value of the normalized time shift Δh_{12}; Δh_{12} is the average of the shifts of the two edges of a pulse (hence the shift of the pulse center), equal to $\frac{1}{2}(\Delta h_1 + \Delta h_2)$, and Δh_1 and Δh_2 are found from (29) (page 33). As mentioned in Section 5.42, trial and error solutions of this equation have been obtained for numerous values of ϕ, ℓ, and a. Carrying out the appropriate averaging process over the r-f phase difference ϕ yields the effective normalized time shift $\overline{\overline{\Delta h}}$ for any combination of values of ℓ and a (see Fig. 132). In the present case of interference, ℓ changes from pulse to pulse (Δprf $\neq$ 0),

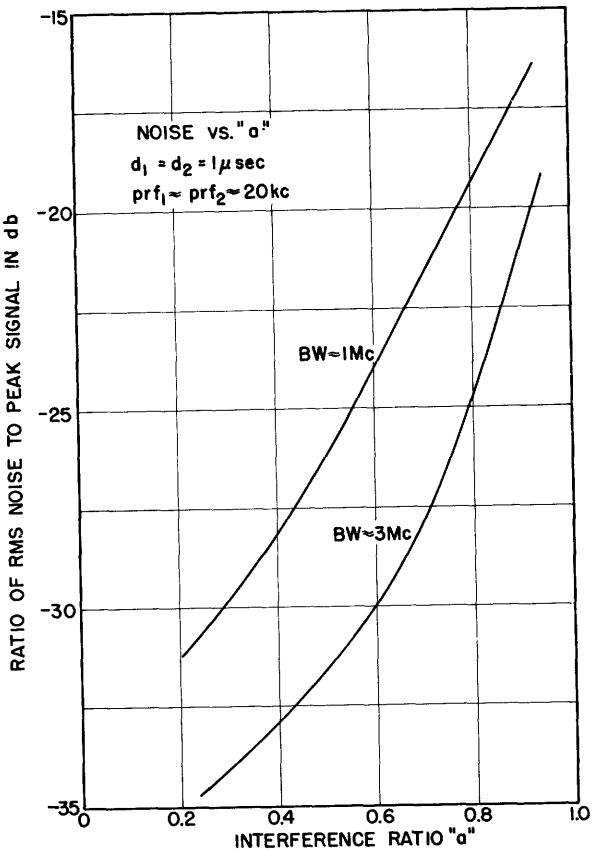

Fig.137 Experimental plot of ratio of noise to signal versus interference ratio for two different system bandwidths. Noise caused by two-station PPM interference (double-coincidence detection).

and another averaging process, this time over ℓ, is therefore required to find the normalized effective time shift $\overline{\overline{\Delta t}}^*$. The results of these lengthy computations are plotted in Fig. 138* together with corresponding experimental results obtained for a system bandwidth of 3 Mc. The results for this bandwidth check very closely with the computed results, particularly in view of the complex nature of the noise and the numerous operations involved in its computation. However, the computed results should actually check experimental results for a considerably smaller bandwidth; the shape of the 3-Mc pulses is more nearly "square" than the gaussian pulses on which the computations are based. The measured noise, in other words, tends to be larger than the computed noise. In addition to the plot of the effective value of Δh_{12} (applicable to double-edge detection), Fig. 138 contains a plot of Δh_1 (one-edge detection) and corresponding experimental results. It is of interest to note that for

* The evaluation of a single point may involve several hundred operations. Values were computed for a = 0.1, 0.2, 0.4, 0.6, and 0.9.

interference ratios up to approximately 0.6 (a < 0.6), the noise is about 4 db lower for double-edge detection. This figure, of course, will vary with the relative durations of the desired and interfering pulses; it tends to be larger if the interfering pulses have longer durations (for $\Delta r\text{-}f = 0$) and smaller for shorter durations, the theoretical lower limit being 3 db.

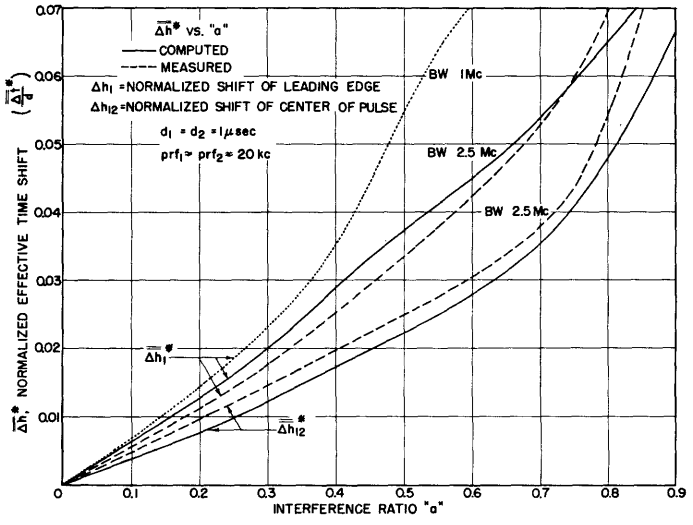

Fig.138 Two-station PPM interference; computed and measured values of normalized effective noise time shift versus interference ratio; one-edge detection: Δh_1, two-edge detection: Δh_{12}.

Interference by CW transmissions or pulse transmissions (e.g., PDM) having larger duty factors than PPM systems causes considerably more severe noise. As the theory predicts, the noise power increases approximately in direct proportion to the interference duty factor. Consequently, CW interference may make intelligibility poor for interference ratios as low as 0.3 and yield a signal-to-noise ratio less than unity for a = 0.9. The radio-frequency difference, $\Delta r\text{-}f$, which was found to have no appreciable effect for short interfering pulses is an important variable in the present case. Variation of $\Delta r\text{-}f$ reveals a succession of minima and maxima in the noise power; there are, in fact, two independent cyclic variations, one with its maxima spaced at 20-kc intervals (corresponding to the pulse-repetition frequency) and the other with its maxima spaced at 1-Mc intervals (corresponding to the reciprocal of the pulse duration). The 20-kc variation has a maximum at $\Delta r\text{-}f = 0$, while the 1-Mc variation has a minimum there; the former is a result of cancellation or reinforcement of the time shifts of successive pulses, and the latter results from cancellation and reinforcement of the time shifts of the two edges of each pulse. Plots of noise-to-maximum-signal ratios are

given in Fig. 139 for two values of Δr-f.

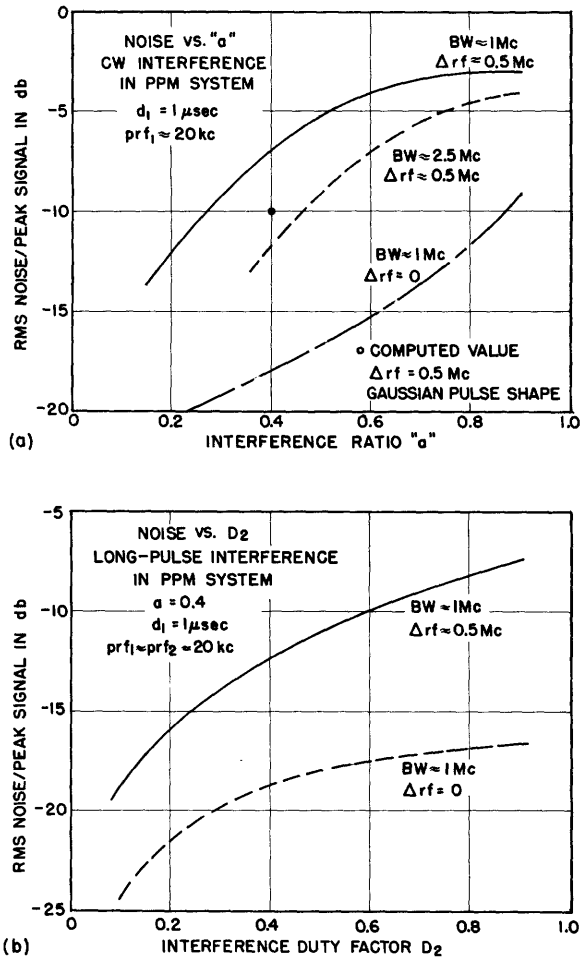

Fig. 139 CW and long-pulse interference in double-coincidence PPM system: ratio of rms noise to peak signal versus (a) interference ratio for CW interference (b) interference duty factor for long-pulse interference.

The nature of the interference noise is by no means random for CW interference (which is always coherent). If the PPM transmitter is a pulsed amplifier, the noise consists principally of one clean beat note which varies in pitch with Δr-f (passing through zero beat at 20-kc intervals). Even if the PPM transmitter is a pulsed oscillator, there is a sufficient degree of coherence to make the noise appear as beats, though not so clean, in the complete absence of position modulation. Continuous modulation, such as music, causes the beats to change to random noise; speech modulation with its frequent gaps results in repeated changes from random noise to beat noise which is very distracting. With pulsed-amplifier operation, of course, coherence is maintained regardless of modulation, and the noise never becomes random. If the interference consists of pulses, coherence is much less likely, since both

the interfering and desired pulse trains must originate from pulsed amplifiers in order that coherence be maintained in the presence of modulation of either or both of the pulse trains. Nevertheless, some degree of coherence is observable even if both pulse trains originate from pulsed oscillators, provided that neither pulse train has time modulation (including "jitter") appreciably larger than the reciprocal of the radio frequency. An audible beat note (Δprf) is generally present, particularly for large values of the interference duty factor and the interference ratio. Time modulation of the interfering pulses does not reach the output under any condition; amplitude modulation of CW interference, on the other hand, does appear at the output with more or less distortion. The extent to which it comes through depends on the interference ratio and the PPM system bandwidth. For example, for a = 0.9 and BW = 3 Mc (100 per cent modulation), cross talk is 10 to 12 db below the desired signal modulation and decreases rapidly with decreasing values of a. For BW = 1 Mc, the level difference is only 6 to 8 db, other conditions being the same.

Figure 139 shows the quantitative results in the form of noise-to-signal ratio plotted against interference ratio, for CW interference, and against interference duty factor for the case of pulsed interference. (The variation of noise *vs.* interference ratio is the same for pulsed interference as for continuous interference, so that the two plots of Fig. 139 give all the information required.) It is clear that CW interference or large-duty-factor pulsed interference is apt to make reception unacceptable even for interference ratios as low as 0.3. The most severe noise results for $\Delta r\text{-}f = 0.5$, since both edges of each pulse are shifted in the same sense. For $\Delta r\text{-}f = 0, 1, \ldots\ldots$Mc, the two edges are shifted in opposite senses and their noise contributions theoretically cancel. In practice, virtually complete cancellation was found possible with careful detector-balancing adjustment, but only for BW > 2 Mc which makes it possible to keep the pulse shape sufficiently symmetrical. For BW = 1 Mc, the noise is never appreciably more than 10 db below the maximum figure obtained at $\Delta r\text{-}f = 0.5$ Mc. Nevertheless, this gain (which is solely a result of the two-edge detection feature) is very helpful, since it may make common-channel interference tolerable in many cases where one-edge detection would yield unacceptable signal-to-noise ratios. It should be pointed out that all the plots in Fig. 139 represent the maximum possible noise with reference to the 20-kc variations; all measurements are made on "20-kc maxima". The minima are much sharper than the maxima and are substantially "washed out"

by normal modulation (PPM) which lowers the noise by approximately 3 db from the plotted values. The effect of system bandwidth, while large for $\Delta r\text{-}f = 0$, is seen to be quite small for $a > 0.5$ but approaches its theoretical proportions for smaller interference ratios (6 db per factor of two in bandwidth). As in previous comparisons between computed and measured signal-to-noise ratios in PPM systems, the computed value based on a gaussian pulse of 1-μsec duration at the half-amplitude level checks the value measured for BW = 2 Mc instead of that measured for BW = 1 Mc.

On the whole, in spite of the advantageous cancellation feature of the detector, the PPM system under discussion does not suppress CW or high-duty-factor interference with much effectiveness. This is a result, primarily, of the limited position-modulation time shift permissible in this system.

Although discussion of equipment performance is being avoided as far as possible, the following observations are of interest here because of their direct bearing on the way in which long-pulse interference affects the double-coincidence PPM system. As previously mentioned, the detector has, in addition to the two-edge feature, a device which is intended to reduce the possible severe effects of "missing pulses". When an occasional pulse fails to reach the detector and can therefore not convey its sample value, the sample of the previous pulse is "held" until a pulse does reach the detector. This feature can readily be removed; a missing pulse then means zero signal (equivalent to a sample of value zero) regardless of the value of the preceding sample. In the absence of modulation, the values of the samples are always zero if the detector is properly balanced, since exactly one-half of each incoming pulse overlaps a pulse of the first reference pulse train and the other half a pulse of the second reference pulse train (see Fig. 124). Therefore, if there is no modulation and the detector is balanced, missing pulses should not produce any disturbance even without the above-mentioned device. In practice this, is borne out to the same extent as the cancellation of the time shifts of the two pulse edges for $\Delta r\text{-}f = 0$; with a wide system bandwidth (BW = 3 Mc, $a = 0.8$, $\Delta r\text{-}f=0$), the r-m-s noise can be kept 16 db below the peak signal without the use of the special device, 18 db if it is used. This two-decibel improvement is unimportant, but if the detector is accidentally unbalanced or only one half (single-edge coincidence) is used, then there is an improvement of approximately 10 db: the signal-to-noise ratio may be as low as 4 db without use of the special device, while it is 15 db with its use. Furthermore, it must be

remembered that even the balanced double-coincidence detector is not balanced instantaneously (only on the average) in the presence of modulation. The following interesting observation bears out the usefulness of the "anti-missing-pulses device": so long as it is used (for the above values of BW, a, and Δr-f), the noise obtained with careful detector balancing in the absence of modulation does not increase noticeably when normal modulation (speech, music, or sinusoidal) is applied, and reception is acceptable. Without the device, the noise increases when modulation is applied; this is particularly noticeable if the modulation is speech, which causes the noise to be modulated at a syllabic rate.

5.52 Two-Station Interference in Flip-Flop-Detection PPM Systems

Consider first interference which is caused by a second PPM system using pulses similar to those of the desired signal. For interference ratios up to one-half, such interference gives rise to the same type of buzzing random noise obtained with the other PPM system. However, for the same bandwidth and interference ratio, the noise is approximately 8 db higher. Of this difference, 6 db is accounted for by the synchronizing pulses -- 3 db as a result of the additional noise picked up by the synchronizing pulses of the desired signal, and 3 db as a result of the fact that the presence of synchronizing pulses in the interfering signal doubles the interference duty factor.* The remaining 2 db (4 db theoretically, see Fig. 138) is attributable to the difference between one-edge and two-edge detection. This 8 db increase is much more than offset by the larger peak signal possible as a result of the larger pulse time shift, which may now be at least 20 μsec instead of $\frac{1}{2}$ μsec; the signal is increased by more than 30 db. (The theoretical maximum modulation swing for prf = 20 kc is approximately 24 μsec or 33.5 db higher than the maximum swing in the other system.) Consequently, the signal-to-noise ratio in the flip-flop system is somewhat more than 20 db higher than in the coincidence system for the same bandwidth and interference ratio. The theoretical and experimental plots of the effective value of Δh_1 (Fig. 138) represent the r-m-s-noise-to-peak-signal ratio, based on a peak signal corresponding to a peak-to-peak time shift of 1 μsec (one pulse duration) and ignoring the presence

* It is assumed that the interfering signal has the same structure as the desired signal. If the interfering signal is of the same type used in the coincidence system (no synchronizing pulses), the second 3-db boost is nonexistent.

of synchronizing pulses. In order to determine the actual signal-to-noise ratios, $1/\overline{\Delta h}_1$ must be increased by a factor of at least 40 (32 db) to account for the larger modulation time shift and decreased by a factor of 2 (6 db) to account for synchronizing pulses in both the desired and interfering pulse trains; this amounts to multiplication by a factor of at least 20 (26 db). A plot of measured and computed noise-to-signal values expressed in db are shown in Fig. 140; the usual tendency of computed results to check with the experimental results measured for bandwidths larger than 1 Mc is again seen to be present, but to a smaller degree, inasmuch as the computed curve averages midway between the curves for BW = 2.3 Mc and 0.9 Mc. It is evident that the effect of the interference is negligible for ordinary communication purposes; it is of the same proportions as light phonograph-needle scratch and is therefore not annoying even with music, except during low passages.

For interference ratios greater than one-half, good reception is possible only if the radio-frequency difference, Δr-f, is 1 Mc or larger. Increasing the interference ratio then simply results in increasing noise as shown in Fig. 140. Interference ratios close to a = 0.9 can be approached with Δr-f > 1 Mc. For larger interference ratios, the trigger action becomes erratic as a result of missing pulses, and reception becomes unacceptable. For smaller values of Δr-f, the transition from good reception to unacceptable reception occurs at interference-ratio values less than 0.9; the borderline value rapidly approaches a = 0.5 as Δr-f decreases below 1 Mc and approaches zero. Common-channel interference with interference ratio larger than one-half is therefore detrimental in the present case, while adjacent-channel interference is relatively inconsequential. There is little doubt that replacement of the active flip-flop (trigger circuit) by a passive circuit (involving diodes and storage capacitors) would improve the performance for large interference ratios. Unlike a flip-flop, such a circuit would not be limited to two choices, that is, to be triggered or not to be triggered by a defective pulse.

Interference from continuous transmissions or pulse transmissions using longer pulses is, of course, more disturbing than the interference from the short position-modulated pulses. It manifests itself in the same way as in the coincidence PPM system, except that the noise averages 3 db higher because of the additional noise introduced by the synchronizing pulses of the desired signal; since the peak signal is approximately 30 db higher than in the

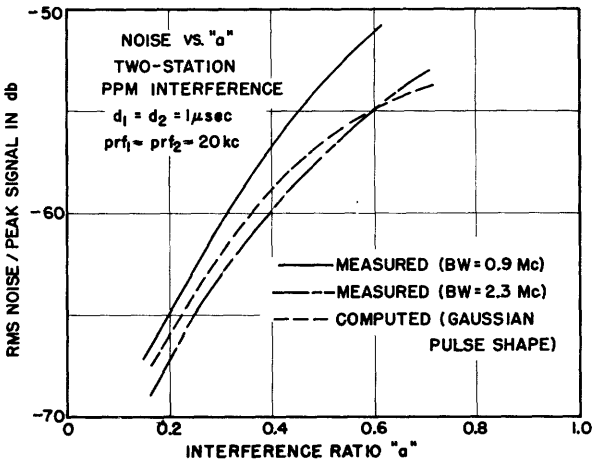

Fig.140 Two-station PPM interference (flip-flop system of detection): ratio of rms noise to peak signal versus interference ratio.

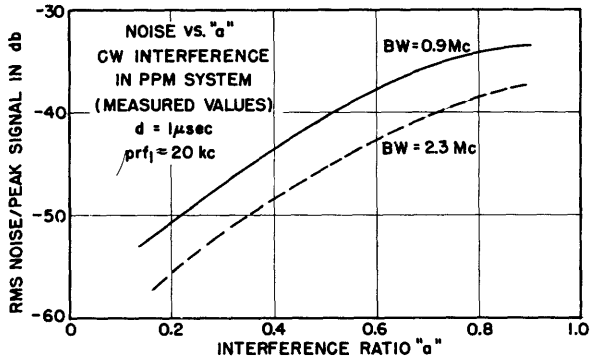

Fig.141 Continuous-wave interference in PPM system using flip-flop detection: ratio of rms noise to peak signal versus interference ratio.

coincidence system, the signal-to-noise ratio is always good so long as the flip-flop does not fail (due to missing pulses). Noise-to-signal ratios measured for CW interference are plotted against a in Fig. 141. They are comparable with those obtained from moderate phonograph-needle scratch. One important respect in which the noise differs from that obtained in the other system is its dependence on $\Delta r\text{-}f$. Since only one pulse edge of each pulse is involved in the detection process, the cyclic 1-Mc variation is completely absent, and the benefit of cancellation obtained for $\Delta r\text{-}f = 0$ with the other system is not obtained here. (The 20-kc variation is obscured by the synchronizing pulses and becomes a 40-kc variation under certain conditions; but these variations with $\Delta r\text{-}f$ disappear completely when modulation is applied and are therefore ignored.) Consequently, there is little variation in noise when $\Delta r\text{-}f$ is changed (a being kept constant), except for the usual gradual decrease in the noise for large values of $\Delta r\text{-}f$; this is a function of the video response of the receiver and amounts to no more than 3 db for $\Delta r\text{-}f$ = 1.5 Mc in the equipment used in this study. The value of $\Delta r\text{-}f$ does have an

important effect in that it determines the largest interference ratio which permits reception without failure (due to missing pulses) of the flip-flop. Unlike pulsed interference, CW interference permits satisfactory operation for interference ratios considerably larger than 0.5, even for $\Delta r\text{-}f = 0$. This must be attributed to the fact that the CW signal has no discontinuities so that differentiating circuits can readily discriminate against it, as borne out by the observation that the degree of differentiation (following the slicer and preceding the flip-flop) has a considerable part in determining the highest permissible interference ratio for $\Delta r\text{-}f = 0$. Typical values of this highest interference ratio permitting satisfactory reception (signal-to-noise ratio as plotted in Fig. 141) are $a = 0.75$ for $\Delta r\text{-}f \approx 0$, $a = 1$ for $\Delta r\text{-}f = 0.5$ Mc, and $a = 1.2$ for $\Delta r\text{-}f = 0.7$ Mc. If the interference is fully amplitude-modulated (the interference ratio being taken as the voltage at the modulation peak relative to the pulse height), the highest permissible values of $\underline{a}$ tend to be slightly lower. So long as these interference-ratio values are not exceeded, the amplitude modulation does not affect the output in any way whatever. If they are exceeded, the resulting noise is too severe to permit acceptable reception.

The noise obtained as a result of interference from relatively long pulses (duty factor 0.1 or larger) differs from that obtained with the position-modulated pulses chiefly in that its power is larger in direct proportion to the duty factor. A distinct beat note (Δprf) is audible in addition to the random noise. The total noise power is slightly more than that which one obtains by multiplying the duty factor by the noise power produced by CW interference; the discrepancy is generally less than 2 db. As in the case of short-pulse interference, satisfactory reception is limited to interference ratios less than 0.5 for $\Delta r\text{-}f = 0$ and to larger values if $\Delta r\text{-}f$ is increased, e.g., 0.8 to 0.9 for $\Delta r\text{-}f = 1$ Mc.

The conclusions for two-station PPM interference are somewhat more definite than for two-path PPM interference; but they cannot be so definite as in the case of PDM systems because of their dependence on the choice of circuitry. Much better signal-to-noise ratios than in PDM were obtained, principally because of the smaller interference duty factor and wider system bandwidths used. The relatively good results obtained with the coincidence system, in spite of the limited modulation time shift, show that adaption of this method to larger time shifts would yield a system which is disturbed

very little by interference from short pulses originating from another similar system. For interference ratios less than 0.5, it is almost solely the small duty factor of the interfering pulse train (not the small duty factor of the desired pulses) which is responsible for the good signal-to-noise ratio. Another feature instrumental in improving the performance is the fact that, for $\Delta r\text{-}f = 0$ (common-channel interference), the time-shift contributions of the two edges of each pulse can be made to cancel, whereas they add in the case of PDM. (This applies only when the interfering pulses are long compared to the desired pulses.) It must be pointed out, however, that neither of the two systems tested incorporates all these possible advantages which can be realized only in a more complex system capable of high modulation and, at the same time, having the characteristics of the coincidence system.

The conclusion, for single-channel systems, may be summarized by stating that, while the two-station interference characteristics of PPM systems are fundamentally superior to those of PDM systems, it is much more difficult to realize this superiority under all conditions. The consequence is that inferior results are obtained under some conditions unless more nearly "ideal" detection systems are used.

More definite conclusions can be stated in the case of multi-channel (time-division multiplex) systems having a large number of channels. Since the modulation time shift in such systems is limited by the channel spacing, the coincidence system is very well suited for this application. For the parameters used in this study (prf = 20 kc, d = 1 μsec) ten channels could readily be incorporated in a system, and the characteristics of each would be completely identical to the single-channel system. If the interference originates from a similar system, its duty factor would be approximately 0.2. The resulting signal-to-noise ratio in any of the channels is tolerable for interference ratios as large as 0.8 for a system bandwidth of only 1 Mc (between 3-db points). A similar PDM system would give acceptable performance only for interference ratio below 0.5. Multi-channel PPM systems are therefore expected to be distinctly superior to multi-channel PDM systems so far as interference characteristics are concerned.

APPENDIX I

ALTERNATE METHODS OF DERIVING THE SELF- AND INTER-CORRELATION FUNCTIONS

The various methods of deriving the correlation functions differ only in the thinking processes used to set up the product of the two functions to be averaged over all time. In the case of the equivalent nonrandom-pulse method used in the text, the first and most difficult step in the procedure is carried out mechanically. This is not so in the case of the following analysis.

The auto-correlation for any value τ is proportional to the overlap between the pulse train and its replica shifted by an amount τ. Instead of considering all pulses and dividing by an infinite period, one may consider one pulse (with all its possible edge time shifts) and divide by one pulse-repetition period. The method can be demonstrated by deriving an expression for the curved portion at one side (right-hand side) of the self- or inter-correlation (for one-edge time shift).

Figure 142 shows a typical pulse, belonging to $f(t)$, which is to be multiplied by another pulse belonging to $f(t + \tau)$. The shaded portions represent the possible positions of the trailing edges. Each pulse has a duration $d_o + x$, where $-x_o < x < x_o$. The overlap between the two pulses is $d_o + x - \tau$, provided that x exceeds $\tau - d_o$; otherwise the overlap is zero.

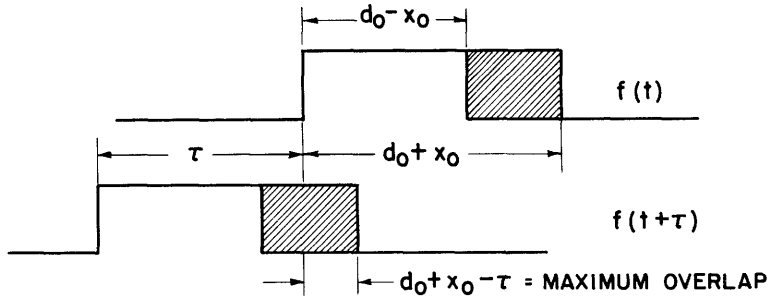

Fig.142 Evaluation of overlap between two typical pulses; the shaded areas represent the possible positions of the trailing edges.

Taking into account all possible values of x between $-x_o$ and x_o, one can define an average value of x as follows:

$$\bar{x} = \frac{\int_{\tau - d_o}^{x_o} xP(x)\,dx}{\int_{\tau - d_o}^{x_o} P(x)\,dx} \quad . \tag{120}$$

The average overlap (omitting all instances in which there is no overlap) is $d_o - \tau + x$; this must be multiplied by the probability of obtaining overlap in order to give the actual average overlap.

$$\text{Average Overlap} = [d_o - \tau + \bar{x}] \int_{\tau - d_o}^{x_o} P(x)\,dx \quad . \tag{121}$$

[$\bar{x}$ is given by (120).] To obtain the auto-correlation, the overlap must be multiplied by E^2/T.

In order to derive the expression for the curved portion at the center of the inter-correlation, one may follow the same procedure outlined above. Figure 142 is redrawn with the two shaded areas partially overlapping. Since the two movable edges overlap, the procedure is more complicated than above; the product must be split into several parts to include the contributions from various components of overlap between the functions to be multiplied. The following result is obtained:

$$\varphi(\tau)\Big|_{-2x_o < \tau + nT < 2x_o} = \frac{E^2}{T}\,(\text{Average Overlap})$$

$$= \frac{E}{T}\left\{ d_o + \int_{-x_o}^{x_o - \tau} P(x) \left[x \int_{x+\tau}^{x_o} P(u)\,du - \tau \int_{-x_o}^{x+\tau} P(u)\,du + \int_{x_o}^{x+\tau} uP(u)\,du \right] dx + \right.$$

$$\left. + \left[\int_{-x_o}^{x_o} xP(x)\,dx - \tau \right] \int_{x_o - \tau}^{x_o} P(x)\,dx \right\} . \tag{122}$$

It can be shown that this leads to the same expression for $\varphi_{\Delta}(\tau)$, (50), as the method used in the text (Section 3.2).

APPENDIX II

ASYMMETRICAL P(x) AND TWO-EDGE TIME-SHIFTS

The purpose of this appendix is to show briefly that the two-to-one relationship between the areas of the center lobe and each side lobe is maintained even if P(x) is asymmetrical. (See page 99).

Consider the "inter-correlation" and more particularly the three departures from triangular shape at the center and each side (see Fig. 31), which determine the center lobe and side lobes, respectively. In the simple case of the double-spike distribution, these lobes are triangular in shape. The center lobe is given by (65); each side lobe is identical except that its height and hence its area is half as great. Now consider the effect of unbalancing the double-spike distribution: instead of letting the probability represented by each spike be one-half, let the probability of $x = x_o$ be P and let that of $x = -x_o$ be 1 - P. The center lobe is still a symmetrical triangle given by (65); its area is directly proportional to the product P(1 - P) which has a maximum for $P = \frac{1}{2}$.

The right-hand side lobe, either for Case 2 or for Case 3, can be obtained from the graphical construction of Fig. 143(a). The right-hand sides of the inter-correlation as well as the self-correlation for Case 2 and Case 3 are indicated by b, c, and e, respectively, for $P = \frac{1}{2}$ (symmetrical distribution). The corresponding broken lines (prime letters) are for P = 1/4 (asymmetrical distribution). By computing the areas of the appropriate triangles, one can show that the side-lobe area (Case 2 or Case 3) equals $P(1 - P)4x_o^2$, which is exactly half the center-lobe area (determined from (65)).

In order to ascertain that the above conclusions are not restricted to the simple case of the double-spike distribution, computations have been carried out for the important case of the half-wave-rectified sinusoid. The self- and inter-correlation functions are plotted in Fig. 143(b). The side-lobe area ($0.595\ x_o^2$) is again found to be half the center-lobe area; it is also recognized as the mean-square value of the a-c component of a half-wave-rectified sinusoid (peak-to-peak amplitude = $2x_o$).

The expressions from which the curves in Fig. 143(b) were plotted are as follows:

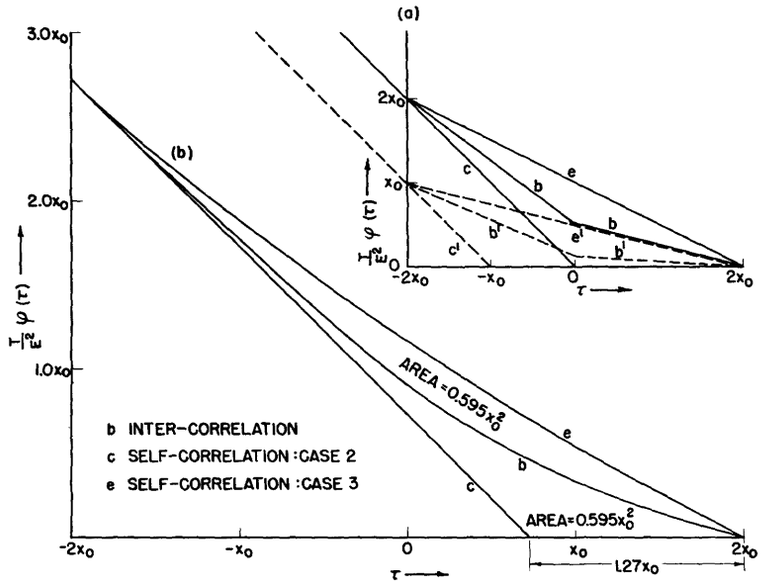

Fig.143 Right-hand extremities of self- and inter-correlations for two-edge time shifts with asymmetrical probability distributions; (a) double-spike distribution (b) distribution of half-wave rectified sinusoid.

e (self-correlation, Case 3)

$$\varphi(\tau) = \frac{1}{\pi}\int_{\tau}^{2x_o} \cos^{-1}\left(\frac{x - 2x_o}{4x_o}\right)dx \quad . \tag{123}$$

b (inter-correlation)

$$\varphi(\tau) = \frac{1}{\pi^2}\int_{\tau - x_o}^{x_o} \left[\cos^{-1}\frac{x - x_o}{2x_o}\right]\left[\cos^{-1}\frac{\tau - x - x_o}{2x_o}\right]dx \quad . \tag{124}$$

for $\tau \geqslant 0$

$$\varphi(\tau) = \frac{1}{\pi^2}\int_{-x_o}^{\tau + x_o} \left[\cos^{-1}\frac{x - x_o}{2x_o}\right]\left[\cos^{-1}\frac{\tau - x - x_o}{2x_o}\right]dx$$

$$+ \frac{2}{\pi}\int_{\tau + x_o}^{x_o} \left[\cos^{-1}\left(\frac{x - x_o}{2x_o}\right)\right]dx \quad . \tag{125}$$

for $\tau \leqslant 0$

$\underline{c}$ (self-correlation, Case 2)

Intersection with zero axis located at $2x_o - 4x_o(0.318)$, the average value of the half-wave-rectified sinusoid.

The actual side lobes for Cases 2 and 3 are obtained by taking the differences of the ordinates of curves c and b, and curves e and b, respectively. These have been plotted in Fig. 144.

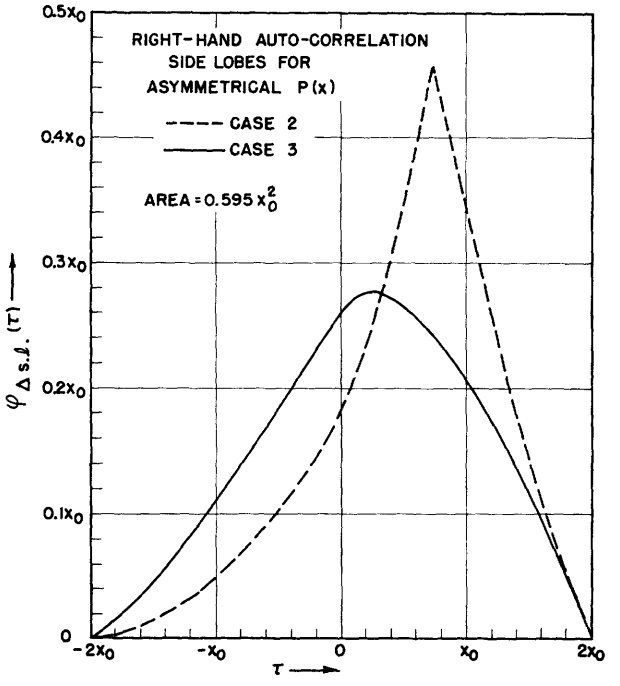

Fig.144 Right-hand auto-correlation side lobes for two-edge time shifts with probability distribution of half-wave-rectified sinusoid. Note: for Case 2 the ordinates are actually negative.

APPENDIX III

POWER SPECTRUM DERIVATIONS

The power spectrum, $\Phi_\Delta(\omega)$, is obtained by taking the Laplace transform of the auto-correlation, $\varphi_\Delta(\tau)$. For the sake of simplicity, the function to be transformed is denoted by $f(t)$, which is the same as $\varphi_\Delta(\tau)$ except for the multiplying constants. (See Table 1, page 63.) The Laplace transform of $f(t)$ is denoted by $g(s)$. The Fourier transform is given by $\frac{1}{2\pi}g(j\omega)$.

A. Triangular Pulse

The pulse can be split into three linear functions (see Fig. 145(a)) and the law of real translation can be applied, as follows:

$$\mathcal{L}(-2t) = -\frac{2}{s^2}$$

$$\mathcal{L}(t + 2x_o) = +\frac{1}{s^2}\, e^{+2x_o s}$$

$$\mathcal{L}(t - 2x_o) = +\frac{1}{s^2}\, e^{-2x_o s}$$

$$g(s) = \frac{1}{s^2}\left[e^{+2x_o s} - 2 + e^{-2x_o s}\right] ;$$

substitute $s = j\omega$ and divide by 2π:

$$\frac{1}{2\pi}\, g(\omega) = -\frac{1}{2\pi\omega^2}\left[e^{j2x_o\omega} - 2 + e^{-j2x_o\omega}\right] = \frac{2x_o^2}{\pi}\left(\frac{\sin x_o\omega}{x_o\omega}\right)^2 . \qquad (126)$$

B. Quadratic Pulse

$$f_1(t) = (t + 2x_o)^2$$

$$f_2(t) = (2x_o - t)^2 - (2x_o + t)^2 = - 8x_o t$$

$$f_3(t) = - (t - 2x_o)^2 \qquad \text{(see Fig. 145(b))}$$

$$\mathcal{L}\ [f_1(t)] = \frac{2}{s^3} e^{2x_o s}\ ,\ \mathcal{L}\ [f_2(t)] = - \frac{8x_o}{s^2}\ ,\ \mathcal{L}[f_3(t)] = - \frac{2}{s^3} e^{-2x_o s}$$

$$g(s) = \frac{2}{s^3} [e^{2x_o s} - e^{-2x_o s}] - \frac{8x_o}{s^2}\ .$$

Substitute $s = j\omega$ and divide by 2π:

$$\frac{1}{2\pi} g(\omega) = - \frac{4x_o}{\pi\omega^2} \left[\frac{e^{2jx_o\omega} - e^{-2jx_o\omega}}{2j\ 2x_o\omega}\right] + \frac{4x_o}{\pi\omega^2} = \frac{4}{\pi} \frac{x_o}{\omega^2} \left[1 - \frac{\sin 2x_o\omega}{2x_o\omega}\right] \qquad (127)$$

C. Cubic Pulse

$$f_1(t) = (t + 2x_o)^3$$

$$f_2(t) = - (24\ x_o^2 t + 2t^3)$$

$$f_3(t) = (t - 2x_o)^3 \qquad \text{(see Fig. 145(c))}$$

Proceeding as in (A) and (B), one obtains

$$g(s) = \frac{6}{s^4} [e^{+2x_o s} - 2 + e^{-2x_o s}] - \frac{24\ x_o^2}{s^2}$$

$$\frac{1}{2\pi} g(\omega) = \frac{3}{\pi} \frac{1}{\omega^4} \left[e^{2jx_o\omega} - 2 + e^{-2jx_o\omega} \right] + \frac{12}{\pi} \frac{x_o^2}{\omega^2}$$

$$= -\frac{12}{\pi} \frac{x_o^2}{\omega^2} \left[\frac{e^{-jx_o\omega} - e^{-jx_o\omega}}{2jx_o\omega} \right]^2 + \frac{12}{\pi} \frac{x_o^2}{\omega^2}$$

$$= \frac{12}{\pi} \frac{x_o^2}{\omega^2} \left[1 - \left(\frac{\sin x_o\omega}{x_o\omega} \right)^2 \right] \qquad (128)$$

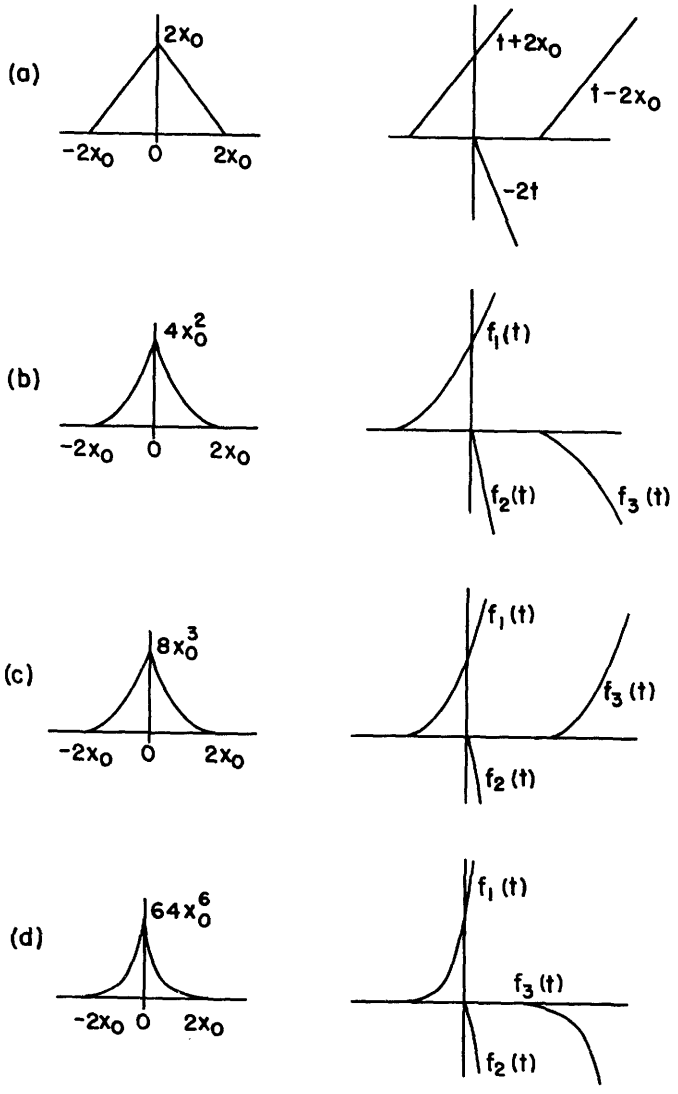

Fig.145 Construction of functions with discontinuous derivatives by the method of translation and sectioning.

D. Sixth-Order Pulse

$$f_1(t) = (t + 2x_o)^6$$

$$f_2(t) = (2x_o - t)^6 - (2x_o + t)$$

$$f_3(t) = -(2x_o - t)^6 \qquad \text{(see Fig. 145(d))}$$

$$\frac{1}{2\pi} g(\omega) = \frac{192}{\pi} \frac{x_o^5}{\omega^2} \left[1 - \frac{5}{(x_o\omega)^2} + \frac{15}{2(x_o\omega)^4} \left(1 - \frac{\sin 2x_o\omega}{2x_o\omega}\right)\right] . \qquad (129)$$

APPENDIX IV

EFFECTIVE VALUE OF Δt

A. One-Edge Time Shift

The effective value of Δt is given by

$$\overline{\overline{\Delta t}} = \sqrt{\overline{\Delta t^2} - \overline{\Delta t}^2} \ .$$

$$\frac{\Delta t}{s\delta}(\phi) = 1 + \frac{a}{s}\cos\phi - \sqrt{1 - \left(\frac{a}{s}\right)^2 \sin^2\phi} \ .$$

[see Section 2.1, (8)]

$$\overline{\frac{\Delta t^2}{s\delta}} = \frac{1}{2\pi}\int_0^{2\pi} \left[1 + \frac{a}{s}\cos\phi - \sqrt{1 - \left(\frac{a}{s}\right)^2 \sin^2\phi}\ \right]^2 d\phi$$

$$= 0.50\left(\frac{a}{s}\right)^2 + 0.094\left(\frac{a}{s}\right)^4 + 0.040\left(\frac{a}{s}\right)^6 + \ldots$$

$$\overline{\frac{\Delta t}{s\delta}} = \frac{1}{2\pi}\int_0^{2\pi} \left[1 + \frac{a}{s}\cos\phi - \sqrt{1 - \left(\frac{a}{s}\right)^2 \sin^2\phi}\ \right] d\phi$$

$$= 0.25\left(\frac{a}{s}\right)^2 + 0.047\left(\frac{a}{s}\right)^4 + 0.020\left(\frac{a}{s}\right)^6 + \ldots$$

$$\overline{\Delta t}^2 = 0.0625\left(\frac{a}{s}\right)^4 + 0.024\left(\frac{a}{s}\right)^6 + 0.012\left(\frac{a}{s}\right)^8 + \ldots$$

$$\therefore \ \overline{\overline{\Delta t}}^2 = 0.50\left(\frac{a}{s}\right)^2 + 0.031\left(\frac{a}{s}\right)^4 + 0.016\left(\frac{a}{s}\right)^6 + \ldots$$

$$\overline{\overline{\Delta t}} \approx 0.71\left(\frac{a}{s}\right) + 0.06\left(\frac{a}{s}\right)^3 \ . \qquad (130)$$

B. Two-Edge Time Shift for $\phi = 180°$

$$\frac{\Delta t(\phi) + \Delta t(\phi + \pi)}{s\delta} = 2\left[1 - \sqrt{1 - \left(\frac{a}{s}\right)^2 \sin^2\phi}\,\right]$$

[see Section 4.5 (109)]

The effective value of this expression is found in the same way as for A.

$$\overline{\frac{\Delta t(\phi) + \Delta t(\phi + \pi)}{s\delta}}^2 = \frac{1}{2\pi}\int_0^{2\pi} 4\left[1 - \sqrt{1 - \left(\frac{a}{s}\right)^2 \sin^2\phi}\,\right]^2 d\phi -$$

$$- \left[\frac{1}{2\pi}\int_0^{2\pi} 2\left[1 - \sqrt{1 - \left(\frac{a}{s}\right)^2 \sin^2\phi}\,\right] d\phi\right]^2$$

$$= 0.13\left(\frac{a}{s}\right)^4 + 0.062\left(\frac{a}{s}\right)^6 + 0.038\left(\frac{a}{s}\right)^8 + 0.026\left(\frac{a}{s}\right)^{10} +$$

$$+ 0.018\left(\frac{a}{s}\right)^{12} + 0.013\left(\frac{a}{s}\right)^{14} + 0.011\left(\frac{a}{s}\right)^{16} + \ldots \quad (131)$$

APPENDIX V

EXPERIMENTAL APPARATUS

A. Circuit Diagrams

Circuit diagrams of the principal equipment used in this research are shown in Figs. 146 - 149. The PDM transmitter shown in Fig. 146 is that used in the PDM two-path interference tests. A variable resistor and a potentiometer control the pulse-repetition frequency and the average pulse duration, respectively. Two switches make it possible to select either pulsed-oscillator or pulsed-amplifier operation, and a third switch permits operation with or without crystal control. Pulsed-oscillator operation is obtained by effectively shunting a tube (6AG7) across the tuned circuit of the oscillator and cutting this tube off only during pulses. Between pulses the tube conducts, and its low impedance prevents the oscillator from operating; in addition, the suppressor grid of the oscillator is held below cut-off during these periods. Pulsed-amplifier operation is accomplished simply by suppressor-grid keying of the output tube. The tube across the tuned circuit of the oscillator is made inoperative so as to allow continuous oscillation.

The PPM transmitter shown in Fig. 147 differs from the PDM transmitter (Fig. 146) only in the video-frequency sections. Asymmetrically duration-modulated pulses are first formed, and their modulated edges are subsequently used to form position-modulated one-microsecond pulses. A simple circuit modification allows the unmodulated edges of the duration-modulated pulses to be converted into one-microsecond synchronizing pulses (as required in the flip-flop system). The average spacing between synchronizing and modulated pulses is adjustable over the entire physically realizable range by means of the potentiometer in the "duration modulator". The potentiometer control in the sawtooth generator makes it possible to change the sawtooth slope by a factor of ten or more.

Figure 148 shows the circuit of the receiver used for PDM and PPM with flip-flop detection. (Pentode suppressor and screen-grid connections are omitted for simplicity.) The first and most important tube of the slicer eliminates the lower part of the positive pulse supplied to it; the setting of the cathode potential determines the level below which the pulses are discarded.

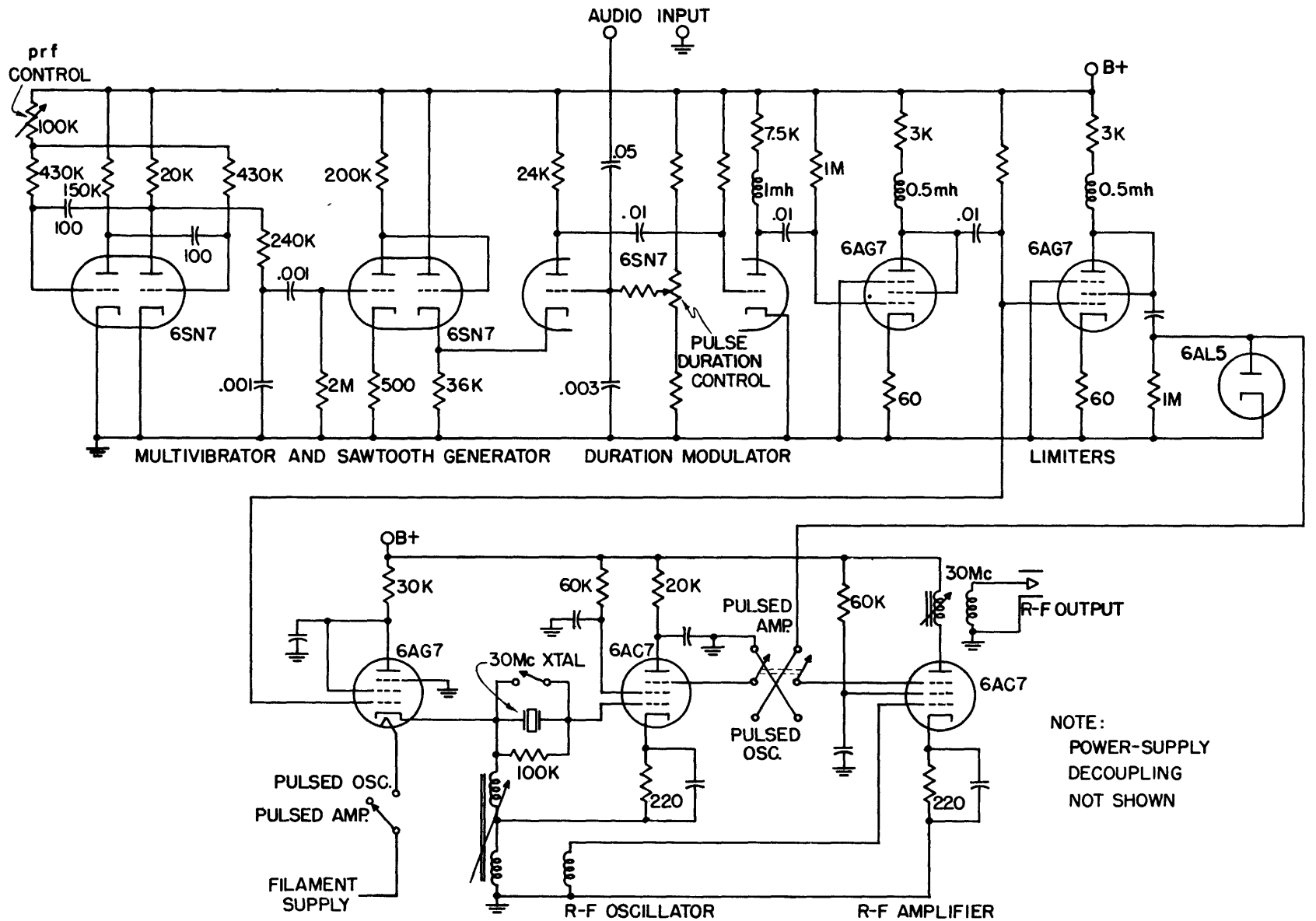

Fig.146 PDM transmitter.

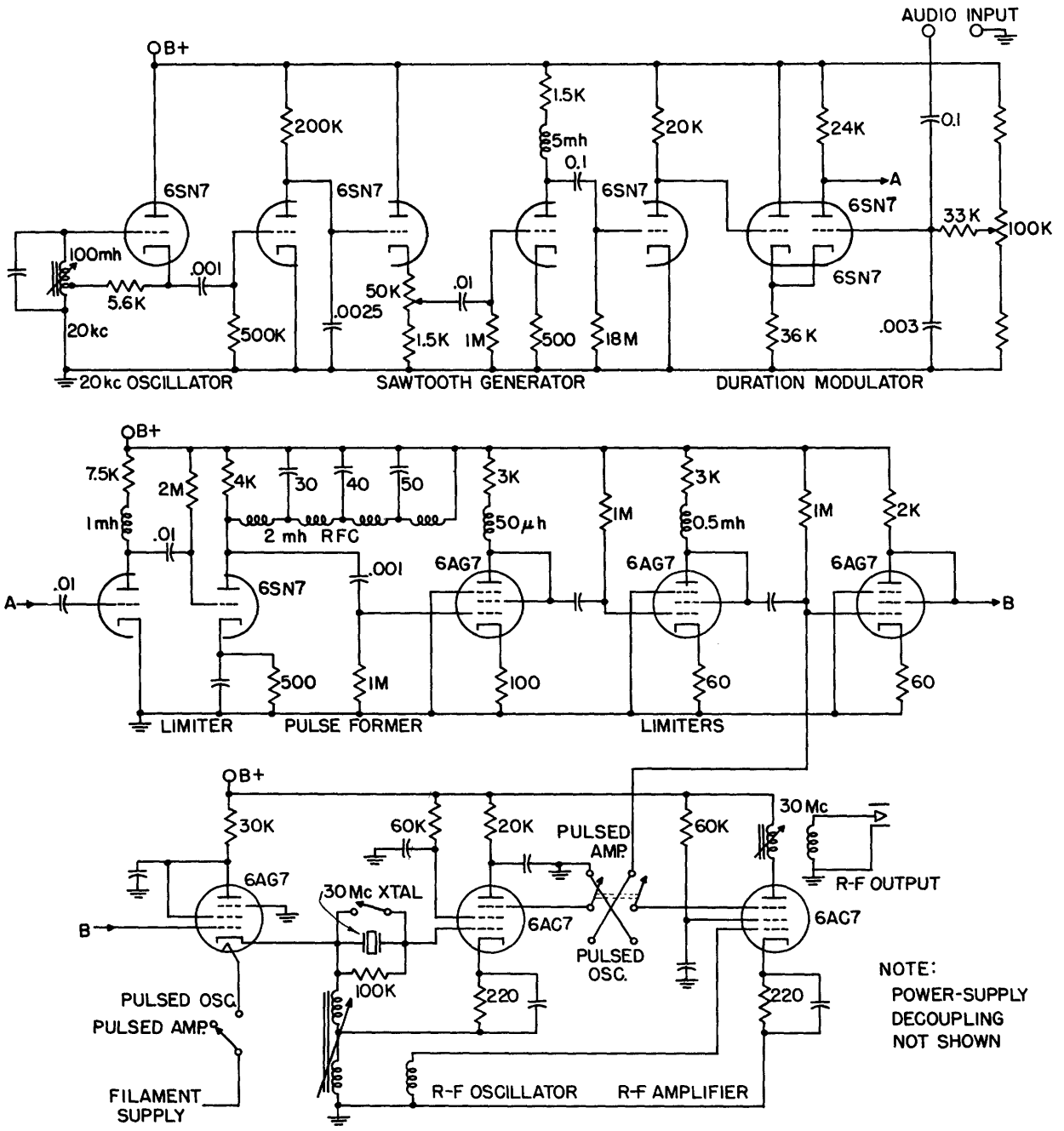

Fig.147 PPM transmitter.

Almost all of the remainder, except for a thin slice above this level, is lost in the second tube of the slicer. Both tubes clip by virtue of control-grid cut-off: the first one forms the "bottom" of the slice, inverts and amplifies the pulse so that the second one cuts the "top" of the slice and again amplifies the slice into a large pulse. The "thickness" of the slice depends on the gain of the first tube, the cut-off voltage of the second tube, and any

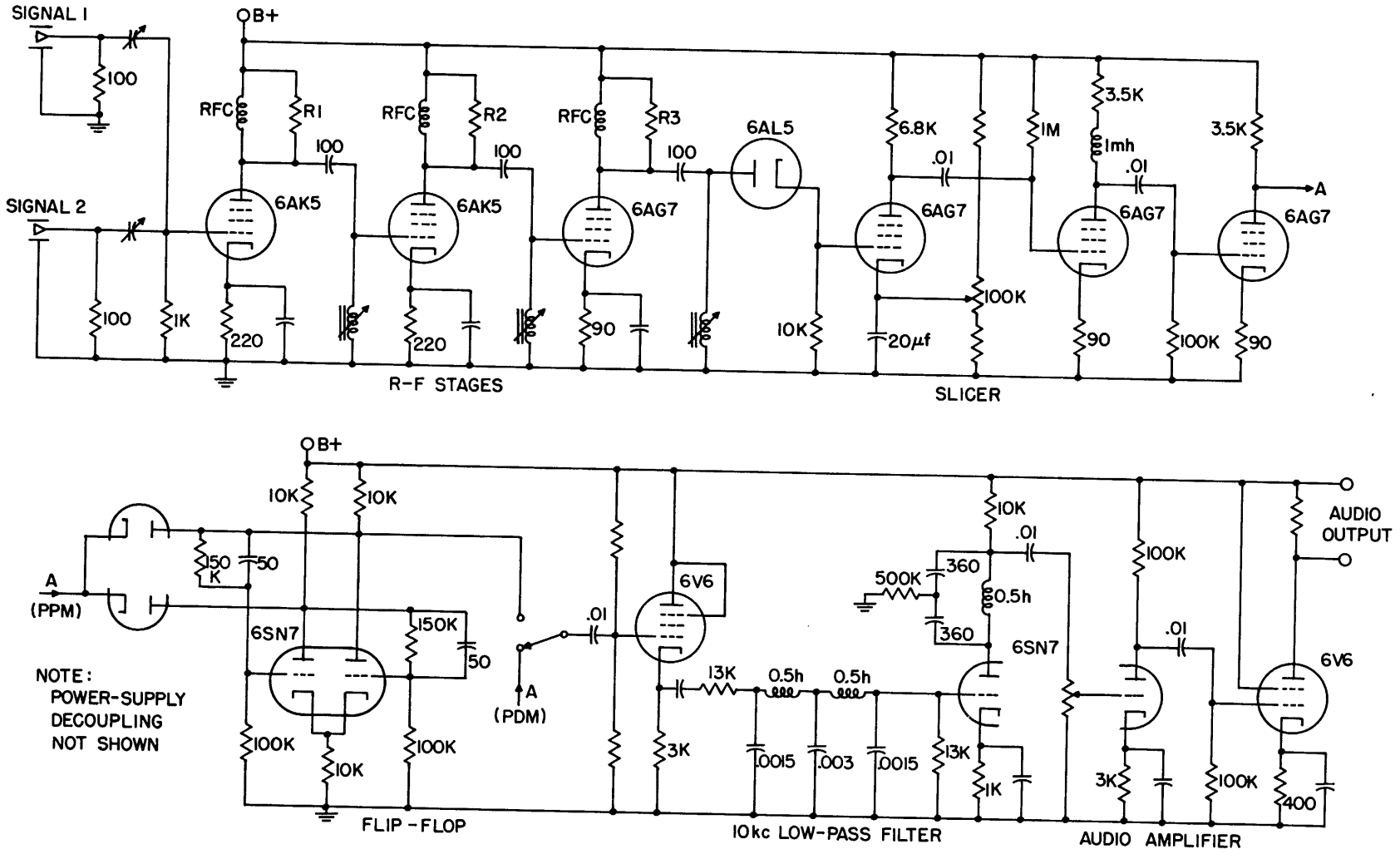

Fig.148 Receiver for PDM and for PPM with flip-flop detection.

subsequent limiting that may take place. The resistors R_1, R_2, and R_3 provide the means for adjusting the r-f (system) bandwidth. The flip-flop, used to convert each set of synchronizing and position-modulated pulses into a duration-modulated pulse is bypassed for PDM reception; otherwise the receiver is the same for PPM flip-flop operation as for PDM operation.

The receiver used for PPM reception with double-coincidence detection is shown in Fig. 149. This receiver incorporates "self-synchronization" and a special feature to minimize the effect of "missing pulses". The r-f stages, detector, and slicer are the same as in the receiver of Fig. 148 (same equipment). Instead of one video-pulse output, three such outputs (A_o, A_1, and A_2), spaced one microsecond (pulse duration) apart are provided. The circuit shown in the middle portion of Fig. 149 generates synchronizing pulses from the modulated pulses (A_o). These synchronizing or reference pulses are compared to two of the modulated pulse trains (A_1 and A_2) in the double-coincidence detector (bottom of Fig. 149); each comparison produces a pulse whose amplitude is proportional to the time shift of either the leading or the trailing edge of the position-modulated pulse - the leading edge in the first and the trailing edge in the second of the two identical channels comprising the double-coincidence detector. Each amplitude-modulated pulse is "held" by trapping it on a storage capacitor until the arrival of the next pulse. One microsecond before a pulse (A_1 or A_2) arrives at either coincidence tube (6AS6), the same pulse (A_o or A_1, respectively) removes the charge (stored one pulse-repetition period earlier) and makes room for the next sample. Should the next sample fail to arrive, then the discharge pulse will also fail to arrive and the previously stored sample is retained until a pulse does reach the detector. In addition, stretching each amplitude-modulated pulse over almost the entire repetition period greatly reduces the magnitude (relative to the audio signal) of the prf component and makes the usual low-pass filtering unnecessary. Furthermore, the push-pull audio connection produces at least partial cancellation of the remaining prf components in the two coincidence channels, with the result that filtering is unnecessary even if the pulse-repetition frequency is in the audible range. Unlike the prf components in the two coincidence channels, the signal components are in phase opposition, and their sum is therefore obtained in the push-pull audio output. It should be noted that the rôles of the modulated pulses and the reference pulses can be interchanged as was done for simplicity in the explanation of the system in

Section 5.41 (Fig. 124).

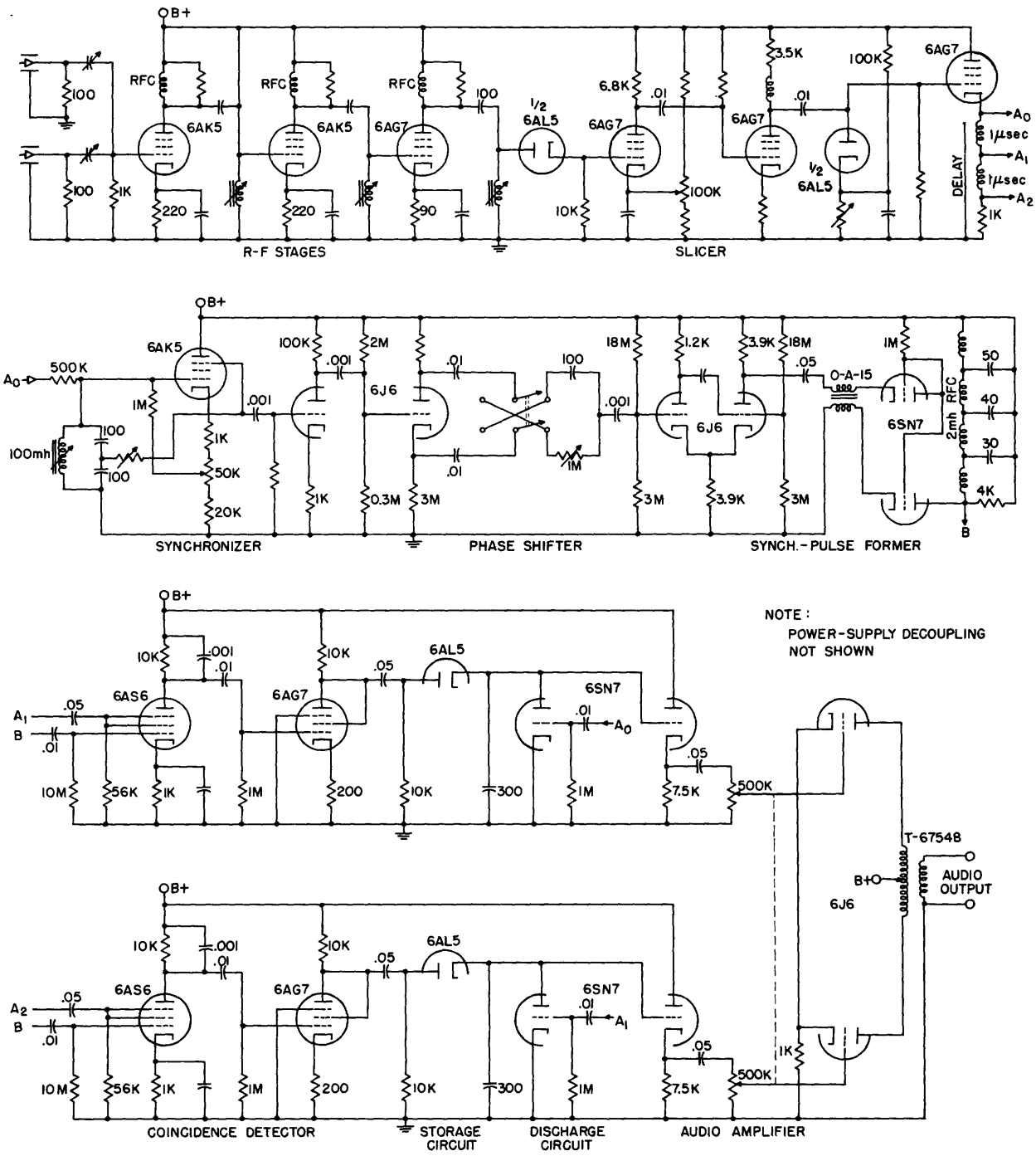

Fig.149 PPM receiver with double-coincidence detection.

B. Oscillograms Showing Circuit Operation

Complete and illustrated descriptions of the manner in which the various circuits function cannot be included here for lack of space, but four representative oscillograms are shown in Figs 150 - 153.

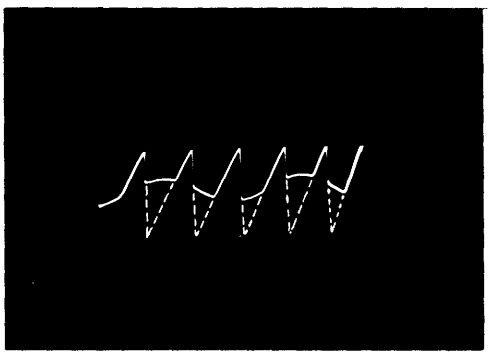

FIG. 150

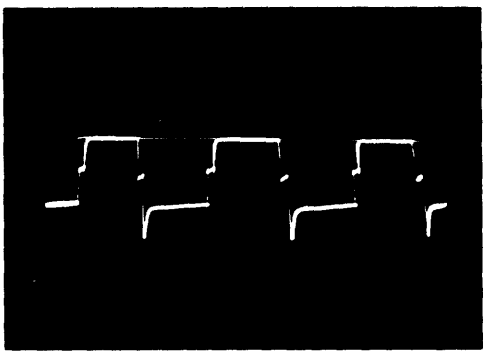

FIG.151

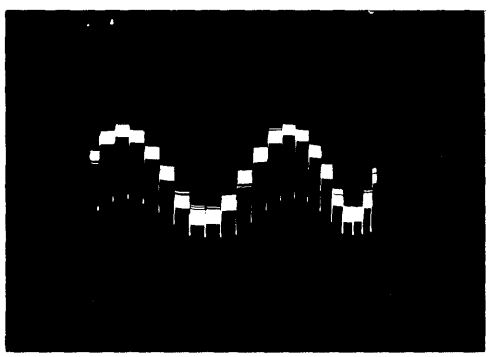

FIG.152

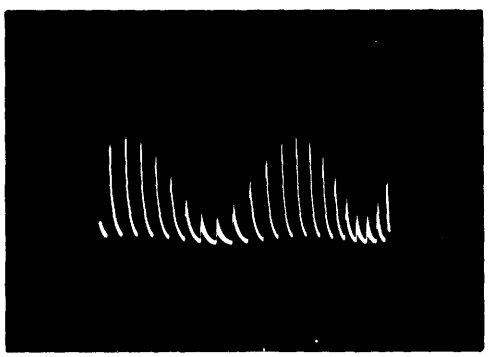

FIG.153

Fig.150 Duration-modulation process: clipping a saw-tooth voltage.

Fig.151 Output of special type of flip-flop acting as PPM detector.

Fig.152 Coincidence-detector output; each sample is stored until 1 μsec before arrival of the next.

Fig.153 Coincidence detector output; each sample is allowed to leak off before arrival of the next.

Figure 150 illustrates the time-modulation process, that is, the clipping of a sawtooth by a sinusoidal modulating signal. Pulse edges are formed at the intersections of the sawtooth and the sinusoidal signal. The oscillogram was taken at the cathode of the "duration modulator" (Fig. 147); at the plate (point "A"), the actual duration-modulated pulses appear.

Figure 151 shows the output of the flip-flop (Fig. 148) modified so as to provide two-edge detection. Ordinarily, the flip-flop is triggered by the leading edges of the short pulses supplied to it. In Fig. 151, it is triggered

only half-way by the leading edge, remains at the half-way or neutral position for the duration of the triggering pulse, and is triggered the remaining distance by the trailing edge. Actual triggering is performed by the trailing edge only, but the triggering pulses, having just half the amplitude of the flip-flop output, are superimposed on this output in such a way as to produce the desired effect.

Figure 152 is the output of one of the two coincidence-detector channels (Fig. 149), observed at the input of one-half of the 6J6 audio amplifier. Each "stair step" represents a sample value extracted from one position-modulated pulse. This value is discharged by the next pulse (approximately 50 μsec later) which, after a small delay, stores its own sample value. The modulating signal is a 2-kc sinusoid, but some noise modulation is also present which causes the stair-step heights to be somewhat different on successive sweeps.

Figure 153 shows the output at the same point as Fig. 152. The circuit has been modified by connecting a leakage resistor (56K) across the 300 μμf storage capacitor and disconnecting the discharge tube normally across this capacitor. Consequently, as soon as the sample-value charge is placed on the capacitor, it begins to leak off and has discharged almost completely when the next sample arrives. Both computations and direct measurements show that the ratio of signal to prf component is approximately 25 db greater in the case of Fig. 153 than in the case of Fig. 152.

C. Performance of Self-Synchronization System

The self-synchronization system (Fig. 149) consists of a pass-band filter used in a regenerative circuit, followed by a phase shifter and a pulse-forming circuit. The filter extracts the fundamental from the position-modulated pulses, as well as some of the low-frequency-modulation side bands (since its pass band has finite width). The sinusoid thus obtained is therefore substantially free of modulation, and the same is true of the pulses which are subsequently formed from the sinusoid. Only some low-frequency position modulation appears on the pulses. This results merely in a modification of the overall frequency characteristic of the PPM system; the overall frequency characteristic is shown in Fig. 154 under three different conditions. If the filter operates as a passive circuit, the result is some loss in low-frequency response, whereas there is a gain in low-frequency response if the filter cir-

cuit is made sufficiently regenerative to operate as an active filter. The explanation lies in the fact that the locally generated pulse (to which the modulated pulse is compared) has some of the same low-frequency modulation as the modulated pulse, but generally shifted in phase by the filter.

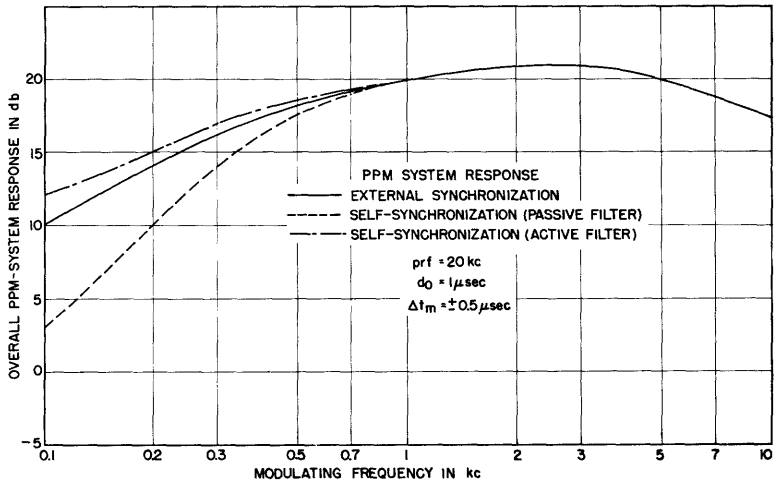

Fig.154 Frequency characteristics of overall PPM system (coincidence detection) with external and self-synchronization.

Figure 155 shows the frequency characteristics of the two low-pass filters used in the experimental part of this study.

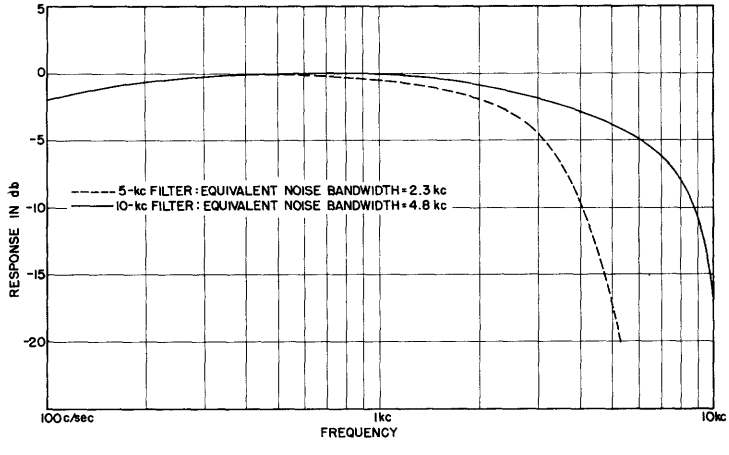

Fig.155 Frequency characteristics of the 5-kc and 10-kc low-pass filters used in the PDM and PPM (flip-flop) receiver.

BIBLIOGRAPHY

1. R. A. Heising, U.S. Patent 1,655,543; granted 1928.

2. R. D. Kell, U.S. Patent 2,061,743; granted 1936.

3. W. A. Beatty, British Patents 523,575, 524,671, 535,384, 535,701; granted 1939-41.

4. E. R. Kretzmer, "Distortion in Pulse-Duration Modulation", Proc. I.R.E., 35, 1230-1235; November, 1947.

5. W. R. Bennett, "Time Division Multiplex Systems", Bell Sys. Tech. Jour., 20, 199-221; April, 1941.

6. C. E. Shannon, "Communication in the Presence of Noise", Proc. I.R.E., 37, 10-21; January, 1949.

7. V. D. Landon, "Theoretical Analysis of Various Systems of Multiplex Transmission", RCA Review, 9, 287-351, 433-482; June and September, 1948.

8. L. J. Libois, "Rapport Signal à Bruit dans Differents Modes de Transmissions Radioelectriques. Spectre d'une Modulation par Impulsions", L'Onde Electrique, 27, 411-425; November, 1947.

9. C. W. Earp, "Relationship between Rate of Transmission of Information, Frequency Bandwidth, and Signal-to-Noise Ratio", Electrical Communication, 25, 178-195; June, 1948.

10. G. L. Fredendall, K. Schlesinger, and A. C. Schroeder, "Transmission of Television Sound on the Picture Carrier", Proc. I.R.E., 34, 49-61; February, 1946.

11. E. M. Deloraine, and E. Labin, "Pulse Time Modulation", Electronics, 18, 100-104; January, 1945.

12. Z. Jelonek, "Noise Problems in Pulse Communication", Jour. IEE, part IIIA, 94, 13, 533-545; 1947.

13. F. F. Roberts and J. C. Simmonds, "Multichannel Communication Systems. Preliminary Investigation based upon Modulated Pulses", Wireless Eng., 22, 538-549; November, 1945.

14. D. D. Grieg and H. Gallay, "Pulse-Time-Modulated Radio Relay System, Radio-Frequency Equipment", Electrical Communication, 24, 141-158; June, 1947.

15. H. J. v. Baeyer, "The Basic Principles of Multichannel Transmission with Modulated Impulses", Brown Boveri Review, 33, 65-69; March, 1946.

16. H. L. Kirke, "The Application of Pulse Technique to Broadcasting", BBC Quarterly, 1, 139-144; October, 1946.

17. J. Zwislocki-Moscicki, "Radioübertragung durch Impulsmodulation", Schweiz. Elektrotech. Verein Bull., 36, 459, 533; July and August, 1945.

18. D. G. Tucker, "Pulse Distortion: The Probability Distribution of Distortion Magnitudes due to Interchannel Interference in Multi-Channel Pulse-Transmission Systems", Jour. IEE, part III, 93, 323-334; September, 1946.

19. N. Wiener, "Generalized Harmonic Analysis", Acta Mathematica, 55, 117-258; 1930.

20. C. E. Shannon, "A Mathematical Theory of Communication", Bell Sys. Tech. Jour., 27, 379-423, 623-656; July and October, 1948.

21. G. I. Taylor, "Diffusion by Continuous Movements", Proc. London Math. Soc., 196-212; 1920.

22. M. F. Gardner and J. L. Barnes, "Transients in Linear Circuits", 1, John Wiley and Sons, Inc., New York, N.Y.; 1942.

23. E. R. Kretzmer, "Analysis of Step Approximation to a Continuous Function", Technical Report No. 12, Research Laboratory of Electronics, Massachusetts Institute of Technology; August, 1946.

24. S. C. Kleene, "Analysis of Lengthening of Modulated Repetitive Pulses", Proc. I.R.E., 35, 1049-1053; October, 1947.

25. W. R. Bennett, "Spectra of Quantized Signals", Bell Sys. Tech. Jour., 27, 446-472; July, 1948.

26. G. A. Miller and W. G. Taylor, "The Perception of Repeated Bursts of Noise", Jour. Acous. Soc. Amer., 20, 171-182; March, 1948.

27. H. B. Huntington, "On Ultrasonic Propagation through Mercury in Tubes", Jour. Acous. Soc. Amer., 20, 424-432; July, 1948.

28. D. Cooke and others, "Pulse Communication", Jour. IEE, part IIIA, 94, 11, 83-105; 1947.

ACKNOWLEDGMENT

The writer wishes to express his gratitude to Professor J. B. Wiesner for supervising this research and to Miss R. J. Harman for assisting in the preparation of this report; to Mr. T. P. Cheatham, Professor Y. W. Lee, Professor L. B. Arguimbau, and Professor H. J. Zimmermann for contributing to the research through valuable suggestions. Much of the work in Chapter 3 is based on material of Professor N. Wiener, ably expanded and presented by Professor Lee in Course 6.563.

Sincere appreciation is expressed for the many indispensable services and facilities of the Research Laboratory of Electronics.